



UNIVERSITÀ POLITECNICA DELLE MARCHE

Doctoral School in Engineering Science
PhD Program in Civil, Environmental, and Building Engineering and Architecture

Doctoral thesis

Physical vulnerability and exposure assessment in Historic City Centers

Development of methodologies and tools for risk reduction measures

PhD Candidate:
Guido Romano

PhD Supervisor:
Prof. Enrico Quagliarini

PhD Co-Supervisor:
Prof. Giuseppe Pace
PhD. Gabriele Bernardini

PhD Program Coordinator:
Prof. Francesco Fatone

Academic Years 2020-2023
XXXVI cycle



UNIVERSITÀ POLITECNICA DELLE MARCHE

Doctoral School in Engineering Science

PhD Program in Civil, Environmental, and Building Engineering and Architecture

Doctoral thesis

Physical vulnerability and exposure assessment in Historic City Centers

Development of methodologies and tools for risk reduction measures

PhD Candidate:
Guido Romano

PhD Supervisor:

Prof. Enrico Quagliarini

PhD Co-Supervisor:

Prof. Giuseppe Pace

PhD. Gabriele Bernardini

PhD Program Coordinator:

Prof. Francesco Fatone

Academic Years 2020-2023

XXXVI cycle

UNIVERSITÀ POLITECNICA DELLE MARCHE

Dipartimento di Ingegneria Civile, Edile e Architettura DICEA

Via Brezze Bianche, Ancona (IT) – 60131

"HEADER"

**"EVERYTHING I DO IS FOR THE
17-YEAR-OLD VERSION OF MYSELF"**

Abloh

"NUMBER"

Abstract

Historic City Centers stand as the most tangible evidence of human history for their cultural significance and architectural heritage, as well as the beating heart of our society thanks to the strong identity value that characterizes them. Their intrinsic significance, indeed, goes beyond mere architectural beauty, and instead represents the cornerstone of the social, cultural, and economic life that shape cities and communities. Consider, for instance, their role in driving tourism, hosting gathering spaces that act as the main stage of social interaction, cultural events, and everyday human activities (including residential, business, and institutional).

Nevertheless, academic and professional debates are still widely open to the research of solutions to evaluate and reduce the risks linked to old and new disasters which every day jeopardize the safety of historic city centers and their inhabitants. It's the case, for instance, of disasters related to natural factors (i.e., seismic areas, floodplains, landslides), human activities (i.e., climate change, pollution, heatwaves, terrorist acts), as well as their combination from a multi-risk perspective. In addition to this, multiple factors such as high population density, narrow streets and layout together with non-updated regulations, preservation constraints to assure historical authenticity, lack of emergency plans, retrofit buildings and infrastructures due to logistic, executive, and economic reasons, further increase the risk in such scenarios.

In this regard, effective solutions should take advantage of holistic approaches, to systematically take into account vulnerabilities, exposures, and hazards that determine the risk, as well as expeditious ones, to speed up the development of methodologies and tools for assessing and reducing the risk itself, and facilitate their application by professionals. Accordingly, interdisciplinary collaboration between urban planners, emergency planners, policymakers, and community stakeholders are paramount in fostering resilience, preparedness and safety of the built environment.

Whitin this context, this thesis addresses the development of methodologies and tools for risk reduction measures in Historic City Centers through sustainable and holistic approaches, with particular attention to integrated analyses of physical vulnerability and exposure. In particular, several dynamics relating to specific or general circumstances are explored according to multiple scales of representation and modeling, ranging:

- from *microscale* to *mesoscale* analyses of the *built environment* (that is from single building and/or street level to neighborhood level);
- from *microscale* to *macroscale* behavioral analyses of the hosted *users* (that is from single pedestrian to groups of them);
- from *normal fruition* conditions to *specific risky* conditions (that is from pre-emergency to emergency conditions, and in particular considering floods);
- from *real-world* to *typological* case studies application.

To support such actions, quick- and easy-to-apply tools and methodologies are developed to speed up evaluation processes, reduce application complexity and economic efforts, and improve replicability also for policymakers and local authorities. Data collection mainly involved rapid surveys and video analyses for databases creation (e.g., mechanical parameters of local masonry typologies, frequencies and conditions of usage of public spaces by users, recurrent human behaviors in specific risk conditions). Risk quantification analyses are performed through the introduction of

synthetic metrics and user-friendly representations (e.g., Risk Indexes, Key Performance Indicators, Risk Maps, specific parameter confidence ranges).

Outcomes, thus, not only *jointly* answer to a wide range of issues according to several perspectives, but also provide customized methodologies and tools to be used for customizable risk reduction analyses, even outside the contexts strictly linked to those herein investigated (e.g., different urban scenarios, different types of hazards). It is therefore a thesis which, in addition to its innovation in the academic field due to its transversality both in conception and in the field of application, is also characterized by a clear practical character to provide immediate feedback on issues that evolve and affect historic city centers and its users. As a result, the next research steps are clear, and will certainly concern the refinement of the proposed tools to provide even more comprehensive and complete analyses also in view of the future challenges that our society will have to face.

List of Contents

1. Introduction	1
1.1 Background	1
1.2 Aims and objectives	3
1.3 Thesis methodology and outline	7
1.4 Previous accomplishments	11
2. Evaluating disaster risk in Historic City Centers: a state of the art	12
2.1 Disaster risk elements' introduction and definitions	12
2.1.1 Hazard	12
2.1.2 Vulnerability	13
2.1.3 Exposure	14
2.2 Evaluating disaster risk for HCCs and their users according to different scales of analysis	14
2.2.1 Different scales for HCCs assessment and representation	14
2.2.2 Different scales for users' assessment and representation	16
2.3 Evaluation of recurring risk conditions: from real-world HCCs to typological scenarios	18
2.4 Key Performance Indicators to quantify the risk	19
3. Phases, methods, and materials	21
3.1 Thesis framework	21
3.2 Physical vulnerability at the microscale: masonry walls classification and mechanical characterization	22
3.2.1 Introduction and motivation	22
3.2.2 Data collection and organization	23
3.2.3 Final database composition	26
3.3 Physical vulnerability at the mesoscale: from real-world case studies to typological scenarios	29
3.3.1 Introduction and motivation	29
3.3.2 Data collection and criteria for scenario creation	29
3.3.3 Typological POS scenarios for flood risk analyses	33
3.4 Spatiotemporal variation of users' exposure and vulnerability in pre-emergency conditions	34
3.4.1 Introduction and motivation	34
3.4.2 Data sources and collection	36
3.4.3 Typological characterization of users	40
3.4.4 Statistical analyses	42
3.5 Users' exposure assessment and modeling in emergency conditions: the case of floods	43
3.5.1 Why floods: introduction and motivation	43
3.5.2 Investigating pedestrian behavioral patterns under different floodwater conditions	44
3.5.3 Comparing custom and generic evacuation simulators based on microscopic approaches	49

3.5.4	<i>Evaluating how pedestrian evacuation behaviors influence the flood risk in riverine HCCs</i>	55
3.5.5	<i>Optimizing shelters and evacuation paths in flood-prone HCCs based on pedestrian behaviors</i>	61
3.6	Hazard assessment and modeling: the case of flood	64
3.6.1	<i>Introduction and motivation</i>	64
3.6.2	<i>Data sources</i>	64
3.6.3	<i>Simulation tool</i>	65
4.	Evaluating physical vulnerability at the microscale: a tool for historical masonry walls classification and mechanical characterization in the context of the Marche Region	67
4.1	Mechanical characterization of recurring masonry walls	67
4.1.1	<i>Compressive strength f</i>	67
4.1.2	<i>Elastic modulus E</i>	69
4.1.3	<i>Shear strength τ_0, shear strength f_{v0}, and shear modulus G</i>	71
4.1.4	<i>Earthen masonry typologies</i>	73
4.1.5	<i>E/f ratio and coefficient of variation</i>	75
4.2	Definition of a tool for historical masonry walls classification and mechanical characterization	76
4.2.1	<i>Outcomes summary and evaluation</i>	76
4.2.2	<i>Results innovation and utility for practitioners</i>	78
4.2.3	<i>Limitations and future aims</i>	79
5.	Evaluating vulnerability and exposure in multi-risk HCC: spatiotemporal impact of different types of areas and users	80
5.1	Square characterization	80
5.2	Users' characterization	81
5.2.1	<i>Hourly characterization</i>	81
5.2.2	<i>Daily characterization</i>	83
5.3	Outcomes evaluation	87
5.3.1	<i>Innovation of the results</i>	87
5.3.2	<i>Policy for stakeholders and practitioners</i>	88
5.3.3	<i>Limitations and future aims</i>	89
6.	How hazard features can affect pedestrian evacuation: investigating behavioral patterns under different floodwater conditions	90
6.1	Observed behaviors and their overall frequency	90
6.2	Statistical frequencies with respect to situational samples	92
6.2.1	<i>Water Depth influence</i>	94
6.2.2	<i>Water Flow influence</i>	95
6.2.3	<i>Water depth equal to or up to the ankles</i>	96
6.2.4	<i>Water depth equal to or up to the knees</i>	97
6.2.5	<i>Water depth equal to or up to the waist</i>	98

6.2.6	<i>Water depth higher than the waist</i>	99
6.3	Most frequent floodwater conditions for behavioral patterns	101
6.4	Outcomes evaluation	103
6.4.1	<i>Implications for modeling approaches</i>	104
6.4.2	<i>Relations with risk-mitigation strategies</i>	104
6.4.3	<i>Limitations and future aims</i>	105
7.	Simplified flood evacuation simulation in HCCs: preliminary comparison between custom and generic simulators	107
7.1	Evacuation curves comparison	107
7.2	Comparison between D_w trend along the pathway	108
7.3	Quartile analysis of trends in pedestrians' evacuation timing	109
7.4	Comparison with real-world observations	111
7.5	Best setup definition	112
7.6	Limitations and future aims	114
8.	How urban layout and pedestrian evacuation behaviors can influence the risk in HCCs: the case of fluvial floods	116
8.1	Floodwater levels in the HCCs	116
8.2	HCCs flood risk with and without pedestrian evacuation behaviors	119
8.3	Outcomes evaluation	122
8.4.1	<i>Typological HCC risk comparison</i>	122
8.4.2	<i>Key findings, work novelties, and future aims</i>	123
9.	Optimizing pedestrian evacuation strategies in flooded HCCs according to a behavioral-based approach	125
9.1	How many, where, how, and which gathering areas and evacuation routes are needed in the HCC-related POS	125
9.1.1	<i>Gathering areas optimal number</i>	125
9.1.2	<i>Gathering areas optimal position</i>	126
9.1.3	<i>Optimal evacuation routes</i>	127
9.1.4	<i>Optimal evacuation units</i>	127
9.1.5	<i>Identification of the best evacuation strategy</i>	128
9.1.6	<i>Comparisons between macroscopic and microscopic modeling approaches</i>	129
9.2	Outcomes evaluation	130
9.2.1	<i>Innovation of the results</i>	130
9.2.2	<i>Policy implications for decision-makers</i>	131
9.2.3	<i>Limitations and future aims</i>	131
10.	Conclusions and future works	133
11.	Appendices	138
11.1	Physical vulnerability at the microscale	138
11.1.1.	<i>Italian National Standard indication: Tables C8.5.I and C8.5.II</i>	138

11.1.2.	<i>Masonry walls texture, façade, and sections</i>	139
11.1.3.	<i>Earthen masonry typologies recurrent in the Marche Region</i>	142
11.1.4.	<i>Literature database</i>	145
11.2	Case studies characterization and typological HCCs definition	148
11.3	Exposure and vulnerability in pre-emergency conditions	154
11.3.1.	<i>Symbols and acronyms</i>	154
11.3.2.	<i>List of case studies</i>	156
11.3.3.	<i>Intended uses full table</i>	158
11.3.4.	<i>Users' temporalities full table</i>	159
11.3.5.	<i>Guide for application</i>	160
11.4	Video-analyses on pedestrian evacuation behaviors	164
11.4.1.	<i>Evacuation behaviors codified and classified in literature</i>	164
11.4.2.	<i>Symbols and acronyms explanation</i>	166
11.5	Specifications on evacuation simulators	168
11.5.1.	<i>Modeling logic</i>	168
11.5.2.	<i>MassMotion specific configuration</i>	169
11.5.3.	<i>Setup symbols and properties</i>	171
11.5.4.	<i>Symbols and acronyms</i>	172
11.5.5.	<i>Detailed KPIs and simulation results</i>	173
11.6	Detailed flood simulation outputs	181
11.6.1.	<i>Flood risk maps</i>	181
11.6.2.	<i>Symbols and acronyms</i>	181
11.7	Mathematical methods for evacuation plan optimization	183
11.7.1.	<i>A minimum cost flow-based Integer Linear Program</i>	183
11.7.2.	<i>Symbols and abbreviations</i>	187
11.7.3.	<i>KPIs and RI detailed results</i>	187
11.8	Characterization of the flood event	189
	Acknowledgements	190
	Dedication	191
	List of Tables	192
	List of Figures	196
	Bibliography	201

1. Introduction

1.1 Background

In the last decades, worldwide cities and society have increasingly been affected by devastating natural disasters [1], [2] to which must be added risks due to human activities [3], [4], thus affecting every day more and more individuals and emergency management authorities [5]. Severity-affecting factors behind this growing trend are multiple, such as the impacts of climate changes, the densification of urban areas, urbanization growth and changes in land use, and the gradual shift in population residence from rural to urban areas [5]–[7].

Cities are hubs of human activity, housing large populations and significant infrastructure, in which the interaction between people (who live, move, and behave differently), and built environment (as the complex system composed of buildings, urban infrastructures, and open spaces) creates a complex dynamic ecosystem that significantly impacts resilience, conservation, and strategies to address whichever kind of disaster [8]–[10]. Understanding these relationships is then essential for assessing the safety and sustainability of cities and their users, and providing answers on how to properly design and secure them in view of the aforementioned current challenges.

Historic City Centers (HCCs) are critical scenarios due to a combination of structural, geographical, and historical factors, and they were not conceived to deal with sustainability, resilience, and contemporary technological issues that every day transform the way users think, experience, and inhabit cities [11]–[15]. Firstly, HCCs were typically constructed using traditional materials and construction techniques that were significant during their time, but often without adequate levels of resilience and structural integrity. Such problems are also exacerbated by frequent constraints on the implementation of structural interventions to protect the authenticity of the artistic and cultural heritage [12], [16]. In addition to this, many HCCs were strategically located near water sources for trade and transportation, exposing them to multiple hydrogeological hazards (e.g., floods and landslides). As a consequence, the organic growth of HCCs often led to unplanned development in vulnerable areas prone to multiple natural risks (i.e., seismic territories, floodplains, or coastal areas) to which further types of risk are being added in recent years (e.g., air pollution, heatwaves, terrorist attacks) [17].

For what it concerns *earthquakes*, the advancements in seismic engineering and dynamics have shown that historical buildings, which were built before the implementation of contemporary seismic standards and principles, are heavily susceptible to damage or collapse. This vulnerability depends on the use of weak materials, techniques, and structural systems that are prone to failure under seismic and vertical forces, as well as the lack of adequate reinforcement [18]–[20]. During *floods*, historic buildings situated in flood-prone areas may suffer from water infiltration, structural damage, and contamination. Inadequate drainage systems, the presence of valuable buildings, and artistic heritage, together with complex and compact urban layouts typical of HCC further exacerbate the risks [21], [22]. In the case of *heatwaves*, historic buildings with limited insulation and outdated cooling systems struggle to provide adequate thermal comfort, putting the occupants at risk. Additionally, the preservation of original features, such as windows or façades, can limit the implementation of modern energy-efficient solutions [23]–[25]. Poor indoor and outdoor air quality is another concern, especially in HCCs facing *pollution* challenges. The inflexible air circulation systems of older buildings can contribute to the accumulation of pollutants, impacting the health and

well-being of occupants and affecting the preservation of cultural heritage [26], [27]. HCCs are susceptible to being targeted in *terrorist attacks* as well, as their cultural and symbolic significance makes them potential targets for intentional harm. Ensuring the safety of occupants and safeguarding heritage require then a delicate balance between preserving the integrity of the structure and implementing effective security measures [28], [29].

Accordingly, risk reduction measures should be complemented with cross-sectional evaluations by considering not only the specific risks for the built environment alone, but also the safety and well-being of its inhabitants through the study of their features, capabilities, and behaviors before, during, and after each type of emergency. In this context, HCCs are generally characterized by even higher **disaster risks**, because of the combination of different factors [30]–[37], such as: (1) their position in areas prone to natural or human-made hazards; (2) their compact and complex layout; (3) the significant building heritage vulnerability; (4) the growing population, densification, and the possible of attractivity for tourists, who can be unaware of the risk and unfamiliar with the urban layout; (5) the lack or shortage of infrastructural (e.g. urban furniture to improve human evacuation, drainage systems against floods, seismic dissipators against earthquakes) and non-structural (e.g. early warning systems, evacuation plans) risk mitigation strategies, due also to the difficulty in integrating these solutions due to heritage preservation regulations, high application impact to historical scenarios, limited spaces for infrastructures, financial constraints, and difficult coordination among stakeholders.

While the exact timing, location, and severity of disasters could be difficult to foresee, our understanding derived from historical occurrences allows us to identify regions most susceptible to specific risks. This awareness enables more effective disaster risk management in anticipation of such events. Scientific literature [38] and international organizations [39], [40] commonly identify four main phases of disaster risk management:

- **Mitigation** involves actions and measures taken to prevent or reduce the long-term cause, impact, and consequences of disasters. This phase aims to address the root causes of disasters and minimize their impact on the built environment and its inhabitants. Mitigation strategies may include land-use planning, building codes, infrastructure improvements, and environmental protection measures.
- **Preparation** focuses on activities and planning done before a disaster occurs to enhance the ability to respond effectively. Preparedness efforts aim to minimize losses of “assets”, i.e., lives, injuries, and property damages. This phase involves developing emergency plans, conducting drills and training exercises, establishing communication systems, and ensuring that resources and personnel are ready for deployment.
- **Response** concerns activities during and immediately after a disaster. Usually, during this phase infrastructure, communication, and other operations do not function normally, thus it involves the mobilization of emergency services, search and rescue operations, medical assistance, and the provision of food, shelter, and other essential services to affected populations. Effective coordination, communication, and rapid deployment of resources are critical components of the response phase.
- **Recovery** is the process of rebuilding and restoring communities in the aftermath of a disaster. This phase aims at restoration efforts to bring the affected area to a stable and sustainable state with regular operations and activities. Recovery efforts include

infrastructure reconstruction, social and economic recovery, mental health support, and long-term community resilience building. The goal is to learn from the disaster experience and create a more resilient environment for the future.

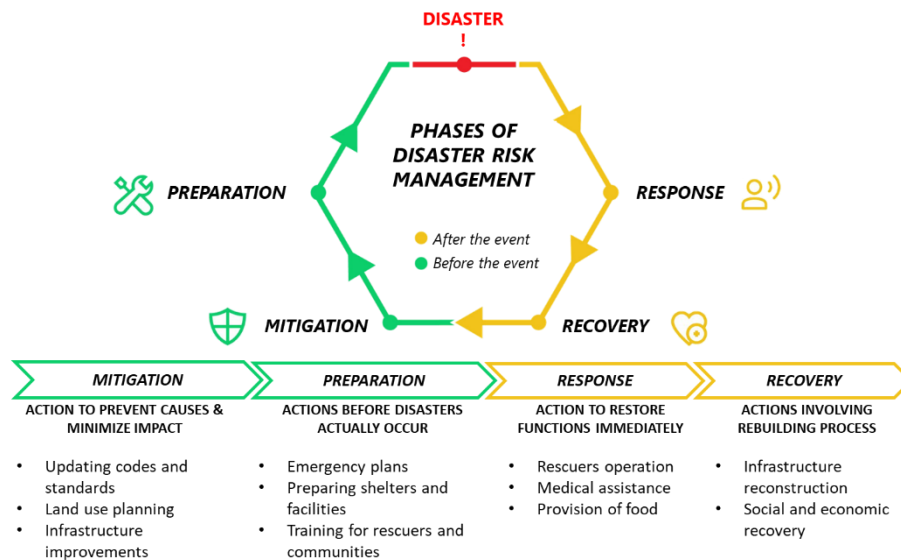


Figure 1: Graphical illustration of the four phases of the disaster risk management: mitigation, preparation, response, and recovery.

In other words, the inner significance of this emergency management cycle is that all communities are in at least one phase of emergency management at any time. This underscores the fundamental importance of activities related to disaster preparedness, mitigation, response, and recovery on a global scale. In particular, rapid and easy tools and methodologies associated with the first, proactive phases of the disaster risk assume a pivotal role in guaranteeing a more robust and comprehensive approach to disaster risk management, contributing to increasing resilience and minimizing the potential impact on communities.

1.2 Aims and objectives

Overcoming the challenges listed above requires holistic and systematic approaches that involve collaboration among stakeholders, local communities, and government authorities towards the development of context-specific risk reduction strategies and methodologies respecting the historical character of the built environment, while also enhancing its resilience to natural hazards. To support such actions, sustainable and resilient analyses, and tailored solutions for risk-prone HCCs are fundamental to guarantee inhabitants a safe and full experience of buildings and public open spaces.

In this sense, quick- and easy-to-apply tools and methodologies to collect and quantify standardized data are necessary, so as to:

- speed up application and evaluation processes to provide timely results toward the reduction of the risks for the whole community [18];
- reduce application complexity and economic efforts to ensure powerful analysis also by non-expert technicians, such as those of local administrations [41];
- improve replicability and take advantage of typological approaches for the definition of recurring conditions that can also lead to common operational frameworks for assessing, identifying, and designing interventions for real-world contexts [10], [21], [42]–[45].

Noteworthy examples in this sense, for instance, are the development of:

- **Risk maps** [41], [46]–[48], as user-friendly tools guaranteeing quick identification of high-risk zones that enable stakeholders to prioritize areas in need of immediate attention or intervention. They are easy to understand and ensure effective communication, helping convey complex information in a simplified manner, which is particularly important when engaging with community members potentially unaware of procedures and risks, or decision-makers who may not have a technical background. Furthermore, risk maps can serve as valuable decision support tools for urban planners as well as emergency management teams to efficiently allocate resources (e.g., how to prioritize rescue operations, investments in infrastructure, early warning systems, urban furniture, and other risk reduction measures). Nevertheless, current approaches for the definition of risk maps often overlook challenges and complexities in HCCs due to the lack of holistic perspectives that jointly integrate factors related to the built environment, the event, and the hosted users features. This gap should be filled to accurately consider the complex nature of HCCs in risk management actions.
- **Simulation tools** [48]–[51], that enable planners and emergency management teams to test different scenarios (in terms of solutions, configurations, temporalities, and disaster type and intensity) and assess the potential impacts on the built environment and its inhabitants. Simulations usually concern disasters (to evaluate effects and extents of damages and vulnerable areas), evacuations (by modeling human behavior and movement during emergencies to test the capabilities of evacuation plans), and infrastructures (by modeling their mechanical features to evaluate their response to various disaster scenarios). Furthermore, they can be used for training purposes to help communities and personnel to understand safety procedures and enhance overall preparedness. Finally, simulators are powerful tools to identify prioritizing areas that require retrofitting and/or to dynamically test the effectiveness of risk reduction measures, as they allow changing conditions over time. This is particularly important for understanding the evolving nature of risks, especially in the context of climate change and other dynamic factors. Nevertheless, current simulation tools should be improved to accurately represent specific human behaviors and motion capabilities during emergencies, especially when the surrounding built environment is deeply modified by the hazard consequences (e.g., floods, earthquakes, but also terrorist attacks). As a result, simulations may provide incomplete or inaccurate assessments of risk and evacuation dynamics, limiting their effectiveness in supporting decision-making processes for risk reduction and resilience planning.
- **Key Performance Indicators (KPIs) and Risk Indexes (RIs)** [49], [52], [53], as quantifiable metrics providing measures on various aspects of risk and the effectiveness of mitigation strategies. These metrics offer a standardized way to assess performance and track changes over time, such as the structural integrity of buildings, built environment resilience, and the effectiveness of evacuation plans. Simplified KPI and RI dashboards focusing on key metrics provide an easy-to-understand overview of critical performances, whose regular monitoring allows for timely identifications of emerging risks and the need for adjustments in strategies. Furthermore, they can also serve as benchmarks to ease comparisons toward predefined standards, as well as enhance communication between different stakeholders (e.g., policymakers, emergency management teams, and

communities), thanks to clear representations conveying complex information in a comprehensible manner. The integration of KPIs and RIs with the aforementioned tools should be pursued toward a more comprehensive view of risk scenarios, although improvements are currently still needed to better clarify the impact of various factors on the overall risk.

- **Surveys** [11], [17], [54]–[60], that collect and organize data in a rapid and collaborative manner across several fields of application. Online and digital survey platforms can reach a wide audience, and the data can be processed rapidly, expediting feedback and analyses. In particular, focusing on HCC risk assessment, survey data assume a paramount role in the systematic collection of feedback from professionals assessing post-disaster damages, vulnerabilities, and performance of structures. Such data facilitates inquiring practitioners' perspectives, offering/providing insights from/for their practical experiences according to a circular logic. Such a collaborative approach extends beyond mere data collection and affords a basis for potential improvement and adaptation of current regulatory standards to the evolving exigencies of structural performance and heritage conservation. In addition to this, surveys also have significant potential in the evaluation of how people behave in the built environment during emergencies and non-emergency situations, so as to improve risk management and space planning, although current practices and approaches seem to overlook such issues. Nevertheless, gathering real-time and historic data on individuals' behaviors, uses, and habits is useful to understand interactions between inhabitants and the built environment, providing critical insights into human responses during emergencies (e.g., evacuation patterns, decision-making processes, utilization of available resources) as well as non-risky circumstances (e.g., usage patterns, preferences, and spatiotemporal interactions during routine activities). In this way, such an informed approach is useful to bolster risk management strategies and optimize spatial planning to better align with human safety, needs, responses, and well-being, thus overcoming current methodology limitations. This comprehensive understanding empowers stakeholders and professionals to create environments that are not only resilient to emergencies but also tailored to the diverse and evolving behaviors of their occupants in day-to-day life. Additional fields of application (even if not investigated in this study) may concern, for instance, the assessment of the environmental impact of buildings and infrastructures to promote energy efficiency and sustainable materials, or the evaluation of accessibility issues focusing on the needs of people with disabilities towards inclusivity standards.

Starting from this overview, this thesis work aims to introduce innovative tools and methodology to assess the risk in HCCs according to sustainable and holistic approaches. Safety of the built environment and its inhabitants are pursued by combining *physical vulnerability*, *exposure*, and *hazard* analyses according to *microscopic* and *macroscopic* scales of analysis applied to real-world and idealized contexts. In particular, significant contributions to the scientific and technical communities are pursued by addressing and solving the following needs.

One of the primary objectives of the thesis is to draw up a ready-to-use abacus of recurring historical masonry walls in the Marche Region, aligning with a specific research goal highlighted also by the Italian National Standards for building construction aimed at assessing the *physical vulnerability* of HCCs. This tool encompasses tables and reference values in accordance with the same principles and fashion by national standards (albeit adapted and updated based on local case studies) and is

supplemented by a huge collection of images to ease the masonry recognition by industry practitioners. Data collection for this study stemmed from surveys conducted by local professionals during their professional activities, thereby enabling future updates to the tool to incorporate advancements in sample data, case studies, and testing techniques.

Besides of the physical vulnerability, a comprehensive and accurate risk analysis requires a proper evaluation of the *vulnerability* and *exposure* of the individuals within the built environment. In this regard, the second research question concerns the lack of a methodology for gathering and estimating such factors and their evolution over space and time. This objective is addressed through the proposal of simple and customizable tools for analyzing public open spaces at the *mesoscale* (as in the case studies herein investigated) as well as entire neighborhoods. Results could be combined also with the previous ones, thus providing the necessary support for highly refined analyses on *single, multi-risk*, and *pre-emergency* conditions in real-world or typological case studies. By integrating these considerations, a more holistic understanding of risk can be achieved, facilitating informed decision-making processes in disaster *preparation* and *mitigation* efforts.

From this perspective, the third and final action fueled in this thesis concerns an in-depth analysis of such issues with reference to the *specific case of flood risk*, as a prevalent and pressing emergency typology necessitating further investigation by the scientific and technical communities. In particular, the risk assessment process is addressed through a simulation-based approach that considers recurring *vulnerability* conditions in flood-prone HCCs in the Italian context and the repercussions due both to the *hazard* features and the *behaviors of the people exposed*. These aspects are combined so as to provide an innovative, holistic risk assessment methodology that relies on multiple tools, going from the production of typological scenarios for the evaluation of standard solutions in relation to characterizing conditions, to the verification and validation of different flood evacuation simulators, until the development of risk indexes and risk maps to rapidly evaluate, rank, and compare scenarios and solutions.

The following subsection introduces specific contents and general organization of the thesis to provide the reader with the key elements to fully understand the gaps to be filled in the research and the solutions consequently proposed.

1.3 Thesis methodology and outline

The thesis work is consequently organized to first highlight overall and specific needs emerging from a comprehensive review of the current state of the art and the prevailing methodologies employed to address aims and objectives previously declared. In particular, Section §2 is organized as follows:

- subsection §2.1 introduces key elements defining disaster risk (i.e., hazard §2.1.1, vulnerability §2.1.2, and exposure §2.1.3) according to relevant sources and international organizations;
- subsection §2.2 concerns the different scales of analysis for risk assessment and modeling by focusing on applications on built environment §2.2.1 and its inhabitants §2.2.2, and ranging from microscale to macroscale approaches;
- subsection §2.3 delves into the study of recurring conditions always according to a broader perspective that varies from the definition of typical uses and behaviors of inhabitants in the built environment, up to the mechanical characterization of buildings and infrastructures. In this way, real-world case studies lead to the definition of typological scenarios useful for fast and standardized analyses;
- subsection 2.4 finally stresses the importance of KPIs as a tool to quantify the risk through metrics and measures differentiated according to the different classifications made in the previous subsections, and to be combined to jointly consider all of them within a single and rapid evaluation tool.

Section §3 states the phases, methods, and materials employed in the research towards the development of methodologies and tools for risk reduction in HCCs. Since the thesis addresses different types of risk and case studies, and, consequently, proposes different solutions, firstly subsection §3.1 graphically summarizes the thesis framework in order to make clear the correlation between the analyses and each of the results illustrated in the following chapters. Subsequently, the following subsection concerns:

- the classification and the mechanical characterization of historical masonry walls in the context of the Marche Region according to a ***microscale approach***, as a relevant example of ***physical vulnerability*** assessment (subsection §3.2). The discussion is organized so as to introduce the motivation behind the choice of the case study (which was selected to provide concrete feedback to a specific suggestion by the Italian building code about the definition of recurring conditions for local masonry specificities), the criteria for the data collection and the composition of a database including experimental tests and photographic material. Collaborations with local professionals (e.g., engineers, licensed laboratories, and local authorities) were fundamental for this purpose. This goal was also agreed with the Order of Engineers of the Province of Ancona, which co-funded this activity to achieve these research aims. This part of the thesis was supervised by Prof. Enrico Quagliarini, and co-supervised by Prof. Giuseppe Pace;
- the realization of typological scenarios for ***physical vulnerability*** assessment according to a ***mesoscale approach***, on the basis of recurring conditions in real-world case studies (subsection §3.3). This part explains which data and statistical analyses are used, taking advantage of a simple approach customizable to any type of context and risk; then provides a focus on the case study of riverine HCCs in the Italian context at risk of flooding, in agreement and to be integrated with other investigations carried out in the following sections

- of the thesis. This part of the thesis was supervised by Prof. Enrico Quagliarini, and co-supervised by PhD. Gabriele Bernardini;
- the assessment of *exposure and vulnerability* spatiotemporal evolution in *pre-emergency conditions* according to a *mesoscale approach* focusing on HCC-related public open spaces (i.e., streets, squares, and their combination) and their inhabitants (subsection §3.4). In particular, the proposed methodology provides a rapid survey form exploited for single case studies, as well as to derive typological, recurring conditions in Italian HCCs. As for the previous sections, the discussion is organized so as to first provide specific motivations behind the choice of the case study, then the criteria for the data collection and organization, the sources, and the statistical analyses performed to identify use patterns in HCCs prone to multi-risk. This research activity was included in the WP3 of the BE S²ECURe¹ project of national interest (PRIN funded by competitive tender, MIUR Grant number: 2017LR75XK) interested in pursuing sustainable and equitable risk-mitigation solutions for users exposed to multi-risk emergency conditions in historic built environments. This part of the thesis was supervised by Prof. Enrico Quagliarini, and co-supervised by PhD. Gabriele Bernardini;
 - an in-depth analysis of the assessment and modeling of *users' exposure in emergency conditions* due to *flood risk* for HCC-related public open spaces (i.e., streets, squares, and their combination) and their inhabitants (subsection §3.5). This part first provides motivations behind the choice of the case study, then collects the fundamental steps for the development of several methodologies and tools for flood risk assessment and mitigation. In particular, starting from the observation of pedestrian behaviors through video-analyses of real-world flood emergencies, different evacuation simulators are developed and compared according to both *microscopic and macroscopic logics* which finally lead to the proposal of assessment tools such as risk indexes and risk maps. Each subsection is organized to discuss specific background and frameworks, criteria for data collection and organization, statical analyses performed, and criteria for simulations and comparisons. This part of the thesis was supervised by Prof. Enrico Quagliarini, and co-supervised by PhD. Gabriele Bernardini;
 - the assessment and modeling of a real-world riverine flood with a return time of 100 years, as a relevant example of the *hazard* to be simulated within the typological scenarios previously defined. The hydrodynamic conditions thus established (output) provide also the basis (input) to test and refine the evacuation simulator developed in the previous subsection. As for the previous sections, the discussion is organized to first provide the specific motivations behind the choice of the case study, then the criteria for the data collection and organization, the sources, and the simulation tool. This part of the thesis was supervised by Prof. Enrico Quagliarini, and co-supervised by PhD. Gabriele Bernardini.

It is important to underline how, in each subsection, measurements and comparisons are performed through the use of customized/customizable KPIs to preserve a synthetic-holistic approach. Finally, the next parts of the thesis concern specific results obtained from the aforementioned analyses, and are organized to provide tools and solutions to cope first with the *mitigation phase* against *generic* disaster risk management (sections §4 and §5), then to the *preparation phase* against a *specific* type of disaster, which is the flood risk (sections from §6 to §9). In particular:

¹ Built Environment Safer in Slow and Emergency Conditions through behaviorally assessed/designed Resilient solutions <https://www.bes2ecure.net/home> (last access: 20/01/2024)

- Section §4 includes the main results obtained from the classification and the mechanical characterization of recurring historical masonry walls in the context of the Marche Region. This research yielded a *textbook for professionals and insiders* [61] including ranges and reference values of mechanical features (compressive strength, elastic modulus, shear strength, and shear modulus) of recurring masonry walls in the Marche Region (subdivided into regulated and unregulated ones) for supporting practitioners in the evaluation of historic buildings safety against vertical and seismic actions. Results include comparisons with the Italian National Standard indications and literature data.
- Section §5 provides the typological description of a sample of 56 squares in Italian HCCs prone to multi-risks (earthquakes, terrorist attacks, heatwaves, and pollution) thanks to innovative KPIs concerning both general features of the built environment, and the users' temporalities affecting vulnerability and exposure issues. Results unveil *usage patterns* considering daily and hourly timetables, differences between user typologies (according to their familiarity with the areas and their motion condition related to their age), and differences between working day and holiday scenarios. *General features of the built environment* are also discussed (e.g., the presence of special buildings, the intended uses, and the frequency and density of indoor and outdoor areas). Promoted in the BE S²ECURE project, the methodology also supports this research for the application of typological scenarios in simulation-based assessment and risk-mitigation strategies development.
- Section §6 discusses relationships between the frequencies of users' behaviors, the water depth (depending on human body parts submerged), flow (distinguishing between still water and flowing water), and the evacuation phase in which they are observed (that is before, during, and after the evacuation). Specific factors like voluntariness, human response, and the presence of reference elements in the flooded built environment are also considered. Such an approach provides cornerstones for the definition of *behavioral patterns* used in the following sections for the development of evacuation simulators.
- Section §7 provides *preliminary setups* of a generic software tool to perform quick and sustainable assessments of pedestrians' flood safety in outdoor spaces, using an easy-to-apply no-code modification approach to include flood peculiar behaviors. Simulation outputs of the setup-based generic software are compared with a custom simulator relying on the same microscopic modeling approach, and with real-world observations for verification and validation purposes. Results provide the best setup of the generic software to reliably represent *evacuation phenomena*, thus encouraging its application also by local authorities.
- In section §8 the aforementioned setup-based generic software has been exploited to unveil how *differences in HCC layout can affect pedestrian evacuation* during flood emergencies. Two different evacuation strategies in six different typological scenarios (characterized by different layouts in terms of street and square positions) are tested under the same flooding event through a simulation-based methodology based on the evacuation process analysis. The first strategy considers that users leave the HCC, thus moving away from the river source of danger. The second strategy adopts gathering areas positioned where the risk is lower. *Risk Indexes and Risk Maps* are provided for the entire scenarios (mesoscale) and each of their outdoor spaces (microscale), depending on evacuation time, flows, path length, and number of casualties depending on hydrodynamic conditions.
- Starting on results obtained from the previous section in terms of the "best evacuation solution" for the "riskiest scenario", section §9 finally addresses the *optimization of*

pedestrian evacuation strategies according to a behavioral-based approach. In particular, results are evaluated by varying the pedestrians' approach to the route choice to optimize the gathering areas' number and position, the evacuation routes to be traveled from each position of the scenario, pedestrian allocation issues, and evacuation units' discretization. Results allow for evaluating security measures to deal with the absence/ineffectiveness of structural ones and could be exploited to assess where/how to implement wayfinding systems, urban furniture, and rescue operations. The best evacuation strategy is determined through a synthetic risk index RI that combines Key Performance Indicators (KPIs) quantifying urban, human, and environmental variables. Since this research goal was tackled through a macroscopic modeling approach, final comparisons are also performed with the microscopic model developed in the previous sections.

Furthermore, outcome innovations, policy for stakeholders, limitations, and future aims are first specifically discussed in each of the previous sections, and finally in an organic manner with respect to a broader horizon that includes all the topics covered in the thesis in the conclusions section (§10). The final sections §11 is dedicated to appendices with supplementary material such as tables for symbols and abbreviations, calculation details, and specific setups used in the simulators.

1.4 Previous accomplishments

Some parts of this Ph.D. thesis were published in previous papers and publications. They mainly are:

- Quagliarini E., Pace G., **Romano G.**, “Murature storiche nella Regione Marche: specificità costruttive e caratterizzazione meccanica sperimentale”, 2023, Edicom Edizioni. ISBN 979-12-81229-04-4 2023
 - Section §3.2 (*data collection and final database*)
 - Section §4 (*results*)
- Bernardini G., **Romano G.**, Soldini L., and Quagliarini E., “How urban layout and pedestrian evacuation behaviours can influence flood risk assessment in riverine historic built environments”, *Sustainable Cities and Society*, vol. 70, 2021, <https://doi.org/10.1016/j.scs.2021.102876>
 - Section §3.3 (*typological scenarios definition*)
 - Section §3.5.4 (*simulations, KPIs, and RIs*)
 - Section §3.6 (*hazard modeling*)
 - Section §8 (*results*)
- Quagliarini E., Bernardini G., **Romano G.**, and D'Orazio M., “Simplified flood evacuation simulation in outdoor built environments. Preliminary comparison between setup-based generic software and custom simulator”, *Sustainable Cities and Society*, vol. 81, 2022, <https://doi.org/10.1016/j.scs.2022.103848>
 - Section §3.5.3 (*setup criteria and simulation outputs*)
 - Section §7 (*results*)
- Quagliarini E., Bernardini G., **Romano G.**, and D'Orazio M., “Users’ Vulnerability and Exposure in Public Open Spaces (Squares): A Novel Way for Accounting Them in Multi-Risk Scenarios”, *Cities*, vol. 133, 2022, <https://doi.org/10.1016/j.cities.2022.104160>
 - Section §3.4 (*data sources and collection, statistical analyses*)
 - Section §5 (*results*)
- Quagliarini E., **Romano G.**, and Bernardini G., “Investigating Pedestrian Behavioral Patterns Under Different Floodwater Conditions: A Video Analysis on Real Flood Evacuations”, *Safety Science*, vol. 161, 2023, <https://doi.org/10.1016/j.ssci.2023.106083>
 - Section §3.5.2 (*data collection and statistical analyses*)
 - Section §6 (*results*)
- **Romano G.**, Marinelli F., Bernardini G., Quagliarini E. (2024), “Optimizing Shelters and Evacuation Paths Against Flood in Historic Urban Built Environments”. In: Endo Y., Hanazato T. (eds) *Structural Analysis of Historical Constructions*. SAHC 2023, 12th -15th Sept 2023, Kyoto (JPN), RILEM Bookseries, vol. 46. Springer Cham. https://doi.org/10.1007/978-3-031-39450-8_100
 - Section §3.5.5 (*Integer Linear Programming*)
 - Section §9 (*results*)

2. Evaluating disaster risk in Historic City Centers: a state of the art

Risk assessment issues are addressed in literature according to multiple approaches depending on the scale of analysis, the representation methodologies, the key factors analyzed, and the tools proposed to solve these issues. This section discusses how these issues are addressed in the current state of the art in the context of HCCs, with a particular focus on the built environment and its users, so as to point out actual needs and research trends, therefore the general outlines followed in this thesis work.

2.1 Disaster risk elements' introduction and definitions

According to general definitions provided in recent literature [39], [40], *disaster risk* can be expressed as the likelihood of loss of life, injury or destruction, and damage from a disaster in a given period of time, and is widely recognized as the consequence of the interaction between severity and frequency of a hazard and the characteristics that make people and places vulnerable and exposed. In the following subsections, hazard (§2.1.1), vulnerability (§2.1.2), and exposure (§2.1.3) are discussed as pillars for defining the overall disaster risk, as shown in .

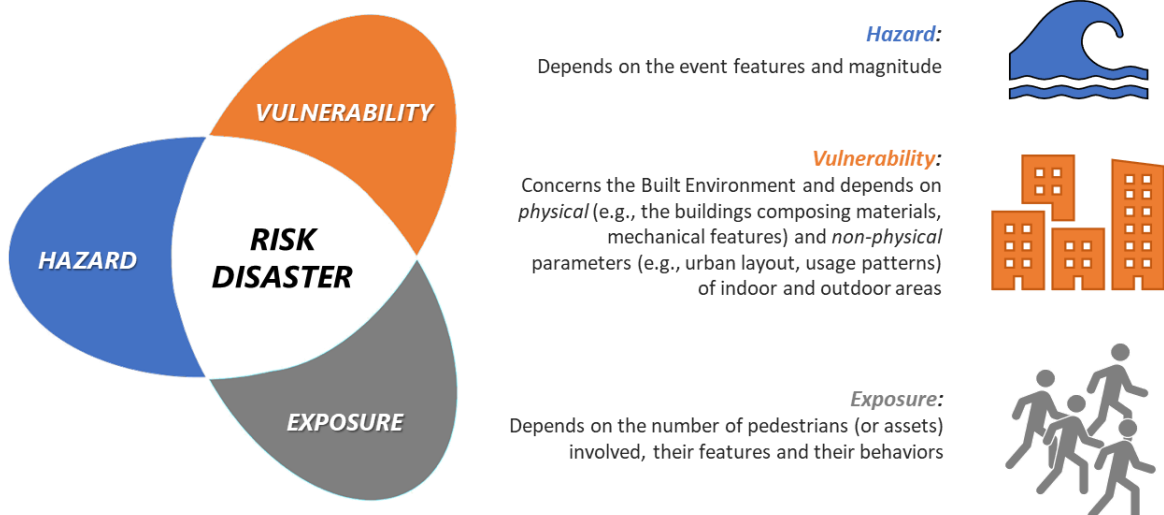


Figure 2: Graphical illustration of the three pillars defining the disaster risk: vulnerability, exposure, and hazard.

2.1.1 Hazard

A *hazard* is a process, phenomenon, or human activity that may cause casualties, health impacts, damages to the built environment, social and economic disruption, or environmental degradation. Hazards can arise from natural, anthropogenic, or socio-natural sources. Natural hazards are primarily linked to natural processes and phenomena, while anthropogenic hazards are induced by human activities (conflicts or social instability are not included, though). Socio-natural hazards result from a blend of natural and human factors, such as environmental degradation and climate change. Hazards may stem from a single source, occur sequentially, or be combined in their origin and effects. They are defined by its location, intensity, frequency, and probability [39], [40].

Hazards, outlined in the Sendai Framework for Disaster Risk Reduction, include geological, hydrometeorological, environmental, technological, and biological factors. *Geological hazards* stem

from internal earth processes, including earthquakes, volcanic activity, and associated phenomena like mass movements and landslides. *Hydrometeorological* hazards arise from atmospheric, hydrological, or oceanographic conditions, including tropical cyclones, floods, droughts, heat waves, and storm surges. *Environmental* hazards encompass chemical, natural, and biological threats, arising from environmental degradation or pollution in air, water, and soil. Some factors, like soil degradation, deforestation, and loss of biodiversity, may be termed hazard drivers rather than hazards. *Technological* hazards result from industrial conditions, dangerous procedures, infrastructure failures, or specific human activities, such as industrial pollution, nuclear radiation, toxic waste, dam failures, and transport accidents. They may also arise directly from the impacts of natural hazard events. Finally, *multi-hazard* include multiple overlap, cascade, or accumulate major events provoking potential interrelated effects [39], [40].

Another classification can be introduced according to the duration of the event. SLow Onset Disasters (SLODs) are defined as hazards emerging gradually over time and can be associated with pollution, heat waves, desertification, and pandemics. On the other hand, Sudden Onset Disasters (SUODs) are triggered by hazardous events that emerge quickly or unexpectedly, and can be associated with earthquakes, terrorist acts, floods, and fires [62]).

In general, hazard events are characterized by different features, the most important ones are their intensity or severity, speed of onset, duration, and the area they cover. Hazards happen at different intensities and timespan (also known as temporal scales), to which scientists associate the concept of return period in terms of probabilities. The longer the return period, the less frequent and more severe the hazard. Difficult challenges arise when multiple hazards coexist, thus highlighting the crucial need to assess risks associated with people and assets according to the full range of hazards [39], [40].

2.1.2 Vulnerability

Vulnerability embraces physical, social, and environmental features that increase the susceptibility of an individual, a community, assets, or systems to the impact of hazards [39], [40], [62], and includes:

- A. The vulnerability due to the built environment, which depends on physical (e.g., the buildings composing materials, mechanical features, design and construction techniques [63]–[66]) and non-physical parameters (e.g., urban layout and intended use of structures, infrastructures, and open spaces [67], [68]) of indoor and outdoor areas that can affect the presence of users;
- B. the vulnerability due to the users, which depends on their physical and social features (e.g., age, gender, disabilities, motion capabilities, culture, socioeconomic status, disaster preparedness, familiarity with the areas) that can alter users' behaviors in terms of utilization and perception of the surrounding environments [69]–[73].

Including vulnerability assessment in disaster risk evaluation means that the overall risk not only depends on the hazard and the number of users/assets exposed, but it reflects their susceptibility to suffer losses and damages. The varying levels of vulnerability (and exposure) elucidate why certain non-extreme hazards can result in severe impacts and disasters, while some extreme events may not. Obviously, the vulnerability evaluation is strictly related to the disaster risk condition to be evaluated (e.g., the surface permeability may be important for flooding risk but not for other risks) [39], [40].

2.1.3 Exposure

Exposure concerns the situation of people, infrastructures, and other tangible human assets located in hazard-prone areas, combined with their capacity to cope with specific vulnerabilities to particular hazards [62], [68]. Many common measures of exposure include the number of users and/or assets in a given area [74], [75]. Population growth, urbanization, and economic development imply people and assets concentration in risk-prone areas, thus exposure changes over time and space [2], [76].

Exposure-related issues on historic/artistic heritage, services, and economic activities are usually considered only with respect to disastrous events that can provoke destruction or damage, such as earthquakes or bombing attacks [77]. Anyway, factors like the density of users over space and time (known also as “temporalities”) [18], [78]–[80], their behaviors and preparedness during emergency and evacuation procedures, the presence of special buildings, sensitive targets, or high-density areas [81]–[84] could significantly affect the users’ safety, health, and wellbeing [67]: a) negatively, since they can be exposed to SLODs [85]–[87] and/or SUODs [88]–[90]; or b) positively, in case they are placed in areas characterized by features or solutions that can mitigate risks, such as green areas, wide square in compact urban layout, built environments implementing structural and non-structural risk reduction solutions [91]–[93].

2.2 Evaluating disaster risk for HCCs and their users according to different scales of analysis

Gathering data on hazard, exposure, and vulnerability improves risk assessment accuracy, leading to more effective prevention, preparation, and financial management measures. A comprehensive disaster risk assessment considers various potential events, their causes, and uncertainties. Therefore, historical analyses can be useful to evaluate (and estimate future trends in) the frequency, severity, and patterns of disasters according to multiple standpoints and types of data. For instance, in areas prone to earthquakes and/or floods, databases collecting modes of failure of buildings and infrastructures could be used as benchmarks for evaluating the effectiveness of existing measures, then to refine regulations and implement updated building codes, zoning laws, and infrastructure improvements [94]–[97]. Similarly, quantitative and qualitative insights on how inhabitants populate, move, and behave in the built environment (both in risky and normal fruition conditions [57]–[60], [83]) can be useful to refine modern tools and techniques, such as hazard modeling and simulators to predict outcomes and probabilities of different events [22], [57], [98], [99].

Such types of analyses and data collection activities can be addressed according to approaches focusing on different levels of detail and therefore providing different perspectives. Some of the factors that can influence the choice of the scale of analysis are: the extension of the areas of interest, the simulation model accuracy, the computational efforts required, the level of complexity suitable for the final users (e.g., simple tools can ease and speed up analyses from non-expert technicians of municipalities), the application to real-world case studies as well as the utilization of idealized case studies to guarantee extensibility and replicability of the results. The following subsections will focus on the different scales of assessment and representation for HCCs and their users.

2.2.1 Different scales for HCCs assessment and representation

There are different approaches for risk assessment in HCC depending on its complexity and extension. Accordingly, different scales of analyses can be distinguished depending on the level of

detail for the evaluation of the HCC features [100], [101], and the scale adopted is able to influence the effects of single and multiple hazards on the physical elements as well as on the hosted users [10], [102], [103]. Within this context, HCC elements and layout can be evaluated through:

- **Microscale analyses** (street level), that examine individual streets and buildings at an extremely fine-grained level [100], [102];
- **Mesoscale analyses** (urban block and neighborhood level), that investigate the composition and layout of building blocks (including their uses and typologies), land use patterns, and open spaces (e.g., squares and streets) [10], [103], [104];
- **Macroscale analyses** (citywide level), that evaluate the overall extension of the HCC at a broader scale, considering its boundary, connectivity with surrounding areas, and regional context [100], [102], [105].

Fine-grained approaches (i.e., at the microscale) allow in-depth analysis and are particularly useful for providing very accurate details about single urban elements, but the resulting findings may lack broader context and generalize patterns and dynamics. On the other hand, low-grained approaches (i.e., at macroscale) consider broader patterns and trends as they look at the city/region as a whole, but they might overlook specific details and features that can be relevant for assessing resilience and developing tailored risk reduction strategies [106]–[109].

Between them, the mesoscale approach allows for achieving an adequate granular and context-specific understanding of the built environment and all of its features (structural, architectural, geometric, typological, etc.). In addition to this, considering also the relationships between the built environment and its users, this is the scale where a wide variety of daily activities (both under normal and/or emergency conditions) that could have implications for the resilience of HCCs take place. Finally, it allows discussing interactions between users and the surrounding built environment in a sufficiently detailed manner [10], [103], [104], [110]–[112].

In particular, public open spaces (POSs) like squares and streets play a pivotal role from a user-related perspective, since their use affects risks for users in a dynamic manner [18]. They are characterized by morpho-typological and construction factors based on the interaction between outdoor and indoor spaces, enclosing building facades, and hosted elements and infrastructure, attracting users who move and engage in individual and collective activities. POSs are particularly relevant and complex for emergency situations, as occupants interact with physical resources (e.g., buildings, emergency-induced damage, layout), social resources (e.g., nearby individuals), and management resources (e.g., rescuers, emergency and evacuation plans) to restore an adequate level of safety. This applies to consequences of both SLODs and SUODs, as well as multi-risk conditions due to overlapping disasters and risk-aggravating conditions such as overcrowding (e.g., during large events). In particular, SLODs can vary the presence of users indoors and outdoors, thus also affecting the attractiveness of specific parts of the POS depending on their features [9], [113], [114]. On the other hand, SUODs could add critical conditions to users in POSs and especially in the squares, depending on the specificities of the emergency response. For instance, in terrorist acts affecting the square, users should evacuate the POS to distance themselves from the attack source, while, in earthquakes, users could gather in the square to minimize interferences with debris while waiting for rescuers' arrival, with respect to the rest of the compact historical urban fabric [115]. Considering the general resilience challenges, the specificities of the POSs, and their rule towards users before and during an emergency, the assessment and reduction of risk for users in the POSs is then a

fundamental goal and should be carried on by using a sustainable and holistic approach [18], [116]–[118].

2.2.2 *Different scales for users' assessment and representation*

Different strategies can be applied to reduce disaster risk [119], [120]. Some of them require permanent or long-term solutions, such as physical constructions or nature-based measures that provide continuous protection against hazards up to a given return period. Anyway, the implementation of these structural solutions could be difficult in existing HCCs because of economic factors, coordination among stakeholders, high application impact with respect to the HCCs features, as well as their effects could be limited especially in case of extreme events [37], [121]. Non-structural solutions relating to evacuation management and planning could be implemented in the HCC to support structural measures in a flexible and effective manner, thus allowing people to reach areas where they can wait for rescuers' arrival in safe conditions [120], [122]–[124]. This is particularly true in case of extreme events and/or sudden disasters that could overcome existing measures, thus preventing pedestrians from adopting the right evacuation strategy due to difficult interactions with surrounding environments deeply modified [22].

Pedestrian dynamics and evacuation planning against natural disasters are commonly addressed through different scale approaches, too [108].

Macroscopic approaches are simple and fast to simulate thanks to low computational costs, as they represent pedestrians as a whole with unique features [125]. They are mainly based on optimization problems and are particularly suitable for scenarios characterized by [109]: wide application scales, complex geometries (e.g., street networks), low-density conditions, monodirectional flows, and few interactions between pedestrians. Prescriptive models are widely exploited to compute optimized evacuation plans through routing algorithms on graphs [125], [126]. Between them, mathematical programming and graph theory emerge as the main prescriptive methodologies for evacuation planning and disaster management [127], with models focused on evacuation paths [125] or on shelter location [128]. Classic approaches rely on the evaluation of the shortest or quickest path on static networks [129], although there are still uncertainties (especially at the urban scale) about the best evacuation strategy from the pedestrian perspective (e.g., if the shortest, the quickest, or the less effortful path).

On the other hand, *microscopic* approaches represent each pedestrian with its own, individual features (e.g., walking speed, decision-making criteria, interactions with other pedestrians), and are capable of reproducing local phenomena and velocity-density relationships, bottlenecks, and slow-down crowd effects [108]. Microscopic approaches are widely adopted to simulate emergency evacuation according to different modeling methodologies, even though their computational cost is noticeably higher. Typical microscopic approaches are cellular automata, agent-based models, and force-based models [124], [130]–[136].

- *Cellular automata* (CA) [137]–[139] are a computational model that consists of a grid of cells that can be one-dimensional, two-dimensional, or even higher-dimensional. Each cell has a finite number of states, determined by its current state and the states of its neighboring cells, and evolves through discrete time steps updated based on the rules of the system. Applications of cellular automata include various field of application, such as physics, biology, computer science, and urban planning.

- *Agent-based models* (ABMs) [131], [135], [140]–[142] are computational models used to simulate complex systems by representing individual entities with individual characteristics, behaviors, and decision-making capabilities (known as agents), and their behaviors and interactions within other agents and the surrounding environment. Such environments can be physical space, as well as abstract (i.e., focusing on conceptual interactions). The rules governing agents-agents and agent-environment interactions are defined within the model. In particular, ABMs are useful to describe complex behavior at the macroscopic level from simple rules at the microscopic level. Randomness or stochastic elements are often introduced in ABMs to account for uncertainties and variations in agent behaviors or environmental conditions.
- *Social force models* (SFMs) [143]–[146] are mathematical and computational models used to simulate the movement of individuals within a crowd or social setting. The fundamental idea is to represent the social forces acting on individuals to predict collective behaviors and quantify motivations to perform certain actions. Such models represent individuals (agents) as entities with specific characteristics (i.e., position, velocity, and desired destination) moving within a shared environment. The interaction between agents and the environment in which they move is then described through social forces classified into various types, i.e., repulsive forces to avoid collisions with obstacles and other agents, and attractive forces towards a desired destination. Agents respond to obstacles and other agents in their vicinity by adjusting their movements to avoid collisions. As a result, each agent has a desired velocity, which is influenced by its goal or destination, and represents the speed and direction it would like to move towards. Some SFMs introduce stochastic elements to account for inherent uncertainties and variations in human behavior over time and space, thus leading to more realistic simulations. Most common SFM applications include evacuation planning (simulating crowd behavior during emergency evacuations to optimize escape routes and strategies), pedestrian dynamics (analyzing crowd movement in public spaces), and urban planning (studying the impact of architectural design and infrastructure on pedestrian flow in urban areas). One of the most famous examples of SFMs is the one proposed by Dirk Helbing and Peter Molnar, which has been influential in the study of pedestrian dynamics and crowd behavior. These models contribute valuable insights into designing spaces and systems that can accommodate the movement of individuals in a safe and efficient manner.

In view of this consideration, microscale approaches are crucial for representing pedestrian dynamics in HCCs for several reasons. Firstly, they provide a detailed understanding of the urban fabric, human-scale design, social aspects, and cultural context, enabling planners and designers to create interventions that enhance both the functionality and the unique character of these historic urban spaces. In particular, microscale approaches allow considering detailed examination and representation of users' interactions with single urban elements and specific features like complex, narrow, and irregular street layouts, and a mix of open spaces and buildings which can influence the users' behaviors and use of indoor and outdoor spaces. In fact, HCC design is often tailored to the human scale, with a focus on walking as a primary mode of transportation. Therefore, microscale analyses capture the interactions between pedestrians and their immediate surroundings, including factors like the street width, the sidewalk design, and the position of urban furniture, allowing including also assessments of accessibility and inclusivity for individuals with different mobility capabilities (i.e., considering the presence of stairs, ramps, and other urban features). HCCs are also

characterized by a wide presence of architectural heritage and preservation requirements, thus microscale approaches can be useful for optimizing urban planning and evaluating interventions considering also the preservation of cultural heritage, as well as identifying areas of congestion and the impact of specific design elements on pedestrian flow. Finally, HCCs often host events, festivals, and markets, thus microscale analysis aids in planning and managing these events by understanding how crowds move and interact within the confined spaces of HCCs.

2.3 Evaluation of recurring risk conditions: from real-world HCCs to typological scenarios

Understanding the risk scenario to which HCCs and their POSs are exposed becomes of paramount importance for assessing the actual risk level for hosted users and designing effective mitigation solutions by public authorities. Most common analyses on risk assessment typically involve real-world scenarios considering actual or possible conditions and features (e.g., building state of conservation, population characteristics, occurrence of a disaster event with a given time of return). Clearly, this type of assessment provides very accurate insights according to the actual conditions and complexities of the studied area, thus of the current vulnerabilities, exposures, hazards, and the following risks, although they require detailed data and information, thus more time and resources [1], [21], [43], [147], [148].

On the other hand, typological (or parametric or idealized) scenarios involve creating simplified, generalized models based on recurring features and situations of relevant case studies. As a result, this type of representation is useful for understanding general trends and patterns thanks to simplified and fast analyses. The creation of risk and multi-risk typological scenarios is based on two aspects: (A) defining recurring conditions that characterize a certain type of POS/HCC/built environment; and (B) their rapid organization for scenario creation [4], [29], [52], [149]–[151].

Recent expedited methods have introduced the use of surveys to collect data to define risk scenarios. For instance, vulnerability and exposure factors are organized thanks to experimental studies and analyses of real events for different types of disasters [11], [54]–[56], [152], [153]. Previous studies have also suggested the possibility of organizing types of built environments thanks to an "idealization" proposed through a limited set of main parameters considering relevant, recurring, and characterizing factors and conditions, and a relative range of variation. The parameters are characterized by analyzing significant real cases, statistically relevant. In terms of single-risk and multi-risk, the main advantage of using typologies for classifying the built environment is the ability to quickly associate a real scenario with an idealized one, whose general safety and resilience trends can be analyzed through simulation approaches [17], [45], [154]. This method has been used, for example, in fire safety practice to analyze prevalent risk conditions for users hosted in relation to the structure layout [155], [156]. Following estimation under idealized conditions because of typological characteristics, it is then possible to refine the risk analysis under the conditions of the actual object of investigation.

However, there is currently a lack of organized methodologies, especially expedited ones, to support designers and local authorities in the organic assessment and representation of possible scenarios to reduce the complexity of the analyses to be developed. Furthermore, while some research efforts have been directed towards typological classifications of morphological, geometric, and construction

aspects, those related to users' vulnerability and exposure seem rather limited, especially considering their spatiotemporal variation and interconnection during emergencies in HCC-POSs [157].

In view of the above, comprehensive risk assessments should aim at combining real-world scenarios, (leveraging their detailed understanding of existing risks) with typological scenarios (which help identify common risk factors and trends applicable to different situations), contributing to the development of faster and more sustainable risk mitigation strategies. Finally, integrating insights from both real-world and typological assessments could help decision-makers develop a more holistic understanding of the risks of a given study area and formulate targeted risk-reduction strategies and tools.

2.4 Key Performance Indicators to quantify the risk

Holistic risk analyses in the built environment can be assessed through various tools and methods suitable for considering all the different nuances of the approaches introduced in the previous sections (i.e., key metrics to measure hazard, vulnerability, and exposure, differences due to the scale of analysis, application to real-world or typological scenarios). However, another fundamental aspect to be guaranteed in addition to the accuracy of the analyses concerns the timeliness and relative simplicity of application since these analyses are often conducted by local authorities non-specialized in the use of specific software and procedures. Easing and speeding up risk analysis for low-trained technicians and local municipalities is then crucial for efficient and timely decision-making in disaster-prone areas.

Among the most relevant tools and methodologies to cope with these needs, it is worth mentioning the development and the use of Key Performance Indicators (KPIs) and their combination into Risk Indexes (RIs) to jointly quantify metrics and parameters measuring *hazard* (e.g., magnitude, frequency, probability), *vulnerability* (e.g., physical vulnerability of structures, social vulnerability of communities), and *exposure* (spatiotemporal distribution of assets, population density, presence of critical structures and infrastructure) factors and their impact on the HCC [64], [158]. Most common KPIs and RIs applications involve measurements of overall risk for HCCs and their users, cost-benefit analysis, social and/or environmental impact, community engagement and awareness, and adaptive capacity. Furthermore, they can be also combined and integrated to boost more refined assessment tools, such as [159]–[164]: (1) risk maps and (2) evacuation plans, organized on the basis of the risk levels, as they can offer a visual overview of the risk distribution across specific areas through quick and easy color-coded identification, and can be useful also to address emergency response and resource allocation; (3) descriptors (i.e., input data) to derive recurring conditions for typological scenarios and perform quantitative risk assessments, e.g., to populate simulation-based case studies and evaluate the risk depending on specific disaster conditions; (4) metrics to compare simulation-based output, e.g., from different scenarios and/or simulators to investigate potential outcomes under various conditions and understand weaknesses and strengths; (5) community surveys and engagement, by involving local community and/or specific practitioners in data collection through surveys or reports that enhance not only gathering valuable information, but also community resilience and awareness. Furthermore, KPIs and RIs can be used to depict specific conditions when they are applied to single case studies, as well as to derive typological conditions (i.e., statistically recurring) when applied to a sample of case studies in the same relevant context.

Therefore, KPIs play a crucial role in providing a quantitative basis for evaluating and managing disaster risk, and their regular monitoring and analysis contribute to informed decision-making by stakeholders and develop strategies to enhance overall resilience and safety. Furthermore, by employing these accessible tools, also low-trained technicians can contribute to quick preliminary risk assessment in the built environment, helping prioritize interventions and allocate resources effectively and rapidly. In this sense, open-access and standardized data sources are useful to speed up evaluations, provide timely results, and improve common operational framework replicability. In fact, thanks to their clarity, simplified tools and visual methods also improve communication between different municipalities and communities, although they can be easily adapted to local context and their specific features.

3. Phases, methods, and materials

3.1 Thesis framework

The conceptual framework shown in Figure 3 summarizes the organization of the next sections of the thesis, highlighting for each of them:

- The disaster risk factors considered (i.e., vulnerability, exposure, and hazard);
- The conditions underlying assessments (i.e., assuming generic pre-emergency conditions or specific emergency conditions, in this case flood);
- the modeling scale adopted (i.e., microscale or mesoscale for the built environment, and microscale or macroscale for the users)
- the following tools and methodologies obtained distinguished based on the phase of the disaster risk addressed (i.e., mitigation or preparation).

Built Environment (BE) for this purpose generically indicates Public Open Spaces (i.e., streets, squares, and their combination) referring to both real-world and typological Historic City Centers scenarios.

	<i>PRE-EMERGENCY CONDITIONS</i>	<i>SPECIFIC EMERGENCY CONDITIONS: FLOODS</i>
PHYSICAL VULNERABILITY of the Built Environment	Section §3.2 BE: microscale	Section §3.3 BE: mesoscale
EXPOSURE AND VULNERABILITY of Users & Built Environment	Section §3.4 BE: mesoscale Users: mesoscale	Section §3.5 BE: micro & meso Users: micro & macro
HAZARD		Section §3.6 BE: micro & meso
METHODOLOGIES AND TOOLS FOR DISASTER RISK REDUCTION	Sections §4 and §5: MITIGATION PHASE IN PRE-EMERGENCY CONDITIONS	Sections from §6 to §9: PREPARATION PHASE AGAINST FLOOD

Figure 3: Conceptual framework illustrating the thesis contents and organization.

3.2 Physical vulnerability at the microscale: masonry walls classification and mechanical characterization

3.2.1 Introduction and motivation

One of the most important issues in the assessment of physical vulnerability for HCCSs concerns the mechanical characterization of existing masonry buildings with appropriate knowledge of the construction typologies and techniques. In Italy, masonry buildings with residential use are frequent: 57% of building heritage is composed of masonry buildings, of which about 20% are in a bad state of conservation according to ISTAT², and their structural retrofitting and preservation represent a major task from a cultural, social, economic, and environmental point of view.

Several masonry typologies were used for construction. Residential masonry buildings' techniques usually involve the use of solid clay bricks and/or stones of different nature, sizes, and processing (e.g.: from rubble to perfect squared stones), assembled with clay or lime mortar, or less frequently, dry-stone constructions. Instead, religious buildings, monuments, and bridges are often constructed with regular squared stone blocks and mortar joints, thus contributing to a large scattering of the mechanical (strength and deformability) parameters with respect to the previous ones [165], [166].

However, even though these issues have been largely investigated by practitioners and insiders, there are still uncertainties about the mechanical characterization of masonry structures, especially in seismic-prone areas like Italy, where the use of different materials, elements, and textures is certainly influenced by ancient knowledge and local materials' availability [167]–[170]. As a consequence, the numerous earthquakes that have recently affected different Italian areas (Friuli 1976, Irpinia 1980, Umbria-Marche 1996–1997, Molise 2002, L'Aquila 2009, Emilia-Romagna 2012, and Central Italy 2016–2017) produced a huge number of damages, collapses, and victims that pointed out how proper and effective interventions cannot be separated from an adequate knowledge of historical buildings through microscale analysis of masonry walls.

To this end, the Italian National Standards (INS, i.e., NTC18 and CSLLPP n.7/2019 [171], [172]) highlight the pivotal role of experimental campaigns through in-situ tests and surveys to reach an adequate “Level of Knowledge”. However, due to executive, economic, and conservation issues, their execution can often be difficult, especially for buildings of historical and cultural significance [165], [173], [174]. Therefore, when experimental campaigns cannot be performed, the INS provides a classification with the most recurrent masonry typologies in the national territory, together with reference values of strength and deformability parameters related to their “Conditions” and “Strengthening Interventions” (Tables C8.5.I and C8.5.II CSLLPP n.7/2019 [172]). However, due to the great variability of techniques and materials available in the national territory, this classification cannot include all the masonry typologies, so the INS itself invites all the Italian Regions to autonomously define “homogeneous areas” in order to consider local specificities [171], [172] whose knowledge and identification would be fundamental to improve professional contribution and community safety.

In view of the above, this section of the thesis elaborates a new **microscale approach** to define **physical vulnerability** in HCCs by considering the mechanical features of its typical masonries [61].

² http://dati-censimentopopolazione.istat.it/Index.aspx?DataSetCode=DICA_EDIFICII (last access: 12/07/2023)

In particular, the proposed case study concerns the context of the Marche Region, for which an abacus of recurring walls has been realized starting from a data collection that involved local practitioners through surveys including tests and photoshoots.

3.2.2 Data collection and organization

The “*experimental*” data collection and organization have been performed through collaborations with local professionals and licensed laboratories, which shared the results of tests carried out for work purposes through a rapid survey oriented towards the classification and characterization of local masonry walls. In particular, the survey is organized into 4 parts (see Table 1), each of which contains the following information provided directly by professionals and laboratories:

- A. *Type of test*, including standard reference and physical quantities measured;
- B. *Masonry wall classification*, according to the classification proposed by the INS (Table C8.5.I [172], resumed in Table 45 in Section §11.1.1), otherwise, if not included in the list, through a short description of the case study (e.g., stone-and-brick mixed masonry, hollow brick masonry with holes > 40%). Similarly, following the prescription of Table C8.5.II [172] (resumed in Table 46 in Section §11.1.1), the possibility of indicating the current “Conditions” and any “Strengthening interventions” was also included to evaluate the impact of masonry in good conditions of conservation;
- C. *Mechanical parameters measured*, according to the indication provided by the INS;
- D. *Photographic material*.

PART A							
Type of test (e.g., double flat-jack, diagonal compression test, shove test...)						<i>Select an option</i>	
Reference standards (e.g., UNI EN ISO, ASTM, RILEM...)						<i>Select an option</i>	
Mechanical parameters measured (i.e., f , E , τ , G)						<i>Select an option</i>	
PART B							
City of the masonry building		<i>e.g., ROME, ITALY</i>					
Sample ID	Masonry typology ⁽¹⁾	Conditions ⁽²⁾			Strengthening interventions ⁽²⁾		
		Good mortar	Stringcourses or edging	Transversal connections	Injections	Jacketing	Reinforced joints sealing
	<i>Select an option</i>	<input type="checkbox"/>	<input type="checkbox"/>	<input type="checkbox"/>	<input type="checkbox"/>	<input type="checkbox"/>	<input type="checkbox"/>
	<i>Select an option</i>	<input type="checkbox"/>	<input type="checkbox"/>	<input type="checkbox"/>	<input type="checkbox"/>	<input type="checkbox"/>	<input type="checkbox"/>
	<i>Select an option</i>	<input type="checkbox"/>	<input type="checkbox"/>	<input type="checkbox"/>	<input type="checkbox"/>	<input type="checkbox"/>	<input type="checkbox"/>
PART C							
Sample ID	f (N/mm²) ⁽¹⁾	E (N/mm²) ⁽¹⁾	τ_0 (N/mm²) ⁽¹⁾	f_{v0} (N/mm²) ⁽¹⁾	G (N/mm²) ⁽¹⁾		
⁽¹⁾ from Tab C.8.5.I CSLLPP 7/2019							
⁽²⁾ from Tab C.8.5.II CSLLPP 7/2019							
PART D							
<i>please insert masonry images here</i>							

Table 1: survey form for the data collection. Mechanical parameters symbology: f = compressive strength; E = elastic modulus, τ_0 = shear strength (from diagonal compression, to be used for irregular masonry), f_{v0} = shear strength (frictional strength at unit-mortar interface without compression, to be used for regular and irregular masonry), G = shear modulus.

Alongside the “experimental” data, “literature” data were also considered in order to provide an even more complete overview. In particular, previous findings from similar relevant studies were collected through the Scopus search engine³ to include:

³ <https://www.scopus.com/search/form.uri> (Last access: 23/12/2023)

- Measurements on the same typologies retrieved in the “experimental” database, including case studies in the Italian national context to provide comparisons also with case studies outside of the Region. Examples of keywords for the search are: “Italian masonry”, “masonry buildings in Italy”;
- Measurements carried out through the same standards (i.e., double jacks carried out according to the ASTM C1197 standard [175], in situ diagonal compression tests carried out according to the ASTM E519 standard [176], shove tests carried out according to the ASTM C1531 standard [177]). Examples of keywords for the search are: “in-situ tests”, “(double) flat-jack test”, “diagonal compression test”, “brick masonry”, “stone masonry”, “tuff masonry”;
- Measurements performed on masonry typologies recognized as local specificities⁴, but still not included in the INS so as to provide first insight also with other country regulations. Examples of keywords for the search are: “(rammed) earth masonry”, “earth walls”, “earth block masonry”, and “adobe/pisè/cob technique”.

All the data thus collected were analyzed through the Shapiro-Wilk and Kolmogorov-Smirnov tests (depending on the sample size, respectively, for distributions smaller or larger than 50 values [178]), to verify the normality of the samples. Samples are distinguished per masonry typology (and obviously per type of test) both for experimental and literature data. Normal samples are organized through quartile-based analyses [179] and arranged in boxplots (also known as “box and whiskers” diagrams) to ease the identification of ranges for comparison purposes with those of the INS. In particular, the comparisons are discussed by referring to the 1 and 3 quartiles of the distributions (the sides of the "box") taken as extreme values of the ranges (min-max). Outliers are calculated through the InterQuartile Range method (limit: 1.5 IQR) [180]. On the other hand, non-normal samples are reported in scatter plots showing their maximum, minimum, and average values, while small (i.e., less than 4 values) samples are discussed with reference to the precise values.

It is important to underline how experimental data measured on case studies characterized by a better “Condition” and/or “Strengthening Interventions” are compared with INS ranges duly amplified through the coefficient(s) reported in Table C.8.5.II [172].

Finally, the following KPIs are introduced and discussed:

- The coefficients of variation (relative standard deviations) RSD_{MP} [-], as the ratios between the standard deviations and the mean values of each mechanical parameter⁵, to quantify the dispersion of the data;
- The E/f ratios [-] considering their average values, to be compared with the recommendations of the current INS [171], [172], Eurocode 6 [181];

by considering each masonry typology, the overall average values, and by distinguishing stone masonry samples from brick masonry samples.

⁴ Pursuant to art. 2 of Legislative Decree no. 490 of 29/10/1999, in 2003 the "Regional Superintendency for Cultural Heritage and Activities" of the Marche Region decreed a restriction for monumental interest for Villa Ficana (MC) due to its historical-cultural value.

⁵ Due to the sample sizes, DSR are calculated only for the compressive strength (DSR_f) and the elastic modulus (DSR_E).

3.2.3 Final database composition

The final experimental database for the mechanical characterization of the masonry walls is composed of 425 tests of the following types:

- 406 double flat-jack tests (DFJT) carried out according to the “*Standard Test Method for In Situ Measurement of Masonry Deformability Properties Using the Flatjack Method*” (ASTM C1197, 2020) [175], used to define compressive strength f and elastic modulus E ;
- 4 diagonal compression tests in situ (DCT) carried out according to the “*Standard Test Method for Diagonal Tension (Shear) in Masonry Assemblages*” (ASTM E519, 2015) [182], used to define shear strength τ_0 and shear modulus G ;
- 9 vertical flat-jack tests (VFJT) carried out according to the procedures illustrated in “*A flat jacks method for in situ testing of brick masonry shear characteristics*” (Armanasco A., Foppoli D., 2020) [183], used to define shear strength τ_0 ;
- 4 shove tests (ST) carried out according to the “*Standard Test Methods for In Situ Measurement Of Masonry Mortar Joint Shear*” (ASTM C1531, 2003) [177], used to define shear strength f_{v0} .

The final composition of the experimental database is resumed in Table 2 and Table 3, in which:

- The masonry typologies are organized in line, by distinguishing a) those included in the INS (ID=M_n°) and those not included (ID=MX_n°), and b) their "Conditions" (sc = standard conditions, gm = good mortar, as indicated in Tab. C8.5.II of the INS [172]);
- The number of values composing each sample is organized in columns.

ID	MASONRY TYPOLOGIES	DFJT Tests [175]	
		f sample [n]	E sample [n]
M1 - sc	Disorganized rubble stone	7	7
M2 – sc	Barely cut stone	6	6
M3 – sc	Roughly cut stone masonry with good texture	8	8
M4 – sc	Irregular soft stone masonry (tuff, limestone, etc.)	3	3
M5 – sc	Regular soft stone masonry (tuff, limestone, etc.)	10	10
M6 – sc	Stone blocks squared	12	12
M7 – sc	Solid clay bricks and lime mortar	87	273*
M8 – sc	Clay hollow bricks with cement-based mortar (holes $\leq 40\%$)	4	17*
M8 – gm	Clay hollow bricks with cement-based mortar (holes $\leq 40\%$) – good mortar	33*	33*
MX1 – sc	Stone-and-brick mixed	20*	20*
MX2 – sc	Solid clay bricks with rubble stone fill	3	1
MX3 – sc	Concrete hollow bricks masonry	0	1

Table 2: experimental database sample composition organized by masonry typology and mechanical parameter measured (compressive strength f and elastic modulus E through double flat-jack tests). ID = M indicates masonry typologies included in the INS, and ID = MX indicates non-included typologies. *Non-normal distributions are indicated in italics. DFJT = double flat-jack tests. Masonry typologies translation from Boschi et al. (2018) [165].

ID	MASONRY TYPOLOGIES	τ_0 sample [n]		f_{v0} sample [n]
		<i>DCT</i>	<i>VFJT</i>	<i>ST</i>
M1 - sc	Disorganized rubble stone masonry	-	2	-
M7 - sc	Solid clay bricks and lime mortar	4	4	4
M8 - sc	Clay hollow bricks with cement-based mortar (holes \leq 40%)	-	2	-
MX1 - sc	Stone-and-brick mixed masonry	2	1	-

Table 3: experimental database sample composition organized by masonry typology and mechanical parameter measured (shear strength τ_0 and f_{v0} , distinguished according to the INS failure mode, namely for diagonal compression or for mortar joint failure). Only one shear modulus value (G) has been registered for the masonry typology M7. ID = M indicates masonry typologies included in the INS, and ID = MX indicates non-included typologies. DCT = diagonal compression tests; VFJT = vertical flat-jack tests; ST = shove tests. Masonry typologies translation from Boschi et al. (2018) [165].

More in general, considering the overall number of tests collected⁶, about 80% of the tests (349 out of 425) concern brick wall typologies (common throughout the national territory), of which almost 85% are made of solid clay bricks with lime mortar (296 total tests, ID=M7) and the other 15% in clay hollow bricks with cement-based mortar (53 total tests subdivided on masonry walls in standard conditions and with “good mortar”, ID=M8). The remaining 20% of the overall number of tests collected concern stone masonry (76 tests), of which 66% are on typologies included in the INS (50 tests, ID=from M1 to M6), and the other 34% on mixed masonry still unregulated by the INS (26 tests, ID=from MX1 to MX3). In particular, between them, the stone-and-brick mixed masonry [35] resulted the third most recurrent masonry typology considering the overall number of tests collected. All the tests are performed on unreinforced masonry walls. Figure 4 resumes the current database composition in terms of geographical information about cities and provinces (all the Marche provinces are included), in terms of masonry typology investigated and in terms of types of tests collected.

⁶ Since f and E were not available for all double flat jack tests collected, their sample sizes are different. Total number of f values: 193; total number of E values: 391; total number of double flat jack tests collected: 408. Tests replicated in the same buildings are included in the samples.

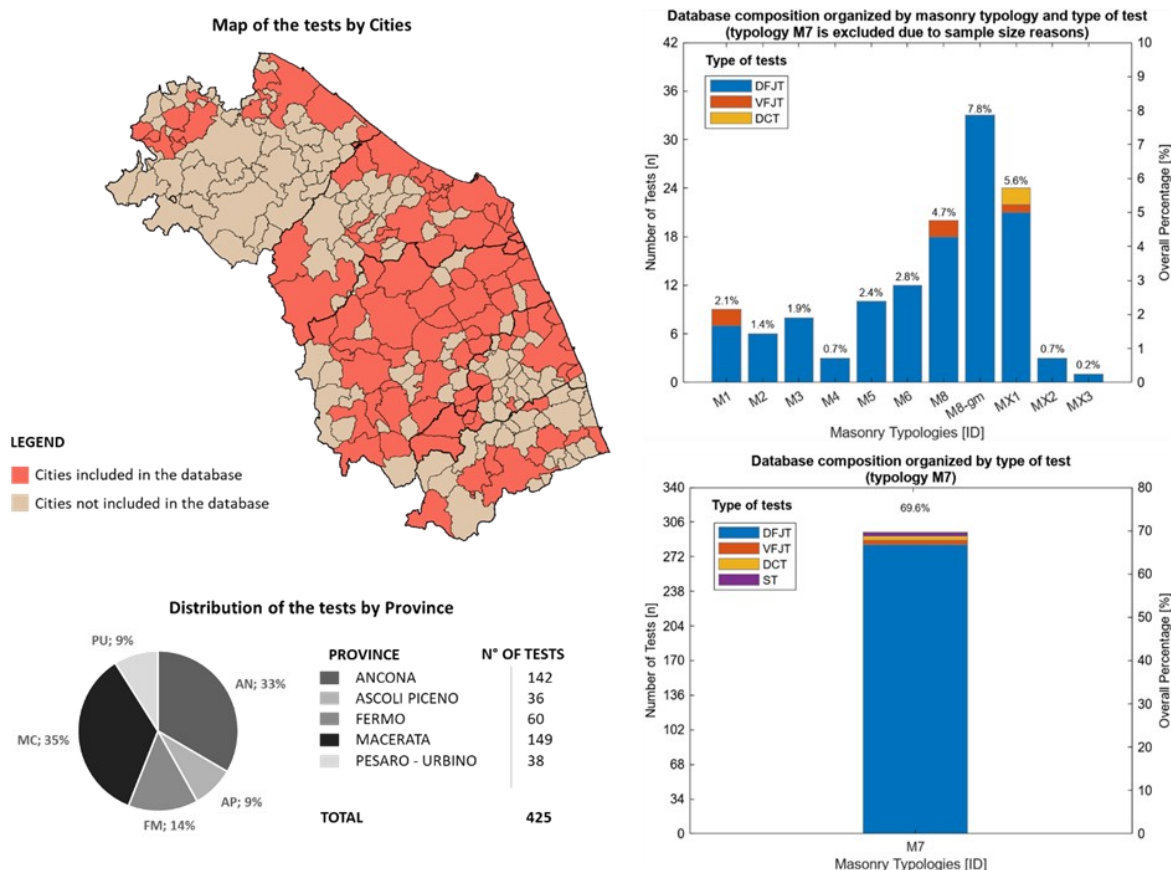


Figure 4: On the right: map of the tests by cities included or not in the database and the following percentage distribution by provinces. On the left: database distribution organized by masonry typology and type of experimental tests. Abbreviations are shown in Table 2 and Table 3. M7 typology (solid clay brick) is shown separately due to the sample size.

Finally, first insights are also provided for what concerns the mechanical characterization of earthen masonries present in the Marche Region (i.e., Adobe, Cob, and Rammed earth, whose features and procedure are resumed in Section §11.1.3, Appendices), which are still unregulated by the INS, even though officially recognized as local specificities (as already introduced in the previous §3.2.2). In particular, due to the absence of tests on local case studies, and the limited availability of similar works in the Italian literature (also given to the restricted presence of this construction technique only in a few other regions, such as Abruzzo, Calabria, Piedmont, and Sardinia), for this typologies the comparisons are made between international scientific literature works (laboratory test on specimens or wallettes done or purpose) and building regulations of countries in which earthen masonry are already regulated.

Besides the construction method of the three aforementioned earthen masonry typologies, Section §11.1.1 also resumes the full list of papers composing the literature database (which mainly includes tests on disorganized rubble stone masonry M1, tuff masonry M4 and M5, brick masonry M7, and earth masonry), together with maps providing indications about the distribution of tests in the regional territory.

3.3 Physical vulnerability at the mesoscale: from real-world case studies to typological scenarios

3.3.1 Introduction and motivation

The urban layout and the geomorphological configuration of outdoor spaces are prominent issues in the evaluation of the physical vulnerability of the HCC at the mesoscale [30], [36], [185]. In particular, many previous studies highlight some of the main factors influencing the physical vulnerability also depending on the type of hazard to be faced, such as [4], [157], [186]: width, length, slope, shape, and direction of streets, squares, and buildings, their distance from the source of danger, the presence of urban furniture, green areas, porches, and special buildings, the paving materials.

As introduced in the previous §2.3, typological scenarios can be exploited to jointly consider the most recurring and/or dangerous characteristics from real-world case studies within one (or more) idealized scenario(s), so as to speed up disaster risk assessment and evaluate common, general solutions against recurring risk factors and trends. Specifically, within the scope of this thesis, they have been used to investigate how **physical vulnerability** at the **mesoscale** influences the flood risk in the context of Italian HCC, due to their impact on hydrodynamic aspects and behaviors of users [21], [37], [187]–[189]. Since the mesoscale analysis involves the composition and layout of building blocks and open spaces (e.g., squares and streets), the case studies and the following typological scenarios concern POSs (as defined in the previous §2.2.1). The criteria adopted to trace the scenarios are introduced in the next subsection. The outcomes of this investigation, pave the way for the development and visualization of several typological scenarios, which will serve as valuable frameworks for performing simulations in the following analyses included in the thesis (see sections §8 and §9).

3.3.2 Data collection and criteria for scenario creation

The first phase for the definition of typological POSs in riverine Italian contexts was the selection of significant case studies to identify the main *vulnerability* modeling inputs. The selected case studies (resumed in Table 4) are characterized by similar conditions in terms of non-complex orography (i.e. essentially flat), presence of a square, paving surface, and proximity to a river with similar features that were recently sources of meaningful floods in the last decades (i.e. since 1960, considering the historic city centers). Figure 5 shows the POS case study of Senigallia (area of “Portici Ercolani”).

City (Province)	Population (updated at 2020)	Recent meaningful floods (last 30 years)	River who crosses the HCC	Name of the area
Albenga (SV)	24042	1994; 2000; 2016	Centa River	Piazza del Popolo
Carrara (MS)	62537	2003; 2012; 2014	Carrione River	Piazza Alberica
Colorno (PR)	9056	2014; 2017	Parma Creek	Piazza Garibaldi
Montevarchi (AR)	24440	1992; 1993	Dogana Creek	Historical City Center
Senigallia (AN)	44616	2011; 2014; 2022	Misa River	Portici Ercolani

Table 4: Case studies selected for the creation of the typological HCC.

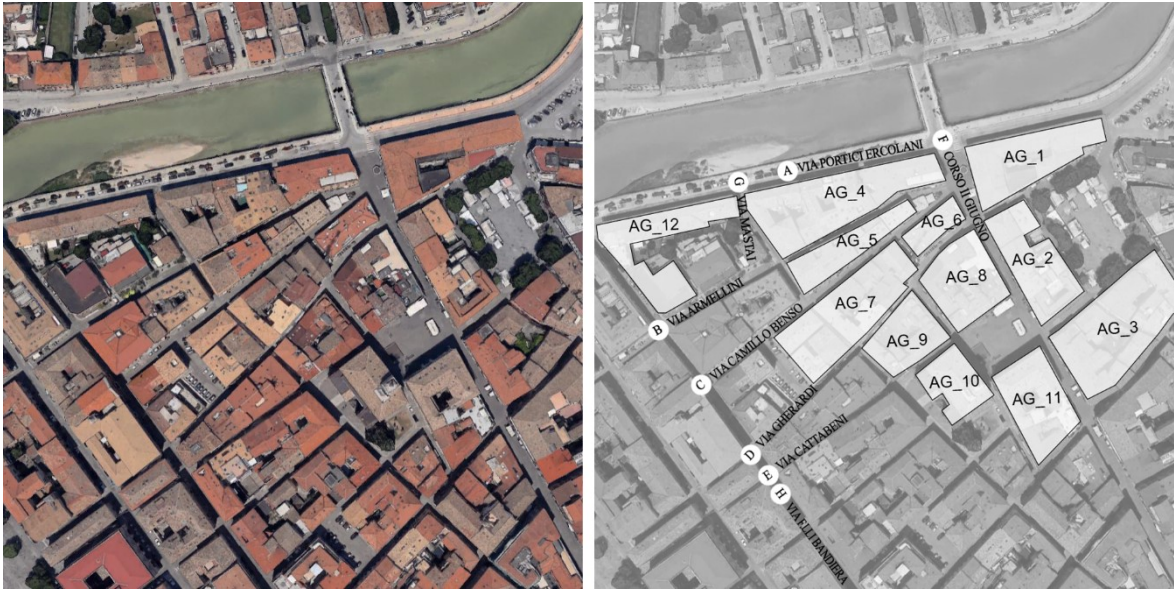


Figure 5: POS "Portici Ercolani" in Senigallia – streets and building blocks included in the case study.

In particular, in order to model the typological POSs, the following input parameters are collected by orthophotos/technical maps from local administrations, and by Google Earth Pro v. 7.3.2⁷ sources [185], [187], [190], [191]:

- a. *streets direction with respect to the river* [°], being parallel (0°) or perpendicular (90°), as shown in Figure 6 for the case study of Senigallia;
- b. *average streets width* [m], to represent them as open channels having a quasi-constant geometry [192]. It was assessed at several points along the development of each street by means of measurements based on orthophotos or regional technical maps (see Figure 6);
- c. *average streets slope* [%], as the ratio between the height difference (from the highest point to the lowest one) and the total street length, according to Google Earth Pro altimetric profiles. Positive slopes indicate that: for parallel streets, upstream spaces are higher than downstream spaces; for perpendicular streets, the altitude increases as you move far from the riverside (see Figure 7);
- d. *dimensions of building blocks*, which are considered non-floodable areas, according to a conservative approach to the simulation of floodwater levels in outdoor spaces. They are assumed in a simplified manner as rectangular shapes with parallel base b [m] and perpendicular length l [m] in relation to the river. Building blocks can have a parallel ($b/l \geq 1$) or perpendicular ($b/l < 1$) trend considering the river (see Figure 8);
- e. *characterization of the squares*, which can ideally behave like detention basins. They are classified in terms of: (1) area⁸ [m²]; (2) position (square adjoining the river; one or more building blocks between the river and the square) and distance of the square barycentre from

⁷ <https://www.google.com/earth/index.html> (data retrieved at: 01/10/2018)

⁸ Porches were considered permeable to the floodwater, since they are characterized by very large openings on the ground floors [212].

the river⁹ [m]; (3) number of streets linked to the square [-]; (4) direction of the major axis of the square considering the river [parallel or perpendicular] (see Figure 9).

Several experimental-based studies performed under different idealized conditions pointed out that the main layout features seem to be: aligned or staggered layout; orientation of buildings with respect to the river flow; the ratio between the building sides length; building length/street width ratio [185], [187], [190], [191]. Therefore, a statistical-based approach is applied to these parameters to define typological HCCs according to a perfect perpendicular street mesh including squared/rectangular paved squares (i.e. with impermeable surfaced) [185], [191], [193]. The streets included in the areas of interest (which are resumed in Section §11.2 - Appendices) have been then divided between streets parallel to the rivers and streets perpendicular to the river. For each parameter, the mode is considered as a reasonable reference value to describe the common experimental-based conditions. Then, the typological HCCs are organized by varying the square presence, positioning, and dimension. In detail, the square dimension is considered as multiple of 1 standard building block.



Figure 6: POS "Portici Ercolani" in Senigallia – streets width and direction data collection.

⁹ The square near Centa River in Albenga is excluded since it represents a specific condition referring to different aggregation in the HCC (parking areas linked to a crossroad junction nearby the main POS area).

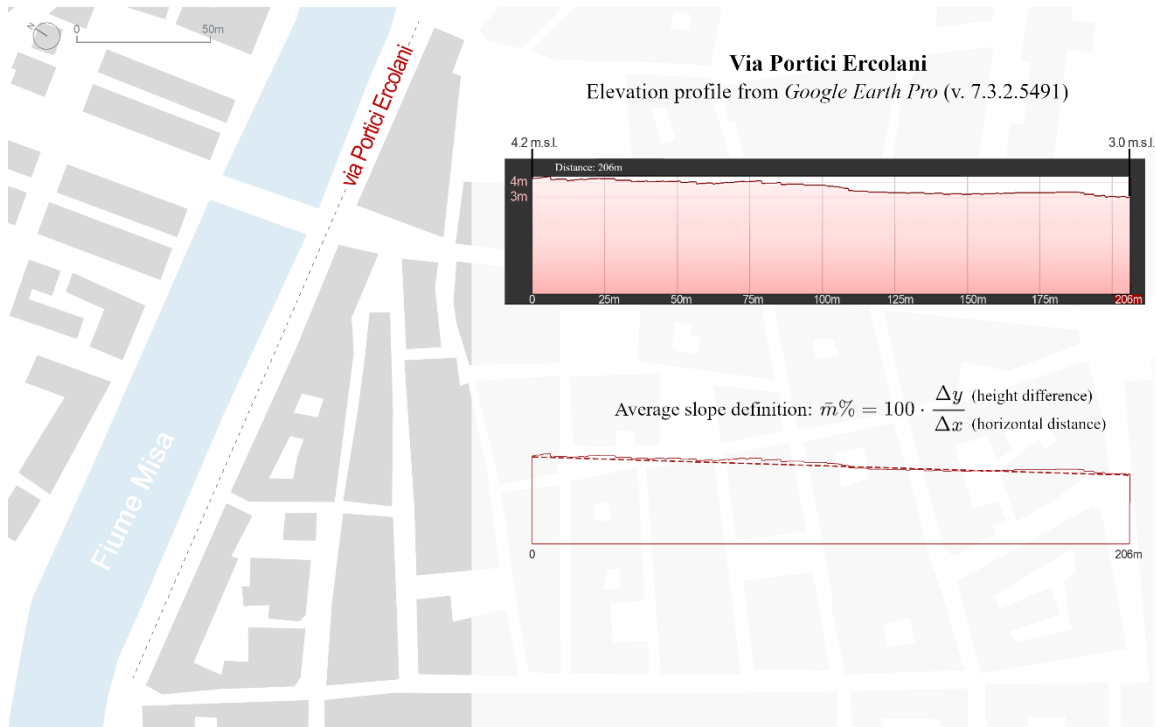


Figure 7: POS “Portici Ercolani” in Senigallia – streets slope data collection.



Figure 8: POS “Portici Ercolani” in Senigallia – building blocks dimension data collection.

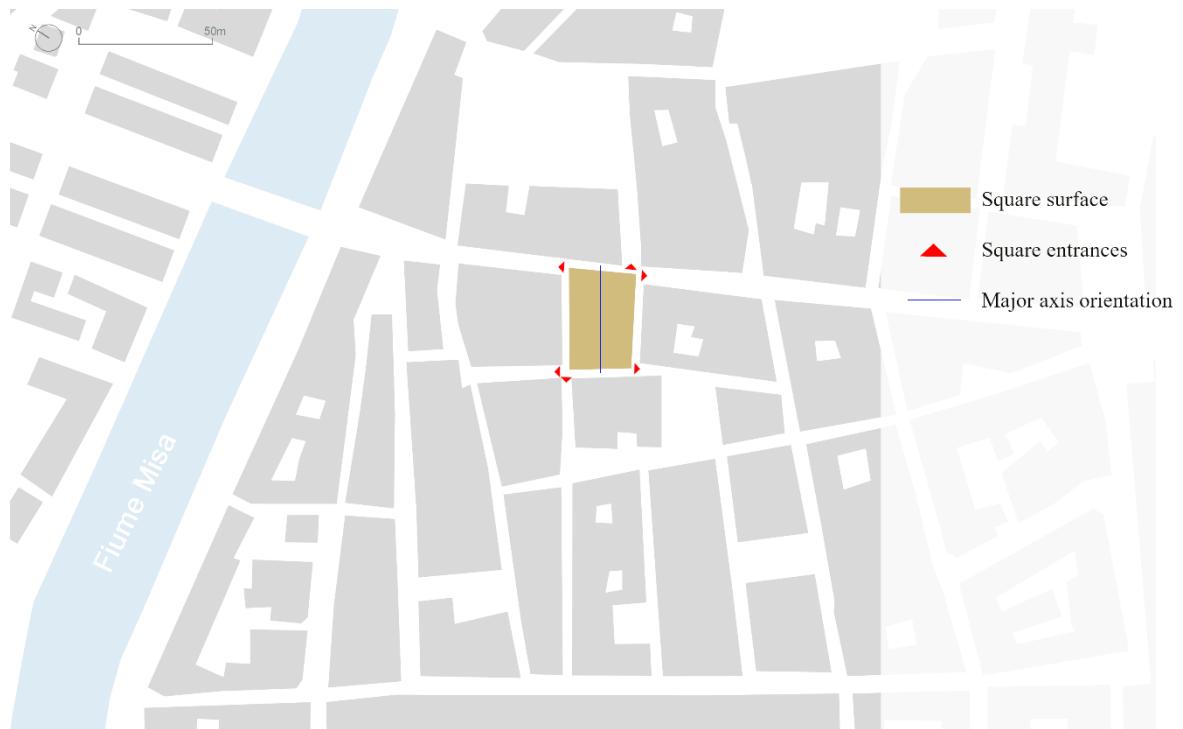


Figure 9: POS “Portici Ercolani” in Senigallia – square features data collection.

3.3.3 Typological POS scenarios for flood risk analyses

Table 5 resumes the values of the parameters describing the physical vulnerability for the case studies according to the aforementioned statistical-based approach. Two groups of typological POSs are derived according to an aligned layout configuration as represented in Figure 10: (1) the compact layout in Figure 10-A (namely, Scenario 1); (2) the 5 layouts including a square in Figure 10-B (namely, Scenarios 2). The two groups have the same basic profile sections (ground elevation along parallel and perpendicular streets), which are shown in Figure 10-C. The full building heights are not considered since they do not affect the results in terms of floodwater spreading into the POS layouts. Furthermore, the two scenario groups are based on the streets’ characterization according to the mode values of Table 5. Table 6 resumes the differences between the typological POSs in Scenarios 2 (A to E), due to the square positions in terms of distance from the river, and of dimensions in terms of modules, that is multiples of building blocks).

Percentile	Parallel streets		Perpendicular streets		Building Blocks b/l ratio [-]
	Section width [m]	Avg Slope [%]	Section width [m]	Avg Slope [%]	
25 th	4.0	0.3	5.1	-1.5	0.6
50 th	6.0	0.8	6.8	0.0	1.2
75 th	9.1	1.7	9.0	2.5	2.3
Mode	4.0	0.3	6.0	-0.6	0.5 (b = 33.0 m; l = 67.0 m)

Table 5: Results from statistical analyses of case studies to define base features of the base typological POSs as in Figure 10-A (Scenario 1).

Case	Area [m ²]; [number of modules]	Distance from the river [m]	Number of streets linked [-]	Major axis of the square direction
A	2211; 1	100-150	8	Perpendicular
B	2211; 1	150-200	8	Perpendicular
C	2211; 1	0-100	8	Perpendicular
D	4554; 2	150-200	10	Perpendicular
E	4824; 2	100-150	10	Parallel

Table 6: Description of Scenarios 2 as in Figure 10-B, by defining the square characterization. Mode parameters are assumed for the POSs, as in Table 5.

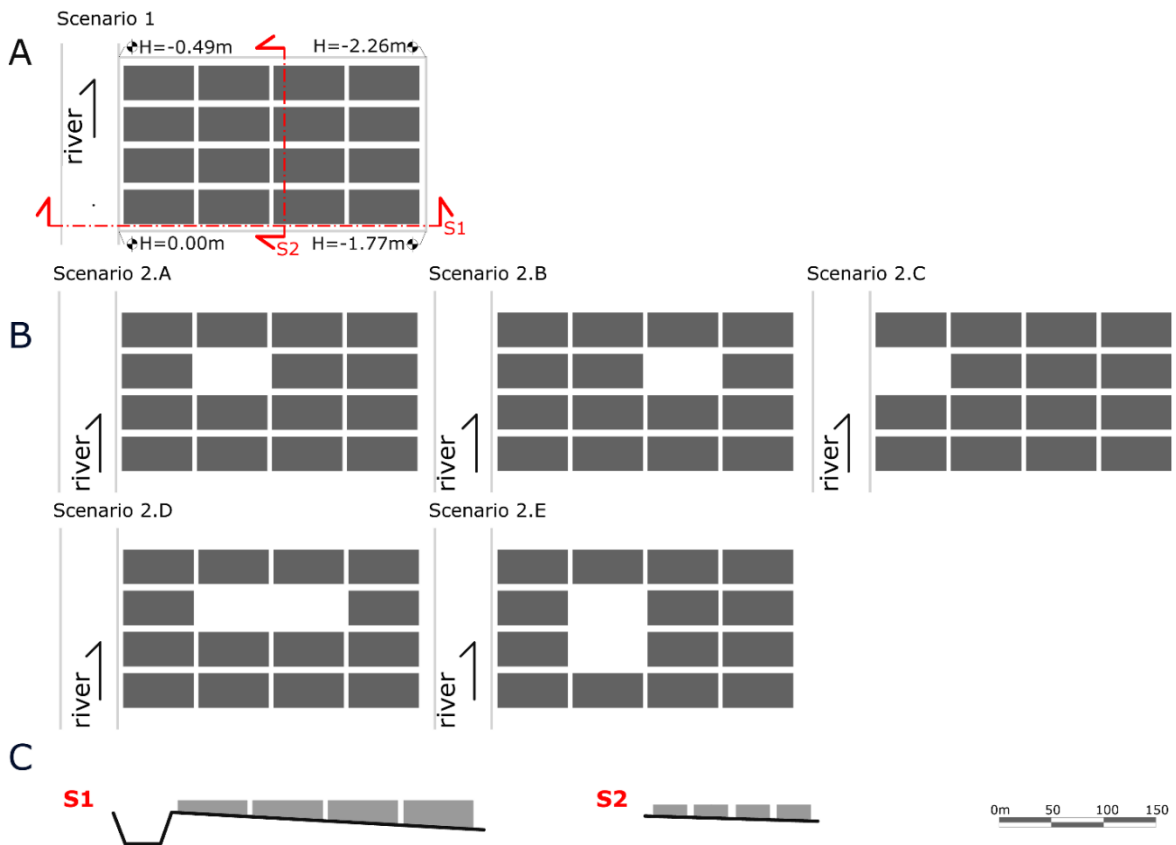


Figure 10: Typological POSs considered in this work: A) compact layout (namely Scenario 1); B) typological POSs layouts including the square (namely, Scenarios 2), having the same basic profile section as for Scenario 1.; c) the basic profile section (ground elevation) according to section lines S1 and S2 in panel A (vertical exaggeration scale: 10x) and metric scale for plan view for all the panels. In each panel, the riverbed is represented between the two gray lines on the left, the arrow points out the river flow direction, and the full-colored gray areas are building blocks.

3.4 Spatiotemporal variation of users' exposure and vulnerability in pre-emergency conditions

3.4.1 Introduction and motivation

Continuing with mesoscale analyses, squares emerge as crucial elements in the HCC and stand out as the most significant open space to be taken into account [194]. Notably, squares within the HCCs frequently host important cultural heritage landmarks, serving as hubs for users' activities and events [194]. The role of squares in the HCCs functioning as hubs of social life [194], is particularly emphasized in the Mediterranean region. Mediterranean squares are described as "the urban element

par excellence," having historically supported various public activities such as religious, commercial, administrative, and leisure pursuits [195]. Consequently, they become focal points for users' exposure and vulnerability, making them of paramount importance for investigation during and after emergencies [17] related to Slow-Onset Disasters (SLODs), which can significantly affect the presence of users indoors and outdoors [9], [113], [114], and Sudden-Onset Disasters (SUODs), which can induce evacuating/gathering depending on the type of hazard [115]. Considering the general resilience challenges, the specificities of the POSs, and their rule towards users before and during an emergency, the assessment and reduction of risk for users in the POSs is then a fundamental goal and should be carried on by using a sustainable and holistic approach [18], [116]–[118].

To support such actions, this section of the thesis aims to define a novel, quick-to-apply methodology to collect and quantify data on *users' vulnerability* and *exposure* in POSs, which are key factors in risk assessment actions [40]. Measuring users' *vulnerability* and *exposure* should involve different levels of analysis according to holistic approaches [11], [62], [80], [196] that allow for considering together different quantities and parameters that dynamically change over time and space (including factors like seasonality, weather conditions, hours of sun, and shadow shapes [83], [197]–[199]). As such, spatiotemporal analyses (known also as "urban temporalities") are fundamental to evaluating how and when things are taking place and estimating the relationships between time and urban spatial dimensions (therefore between uses and users) [11], [41], [200]. Anyway, temporalities are still limitedly considered for user-related analyses, especially while dealing with risk quantification and assessment, and should be evaluated through KPIs not only at the macroscale (that is at the whole urban scale [198], [201]), but also at the mesoscale [10]. Possible applications to POSs, and, in particular, to urban squares [11], are then needed, mainly because they can contribute to reliable scenario creation for single and multi-risk analysis, including those using simulation tools [18], [150], [202].

To cope with these needs, quick and easy-to-apply approaches relying on rapid tools and open-access, standardized data sources are necessary, so as to: a) speed up the evaluation of the users' *vulnerability* and *exposure*, and provide timely results towards the reduction of the risks for the whole community [18]; b) reduce application complexity and efforts also by non-expert technicians, such as those of local administrations [41]; c) improve replicability and take advantage of typological approaches for the definition of recurring conditions that can also lead to common operational frameworks for assessing, identifying, and designing interventions for improving POSs in real-world contexts [10], [21], [42]–[45].

In this work, we focused on the characterization of squares as relevant urban POSs, also considering the following common base assumptions [11], [76], [83]: (1) both outdoor and indoor areas directly face the POS and are connected to the POS itself; (2) data and temporalities are assessed in **pre-emergency** conditions, to allow using collected data on users' vulnerability and exposure as general inputs for different kinds of SLODs and SUODs; (3) the POS is the only attractor of users. The work investigates a homogeneous sample of POSs (56 squares, resumed in Section §11.3.2 - Appendices), which: (1) share similar morphological and constructive characteristics (regular shape, i.e. convex); (2) are placed in historic cities sharing common features (historic Italian cities among provincial capitals, cities with over 20,000 inhabitants, and cities as attractor poles in the surrounding territories); (3) are prone to at least one of the following risks: earthquake, terrorist attack (SUODs); heatwave, pollution (SLODs) [45].

3.4.2 Data sources and collection

The work is mainly structured in three main phases (Figure 11): 1) assessment of users' vulnerability and exposure factors through open-access tools and data sources to characterize the POS; 2) organization of data in quantitative parameters (KPIs); 3) statistical analysis to trace possible typological scenarios depending on the general recurring conditions of the considered POSs.

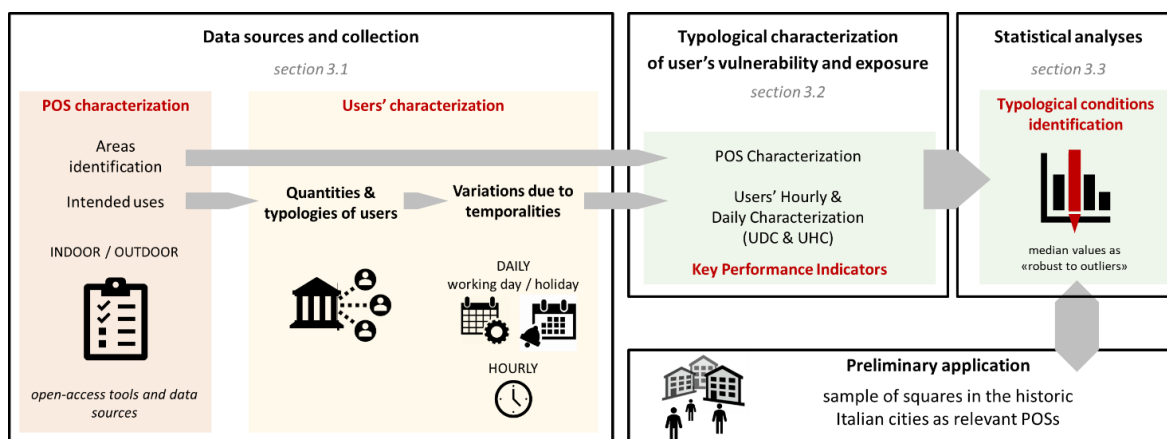


Figure 11: Specific framework for this section - from data sources to statistical analyses.

All the sources used for the present analysis are remote-based, open-access (e.g., local maps, census databases, free online tools [54], [203]), and available for whatever POS, city, and country. It is worth noticing that the current methodology considers the intended uses of the squares in similar, standardized, pre-emergency conditions, therefore it represents a first step towards the users' *vulnerability* and *exposure* assessment by pursuing a conservative, quick- and easy-to-apply approach, connected with related tools and sources (that can be easily replaced in presence of specific tools/data provided by single municipalities for more up-to-date/in-depth analyses). In particular, data sources and collection are set up to quantify the maximum number of users to consider within the POS through the breakdown analysis of (1) the *type of areas* occupied by the users [80], (2) the organization of demographic data into *age ranges* [41], and (3) the impact of temporalities evaluated by the daytime (day or night) and day type (working day or holidays) [11].

The *type of areas* occupied by the users have been distinguished as *outdoor* and *indoor* (Figure 12). In particular, five different types of *outdoor areas* are distinguished in terms of their intended uses: (1) *carriageable areas* CA are primarily used/occupied by vehicles, e.g. carriageway and parking lots; (2) *walkable areas* WA are accessible by pedestrians, e.g. sidewalks, accessible/non-fenced green areas, and gardens; (3) *unwalkable areas* UA are occupied by monuments, fountains, greeneries, other fenced areas and stairs; (4) *dehors* D are open-air terraces of restaurants, open markets, and other outdoor areas hosting a specific intended use or connected to a specific building, placed at the ground levels, and they include both temporary (removable) and permanent structures; (5) *private courtyards* CY are generally inaccessible to the public, e.g. fenced courtyards of dwellings. Although porticos can be mainly classified within these areas depending on their use, they are not considered in this work as *outdoor areas* since their dimension identification via quick analysis tools of aerial views is difficult to perform.



Figure 12: Identification of Public Open Space areas for the case study of Piazza Duomo in Reggio Calabria (see Section §11.2) by: A) distinguishing between outdoor (in orange) and indoor (in yellow) areas; B) recognizing outdoor areas types as carriageable - CA (in blue), walkable - WA (in magenta), unwalkable - UA (in gray), dehors - D (in yellow), and private courtyard – CY (in green); C) identifying the POS in the urban fabric.

The *indoor areas* considered are those of the buildings directly connected to the *outdoor areas* through elements such as doors, passages, and gates. Their identification has been supported by Google Maps and Street Maps¹⁰ tools, which allow checking the number of building floors, and their intended uses. *Indoor areas* non-directly connected to the *outdoor area* are herein excluded. According to the adopted quick-to-apply approach [41], [78], *indoor areas* are classified depending on their intended use, such as residential buildings, commercial activities, and private/public services and institutions. Furthermore, strategic buildings and special uses that can be subject to terrorist attacks have been classified into homogeneous groups depending on the combination of the intended uses, temporalities, crowd conditions, and emergency-related issues [28], [45], [204], [205]:

- “Theatres, Museums, Religious buildings”, as buildings freely open to the public and generally characterized by the most significant occupant loads, up to overcrowding;
- “Government buildings” (such as city halls, courts, and police stations), as public buildings that are generally used as offices, can have a role in disaster conditions, and can ideally be hard targets for terrorist acts;
- “Metro - Rail stations”, as public buildings where users are in transit;
- “Hospitals, Schools, Universities” as specific public buildings with a strategic rule in the city, also hosting vulnerable users.

Table 7 resumes the aforementioned *types of areas* together with the type of users occupying each of them, and the relative occupant load OL_i [pp/m²] and temporalities defined by Italian regulation [204] (see Section §11.3.3, Appendices) evaluated considering daily and hourly timetables. In particular, Only Outdoor users (OO) and Residents (R) are non-variable components, while Prevalent Outdoor users (PO) and Non-Residents (NR) strictly depend on the opening time of the intended uses. Daily temporalities are provided by distinguishing between Working days (as the most

¹⁰ available at <https://www.google.it/maps/?hl=it> (last access on 25/07/2021).

recurring conditions during the year) and Holidays (representing Sundays and other national holidays), while hourly temporalities of the POS are evaluated for each hour of the day (1-24) [80]. In this work, mass gathering events or one-off events (such as local fairs or festivals) are ignored as exceptional situations for crowding conditions. Furthermore, areas with variable temporalities (e.g., open markets in the morning/working days as D, pedestrian areas as WA, or parking lots in the afternoon/night/holidays as CA) are characterized by time-dependent *OL* values according to those in Table 7. Finally, the familiarity of the users with the POS (and the evacuation procedures) has been also indicated, and only R are conservatively considered as familiar [18].

Type of areas [m ²]	Type of users (position, familiarity)	{Daily timetable when applied} Occupant Load OL_i [pp/m ²] (hourly timetable when applied)
Carriagable areas (CA)	- the use of carriageways is only assigned to vehicles with no distinction with the daytime and type [206].	{W and H}: 0.0 pp/m ² (1-24)
Walkable areas (WA)	Only Outdoor Users OO (outdoor, unfamiliar)	{W and H} [*] : 0.1 pp/m ² (7-24) 0.0 pp/m ² (1-6)
Unwalkable areas (UA)	- these areas are not available for users as they represent an obstacle in the POS	{W and H}: 0.0 pp/m ² (1-24)
Dehors (D)	Prevalent Outdoor Users PO (outdoor, unfamiliar)	{W and H}: 0.4 pp/m ² (intended uses opening time) 0.0 pp/m ² (intended uses closing time)
Private courtyards (CY)	- these areas are occupied by the same users of the indoor areas linked to them	{W and H}: 0.0 pp/m ² (1-24)
Indoor areas as Non-residential areas (IO₁)	Non-Resident Users NR (indoor, unfamiliar)	{W and H}: Depending on the intended use (intended use opening time)**
Indoor areas as Residential areas (IO₂)	Residents Users R (indoor, familiar)	{W and H}: 0.05 pp/m ² (0-24)

* Considering a low level of crowding in ordinary conditions (under the level of service A threshold [207]) only during the daily hours (i.e., from 7 to 24 every day) [114], [141].

** See Section §11.3.3 and §11.3.4 (Appendices). The main values are: 0.4pp/m² for intended uses open to the public (e.g., restaurants, bars, shops, public offices); 0.7pp/m² for churches; 0.1pp/m² for intended uses close to the public. Churches' opening times refer to Sunday service timetables.

Table 7: Summary of the users' temporalities according to the types of areas. *W* is for Working days, *H* is for Holidays (full list of abbreviations in Section §11.3.1, Appendices).

The effective surface SU_i [m²] of each *outdoor area* (CA; WA; UA; D; CY) and *indoor area* (IO_i) has been calculated through the freeware online tools Calcmaps¹, which allows measurement analysis on aerial views. In detail, in this process, the gross areas are considered rather than the net internal ones, thus slightly overestimating the following maximum users' number evaluation moving toward a conservative approach in the users' vulnerability and exposure quantification [41], [78]. Google Street Maps¹ views and photos are used to support the areas and buildings characterization (i.e., to check intended uses and opening times during the different days of the week, number of floors, presence of porticos, and presence of doors, passages, or gates connecting indoor and outdoor areas) [41], [80]. In case of missing data, the opening time has been assessed through databases containing

information on companies¹¹, social network pages, or according to national (or local) regulations on timetables of buildings open to the public¹², considering the specific application context (i.e. in this work, the Italian context).

Similarly, in Table 8 users are listed in *age ranges* [41], [78], so as to consider possible common conditions in motion [208]. Moreover, temporalities are considered by means of a “presence coefficient” *cp* [-] evaluated on the basis of the users’ age range, familiarity with the POS, and daily and hourly timetables (which is equal to 1 if users are present, 0 if users are absent, and 0.09 to consider unemployed¹³ users spending their time at home).

Type of Users [age range, motion conditions]	Familiar Users - R {Daily timetable} (Hourly timetable // Presence coefficient <i>cp</i> [-])	Unfamiliar Users – OO, PO, NR {Daily timetable when applied} (Hourly timetable when applied // Presence coefficient <i>cp</i> [-])
Toddlers (TU) – [0-4, assisted: directly dependent on their parents]	{W and H}: (1-24 // 1) – at home	{W and H}: (intended use opening time // 1); (intended use closing time and offices* // 0)
Parents-assisted Children PC [5-14, assisted: can autonomously move but are generally assisted by their parents]	{W}: (8-13 // 0) – at school (1-7 and 14-24 // 1) – at home {H}: (1-24 // 1) – at home	{W and H}: (intended use opening time // 1); (intended use closing time and offices* // 0)
Young Autonomous YA [15-19, autonomous: can be considered as autonomous users, and relate to students]	{W}: (8-13 // 0) – at school** (1-7 and 14-24 // 1) – at home {H}: (1-24 // 1) – at home	{W and H}: (intended use opening time // 1); (intended use closing time and offices* // 0)
Adults AU [20-69, autonomous can be considered as autonomous users, and relate to workers or university students]	{W}: (8-18 // 0.09) – at work/university (1-7 and 14-24 // 1) – at home {H}: (1-24 // 1) – at home	{W and H}: (intended use opening time // 1); (intended use closing time // 0)
Elderlies EU [70+, assisted: may have poorer motion capabilities]	{W and H}: (1-24 // 1) – at home	{W and H}: (intended use opening time // 1); (intended use closing time and offices* // 0)

* Offices include intended uses close to the public and are considered occupied only by Adult users.

** According to the common Italian teaching timetable, even if they could change if specific sources on daytime openings are available, such as in full-time primary or secondary schools (see also Sections §11.3.3 and §11.3.4).

Table 8: Summary of the users’ temporalities according to the age range and familiarity with the POS. *W* is for Working days, *H* is for Holidays (full list of abbreviations in Sections §11.3.1, Appendices).

Data about the population distributions (age and gender) can be obtained from local registers or census databases. For what concerns the Italian Municipalities, the online website of the ISTAT provides the percentage distribution of the population based on the annual reports¹⁴, allowing the organization of the data per age range (AP_a [%] where *a* indicates the ranges of Table 8) and for

¹¹ main considered free-access databases on timetables of companies and activities open to the public: <https://www.paginegialle.it/>, <https://www.oraridiapertura24.it/> (last access: 09/02/2021 – in Italian)

¹² regulations on opening timetables: <https://www.mise.gov.it/index.php/it/mercato-e-consumatori/concorrenza-e-commercio/risposte-ai-quesiti/orari-di-apertura-e-chiusura> (last access: 09/02/2021 – in Italian)

¹³ According to national data from www.istat.it/it/archivio/occupati+e+disoccupati, last access 09/02/2021

¹⁴ for 2020: <http://demo.istat.it/popres/index.php?anno=2020&lingua=ita> (last access on 25/07/2021). As an alternative, data from tuttitalia.it website could be used (e.g., <https://www.tuttitalia.it/lazio/33-roma/statistiche/popolazione-eta-sesso-stato-civile-2020/> (last access 25/07/2021) as 5 years-wide classes of population are already available.

gender (Mp for male and Fp for female [%]). According to the purpose of a quick-to-apply approach [18], [78], these distributions are reasonably assumed valid considering the POS as a part of the whole urban scenario to which Municipalities-related data are referred.

In view of these considerations, the maximum number of users NU [pp] to consider within the POS has been first evaluated on hourly sampling according to Equation 3.1:

$$NU = \sum_{i,a} SU_i \cdot OL_i \cdot AP_a \cdot cp \quad (3.1)$$

Where:

- SU_i [m²] is the effective surface of the i-th type of area (first column of Table 7);
- OL_i [pp/m²] is the Occupant Load of the i-th type of area (third column of Table 7);
- AP_a [%] is the users' age percentage distribution of the a-th age range (first column of Table 8);
- cp [-] is the presence coefficient (second and third columns of Table 8).

3.4.3 Typological characterization of users

In this section, the data previously collected are converted into KPIs useful to perform local-scale analyses on single case studies. The KPIs are resumed in the following according to three classes, together with their specific calculation methods and meanings:

1. **Public Open Space Characterization (POSC):** they do not directly express the users' quantification and typologies, but they trace exposure- and vulnerability-influencing issues depending on the general square features and regardless of the daily/hourly POS use (Table 9).

<i>KPI [unit of measure]</i>	<i>C: Calculation methods M: Meaning</i>	<i>Specific conditions and related symbols [unit of measure if needed]</i>
Percentage of outdoor areas per typology [%]	C: the ratio between specific and overall outdoor areas M: tracing areas with particular use patterns depending on their accessibility and use rules	Percentage values per typology: carriageable areas CAp , walkable areas WAp , unwalkable areas UAp , dehors Dp , private courtyards CYp
Presence of special buildings or special uses [Boolean], [number of items per POS]	C: presence or not of special buildings or uses M: defining special buildings or uses to be considered in the square as possible attractors for temporalities, exposure, and specific individual vulnerabilities	Presence of special buildings/uses SB [Boolean] Number of special buildings/uses SBn [number of items per POS]*
Ratio between indoor and outdoor features [-]	C: the ratio between the specific indoor and outdoor areas of the POS M: rapidly characterizing the built environment and defining the spaces in which vulnerability and exposure are higher	Ratios between the indoor area and the outdoor area AIOr

* The median area of the special buildings **SBA** [m²] has been also calculated for the most recurrent category of special buildings and uses

Table 9: POSC-related KPIs.

2. **Users' Hourly Characterization (UHC):** they provide a detailed overview of the users' distribution based on an hourly sampling methodology (Table 10).

<i>KPI [unit of measure]</i>	<i>C: Calculation methods M: Meaning</i>	<i>Specific conditions and related symbols [unit of measure if needed]</i>
Users' density considering the outdoor areas [pp/m²]	C: the ratio between the users' overall number and the <i>outdoor area</i> M: it essentially considers that all the users can contemporarily move out of the buildings, e.g. as for evacuation scenarios in SUODs	users' overall outdoor density UOod , considering both outdoor and indoor users out of the buildings
Percentage of users considering familiarity with the POS [%]	C: percentage ratio between specific users' typologies and the users' overall number UOn M: scaling the number of users into the POS with respect to main behavioral issues such as those due to risk-perception and preparedness issues	calculated for: only outdoor users OOp ; prevalent outdoor users POp ; residents Rp ; non-residents NRp .

Table 10: UHC-related KPIs.

3. **Users' Daily Characterization (UDC):** they provide a general overview of the users' distribution considering the days as a whole (Table 11).

<i>KPI [unit of measure]</i>	<i>C: Calculation methods M: Meaning</i>	<i>Specific conditions and related symbols [unit of measure if needed]</i>
Users' density considering the indoor areas [pp/m²]	C: the ratio between the (specific) maximum number of users and the <i>indoor area</i> M: it essentially considers an average density of users in <i>indoor areas</i> and the possibility that outdoor users contemporarily move into <i>indoor areas</i> , e.g. as for invacuation scenarios in SUODs or heatwave conditions	users' overall indoor density UOid , considering both outdoor and indoor users in the buildings users' indoor density Uid , considering the normal fruition of the buildings (R+NR)
Users' density considering the outdoor areas [pp/m²]	C: the ratio between the users' overall number and the <i>outdoor area</i> M: it essentially considers that all the users can contemporarily move out of the buildings, e.g. as for evacuation scenarios in SUODs	users' overall outdoor density UOod , considering both outdoor and indoor users out of the buildings
Ratio between indoor and outdoor features [-]	C: the ratio between the number of users of the indoor and outdoor spaces M: it allows evaluate how users are distributed in <i>indoor</i> and <i>outdoor areas</i> during the day	ratios UIOr between users in <i>indoor areas</i> (R+NR) and users in <i>outdoor areas</i> (OO+PO)
Percentage of users considering familiarity with the POS [%]	C: percentage ratio between specific users' typologies and the users' overall number UOn M: scaling the number of users into the POS with respect to main behavioral issues such as those due to risk-perception and preparedness issues	calculated for: only outdoor users OOp ; prevalent outdoor users POp ; residents Rp ; non-residents NRp .
Percentage of users considering individual vulnerability [%]	C: percentage ratio between specific users' typologies and UOn M: scaling the maximum users' number into the POS with respect to main individual vulnerabilities affecting response and motion	calculated for: toddlers TUp , parent-assisted children PCp , young autonomous YAp , adult AUp , elderly EUp . depending on their gender: male Mp , female Fp

Table 11: UDC-related KPIs.

UHC- and UDC-related KPIs are organized both for working days and holidays, and Table 10 and Table 11 also remark on how they are able to trace the conditions for the overall users' sample, as well as distinguish users by their familiarity with the POS and by age ranges. It is also worth noting that some KPIs could have different meanings for different types of disaster assessment. For instance,

users can decide to move indoors or outdoors depending on the type of hazard. In this sense, critical interaction conditions in *indoor areas* and *outdoor areas* of the POSs (as the sum of WA, D, and CA, and so considering the carriageable areas as available for users gathering in case of emergency) are assessed through the users' density [pp/m²] [80], [209].

3.4.4 Statistical analyses

KPIs introduced in the previous subsection are organized according to the following statistics to trace typological scenarios depending on the general recurring conditions of the considered POSs, and so, in this study, of the whole sample of squares.

For *POSC-related KPIs*: (a) Boolean parameters (i.e. SB) are investigated according to two possible classes (true or false), and the recurring condition of the sample is represented by the class with the higher frequency. (b) Parameters expressed in discrete classes, such as the number of items (i.e. SBn), are assessed through a quartile-based approach [179], [180], which has been also adopted by previous works on built environment typologies definition [45], [210]. Outliers are retrieved according to the InterQuartile Range IQR method (fence: 1.5 IQR) [180], so as to define boundary conditions in the sample that cannot be considered typologically relevant. In this case, the mean value calculation is excluded because of the discrete value of this KPI, while the median value of the KPI is used to derive the typological description of the squares sample in a “robust to outliers” perspective [180].

UHC- and UDC-related KPIs, as well as continuous *POSC-related KPIs* (i.e. Percentage of outdoor areas per typology, AIOr), are assessed through the same quartile-based approach. In particular, *UHC-related* values are firstly organized considering the whole sample of squares, and the quartile-based approach allows tracing the overall distribution of each KPI by pointing out extreme (i.e. maximum and minimum, excluding outliers according to the IQR methods), and other recurring values, i.e. the median.

Then, *UHC-related* values are merged for each of the squares, in a separate manner, to trace the related *UDC-related* values. Minimum and maximum values for each square have been collected together to provide separated subsets of data, respectively representing under/overcrowding conditions of the sample. Similarly, median values are collected into a separate subset to represent recurring conditions of use. These three subsets have been separately analyzed using the same quartile-based approach, by also applying the IQR method. In this way, quartile-based representations of maximum, minimum, and median KPI values for the whole sample of squares have been retrieved for each subset.

3.5 Users' exposure assessment and modeling in emergency conditions: the case of floods

3.5.1 *Why floods: introduction and motivation*

Worldwide, floods are the most common and devastating threat for HCCs, affecting each year more individuals than any other disaster [1], [2], [5]. Reliable but quick analyses are then necessary to promote flood risk assessment actions and effective risk-mitigation strategies [211]–[214]. In this context, mesoscale analyses seem to have a paramount relevance since POSs (i.e., streets, squares, parks, other open spaces, and their combination) affect the flood spreading within the HCCs [34], [130], [219]–[222], [133], [134], [189], [191], [215]–[218], which become critical environments for the users' safety, especially during emergency conditions, i.e. in the evacuation process [124], [131], [136], [223].

Previous works pointed out how risk assessment tasks, related risk mapping actions, and evaluations on risk-mitigation strategies should take advantage of simulation models in view of the complexity of the overall system, which comprises the HCC physical vulnerability (§3.3), the hazard characterization (§3.6), and the users' **exposure** and in emergency conditions [124], [136], [201], [219], [220], [224]–[226]. In particular, efforts to include users' spatiotemporal dynamics and behaviors in flood conditions have been provided [124], [130], [134], [136]. Such models allow for evaluating the effects of interactions between the pedestrians, the floodwater conditions, and the surrounding built environment on users' risks and possible casualties, mainly based on the effects of floodwater depth and speed on pedestrians' speed reduction, buoyancy phenomena, and body failure [134], [135], [227]–[231].

Simulation tools have been applied for preliminary evaluations of the effectiveness of emergency solutions [123], [134], [188], [196], [218], [232], [233], especially those directly aimed at helping people when structural solutions fail/miss or massive events occur (e.g., evacuation plans, safe areas identification). However, such simulators are generally considered as custom software, mainly developed for research purposes, and characterized by a high complexity level in terms of use, functionality, and interoperability that could slow down (or impede) crucial analyses for the risk assessment, especially considering uses by Local Authorities technicians who can have a low training level on the matter.

Generic evacuation simulation tools, on the contrary, would represent a powerful solution to improve sustainable applications of evacuation simulation tools, since they are widely implemented in more user-friendly software, especially considering commercial ones. They are oriented towards general-purpose evacuation simulation and use behavioral and motion quantities from related databases [208], [234], [235]. Their general verification and validation process has been provided according to standard testing conditions [155]. Nevertheless, generic software needs adequate modifications to represent flood-related behaviors. To solve this issue in a quick, easy-to-apply, standard-based and so sustainable way, specific software setups can be developed, thus avoiding complexity-increasing operations on the source code or the implementation of dedicated plug-ins and additional tools.

Within this framework, this section of the thesis is aimed at the development of new preliminary tools for supporting technicians and designers in carrying out quick and sustainable assessments of pedestrian safety in flooded outdoor spaces. In particular, the next subsections are organized so as to provide:

- §3.5.2: Preliminary video analyses on human behaviors for a comprehensive understanding of how individuals behave in emergency situations, providing valuable insights into their decision-making processes, movement patterns, and interactions [57], [59], [98], [99], [236]–[238]. This preliminary analysis serves as a crucial step in creating more effective and reliable evacuation simulation software since analyses of real-world behaviors can improve the accuracy and realism of evacuation simulations, differently from traditional laboratory tests that involve the use of mannequins, equipped volunteers or stuntmen, and controlled floodwater conditions that do not fully represent the complexity of real flood events [50], [231], [239]–[243];
- §3.5.3: Preliminary setups of a generic software tool using an easy-to-apply no-code modification approach to include flood peculiar behaviors. Simulation outputs of the setup-based generic software are compared with a custom simulator relying on the same *microscopic* modeling approach, with real-world observations, and moving towards the verification and validation process according to standard testing conditions. The testing scenario consists of a straight and flat street in stationary flood conditions where small compact groups of pedestrians are evacuating. Results provide the best setup of the generic software to reliably represent evacuation phenomena.
- §3.5.4: Evidence on how accounting or not pedestrian evacuation behaviors can affect flood risk assessment and emergency strategies evaluation. Risk indexes and risk maps are developed with respect to microscale (i.e., outdoor space) and mesoscale (i.e., the whole POS) assessments. The testing scenario consists of the typological POSs previously defined (see §3.3) under the same hazard conditions (that will be introduced in next) §3.6. The simulations were performed through setup-based generic software;
- §3.5.5: A risk-based methodology to determine the optimal strategy for on-foot evacuations in flooded urban areas. In this case, a *macroscopic* approach (an Integer Linear Program solving an optimization flow problem on a graph street network) is adopted to simulate the evacuation, which allows for minimizing the number of casualties and, in turn, the evacuation routes' length, time, and effort. The best evacuation strategy is determined through a synthetic risk index RI that combines Key Performance Indicators (KPIs) quantifying urban, human, and environmental variables. The testing scenario consists of the riskiest typological POS according to the previous subsection outcomes. Criteria for comparisons between previous microscopic and macroscopic approaches are included. Results allow for evaluating safety measures to deal with the absence/ineffectiveness of structural ones and could be exploited to assess where/how to implement wayfinding systems, risk maps, urban furniture, and rescue operations.

3.5.2 Investigating pedestrian behavioral patterns under different floodwater conditions

3.4.2.1 Background and research framework

As for other kinds of disasters affecting HCCs, flood evacuation is characterized by different types of behaviors according to which three main evacuation phases are generally distinguished [58], [244], [245]: (1) a *pre-movement* phase, involving behaviors performed before the evacuation starting that generally concerns the recognition/evaluation of the hazard, and are still unrelated with searching and reaching a safe area (e.g., trying to save other people or personal belongings, spending time

recording with smartphones); (2) a *motion towards the evacuation target* phase, referred to the actual physical evacuation of people from the flooded areas; (3) a *post-evacuation* phase at the end of the motion process, after the arrival to a safe area.

In addition to this, previous studies also identify further classifications based on other factors, such as: a) the *type* of emergency in which they are noticed, distinguishing between peculiar behaviors when they are characteristic only of the flood evacuation, or common behaviors and when they are noticeable also in other emergency conditions [223]; b) the *voluntariness* in performing the behavior as a result of a decision, as deliberately chosen or passively suffered [246]; the people's *response* against the hazard, in terms of protective behavior directly aimed at saving their own and/or other's lives, or hazardous behavior [247]; the required presence of *reference elements* for people to activate the behavior, such as environmental elements (e.g., obstacles, debris, urban furniture, tools furnished by rescuers), or human elements (i.e., other evacuees or rescuers) [223]. Section §11.4.1 (Appendices) provides a general overview of all the behaviors already codified in the literature.

Video-sharing platforms like YouTube, Twitter, Facebook, and Instagram offer a huge and free database of emergency-related multimedia content already used for several applications concerning behavioral analyses, but only reliable sources should be taken into account (e.g. mass-media channels, law enforcement agencies, rescuers, local authorities) [58]. Previous works also provided some flood monitoring, mapping, and modeling applications to extract the event's main features (i.e., floodwater depth, flow) from images and videos through comparison with objects having known dimensions (e.g., pedestrians standing in the water, wheels of cars, road signs) [248]–[252]. However, even though modern technologies allow detailed estimations, these kinds of approaches generally require long-time analyses and high-framing quality multimedia content [248], [253].

Although videotape analyses are consolidated, and detailed quantitative insights already explain “why” and “which” behaviors are performed [99], [223], literature works still demonstrate a general lack of connecting “how” floodwater conditions qualitatively affect the pedestrians' behaviors (and so their bodies). In this sense, the following gaps should be considered according to previous investigations: (a) the water depth in relation to notable human body parts (namely the ankle, the knees, and the waist) or vehicle parts (for drivers inside vehicles moving in the floodwaters) [50], [231], [241], [248]; and (b) the water flow by distinguishing between still water and flowing water (that is zero and non-zero in terms of water speed) [99], [227].

The video analysis is then organized in two steps, adapting a previous methodology tested on terrorist acts and people's behaviors [58] to fit the flood evacuation scenarios analysis. The first step concerns the videotape collection and the definition of criteria on how to classify the behaviors depending on the floodwater conditions (i.e., water depth and flow), and the people involved (section §3.4.2.2). Afterward, the second step concerns the analysis of the behaviors and their statistical frequency depending on the criteria introduced in the first step task (section §3.4.2.3).

In the overall process, even though previous literature approaches suggest the use of the number of “scenes” or videotapes to evaluate the frequency of each behavior [57], [58], in this case, the frequency has been calculated considering the number of people within the videotapes scenes in combination with the floodwater and built environment conditions, which is a measure of how much a given behavior is activated rather than observed. In this way, the proposed approach also reduces the possibility of a biased selection of the overall sample of assessed scenes, mainly due to specific

floodwater conditions more or less frequent in the sample. Besides, it allows separate evaluation of how floodwater conditions affect each individual (i.e., same water depth but different body parts submerged depending on the individual height).

3.4.2.2 Data collection and organization

139 videotapes freely available on local news websites¹⁵ and verified YouTube and Twitter channels have been analyzed involving the clear presence of people interacting (by foot or vehicles) with flooded outdoor BEs scenarios from all over the World. The videotape collection has been carried out by searching in the search engine of the aforementioned repositories the following keywords: “flood(ing)”, “urban flood(ing)”, “flood(ing) evacuation”, and “flooded areas”. The selected videotapes are identified by a number reported in curly brackets ($\{num\}$) and are available at [{Flood videotapes SafetyScience}](#). Each videotape has been divided into one or more “scenes” characterized by the same evacuation (i.e., floodwater) conditions [58], [98] in terms of the water depth and flow, in the same built environment scenario. Figure 13-A and Figure 13-B resume the general features (in percentage terms) of the collected videotape database, respectively in terms of floodwater conditions and geographic area distributions.

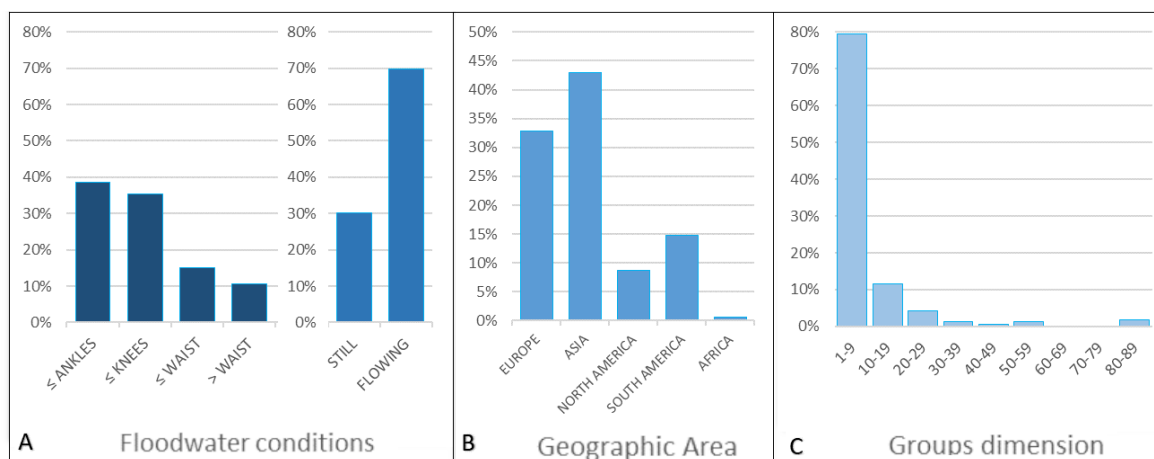


Figure 13: videotapes general features in percentages terms according to: (A) the floodwater conditions (water depth and flow); (B) the geographic area; (C) the groups' dimensions.

In particular, considering floodwater conditions, the water depth - in the following, referring to the subscript d - has been evaluated according to the human body parts submerged by the flood, that is equal to or up to ankles (A), knees (K), waist (W), and higher than the waist (HW) [231], [241], [248]. Such an approach ensures the quick application of such analysis on a wide sample by referring to critical body parts submerged by floodwaters, also in case of different heights between the investigated individuals on the scene, which can potentially affect the level of floodwater experienced and the types of behaviors exhibited. However, although differences between individuals can obviously exist due to anthropometric issues, in view of the quantification of such body parts measures, such levels can be roughly traced back to 0.10m for the ankles, 0.40m for the knees, and 0.90m for the waist considering the average measures of an adult [231]. In particular, in the case of videotapes with adult-assisted children (whose physiological measurements highly differ

¹⁵ e.g.: <https://www.ilfattoquotidiano.it/2021/07/15/germania-la-forza-del-fiume-esondato-nelle-strade-e-impressionante-lacqua-porta-via-le-auto-video/6262834/> (last access: 02/11/2022)

from adults), the same approach was adopted, and the adults' body was considered as a benchmark. This assumption is consistent with the adults' active role in children's safety from both a physical and decisional point of view [197]. Videotapes with only children were not found. For what it concerns vehicles, the dimensions¹⁶ of wheels and car body have been used to trace back the water depths to the four levels previously defined.

The water flow - in the following, referring to the subscript f - has been distinguished between still water (S) when the surface water seems to be calm (speed close to zero) or not flowing¹⁷, and flowing water conditions (F) when the surface water speed is visibly different than zero (traceable also with the aid of elements such as waves, dragged objects within the videotapes) [99]. All the floodwater conditions obtained by crossing the water depth and flow levels are resumed in Figure 14.

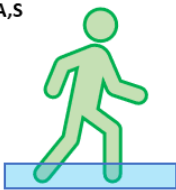
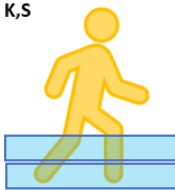
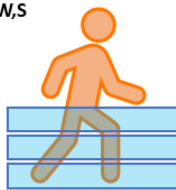
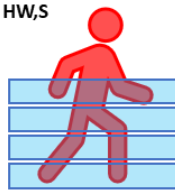




	ANKLES ($\approx 10\text{cm}$)	KNEES ($\approx 40\text{cm}$)	WAIST ($\approx 90\text{cm}$)	HIGHER
STILL	A,S 	K,S 	W,S 	HW,S 
FLOWING	A,F 	K,F 	W,F 	HW,F 

Figure 14: Illustration of all the floodwater conditions organized per water depth (rows) and water flow (columns), including related acronyms for subsample creation. Numerical values are referred to adults [231].

A total number of 1269 people have been inspected, distributed in groups of up to 82 individuals, with a medium group dimension equal to 10 individuals. In particular, the number of people featured in each scene has been organized according to the parameters shown in Table 12 and illustrated in Figure 15. According to the original method adopted by this work [58], the following assumptions were made:

- people not clearly and completely visible were not considered, as well as those behind smartphones and cameras hypothetically involved in “curiosity” effect behavior (PM2) since fundamental factors such as if they are in a safer position and/or if they are reporters (thus filming for job reasons) are unknown. People filming while evacuating were not found;
- *moving through the water with vehicles* (M5) were not considered in relation to empty vehicles or with a not clearly visible presence of people inside. In this case, the analysis of

¹⁶ Cars' dimensions have been estimated through the official web pages when the models were recognizable, otherwise online sources like <https://www.pneumatici.it/calcolatrice-pneumatico> were used to estimate the wheels height depending on the cars' model (e.g., city-cars, sedans, station-wagons, SUVs, trucks...).

¹⁷ According to an expeditious approach, there is an inherent margin of error due to image quality and perception.

behaviors was performed in relation to the number of vehicles (i.e., of drivers) crossing the floodwater was considered, rather than considering the number of passengers [246].

Parameters [pp]	Meaning
PO - People overall	The total number of people who could actually perform a given behavior (Figure 15). The number of people has been also classified considering the presence of reference elements if their presence is necessary to activate the behavior (e.g., the presence of unmovable obstacles to be attracted by them).
PI - People involved	Total number of people who perform a given behavior (Figure 15).
PI_d - People involved per water depth	Total number of people performing a given behavior under the same water depth, that is equal to or lower than the ankle, the knees, the waist, or higher than the waist ($d = [A; K; W; HW]$).
PI_f - People involved per water flow	Total number of people performing a given behavior under the same water flow, that is still or flowing ($f = [S; F]$).
PI_{d,f} - People involved per floodwater conditions	Total number of people performing a given behavior under the same floodwater conditions, that is combining the water depth and flow conditions.

Table 12: Parameters to quantify the number of people [pp] featured in the videotapes.

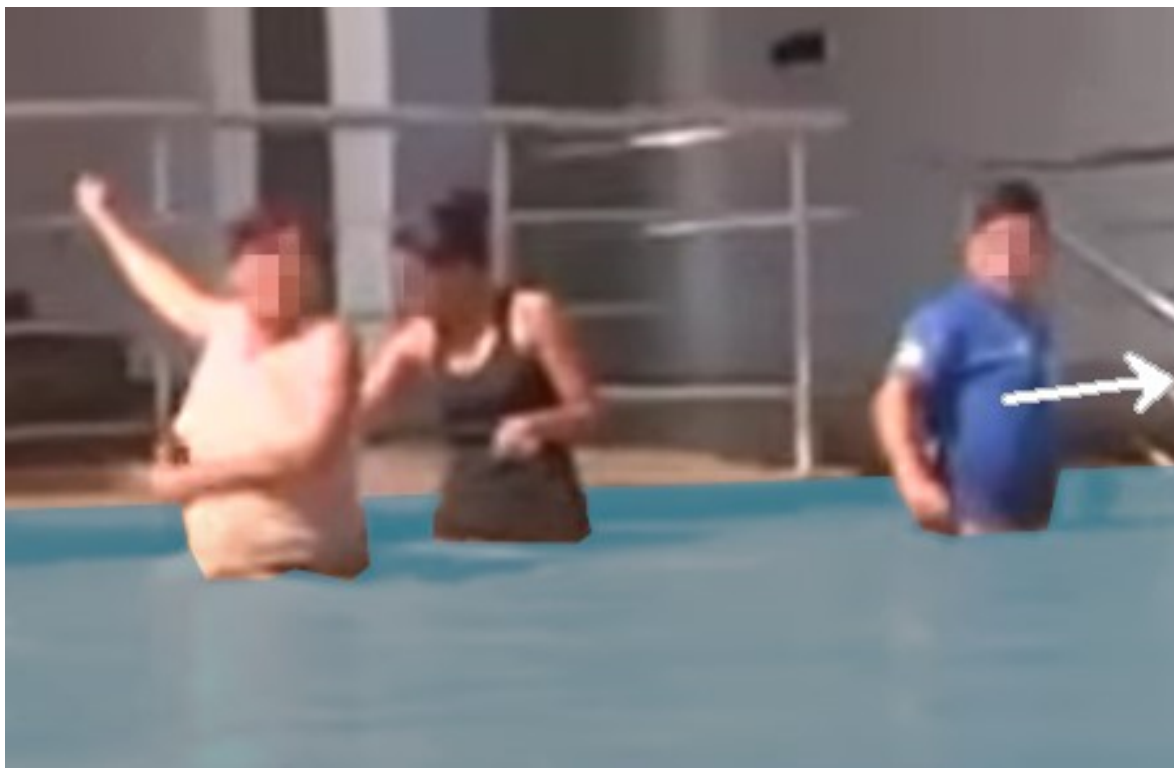


Figure 15: Example of 2 pedestrians (on the left) performing attraction towards unmovable obstacles M2, while the pedestrian on the right is moving away from the fence (the white arrow indicates his direction). The following parameters are considered in this scene: $PO=3$, $PI=2$, $PI_w=2$, $PI_{w,s}=2$ (reference videotape: {95}).

3.4.2.3 Behavioral patterns definition with respect to water depth and flow

The behavioral patterns definition has been performed by considering frequent *by-literature* behaviors (those resumed in section §11.4.1), and inquiring about *new-noticed* ones, as suggested by the methodological reference work [58]. In particular, the *new-noticed* behaviors have been classified according to their related evacuation phase, type, voluntariness, human response, and presence of reference elements.

Then, the statistical frequencies of the *observed behaviors* (i.e., both *by-literature* and *new-noticed* ones) have been calculated by considering overall and situational samples in relation to the number of people and the floodwater conditions (i.e., the water depth and flow), as shown in Table 13, which

also resumes the assessed frequency percentage depending on *deliberately chosen* and *passively suffered* behaviors.

Statistical Frequency percentage [%] and related calculation	Meaning
Overall frequency $PI/PO*100$	Since this percentage is an expression of the voluntariness in performing a given behavior, it is only evaluated for <i>deliberately chosen</i> ones (that is excluding behaviors M7 and M8 for which the evaluation of PO strictly depends on physical features not deducible through images, such as the people's age, gender, health, foot size [227], [241]).
Situational frequencies $PI_d/PI*100$; $PI_f/PI*100$	These percentages show in which condition the behaviors are more frequent respectively in relation to the water depth and flow. Both <i>deliberately chosen</i> and <i>passively suffered</i> behaviors are considered.
Situational frequency per water depth $PI_{d,t}/PI_d*100$	This percentage shows in which flow conditions the behaviors are more frequent given the same water depth, also in view of comparisons with previous works' general trends depending on the human kinematics [50], [99], [227], [231]. Both <i>deliberately chosen</i> and <i>passively suffered</i> behaviors are considered.

Table 13: Statistical frequencies of behaviors (and their meaning), evaluated with respect to the number of people (according to Table 12) and the floodwater conditions (in terms of water depth and flow).

Results are first discussed according to less and more frequent floodwater conditions in which behaviors are observed, then inferential statistical analyses are provided to assess relationships between situational frequencies. In particular, Chi-squared tests of independence are performed for categorical data by considering 3 sets of values expression of the performed behaviors and the specific conditions in which they occur, namely: (a) Behaviors x Water depth (14 x 2); (b) Behaviors x Water flow (14 x 4); (c) Behaviors x Water conditions (14 x 8) all of which measured in terms of PI [pp] so as to consider only behaviors actually performed (see Table 12). Finally, behavioral patterns are defined with respect to the most frequent floodwater conditions.

3.5.3 Comparing custom and generic evacuation simulators based on microscopic approaches

3.5.3.1 Background and research framework

This section aims to provide preliminary, innovative support to technicians and safety designers on how to adapt generic software to carry out quick and sustainable assessments of pedestrian safety in flooded outdoor spaces. A proper setup of an existing generic software based on microscopic evaluation modeling (Oasys MassMotion [254]), generally used for indoor evacuation analysis purposes, is provided to include main pedestrians' flood behaviors, thus focusing on a few simple setup parameters. Then, reliability analyses of such a setup-based generic model are provided according to literature standards and using a simple testing scenario (a linear and flat street), by analyzing different configurations on the selected setup parameters [130], [134], [155], [235].

First, comparisons with an existing custom flood simulation software are provided. Since the selected generic software adopts a Social Force Model (SFM) approach for the evacuation simulation [255], the selected custom simulator (Flooding Pedestrians' Evacuation Dynamics Simulator - FlooPEDS) [134] is similarly based on the same approach. FlooPEDS has been also developed and preliminarily validated according to real-world observations for flood evacuation purposes, as well as applied to real-world contexts for the analysis of risk-mitigation solutions [132]. Second, additional comparisons with observations of pedestrians' motion from real-world floods are also used to evaluate the setup-based generic software reliability [223], [256].

The testing scenario is quite simple and concerns stationary flood conditions where small compact groups of pedestrians are evacuating. Nevertheless, as in general aims of standard testing conditions for verification and validation of evacuation simulators [130], [134], [155], [235], if the comparison is not effective in such a simple scenario, more sensible differences between the simulators will surely appear in more complex POSs or conditions. Even though such kind of analysis cannot be always defined as a fair and exhaustive comparison (due to the peculiarities of the modeling logic and the specific conditions of real-world floods), however rough and preliminary evaluations of differences and behavioral uncertainties in simulation outputs can be provided (e.g. evacuation timing, trends of distances between pedestrians, and unmovable obstacles).

3.5.3.2 Basic criteria to replicate pedestrian behaviors

According to findings from the previous sections (results will be shown in §6) and from relevant literature research [51], [131], [134], [135], the characterization of the pedestrian behaviors in flood in the generic software is based on three main drivers: (1) the evacuation speed v_i [m/s], (2) the body instability, and (3) the attraction towards unmovable obstacles.

Concerning v_i , Equation 3.2 [223] calculates the experimental-based evacuation speed for a given floodwater depth D_f [m] and speed V_f [m/s] (g is the gravitational acceleration [m²/s]). The higher D_f and v_f , the lower the evacuation speed v_i . Additional differences in motion speeds depending on age, motion abilities, and gender can be considered by modifying the numerical parameters in Equation 3.2 [243].

$$v_i = 0.52 \left(\frac{D_f \cdot V_f^2}{g} + \frac{D_f^2}{2} \right)^{-0.11} \quad (3.2)$$

Concerning body instability, general consolidated thresholds for adults¹⁸ can be traced back to situations in which $D_f \geq 1.20\text{m}$, $V_f \geq 3.00\text{m/s}$, or $D_f V_f \geq 1.20\text{m}^2/\text{s}$ [227].

Previous works pointed out the possibility of considering homogeneous floodwater conditions for the street/square in the POS, or a part of it (e.g. the outdoor part between two consecutive crossroads), thus dividing the space in a grid [124], [131], [132], [136]. This choice can be sustainable since it reduces the implementation and computational complexity of local D_f and V_f effects on v_i and body stability. According to such an approach, in a full-scale application scenario, the motion space can be divided into different areas to represent streets/squares in the POS or a part of them (as for floors in the case of building evacuation simulators [254]). Each area can be characterized by D_f and V_f values which are constant in the area, but dynamic over the simulation time, depending on the floodwater spreading simulation [132], [191], [196], [220].

Concerning the attraction towards unmovable obstacles, literature data concerning real-world observations of pedestrian behaviors along flooded streets noticed that pedestrians prefer to stay closer than about 3m from building walls, fences, and other continuous and unmovable elements in any case [134].

¹⁸ Pedestrians with a mass per height higher than 50 [kg·m].

3.5.3.3 *Tested scenario*

The setup-based version of MassMotion and FlooPEDS are applied to the same typological scenario for comparison purposes. The tested scenario is quite simple in adherence with the consideration of the previous subsection (see also §11.5.1), and it consists of a linear and flat pathway representing a common outdoor open space such as a street, with stationary flood conditions and small compact groups of pedestrians evacuating. This configuration allows focusing on the pedestrians' elementary motion contingencies since constant floodwater conditions are imposed¹⁹. In this sense, it is representative of a street for a simple but critical layout in urban open spaces and it is also consistent with the IMO (International Maritime Organization) test 1 layout [155]. Indeed, as in the general aims of standard testing conditions for verification and validation of evacuation simulators, if the comparison is not effective in such a simple scenario (that is considering linear trajectory by the pedestrians, stationary environmental conditions over time and space, small groups of pedestrians, flat and linear pathway), more sensible differences between the simulators will surely appear in more complex POSs or conditions (e.g., due to unexpected variability in human behavior, presence of floating obstacles).

In detail, this testing scenario is 17.6m wide and 87m long, with no internal crossroads. Two continuous buildings are considered placed alongside the pathway, one on each pathway side. It hence represents a typical real-world urban built environment, i.e. composed of orthogonal urban fabric, according to previous FlooPEDS testing conditions [134]. Section §11.5.2 (Appendices) resumes the overall details on the setup of the generic software for the scenario implementation, while runs performed with FlooPEDS according to previous works results consider a cad file representing the same scenario.

The following general rules are applied for simulations in the tested scenario reference work for both MassMotion and FlooPEDS [134]. Tests are carried out by considering compact groups of 10 pedestrians per side starting the evacuation at the same time, to point out the overlapped effects of SFM attractions between the pedestrians themselves, and between the pedestrians and the buildings. The number of simulated pedestrians is provided by considering that the average number of exposed pedestrians (coming from buildings) per square meters of outdoor open spaces could refer to low-density conditions (LOS A, free circulation, lower than 0.08pp/m² [257]). Such values are consistent with input data on pedestrians' densities from previous works [135], [230]. Pedestrians are generated at the start of the pathways, being initially placed at a maximum distance of about 3.5m from the building. They move towards the end of the pathway, where the evacuation test is considered to end.

3.5.3.4 *Setup criteria: variable parameters of the generic simulator*

The properties of *portals* and *servers* are the variable parameters for the setup of MassMotion (see Section §11.5.2 (Appendices)), thus pursuing a sustainable and rapid configuration of the generic software for flood evacuation simulation. *Portals* represent both the entrances into the simulation and the pedestrians' destinations. *Servers* are used to model queues and, more in general, to vehiculate the pedestrians' movements and behaviors, therefore they can be used to model pedestrian-unmovable obstacles attraction without modifying the source code. The following criteria

¹⁹ There is no influence due to the floodwater direction and so effects of pedestrian-pedestrian and pedestrians-obstacles interactions can be better highlighted.

for the setup configurations of *portals* and *servers* are considered, as graphically resumed in Figure 16 and Table 14:

1. *Entrance portals shape*. Two configurations are tested to represent the moment from the building exit by pedestrians who try to start the evacuation together, because of group behaviors:
 - a. in the *rectangular* one, entrance *portals* have a dimension of 3x1m and are adjacent to the walls. The pedestrian density is about 3pp/m² in order to increase the interaction between them, starting the simulation closer to each other and lower than 3.0m away from the unmovable obstacle;
 - b. in the *squared* one, where entrance *portals* have a dimension of 3x3m and are placed 1m away from the walls. The pedestrian density is about 1pp/m² to replicate the custom simulator starting setup.
2. *Servers number, positioning, and properties*. Servers are placed along the pathway (in the following, “first servers”) and at the end of the *floor*, that is near the exit *portals* (in the following “second servers”) to simulate the attraction of the pedestrians towards the buildings. Considering the *floor*'s length, each pedestrian's journey is aimed at using: 1 entrance *portal* at the beginning of the *floor*, 1 “first server” placed along the *floor*, 1 “second server” at the end of the *floor*, and finally 1 exit *portal*. The reference work distinguishes three main classes of distance from unmovable obstacles: 0 to 1m, 1 to 2m, and 2 to 3m [134]. Therefore, three “first servers” per side of the *floor* are tested. An alternative configuration of only two “first servers” is also studied to increase the interaction between pedestrians. In both cases, only one “second server” per side of the *floor* is tested to increase the attraction of unmovable objects near the crossroads. These multiple setups are evaluated by placing servers in the middle (e.g. for the 0 to 1m class, 0.5m) or at the maximum value of each distance class (in the same example, 1m). Furthermore, the “first servers” position along the pathway is tested according to three configurations, according to a parametric approach. Tested positions are at *halfway*, at *a quarter*, and at *an eighth* of the pathway. These configurations allow investigating the impact of interferences between pedestrians at the passage points (i.e. servers), hence if behavioral uncertainties towards the unmovable obstacles exist. Finally, the probability that a pedestrian selects one of the “first servers” is assumed according to two configurations: *homogeneous*, if each element has the same probability; *by-literature*, according to the real-world observations about the frequency for each class of distance from unmovable obstacles.

These criteria lead to obtaining 36 different setups, which are organized by grouping them by the entrance *portal* shape (R for rectangular; S for squared - in yellow in Figure 16) and the “first servers” position along the pathway (8 for position 1/8 of the path length; 4 for position 1/4 of the path length; 2 for position 1/2 of the path length - in magenta in Figure 16), as shown in Figure 16. Furthermore, each group of setups is also characterized by the probability a pedestrian can choose a *server* (H: homogeneous; L: by-literature), and the *servers*' number and position with respect to the wall (in orange in Figure 16), as resumed in Table 14.



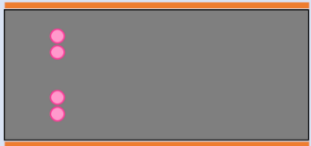
			Entrance portals shape		
			Rectangular (3*1m) - R	Squared (3*3m) - S	
First servers positioning in respect to the start	Halfway - 2	43.50m		<p style="text-align: center;"><u>GROUP R1</u></p> AH2R BL2R AL2R CL2R BH2R DH2R	<p style="text-align: center;"><u>GROUP S1</u></p> AH2S BL2S AL2S CL2S BH2S DH2S
	A quarter - 4	21.75m		<p style="text-align: center;"><u>GROUP R2</u></p> AH4R BL4R AL4R CL4R BH4R DH2R	<p style="text-align: center;"><u>GROUP S2</u></p> AH4S BL4S AL4S CL4S BH4S DH4S
	An eight - 8	10.87m		<p style="text-align: center;"><u>GROUP R3</u></p> AH8R BL8R AL8R CL8R BH8R DH8R	<p style="text-align: center;"><u>GROUP S3</u></p> AH8S BL8S AL8S CL8S BH8S DH8S

Figure 16: Organization of the setup groups depending on the entrance portals' shape (columns) and the "first servers" position along the pathway (rows). The setup code is composed of four characters: the number and position of the servers with respect to the wall (A-B-C-D) as in Table 14, the probability a pedestrian can choose a server (H-L), the server position with respect to the start (2-4-8), and the shape of the entrance portal (R-S). Entrance portals are in yellow, exit portals in red, first servers in magenta, and buildings walls in orange.

Setup code	"First servers" features		"Second server" features	
	Number [-]	Distance from the wall [m]	Number [-]	Distance from the wall [m]
A	2	1; 2	1	1
B	2	0.5; 1.5	1	0.5
C	3	0.5; 1.5; 2.5	1	0.5
D	2	1; 2	1	0.5

Table 14: Setup code for the servers' position by considering their number and distance with respect to the side of the floor (i.e., the walls of the buildings).

3.5.3.5 Simulation outputs and comparison criteria

Simulations are repeated 10 times due to the probabilistic rules in motion simulation [155]. Table 15 summarizes the outputs of the simulations performed through the generic and the custom software. They are selected in order to provide both a macroscopic (EC , t_{max} , W , and F) and a microscopic (D_w trends) description of the models, together with the necessity of comparison with real-world observations (D_w percentage distribution).

The comparison between the graphical outputs (i.e., EC and D_w trends) is performed according to previous works Key Performance Indicators (KPIs) resumed in Table 16 [155], [162]. Results are discussed through KPIs mean and standard deviation values for each of the 6 setup groups identified in Figure 16, while extended results for all the 36 setups are reported in Section §1.5.5 (Appendices).

OUTPUT	DESCRIPTION
Graphical outputs	
Evacuation Curves EC	Evaluated as the percentage of arrived pedestrians [%] over the simulation time [s]. The average evacuation curve is considered for each tested condition.
D_w trends [m]	Distance between each pedestrian and the side of the building during the evacuation tracked over the pathway length. The outcoming curves describe how the attraction from unmovable obstacles affects the pedestrians' trajectory along the path, depending on the input setup. To elaborate such curves, D_w data are organized in quartiles. Data are grouped over 3m-long pathway steps, according to the distance threshold for repulsive phenomena in motion considered by FlooPEDS and based on previous works relating to the SFM
Numerical outputs	
Maximum evacuation time t_{max} [s]	The overall time during which the pedestrians remain in the outdoor BE.
Waiting time percentage W [%]	Calculated as the maximum waiting time t_w [s] (i.e., that is the time in which a pedestrian remains stationary at a <i>server</i>) normalized by the maximum evacuation time t_{max} . This parameter evaluates the impact of possible queuing phenomena simulated by the generic simulator at the <i>servers</i> and considers how the effect of group dynamics can force pedestrians to spend time in non-movement activities because of simulator logic (in MassMotion, <i>servers</i> attract people towards the buildings but could represent deadlocks).
Evacuation flow F [pp/s]	Calculated as 5-to-95 th percentiles of pedestrians to estimate the speediness of the evacuation process on a sample of 100 pedestrians (10 simulation repetitions of scenarios involving 10 pedestrians) to reduce the impact of outliers due to particular simulation aspects in crowd motion [155], [258], such as those related to starting positions less or more favorable, neighbors behaviors, deadlocks phenomena, etc.
D_w percentage distribution [%]	Percentage distribution of the distance between each pedestrian and the side of the building during the evacuation tracked over the pathway length, evaluated by considering the three literature-based main classes [134]: lower than 1m; from 1m to 2m; higher than 2m.

Table 15: List of parameters for the comparison between the generic and the custom simulator.

KPI	MEANING
Secant Cosine SC [-]	to measure the differences in shape between two curves, as their first derivative (for SC next to 1, the shapes of the curves can be considered similar)
Euclidean Relative Difference ERD [-]	to measure the overall agreement between two curves, as the norm of the difference between two vectors (for ERD next to 0, the curves can be considered close)
Euclidean Projection Coefficient EPC [-]	to measure the scale factor, which is the best possible fit between two curves (for EPC next to 1 the curves can be considered similar)
Difference between the graphic Areas Under the Curves $DAUC$ [%]	to investigate if underestimating/overestimating contingencies exist (positive values point out that predictions for the generic simulator are over those of the custom one)

Table 16: KPIs to perform the comparison between the graphical outputs (evacuation curves EC and D_w trends) and their meaning [155], [162].

Finally, the criteria for the comparison between the numerical outputs (i.e., t_{max} , F , W , and D_w percentage distribution) are resumed in Table 17. Quartile-based analyses are organized depending on the shape of the *portals* to describe general uncertainties for the whole set of considered input setups, then notable values are compared with custom software and real-world observations. Concerning the percentage distributions, differences due to the modeling logic at both microscopic and macroscopic levels are assessed to be compared with acceptability thresholds, which are up to about 10%-20% [103], [258], [259].

OUTPUT	COMPARISON CRITERIA
t_{max} [s]	Quartile-based analyses and comparison with custom software outputs
F [pp/s]	Quartile-based analyses and comparison with custom software outputs
W [%]	Quartile-based analyses
D_w percentage distributions [%]	Comparisons with custom software and real-world observations

Table 17: Numerical outputs comparison criteria: as the custom simulator does not consider deadlocks in the building attraction, W outputs are discussed independently to evaluate the impact of the queuing phenomena on the evacuation timing in the generic simulator.

3.5.4 Evaluating how pedestrian evacuation behaviors influence the flood risk in riverine HCCs

3.5.4.1 Background and research framework

As for other kinds of disasters such as earthquakes, fire, and terrorist acts [22], [260], [261] and according to the previous, general definition of disaster risk reduction²⁰, flood risk assessment depends on the combination of the *vulnerability* of the HCC (and, in particular, the *physical vulnerability*), the *hazard*, and the *exposure* (see §2.1). Most of the current approaches generally only take into account *physical vulnerability* and *hazard* evaluations [30], [31], [35] or just combine such factors with the number and location of exposed individuals [36]. Besides, existing approaches generally provide mesoscale results to suggest risk-mitigation strategies concerning the best position of gathering areas in wide urban scenarios and the modification to the emergency path configurations with respect to the layout [124], [135], [221]. At the same time, contrarily to other kinds of disasters affecting the urban layout such as earthquakes [48], the meso- and micro-scale analyses of the outdoor spaces affecting the pedestrians' safety seem to be generally neglected [134], although differences in HCC layout can imply differences in flood risks. Furthermore, a limited number of research combines the number of exposed pedestrians, their evacuation behaviors, and the emergency management strategies adopted [124], [262], while no work directly addresses the particular but widespread context of riverine HCCs and risk assessment with and without evacuation behaviors, which can lead to underestimating or overestimating the risk.

Within this context, this section of the thesis provides a new, innovative methodology to compare how accounting or not accounting the pedestrian evacuation behaviors can affect flood risk assessment and emergency strategies evaluation. Previously defined typological POSs are adopted as case studies, and existing tools for hydrodynamic and pedestrian evacuation simulation are applied to them. The latter, in particular, exploits the same setup configuration tested in the previous section on a generic simulator. Risk indexes for the whole POSs (mesoscale) and each of its street/square (microscale) are provided to assess the risk with and without the pedestrian evacuation behaviors, by innovatively adopting the two scales of application in a combined manner:

- the mesoscale analysis, concerning the POS as a whole, can globally compare and rank different POSs and emergency management strategies;
- the microscale analysis, concerning each outdoor space (street, square, or a part of them) can provide data on where and how to introduce interventions for supporting the pedestrians' evacuation in each typical HCC.

²⁰ <https://www.undrr.org/terminology>, last access: 10/12/2020

3.5.4.2 Simulation criteria and outputs organization

The first part of the proposed methodology concerns the definition of the case studies, which mainly consists of:

- 1) The choice of testing scenarios (*physical vulnerability*), which are the typological POSs in riverine HCCs introduced in subsection §3.3, and are shown in Figure 17 to ease the read;
- 2) The pedestrian evacuation behaviors simulation (*exposure*), which are performed through the setup-based simulator introduced in §3.5.3. In particular, two different evacuation strategies are considered (i.e., choice of the evacuation target), namely “*leaving*”, in which the gathering areas are placed at the downstream exit of the POS, or “*sheltering*”, in which the gathering areas are placed in streets and squares characterized by more favorable hydrodynamic conditions (i.e., outdoor spaces where the maximum $D_f V_f$ is lower than $0.6 \text{ m}^2/\text{s}$). The shortest path approach is adopted, and pedestrians cannot move upstream or towards the river, as in experimental-based behaviors [134].
- 3) The river overflow (*hazard*), whose modeling is resumed in the next §3.6, allows tracing the hydrodynamic conditions established in the typological POSs in terms of D_f , V_f , $D_f V_f$. In particular, such parameters are used to depict pedestrian motion behaviors by considering their maximum values (namely, D_i and V_i , which are used to calculate the *pedestrian speed* v_i according to Equation 3.2, and $DV_{\max,i}$ [m^2/s] to evaluate ultimate stability thresholds)²¹.

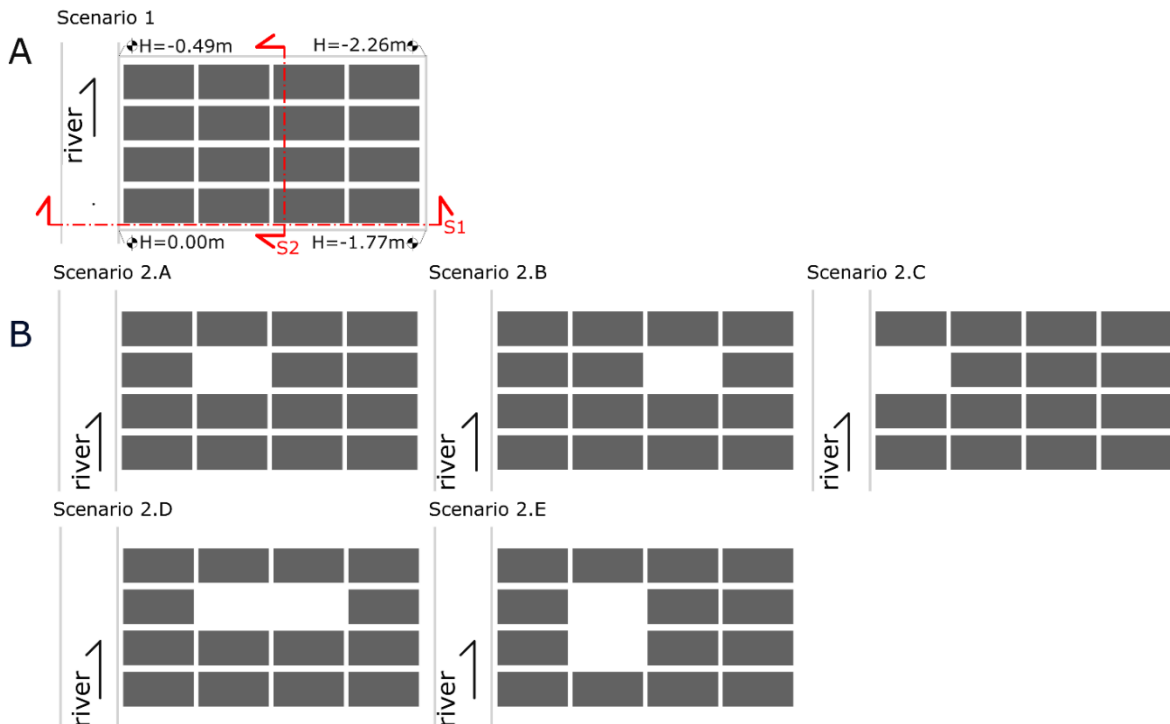


Figure 17: Typological POSs as testing scenarios (A: compact layout; B: layouts including a square). More details at §3.3.

Evacuation simulations are performed by considering an overall simulation time t_{sim} [s] of 20 minutes (1200 s), which is a time span long enough within which DV reaches its maximum values in the

²¹ Each parameter is also analyzed to point out if general homogeneous conditions of floodwater spreading in the POSs exist over time, by verifying that their variations are lower than 10%.

POSSs, and that ensures that v_i and DV_i variations are lower than 10%. This threshold allows considering simplified quasi-constant environmental conditions affecting pedestrian motion [134]. Moreover, in view of the general timeline for flood emergency management [263], the simulation time is compliant with previous works on evacuation simulations in the urban environment focusing on the evacuation process [134]. Accordingly, the final setup concerned the following points:

- the pedestrian speed v_i in each street/square of the typological POSSs depends on the D_f and V_f conditions where he/she is placed, according to Equation 3.2;
- pedestrians placed where $DV_i \geq 1.2 \text{ m}^2/\text{s}$ are considered unable to arrive at a gathering area, thus being trapped in the outdoor spaces;
- pedestrians move along “preferential lanes”²² placed 1m and 2m far from the building walls, to replicate attraction towards unmovable obstacles. Simulation interactions between the pedestrians along these “preferential lanes” could provide variations of distance values between the pedestrian and the unmovable obstacles, thanks to pedestrian-pedestrian repulsive phenomena in motion.

In the next subsections, the simulation results are organized into KPIs concerning only the *physical vulnerability* and the *hazard* modeling (§3.5.4.3) or including the *exposure* too (§3.5.4.4). Finally, KPIs are organized into Risk Indexes with and without considering pedestrian evacuation behaviors (§3.5.4.5). Both KPIs and Risk Indexes are designed to range from 0 (no impact on risk) to 1 (maximum impact), and are arranged by distinguishing the conditions of:

1. the overall POS, according to a mesoscale standpoint, thus providing a unique value for each typological POS, expressed by the indexes subscript M ;
2. each outdoor space in the POS, according to a microscale standpoint, thus providing, for each typological POS, a specific value for each outdoor space, expressed by the indexes subscript m . In addition, a map view is offered to graphically trace the risk values on the POS layout.

3.5.4.3 KPIs based on physical vulnerability and flood hazard

Table 18 resumes the KPIs concerning physical vulnerability and flood hazard, in view of the floodwater spreading simulation results.

According to the microscale point of view, DV_i maps over the POS layouts are firstly traced to investigate the role of intrinsic features for streets and squares in the floodwater spreading in the typological POS scenarios. DV_i are organized into five risk classes considering the related conditions for adults’ stability [227]: 1) *safe*, that is a null risk if DV_i is equal to $0.0 \text{ m}^2/\text{s}$; 2) *low*, if up to $0.6 \text{ m}^2/\text{s}$; 3) *moderate*, if ranging from 0.6 to $0.8 \text{ m}^2/\text{s}$; 4) *significant*, if ranging from 0.8 to $1.2 \text{ m}^2/\text{s}$; 5) *extreme*, if over $1.2 \text{ m}^2/\text{s}$.

Then, the mesoscale standpoint is investigated through the *average $D_f V_f$ value weighted by the outdoor spaces areas $DV_{a,M}$ [m^2/s]*, which considers all the DV_i values of the outdoor spaces and sub-spaces in the POS. $DV_{a,M}$ is normalized by the upper limit of stability ($1.20 \text{ m}^2/\text{s}$) to provide the

²² “server” objects, characterized by “a conceptual entry point”, “an exit point” and a connecting line along which the simulated pedestrians can move according to queuing-based criteria to maintain their overall trajectory (see 11.5.2).

stability index for the whole POS $I_{DV,M}$ [-]. Thus, $I_{DV,M}$ can compare different scenarios. This work assumes $I_{DV,M} = 1$ in case of $DV_{a,M} > 1.20 \text{ m}^2/\text{s}$ to stress similar unacceptable conditions for stability.

In a similar manner, the *stability index for each outdoor space* $I_{DV,m}$ [-] depends on the ratio between $DV_{max,i}$ [m^2/s] and the critical threshold for adults' stability ($1.20 \text{ m}^2/\text{s}$), thus analyzing risks from a microscale standpoint. In addition, the *normalized distance of the outdoor space from the river* $D_{r,m}$ [-] takes into account the Euclidean distance between the river and the barycentre of each outdoor space or sub-space (d_r). In particular, it depends on $d_{r,MAX}$ [m], which is the maximum d_r value in the POS, and it ranges from 0 to 1.

KPIs name, symbol [unit of measure]	KPIs calculation method	Evaluation of results
Average DV value weighted by the outdoor space areas, $DV_{a,M}$ [m^2/s]	$DV_{a,M} = \frac{\sum DV_i A_i}{\sum A_i}$ [Eq. 2]	The higher $DV_{a,M}$, the more critical the overall POS conditions for stability
Stability index for the POS $I_{DV,M}$, and for each outdoor space $I_{DV,m}$ [-]	$I_{DV,M} = \min\left(\frac{DV_{a,M}}{1.20 \text{ m}^2/\text{s}}, 1\right)$ [Eq. 3]	The higher this index, the more probable the loss of body stability (maximum value equal to 1)
	$I_{DV,m} = \min\left(\frac{DV_{max,i}}{1.20 \text{ m}^2/\text{s}}, 1\right)$ [Eq. 4]	
Normalized distance from the outdoor space to the river $D_{r,m}$ [-]	$D_{r,m} = 1 - \frac{d_r}{d_{r,MAX}}$ [Eq. 5]	The higher $D_{r,m}$, the more rapid the arrival of the flood because of the shortest distance from the river

Table 18: KPIs for the microscale and mesoscale risk assessment concerning physical vulnerability and hazard.

3.5.4.4 KPIs based on exposure

Evacuation simulation results are organized into the mesoscale-related KPIs described in Table 19. These KPIs trace the effects of interactions between pedestrians and floodwaters, depending on the adopted emergency evacuation strategy.

Considering 240 simulated pedestrians P [pp]²³, the following values are assessed for each scenario: (1) the maximum evacuation time $t_{max,evac}$ [s], that is the evacuation time of the last pedestrian arriving at a gathering area; (2) the longest evacuation path d_{max} [m]; and (3) the number of pedestrians unable to arrive in a gathering area n_a [pp]. Maximum values are considered according to a conservative approach in simulation evaluations since they offer different evacuation-related issues depending on the DV conditions in the outdoor spaces [134].

If at least 1 pedestrian has to stop because of DV conditions, $t_{max,evac}$ is conservatively assumed as the overall simulation time t_{sim} [s], that is 1200s (20 minutes). The pedestrian flow at the gathering areas f_{e95} [pp/s] is calculated considering the 5th to 95th percentiles of pedestrians who can reach a gathering area. In this way, it is possible to exclude effects due to pedestrians who are: (1) initially placed in a particularly favorable position, such as close to the gathering areas, by referring to the 5th percentile as a threshold; or (2) involved in critical conditions for the evacuation flows, such as queuing

²³ The number of simulated pedestrians has been defined to reproduce free-flow walking conditions for pedestrians placed along the streets before the flood. The threshold of pedestrians' densities $\leq 5.6 \text{ m}^2/\text{pp}$ is adopted according to the Level of Service A threshold, according to which pedestrians move in desired paths without altering their movements in response to other pedestrians" [207]. The pedestrians were homogeneously positioned in the POS at the event peak time, to conservatively represent pedestrians, such as visitors, who cannot reach a building and move upstairs [36], [122], [223].

phenomena, by referring to the 95th percentile as a threshold. The maximum value $f_{e95,MAX}$ [pp/s] for all the compared POS scenarios is also used as pointed out in Table 19.

KPIs name, symbol [unit of measure]	KPIs calculation method	Evaluation of results
Normalized evacuation time, $T_{e,M}$ [-]	$T_{e,M} = \frac{t_{max,evac}}{t_{sim}}$ [Eq. 6]	The higher $T_{e,M}$, the higher the time a pedestrian is exposed to risk
Normalized traveled distance, $D_{t,M}$ [-]	$D_{t,M} = \frac{d_{max,i}}{d_{MAX}}$ [Eq. 7]	The higher $D_{t,M}$, the higher the possibility for the pedestrian to face additional threats (e.g. DV condition, obstacles dragged by floodwaters)
Percentage of non-arrived pedestrians, $N_{a,M}$ [-]	$N_{a,M} = \frac{n_a}{P}$ [Eq. 8]	Higher $N_{a,M}$ values relate to higher risk
Presence of trapped pedestrians in a given outdoor space, $N_{a,m}$ [boolean]	$N_{a,m} = 1$ if $\frac{n_a}{P} \geq 0.05$; $N_{a,m} = 0$ elsewhere [Eq. 9]	Higher $N_{a,m}$ values relate to higher risk due to loss of stability or latecomers in the given outdoor space
Normalized pedestrian flow, $F_{e,M}$ [-]	$F_{e,M} = 1 - \frac{f_{e95}}{f_{e95,MAX}}$ [Eq. 10]	“Slower” evacuations are characterized by “lower” $f_{e,95}$ values. Thus, higher $F_{e,M}$ values represent higher risk, since pedestrians take longer to reach shelters.

Table 19: KPIs for the mesoscale and microscale risk assessment concerning pedestrian evacuation behaviors.

Finally, from a microscale analysis standpoint, the *presence of trapped pedestrians in a given outdoor space*, namely $N_{a,m}$ [boolean], is evaluated. $N_{a,m}=1$ is conservatively assumed if the percentage of trapped pedestrians in the outdoor spaces is equal to or higher than $0.05 \cdot P$, according to general criteria for fire safety and evacuation simulation assessment [264]. In fact, this threshold considers the effective risk conditions of 95% of the pedestrians, thus limiting the effects of local conditions affecting latecomers’ motion such as the initial positions of pedestrians, or the uncertainties in pedestrian interactions in the simulation model [162], [258]. Elsewhere, $N_{a,m}=0$.

3.5.4.5 Risk Indexes with and without the evacuation process

Risk Indexes are calculated by excluding and including evacuation-related issues, both at the mesoscale and microscale levels, by combining the KPIs through the Analytic Hierarchy Process methodology [265]²⁴. The Analytic Hierarchy Process allows assigning priorities to the KPIs, which are assumed as criteria, according to pairwise comparisons between them. Each KPI weight W_k [-] permits a distinct evaluation between the single criterion importance and its global impact on the overall risk rating. Finally, KPIs are combined through Eq. 3.3, which outlines a *generic Risk Index RI* through the normalization with respect to its maximum value, where p is the overall number of KPIs considered for the *RI* calculation. In particular, Equation 3.3 is based on the *RI* representation according to the Euclidean norm of a vector in a vector space of dimension equal to p and has a field of existence included in the range $[0, 1]$, where 0 is the minimum risk and 1 represents the maximum risk. A classification of *RI* values is also proposed as follows to perform comparisons: $RI < 0.15$; $0.15 \leq RI < 0.30$; $0.30 \leq RI < 0.45$; $0.45 \leq RI < 0.60$; $0.60 \leq RI < 0.75$; $RI \geq 0.75$.

²⁴ Analytic Hierarchy Process calculator available at : https://bpmmsg.com/academic/ahp_calc.php (last access: 10/06/2020).

$$RI = \sqrt{\frac{\sum_{k=0}^p W_k^2 \cdot KPI_k^2}{\sum_{k=0}^p W_k^2 \cdot 1^2}} \quad \text{Eq. 3.3}$$

For what concerns the risk indexes *without pedestrian evacuation behaviors*:

- The *mesoscale* index $RI_{POS,M}$ [-] is equal to IDV,M .
- The *microscale* index $RI_{POS,m}$ [-] considers IDV,m and $D_{r,m}$ by reasonably assuming that both of them have the same priority since they refer to POS and flood-related conditions ($W_k=0.5$).

On the other hand, the risk indexes *with pedestrian evacuation behaviors* are founded on the KPIs defined in Table 20. In particular:

- For the *mesoscale* index $RI_{evac,M}$ [-], it is assumed that IDV,M and $N_{a,M}$ are the most important indicators since they describe the effect of POS conditions on *pedestrian evacuation behaviors*. Hence, when focusing on data related to each pedestrian, the priority is given to the possibility of reaching a gathering area rather than to the evacuation time and distance. Furthermore, $T_{e,M}$ and $F_{e,M}$ are considered on the same level of importance being both time-dependent indicators, even if they represent different evacuation issues.
- For the *microscale* index $RI_{evac,m}$ [-] three KPIs were considered on the same level of importance.

Table 20 resumes the weight calculation for $RI_{evac,M}$ and $RI_{evac,m}$, having a Consistency Ratio CR under acceptability thresholds ($CR_M=0.3\%<10\%$; $CR_m=0\%<10\%$).

KPI	mesoscale RI _M				microscale RI _m			
	$T_{e,M}$	$D_{t,M}$	$N_{a,M}$	$F_{e,M}$	IDV,M	$D_{r,m}$	$N_{a,m}$	IDV,m
W_k [-]	0.076	0.148	0.380	0.076	0.320	0.333	0.333	0.333

Table 20: weights W_k for RI with pedestrian evacuation behaviors obtained via Analytic Hierarchy Process.

Finally, due to their existence field $[0, 1]$, the proposed risk indexes are used as comparing elements to point out:

- *the differences of RI with and without pedestrian evacuation behaviors*, from both mesoscale and microscale standpoints, by discussing reasons for differences, also in relation to the outdoor spaces (using risk maps in the POS layout);
- *according to a “mesoscale” point of view*: a) for *RI without pedestrian evacuation behaviors*, differences of risk levels in different typological POS scenarios; b) *RI with pedestrian evacuation behaviors*, how different emergency evacuation strategies can affect the pedestrians' safety, by comparing “leaving” to “sheltering” strategies;
- *according to a “microscale” point of view*, to highlight the main outdoor spaces in the POS where the risk is higher and risk-reduction interventions should be hence applied, by discussing differences due to *RI with and without pedestrian evacuation behaviors*.

3.5.5 Optimizing shelters and evacuation paths in flood-prone HCCs based on pedestrian behaviors

3.5.5.1 Background and research framework

Although comparisons of different types of emergency management strategies were made in the previous section (namely, “leaving” and “sheltering”), uncertainties still concern the optimization of gathering areas (i.e., their number and position), the best evacuation paths to reach them, and how to allocate pedestrians to evacuation units [126], [266], [267]. Evacuation solutions in case of natural disasters are generally addressed through macroscopic approaches (i.e., by routing algorithms on graphs [126], [267], [268]). In particular, they are mainly based on optimization problems and are particularly suitable for scenarios characterized by [109]: wide application scales, complex geometries (e.g., street networks), low-density conditions, monodirectional flows, and few interactions between pedestrians. Prescriptive models are widely exploited to compute optimized evacuation plans [125], [126]. Between them, mathematical programming emerges as the main prescriptive methodology for evacuation planning and disaster management [127], with models focused on evacuation paths [125] or on gathering area locations [128]. For instance, in the case of earthquake emergencies, many studies adopt the Dijkstra algorithm approach to evaluate the safest paths depending on factors such as obstruction, visibility, and the capability of the streets [269], [270]. For what it concerns floods, classic approaches rely on the evaluation of the shortest path [271], [272] or the shortest time [273], but there are still actual uncertainties (especially at the micro- and mesoscale, i.e., public open spaces and sub-spaces) about the right approach for the path choice (e.g., if the shortest, the quickest, or the less effortful path), and consequently on how, where, which, and how many gathering areas and evacuation paths are needed to guarantee the pedestrians’ safety.

To this end, this section will introduce a new methodology to evaluate the best evacuation solutions in case of floods in HCCs, and in particular to optimize the number and position of gathering areas together with the evacuation paths to reach them depending on the approach for the path choice. The application scenario is the riskiest typological POS between those tested in the previous sections, assuming the same hydrodynamic conditions (see §3.6) to derive the pedestrians’ motion conditions (i.e., speed v_i , stability $D_f V_f$, and effort $D_f V_f S$ to trace a correlation between the path length and the faced floodwater conditions [236]). Since in previous sections evacuation planning and management are addressed through microscopic approaches, a final comparison is also provided through a Risk Index RI [-] that jointly considers aspects inherent to the urban layout (*physical vulnerability*), the human factor (*exposure*), and the event intensity (*hazard*) to point out possible differences between the two modeling approaches.

3.5.5.2 Evacuation optimization through Integer Linear Programming

The street network of the typological POS is described by an oriented graph $G = (V, E)$ (shown in Figure 18) where:

- nodes $V = \{1, \dots, |V|\}$ are associated with the barycentres of all the streets and crossroads (indicated with numbers), plus the vertices and the barycentres of the four quadrants that compose the square²⁵ (indicated with letters).

²⁵ The variations of all the parameters D, V, DV, and V_p are $\leq 10\%$ within the reference area of each node.

- links $(u,v) \in E = \{1, \dots, |E|\}$ are associated with segments of streets (or paths in the square) connecting nodes u and v . Possible movement directions of the pedestrians are defined considering that pedestrians always move away from the source of hazard and cannot move upstream [134], [186]. Thus, links corresponding to streets parallel to the river are not oriented (and therefore can be traveled in both directions), whereas those corresponding to perpendicular and oblique streets are oriented (away from the river). However, exceptions to these rules occur when moving upstream is the only way to stay in the testing scenario, as in the case of the streets furthest from the river.

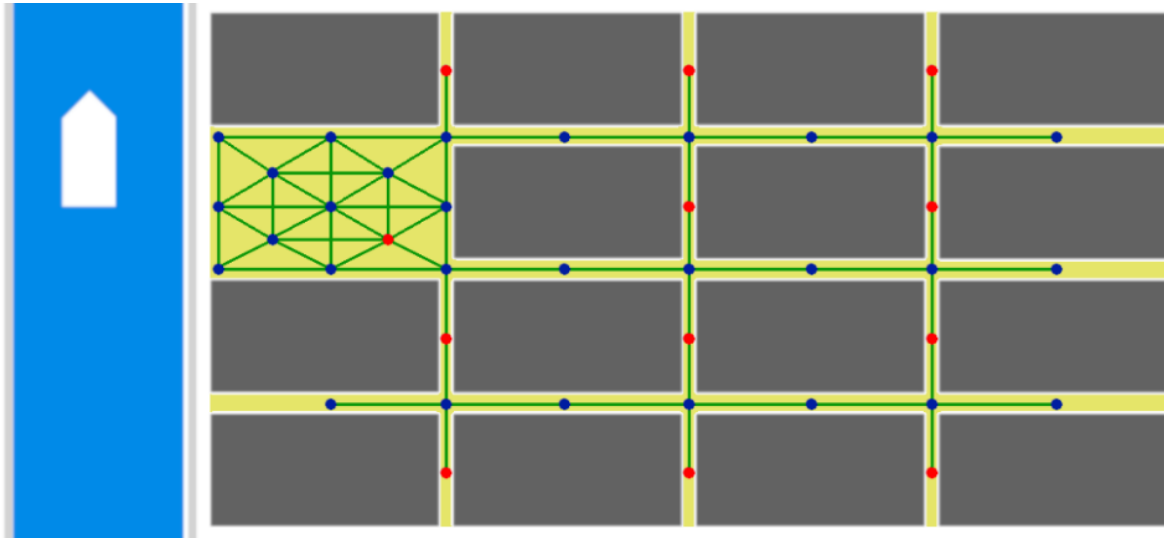


Figure 18: Illustration of the graph that models the street network. Blue dots are starting points; red dots can be both starting points and/or potential shelters. Links are marked in green: those parallel to the river can be traveled in both directions, the others only away from the river.

In order to model the optimal evacuation problem in terms of a particular minimum cost flow problem on G , nodes are considered as:

- starting points (41 blue and red nodes in Figure 18), in which 240 pedestrians are homogeneously distributed to reproduce random positions before the event (86 pedestrians in the square, 11 pedestrians in each street perpendicular to the river, and 4 pedestrians in each street parallel to the river);
- potential gathering areas (12 red nodes in Figure 18), which will be chosen on the basis of the hydrodynamic conditions (basically dry or quasi-dry areas where $D_f V_f \approx 0 \text{ m}^3/\text{s}$) obtained from the hazard simulation (see sections §3.6 for modeling criteria, and §8.1 for the following results). In particular, the gathering areas placed in the parallel streets simulate the entrance to indoor safe areas, while the gathering areas in the square simulate an outdoor, raised safe area.

The pedestrians' motion conditions during the evacuation, which depend on the hydrodynamic conditions of the floodwater spreading within the typological POS, are modeled by associating a *cost* c_{uv} to each link (u,v) of the graph that takes into account the *human speed* and the *stability* computed by Eq. (3.2). Clearly, links connecting dummy nodes have dummy costs: for all $u \in V$, $c_{uu} = 0$ and $c_{uz} = \text{big}C$ where *big* C is a big-enough constant needed for implementing the hierarchical optimization described below.

Different scenarios are defined depending on the approach i (being $i = 1 \rightarrow 3$) adopted for the path choice, i.e., the shortest, the quickest, or the cheapest (see Table 21), and the number M (being $M = 1 \rightarrow 12$) of available gathering areas. For each scenario (i, M) , the model hierarchically minimizes the number $N_{a(i, M)}$ of pedestrians who cannot complete the evacuation and the sums of the costs $[\sum_{(u,v) \in E} c_{uv}]_{i,M}$.

i	Approaches for the path choice	Criteria for the optimal solution calculation	Link Cost c
1	Shortest	Minimization of the evacuation length	S [m]
2	Quickest	Minimization of the evacuation time	T [s]
3	Cheapest	Minimization of the evacuation effort	$DV \cdot S$ [m ³ /s]

Table 21: Definition of the approaches for the path choice and their calculation method depending on the link cost. Links with $D \geq 1.20m$, $V \geq 3.00m/s$, or $DfVf \geq 1.20m^2/s$ cannot be traveled [227]. The time T is evaluated as the ratio between S and v_i in each link.

The minimum cost flow on G which uses at most M available shelters is formulated as an Integer Linear Program (ILP), and solved through the commercial package IBM-CPLEX²⁶ (see Section §11.7 for further modeling details). As a result, 36 different optimal solutions are obtained, organized in 3 sets (one for each approach for the path choice) of 12 (depending on the number of gathering areas available). The optimal solution of scenario (i, M) provides:

- the gathering area(s) position that minimizes the cost with respect to the adopted approach for the path choice;
- the evacuation paths to arrive at the gathering areas from each node of the graph;
- the number of pedestrians who cannot complete the evacuation $N_{a(i,M)}$;
- an array $C_{AVG(i,M)} = [S_{AVG}; T_{AVG}; DVS_{AVG}]_{i,M}$ listing the mean cost values evaluated with respect to the $(240 - N_{a(i,M)})$ pedestrians who manage to conclude the evacuation.

Since the model acts as a decision-maker that coordinates evacuation operations, evacuation paths are assigned to pedestrians in a collaborative setting. Moreover, minimizing the sums of the costs considering all 240 pedestrians rather than the least favored one promotes the group dynamics rather than those of the single pedestrian. However, if the links of G are not capacitated, i.e., in the absence of congestion, the solutions describe evacuations where each pedestrian always chooses a path of minimum cost.

3.5.5.3 KPIs and RI to select the best evacuation solution

The selection of the best evacuation solution(s) is finally performed by means of a Risk Index $RI_{i,M}$ [-] that jointly considers specific Key Performance Indicators (KPIs) depending on the environmental conditions established by the event (*hazard*), the pedestrians' behaviors in floodwaters (*exposure*), and the POS layout (*vulnerability*). The KPIs for this purpose are obtained by normalizing the arrays $C_{AVG(i,M)}$ with respect to the costs' absolute maximums $MAX|C_{AVG}|$ (that is considering all the three sets of solutions) according to the rules resumed in Table 22.

²⁶ <https://www.ibm.com/it-it/analytics/cplex-optimizer> (last access: 03/01/2022)

k	KPI [-]	Calculation method	Definition	W_k [-]
1	$d_{i,M}$	$S_{AVG(i,M)} / \text{MAX } S_{AVG} $	Normalized average evacuation length	0.2
2	$t_{i,M}$	$T_{AVG(i,M)} / \text{MAX } T_{AVG} $	Normalized average evacuation time	0.2
3	$dvs_{i,M}$	$DVS_{AVG(i,M)} / \text{MAX } DVS_{AVG} $	Normalized average evacuation effort	0.2
4	n_a	$N_a(i,M) / 240$	Missing pedestrians' ratio	0.4

Table 22. Key Performance Indicators calculation method and definition.

The related weights W_k are assigned according to the Analytical Hierarchy Process [265] by assuming the number of pedestrians unable to complete the evacuation as the riskiest parameter, and the other on the same level of importance (Consistency Ratio is 0%, which is lower than the maximum acceptability threshold of 10%). KPIs are combined in Eq. (3.4) so as to outline the Risk Index $RI_{i,M}$ as the Euclidean norm of a vector in a vector space of dimension equal to k , and with a field of existence included in the range $[0, 1]$, where 0 is the minimum risk and 1 represents the maximum risk.

$$RI_{i,M} = \left[\sqrt{\frac{\sum_{k=1}^4 W_k^2 \cdot KPI_k^2}{\sum_{k=1}^4 W_k^2 \cdot 1^2}} \right]_{i,M} \quad (3.4)$$

Finally, results are discussed so as to provide:

- the best evacuation solution (i.e., the optimal number and position of the shelters and the paths to reach them from each point of the POS) depending on the values assumed by $RI_{i,M}$ for each of the 36 solutions, organized for comparison purposes in 3 sets according to the aforementioned approaches for the path choice;
- comparisons between results obtained through the macroscopic model (i.e., the ILP introduced in this section), and the microscopic model (i.e., the setup-based generic simulator) considering only the best evacuation solution configuration in terms of gathering areas and evacuation paths configuration.

3.6 Hazard assessment and modeling: the case of flood

3.6.1 Introduction and motivation

Adequate holistic assessments cannot ignore the evaluation of hazard features and consequences, whose analysis should be included in a general framework within which all the factors that influence the overall risk are jointly considered (namely, hazard, vulnerability, and exposure). To this end, this subsection will explain how to model and assess the hazard in HCCs according to the same typological-and-mesoscale approach used in the previous sections. In particular, the event selected for this purpose concerns a flood in an HCC-POS due to a river overflow, in order to investigate its effect on the outdoor spaces (which are the typological POS introduced in §3.3) and its users (considering specific evacuation behaviors introduced in §3.5) [30], [274].

3.6.2 Data sources

The objective at this point of the work is therefore to define the characteristics of the watercourse that crosses the previously defined typological POSs, and, consequently, to determine the characteristics of the event that provide the input for the evacuation simulations (sections §8 and §9).

In particular, the choice of the watercourse was essentially dictated by two issues: 1) the availability of sufficiently accurate data about the geometry of the watercourse and the flow rate i.e., flood

hydrograph and river cross-sections; 2) a watercourse characterized by similar features to those of the selected case studies, which are resumed in Table 23. The watercourse taken as a reference for hazard modeling input definition is the Esino River, one of the most important watercourses in the Marche Region in terms of the size of the hydrographic basin and average annual flow rate.

In detail, the hydrometer station located at Moie, placed in the central part of the Esino River basin, is selected due to the frequent flood events registered since the 1960s and its river section width [m]. The model considers the overflow of the river placed in the HCC, in a short time span. This condition implies that pedestrians could not reach safe areas before the event. The model is based on the Esino hydrograph related to the 18/11/1975 flood [275] and on the application of the Giandotti theory [276] to the Esino River at the Moie section. Section §11.8 (Appendices) shows the calculation, which leads to a 100-year maximum flow rate of 1148 m³/s.

River - City	River basin area [km ²]	River length [km]	Maximum section width [m] (**)
Centa River – Albenga	432.0	45.0	95.0
Carrione River – Carrara	46.6	15.4	10.0
Parma Creek - Colorno	618.0 (*)	-	50.0
Dogana Creek - Montevarchi	27.8	-	15.0
Misa River - Senigallia	380.0	48.0	35.0
CASE STUDY: Esino a Moie Station	801.7	71.4	56.0

(*) this value refers to the closing section of the Ponte Bottego station, Parma (16 km upstream to Colorno)

(**) assessed in proximity to the city center.

Table 23: Comparison between the river basin of the selected case studies (§3.3) and the one adopted for hazard modeling.

The following assumptions are taken into consideration to increase the effects of floodwater spreading in the outdoor spaces [134], [185], [192]:

- Building blocks are conservatively modeled as completely impermeable and with no surface roughness, thus inducing no dumping of floodwaters, no shear stress, and no speed reduction near the buildings;
- The bottom roughness of the open channels is represented through the Manning coefficient [s/m^{1/3}] by considering a value equal to (1) 0.030 for the riverbed, to model a natural stream having maximum width lesser than 30m at bankfull stage, non-vegetated and straight development; (2) 0.013 for the streets and squares, to model stone paving, which is typical of the considered Italian HCCs.

3.6.3 Simulation tool

An existing commercial software is selected to boost the application process and demonstrate the methodology capabilities also considering the use by local technicians in real HCCs. In particular, the floodwater spreading simulations are performed by Delft3D (version 4.03.0127), because of reliable previous research on its development, verification, and application in urban contexts, including river overflow scenarios [277]–[280]. The software evaluates the effects of the fluvial flood

²⁷ Available: <https://oss.deltares.nl/web/delft3d> (downloaded at 01/12/2018)

on the outdoor spaces, by calculating water depth D [m] and speed V [m/s] values²⁸ during the whole event, with time steps of 60 s, on a solving mesh composed of 1m x 1m cells. According to previous work criteria [185], the gauging points to measure D and V are placed:

- at each crossroad barycentre;
- at each street barycentre;
- in different points of each square by using a chessboard-based scheme according to Figure 19, to verify the possible effects due to floodwaters coming from the linked streets.

Figure 19 shows an example of the division of squares into 4 sub-spaces for each module by evidencing the river axis, the buildings (gray areas), the position of the gauging points inside the square according to a chessboard scheme (blue dots), and the sub-spaces division (given by the dashed lines in the square).

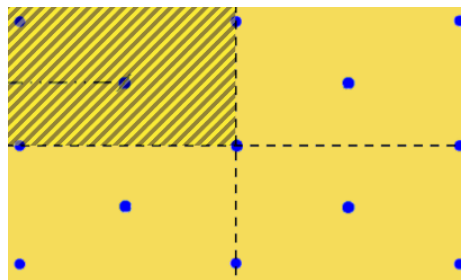


Figure 19: Scheme of gauging points positions (blue dots) and sub-spaces areas (divided by the dashed lines) in a typical square of the typological POSs for simulation purposes (example dimension equal to 1 module).

²⁸ V is averaged on the D .

4. Evaluating physical vulnerability at the microscale: a tool for historical masonry walls classification and mechanical characterization in the context of the Marche Region

4.1 Mechanical characterization of recurring masonry walls

The following sections are organized into three main parts to discuss results about compressive strength f (§4.1.1), elastic modulus E (§4.1.3), and the shear strength τ_0 and f_{v0} (Section ...) describing specific microscale features of the HCC. Specific comparisons are provided for each masonry typology by comparing INS ranges and experimental ones traced according to criteria introduced in Section §3.2.2. Wall textures, façades, and sections of each masonry typology are shown in Section §11.1.2 (Appendices).

4.1.1 Compressive strength f

Figure 20 resumes the comparisons between the minimum-maximum ranges provided by the INS (in blue), and the experimental data organized by boxplots (normal samples, by referring to the ranges between quartiles 1 and 3), or by minimum, mean, and maximum values (non-normal sample).

- **Disorganized rubble stone (M1):** the range identified by the experimental data is lower than the one provided by the INS by 0.60 MPa circa, meaning that regional data seems to be halved compared to the national standard (median experimental values are in line with the minimum provided by the INS, which is about 1.00 MPa). However, considering the elements features (e.g., the variability of the stones shape and size), the experimental sample exhibits a relatively low dispersion ($RSD_{f,M1}=0.43$).
- **Barely cut stone (M2):** comparisons in this case are influenced by the fact that the INS only provides a single threshold for the compressive strength (2.00 MPa). Accordingly, the experimental range turned out to be outside of the INS provisions, and on average is worth half, since the experimental mean value is about 1.00 MPa. Similarly to the previous case, despite of the variability of some of the stones shape and size, the experimental sample exhibits a relatively low dispersion, too ($RSD_{f,M2}=0.42$).
- **Roughly cut stone (M3):** similarly to the masonry typology M1, in this case the experimental range is lower than the one provided by the INS, and is translated of about 1.00 MPa. This difference is confirmed also comparing the mean values (respectively, 2.20 MPa for the experimental data and 3.20 MPa for the IBC provisions). Furthermore, since the quality of the stone elements generally improve compared to the previous typologies, the dispersion consequently decreases ($RSD_{f,M3}=0.32$).
- **Irregular soft stone (M4):** only 3 tests have been collected for this masonry typology, thus the comparison with the INS is proposed on the basis of the individual measured values (black asterisks in Figure 20). In particular, only one measurement is currently comparable with the INS provisions (the lower one, equal to 1.80 MPa), while the other ones (equal to 2.58 MPa and 2.79 MPa) are closer to the ranges provided for the regular soft masonry, which is discussed in the following.

- **Regular soft stone (M5):** the experimental range is slightly lower than the INS provisions, and they differ of about 0.50 MPa. In particular, both the mean and the upper threshold of the experimental sample are comparable, respectively, with the minimum threshold and the mean of the range provided by the INS (2.00 MPa and 2.60 MPa respectively). Furthermore, the dispersion is higher than the previous cases ($RSD_{f,M5}=0.50$), despite the regular texture.
- **Stone blocks squared (M6):** differently from the previous typologies, results highlight a clear difference between regional and national ranges, as the experimental bounds are more than halved compared to the thresholds provided by the INS. Furthermore, the data dispersion is quite small due to the regular texture ($RSD_{f,M6}=0.38$).
- **Solid clay brick and lime mortar (M7):** this is by far the most tested masonry typology in the experimental database, as well as one of the most widespread both in the regional and national territory [224]. The huge amount of tests collected probably determined a higher dispersion ($RSD_{f,M7}=0.54$) in spite of the regular texture and the use of mass-produced elements. However, the data sample is normal, and the experimental range is almost overlapped with the INS provisions (except for a slight difference of about 0.70 MPa between the minimum thresholds).
- **Clay hollow bricks in standard conditions (M8) and with good mortar (M8-gm):** similarly to the previous case, also the clay hollow bricks masonry (holes percentage area $\leq 40\%$) is widespread throughout the regional and the national territory [225], as also evidenced by the second place among the most recurrent typology in the current database. Results demonstrate that, regardless of masonry “conditions”, the experimental data are characterized by a high dispersion ($RSD_{f,M8}=0.43$ and $RSD_{f,M8-gm}=0.50^{29}$), and a significant gap with the INS provisions (more than 5.00 MPa on average). In particular, only the maximum value collected for the sample in “good condition” (7.30 MPa, non-normal distribution) is comparable with the mean value of the INS range (7.80 MPa).
- **Stone-and-brick mixed masonry (MX1):** Despite being commonly acknowledged as a common typology throughout the national panorama [91] (as also demonstrated by the third place among the most numerous sample in the database), this masonry typology is still unregulated by the INS³⁰. Accordingly, results only concerns experimental data, and they are mapped considering minimum, mean, and maximum values of the sample as the distribution is non-normal (probably due to possible differences in the percentages of stones and bricks both in the façades and/or in the sections of the tested walls³¹). Accordingly, the collected sample also shows out a significant data dispersion ($RSD_{f,MX1}=0.59$). However, making a comparison with previous stone-made typologies, the interval included between the minimum and average values can be compared with the INS values of M1 typology, and with experimental values of M1 and M2 typologies, that are the weakest ones.
- **Other typologies (MX2 and MX3):** no data were collected for the concrete hollow brick masonry (MX3), while for the solid clay bricks with rubble stone fill typology (MX2) results

²⁹ Probably due to possible differences in the hole percentage areas between the masonry walls tested.

³⁰ Excluding the stone masonry with brick stringcourses [93].

³¹ It is important to underline that the tests were performed by laboratories that not always provided accurate descriptions and photos of the masonry walls, therefore no further information on the percentages of stones and bricks is available.

are close to the disorganized rubble one. However, it is worth noticing that this masonry typology is commonly characterized by the total absence of transversal connection between the external facings and the internal core, the latter having a non-negligible thickness than the former. These characteristics can certainly influence the measurements carried out with double flat-jacks, therefore these results will need to be compared with more exhaustive tests in the future.

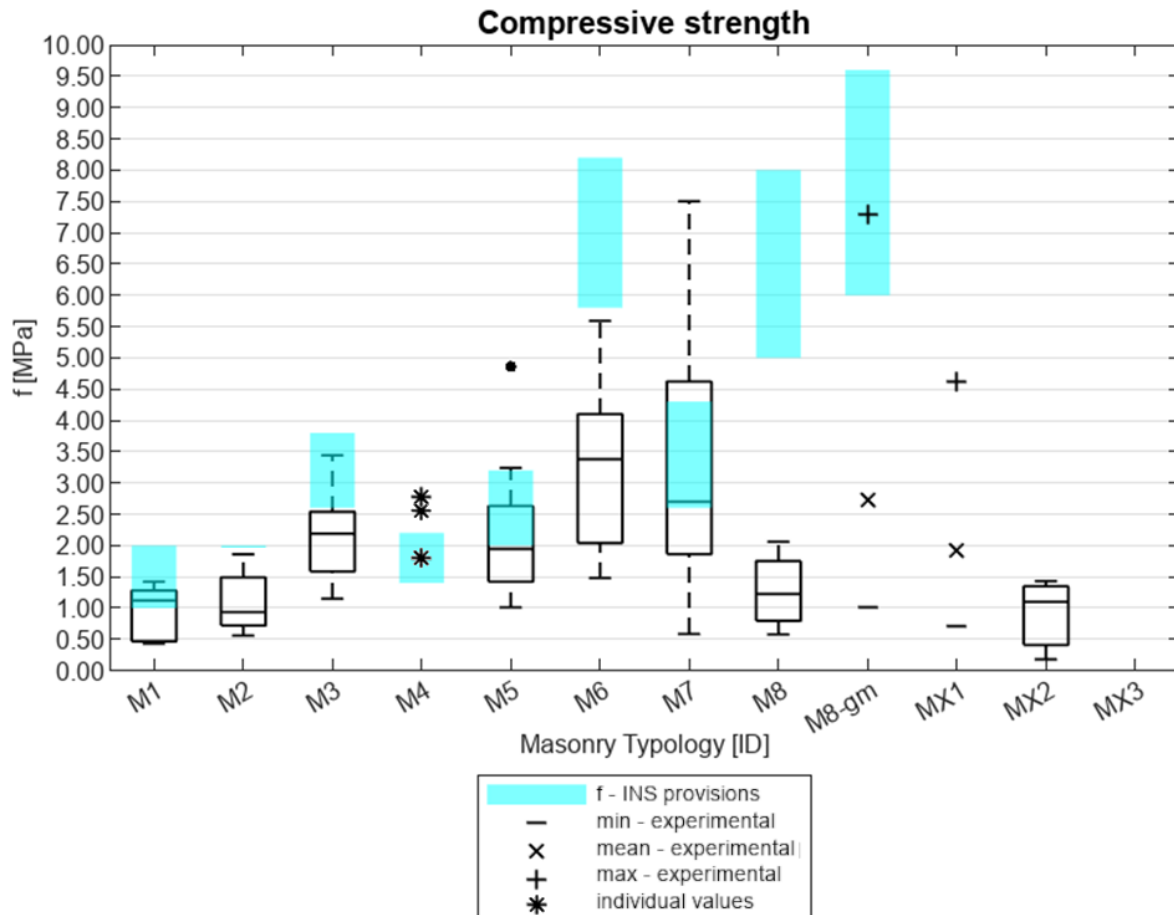


Figure 20: Compressive strength graphical comparison between the experimental data (boxplots and black markers), and the INS provisions (blue areas).

4.1.2 Elastic modulus E

Figure 21 resumes the comparisons between the minimum-maximum ranges provided by the INS (in green), and the experimental data organized by boxplots (normal samples, by referring to the ranges between quartiles 1 and 3), or by minimum, mean, and maximum values (non-normal sample).

- **Disorganized rubble stone (M1):** the experimental data are characterized by a high dispersion ($RSD_{f,M1}=0.65$), thus the experimental range is wider than the INS one, although their mean and median values, respectively, are comparable (around 900 MPa). Vice versa, extending the comparison to literature findings (resumed in Table 47, Section §11.1.4, Appendices), it can be noticed how their values are significantly higher (the lowest literature values are comparable with experimental and standard maximum thresholds), although such outcomes can certainly depend on the use of specific materials and technologies strongly influenced by local knowledge and availabilities.

- **Barely cut stone (M2):** experimental data and INS provisions are perfectly comparable since their mean values are about 1200 MPa, while minimum and upper bounds slightly differ although a small dispersion of the experimental sample ($RSD_{f,M2}=0.36$).
- **Roughly cut stone (M3):** in this case the elastic modulus is characterized by a higher dispersion ($RSD_{E,M3}=0.57$). For what concerns the comparison between national and regional data, the lower bound of the experimental range (quartile 1) is comparable with the minimum threshold provided by the INS, while the upper bound (quartile 3) is almost 2.5 times higher than the INS maximum threshold.
- **Irregular soft stone (M4):** only 3 tests have been collected for this masonry typology, thus the comparison with the INS is proposed on the basis of the individual measured values (black asterisks in Figure 21). Similarly to the compressive strength, only one measurement is currently comparable with the INS provisions (the lower one, equal to 794 MPa), while the other ones (equal to 1733 MPa and 2107 MPa) are closer to the ranges provided for the regular soft masonry, which is discussed in the following.
- **Regular soft stone (M5):** the experimental lower bound and the INS minimum threshold are comparable (respectively, 1100-1200 MPa), as well as their mean values (respectively, 1400-1500 MPa), while the upper bound of the experimental data (quartile 3) is about 1.3 times greater than the INS maximum threshold. Such outcomes find confirmation from the comparison with literature data retrieved from previous works (resumed in Table 47, Section §11.1.4, Appendices), which are comparable with the lower bound identified through the in-situ measurements. Finally, the dispersion is almost the same as that of the compressive strength ($RSD_{E,M5}=0.49$).
- **Stone blocks squared (M6):** in this case the dispersion of the experimental data is such high ($RSD_{E,M6} =0.59$) to compromise an effective comparison with the INS range.
- **Solid clay brick and lime mortar (M7):** since the experimental data sample is non-normal, the comparison with the INS range is provided in terms of maximum, minimum, and mean values. In particular, similarly to the previous case, the dispersion of the experimental data is such ($RSD_{E,M7} =0.73$) to compromise an effective comparison with the INS range (which are also in line with literature data resumed in Table 47, Section §11.1.4, Appendices), and implies a significant discrepancy especially considering the maximum values.
- **Clay hollow bricks in standard conditions (M8) and with good mortar (M8-gm):** similarly to the previous case, the experimental data samples are non-normal and the data dispersion is such ($RSD_{f,M8}=0.69$ and $RSD_{f,M8-gm}=0.70$) to compromise an effective comparison with the INS range (the experimental mean value anyway is about half of the INS one).
- **Stone-and-brick mixed masonry (MX1):** as for the compressive strength, in this case results only concerns experimental data, and they are mapped considering minimum, mean, and maximum values of the sample as the distribution is non-normal and the dispersion is even higher ($RSD_{f,MX1}=0.85$). However, the comparison with other stone-made typologies shows that the experimental minimum and mean values can be compared with the INS values of M1 and M3 typologies, that are between the weakest ones.

- **Other typologies (MX2 and MX3):** only one value was collected for such typologies (solid clay bricks with rubble stone fill and concrete hollow bricks), and they are respectively comparable with the INS provisions for the M1 typology (disorganized rubble stone, the weakest one) and the M8 typology in good conditions (clay hollow bricks with cement-mortar, the strongest one). Results however will need to be compared with more exhaustive tests in the future.

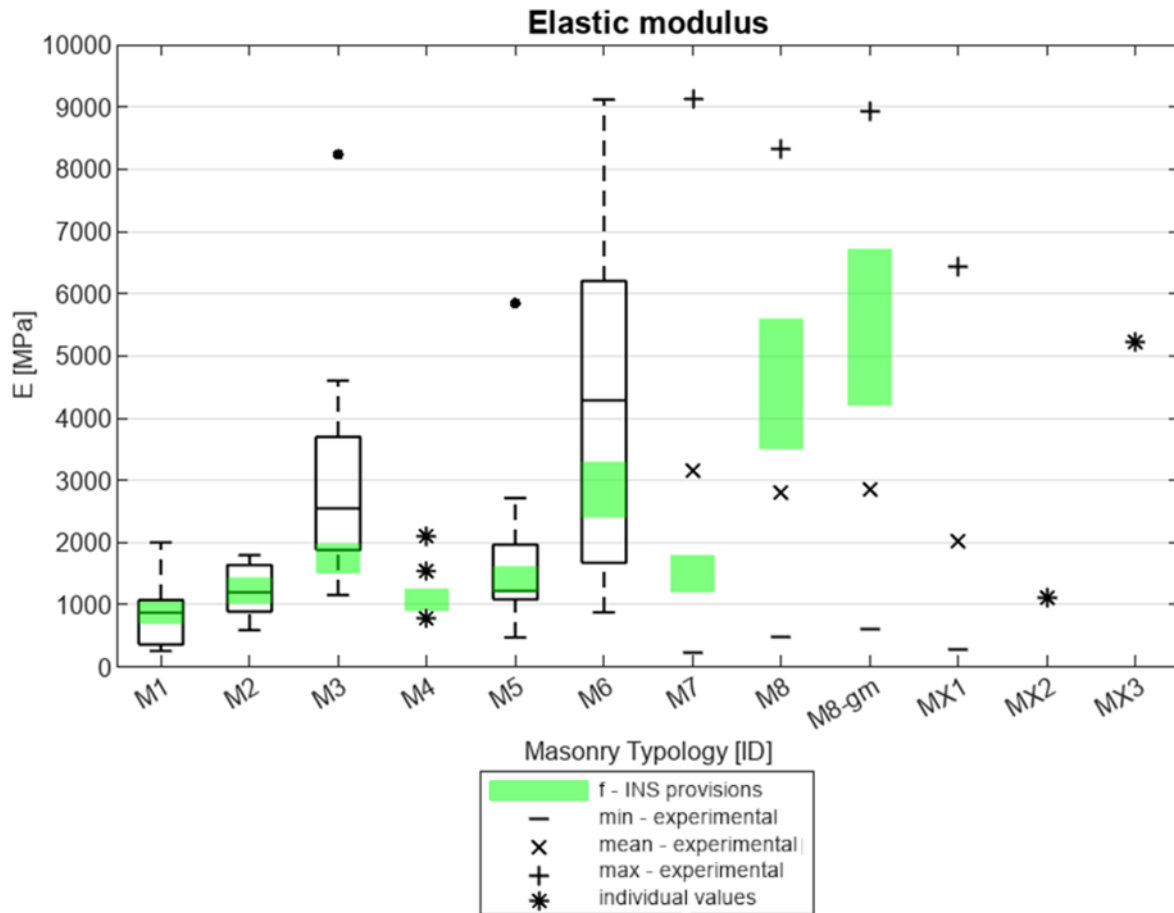


Figure 21: Elastic modulus graphical comparison between the experimental data (boxplots and black markers), and the INS provisions (green areas).

4.1.3 Shear strength τ_0 , shear strength f_{v0} , and shear modulus G

The shear parameters are discussed with respect to the single values recorded from the experimental tests, since the sample size is not large enough to trace statistically reliable reference ranges (see Table 3). Figure 22 resumes the comparisons with the minimum-maximum ranges provided by the INS by distinguishing:

- the shear strength for diagonal compression for both regular and irregular masonry typologies (τ_0 , indicated by the blue area and to be compared with the blue markers), evaluated through diagonal compression tests (DCT) and vertical flat-jacks tests (VFJT);
- the shear frictional strength at unit-mortar interface without compression only for irregular masonry typologies (f_{v0} , indicated by the red area and to be compared with the red markers), evaluated through shove tests (ST).

The shear modulus results (G) are not illustrated graphically as only one value was collected.

- **Disorganized rubble stone (M1):** being an irregular masonry, the comparison only concerns τ_0 . In particular, two experimental data are collected through vertical flat-jack tests, of which one is comparable with the INS range (≈ 0.03 MPa) while the other one greatly exceeds the range. No experimental measurements have been found regarding the shear modulus G .
- **Solid clay brick and lime mortar (M7):** as for the double flat-jacks tests, also for the shear parameters measurements the solid clay bricks masonry is the typology with the most tests collected, both in terms of number of measurements and in terms of variety of tests. In particular, 12 measurements are collected, equally distributed between three types of experimental tests, namely: 4 vertical flat-jack tests (VFJT, blue circles), 4 diagonal compression tests (DCT, blue triangles), and 4 shove tests (ST, red crosses). Results show that, considering the diagonal cracking τ_0 failure mechanism, the experimental data are mostly comparable with the INS provisions (in blue). In particular, all the measurements performed through diagonal compression tests are included in the INS range, while those performed through vertical flat-jacks tests on average provide slightly higher values (average of the 4 measurements equal to 0.16 MPa, compared to the INS maximum threshold of 0.13 MPa). Differently, as regards f_{v0} two measurements are above the maximum threshold indicated by the INS (respectively, 0.44 and 0.36 MPa against 0.27 MPa), while the other two are below the minimum threshold (respectively, 0.06 and 0.05 MPa against 0.13 MPa). Finally, a shear modulus G value was also measured through a diagonal compression, and it is comparable with the INS minimum threshold (respectively, 397 and 400 MPa).
- **Clay hollow bricks in standard conditions (M8):** in this case, the masonry walls tested were all in "standard conditions" of conservation (code "sc"). Only vertical fat-jack tests have been collected, thus the comparison is discussed only with respect to shear strength τ_0 (in blue), and the experimental data collected are significantly higher than the INS provisions (respectively, 0.55 and 0.39 against 0.17 MPa). Finally, no experimental measurements were found for what concerns the shear modulus G .
- **Stone-and-brick mixed masonry (MX1):** due to the absence of indications by the current INS, for this masonry no specific graphical comparisons are provided. Experimental data have been collected by means of two types of tests, which show that diagonal compression results (0.25-0.26 MPa) differ by an order of magnitude from the single value measured through a vertical flat-jacks test (0.025 MPa, which is comparable with the INS provisions for the disorganized rubble stone masonry, as shown in subsections §4.1.1 and §4.1.2).

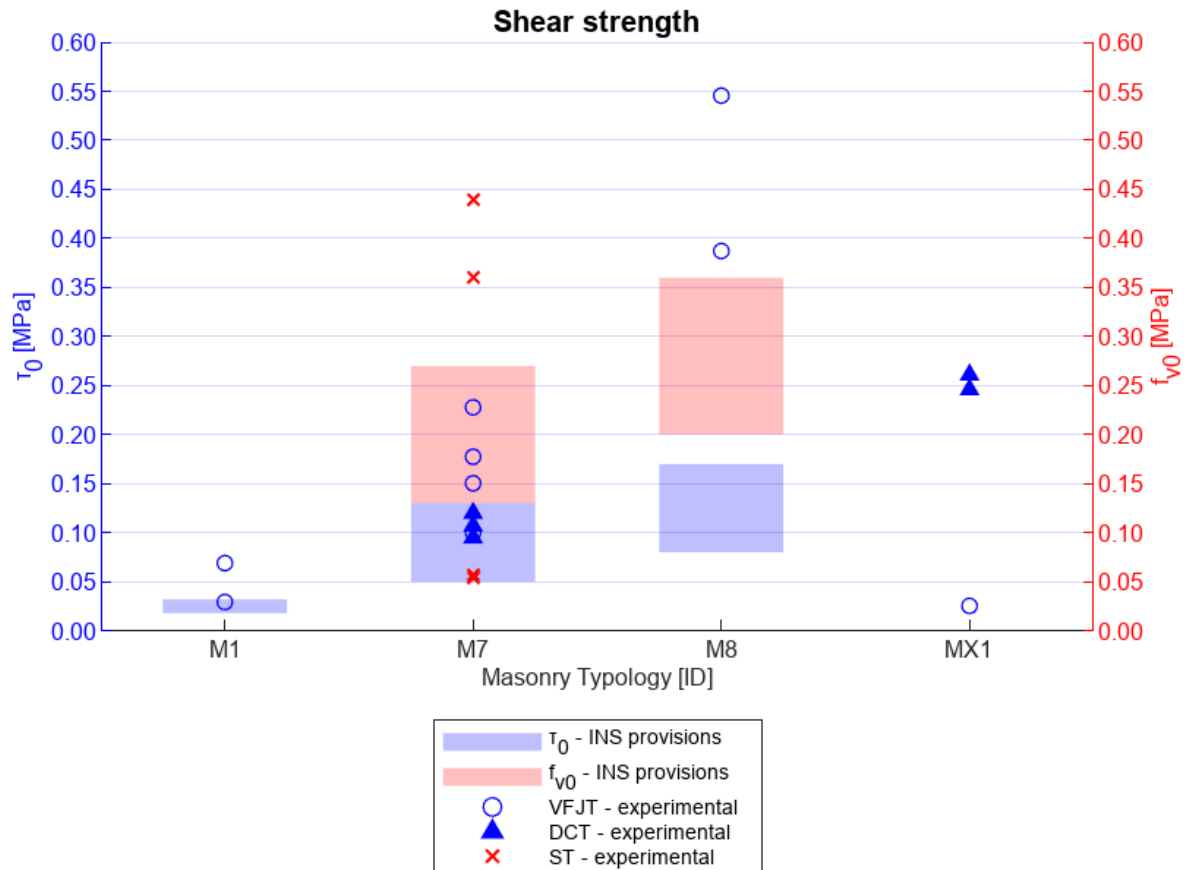


Figure 22: Shear strength graphical comparison between the experimental data and the INS provisions. Blue areas and blue markers indicate τ_0 , red areas and red markers indicate f_{v0} .

4.1.4 Earthen masonry typologies

As already introduced in the previous §3.2.3, at a regional level the 3 earthen typologies present in the Marche Region are Adobe, Cob, and Rammed earth, of which preliminary insights are provided in this section. In particular, due to the absence of in situ measurements in the experimental database and of reference values in the INS, the values herein discussed are based on literature data obtained from national and non-national studies and national standards from countries in which the typologies are already regulated.

- For what concerns Adobe, Figure 23 shows a graphical comparison between the literature range (gray boxplot), the range proposed by the Spanish standard (orange area, source [283] ref. MOPT 1992 [284]), and the values obtained from scientific research about case studies in the Marche Region (blue markers - see §11.1.4 in Section §11.1.2, Appendices). In terms of compressive strength, there is a good correspondence between the two ranges, with a slight underestimation of the literature sample (0.50-1.80 MPa) compared to the Spanish standard provisions (0.75-2.25 MPa). Values collected from literature studies on regional case studies perfectly matches with these ranges (1.20 and 0.77 MPa [285]). For the elastic modulus, the MOPT does not provide indications, while the values obtained from regional studies are comparable (135 MPa [286]) or slightly lower (40 and 26 MPa [285]) than the minimum values founded from international research (which ranges between 55 and 225 MPa, with the presence of two outliers of about 800 MPa).

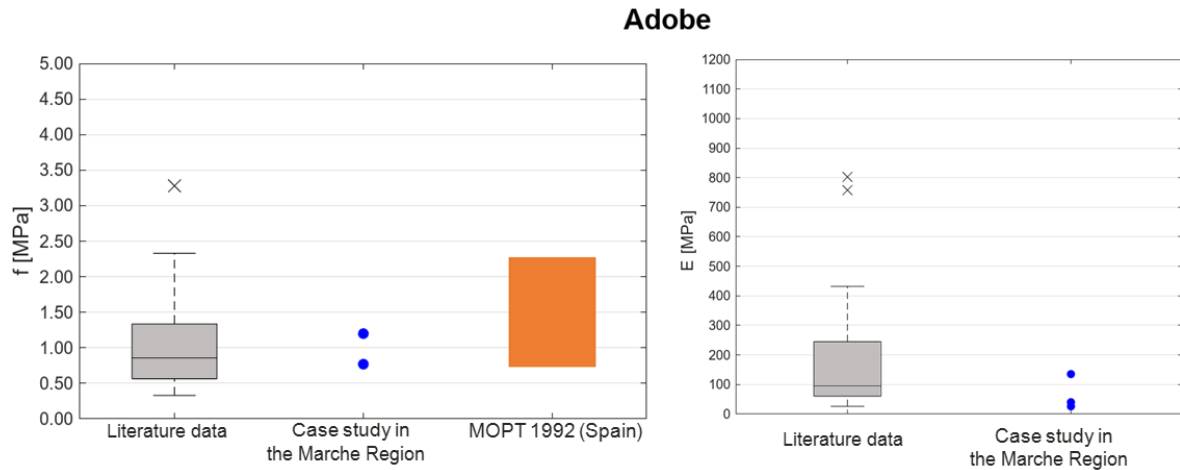


Figure 23: Adobe masonry – Graphical comparison in terms of compressive strength f (on the left) and elastic modulus (on the right) between literature ranges (gray boxplots), the Spanish standard (orange area), and the values obtained from literature studies on regional case studies (blue markers). Outliers are indicated by the gray crosses.

- Worldwide, the Cob typology is less widespread than the other two herein investigated, therefore literature data collected for estimating ranges shown in Figure 24 (gray boxplots) mainly refer to case studies relating to the Marche Region (blue circles, about one-third of the reference sample, which is fully reported in Section § 11.1.4, Appendices), in which it is more common. In particular, for the compressive strength there is an excellent agreement between the literature data sample (0.45-1.20 MPa), and the values obtained from regional research (all between 0.25 and 1.60 MPa). On the other hand, for the elastic modulus, the range of the literature studies is between 15 and 150 MPa, and the regional data are closer to the lower threshold (blue markers).

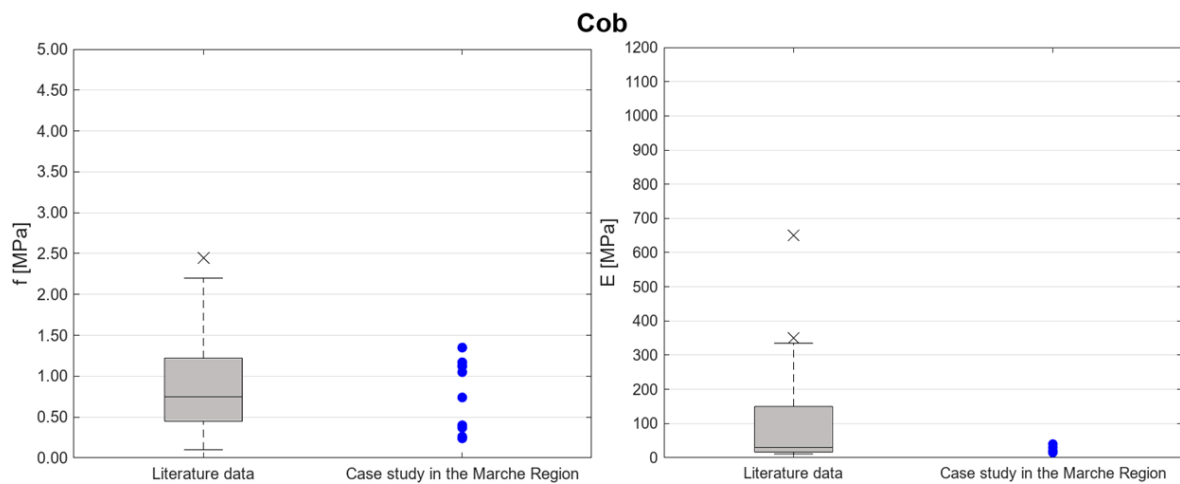


Figure 24: Cob masonry – Graphical comparison in terms of compressive strength f (on the left) and elastic modulus E (on the right) between literature ranges (gray boxplots) and the values obtained from literature studies on regional case studies (blue markers). Outliers are indicated by the gray crosses.

- Although there is evidence of the presence of Rammed earth masonries in the Marche Region [287], currently no scientific research investigating local case studies has been found. Accordingly, Figure 25 shows a comparison between the ranges defined through international literature data (gray boxplots), and the standard provisions of the following countries:

- Australia (ref. *Australia Standards HB 195:2002* [288], via [289]), indicated by the blue area (compressive strength between 0.40-0.60 MPa) and the blue circle (elastic modulus equal to 500 MPa);
- Zimbabwe (ref. *Standard Association Zimbabwe SAZ724:2001* [290], via [283]) indicated by the green area (compressive strength equal to at least 1.50 MPa for single-story buildings, and 2.00 MPa for two-story buildings);
- Spain (ref. *MOPT 1992* [284], via [283]), identified by the orange area (compressive strength between 0.60-1.80 MPa);
- New Zealand (ref. *Edict of Government, NZS 4297:1998* [291] via [289]), identified by the brown square markers (compressive strength equal to 0.50 MPa, elastic modulus equal to 300 times the strength compression);
- New Mexico, USA (ref. *NMAC 14-7-4:2016* [292], via [289]) identified by the pink triangular marker (compressive strength equal to 2.07 MPa).

As regards the compressive strength, the literature range (1.00-2.00 MPa) has quite good agreement with the provision of the Spanish, Zimbabwean, and US standards, which indicate a maximum threshold included between 1.80-2.00 MPa. However, some outlier values above the threshold of 3.50 MPa exist. On the other hand, for the elastic modulus, the Australian and US (New Mexico) standards are perfectly comparable, respectively, with the 3rd and 2nd quartiles traced by the literature data sample (150-500 MPa).

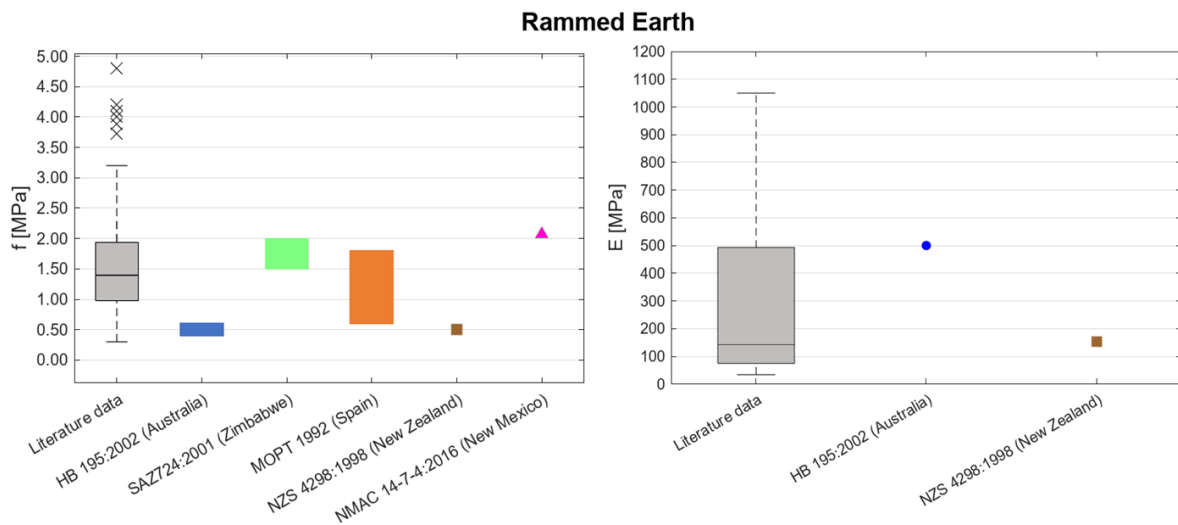


Figure 25: Rammed earth masonry - Graphical comparison in terms of compressive strength f (on the left) and elastic modulus (on the right) between literature ranges (gray boxplots) and the Australian, Zimbabwean, Spanish, New Zealand, and US (New Mexico) standards. Outliers are indicated by the gray crosses.

4.1.5 E/f ratio and coefficient of variation

Results obtained through quartile-based analyses offer interesting insights into the mechanical characterization of the different masonry typologies. In general, the ranges identified for the compressive strength revealed a fair correspondence between the experimental data and the INS provisions, while the elastic modulus data are characterized by a great dispersion that implies wider ranges, making often the comparison difficult (on average, $RSD_f=0.43$ and $RSD_E=0.60$ considering the entire data sample collected).

As regards earthen masonry, the dispersion is significantly greater both for the compressive strength ($RSD_{f,ADOBE} = 0.62$; $RSD_{f,COB} = 0.62$; $RSD_{f,PISÈ} = 0.63$) and, even more higher for the elastic modulus ($RSD_{E,ADOBE} = 1.15$, $RSD_{E,COB} = 1.40$, $RSD_{E,PISÈ} = 0.98$).

On the other hand, the values assumed by the E/f ratios highlight a good agreement between the values prescribed by both the INS and the Eurocode ($E/f=1000$) [171], [172], [181], and those obtained from experimental data ($E/f \approx 1000$) considering: a) the entire sample of masonry (AVG), b) the sample of stone masonry (STO), and c) the sample of brick masonry (BR), all summarized in Table 24. In particular, such values are always confirmed for all the masonry typologies investigated, except for the following cases:

- Clay hollow bricks masonry in “standard conditions” (M8-sc), where the E/f ratio is almost doubled mainly due to the extremely low values of compressive strength compared to those proposed by the INS;
- Irregular (M4) and regular (M5) soft stone masonries, for which the values are anyway comparable with those reported in the scientific literature [293]–[296] (see Table 48 in Section §11.1.4) and with those obtainable using the ranges of E and f provided by the INS, i.e. around 600 for the first, and between 600-800 for the second [171], [172];
- earthen typologies (Adobe, Cob, Pisè), for which the E/f ratios vary between 150-190, thus substantially lower than the 300 proposed by the Australian standards introduced in the previous subsection §4.1.4 [288].

	M1	M2	M3	M4	M5	M6	M7	M8-sc	M8-gm	MX1	AVG	STO	BR
<i>E/f</i>	918	1126	1403	646	676	1396	1040	2193	1108	1046	1150	1125	1079

	Adobe	Cob	Rammed
<i>E/f</i>	155	125	190

Table 24: *E/f* ratios [-] singularly evaluated for each masonry typology and on average, considering: the overall sample (AVG), the stone masonries sample (STO, that include typologies from M1 to M6), and the brick masonries sample (BR, that include typologies M7, M8-sc, and M8-gm). “sc” stands for standard conditions, “gm” stands for good mortar.

MASONRY CODES: M1= disorganized rubble stone; M2=barely cut stone; M3=roughly cut stone; M4=irregular soft stone; M5=regular soft stone; M6=stone blocks squared; M7=solid clay bricks; M8=clay hollow bricks; MX1=stone-and-brick mixed.

In this regard, however, it is noteworthy to highlight that, while considerations and insights for stone masonry typologies can be considered relevant *only* for the Marche regional context (since the use of specific materials and/or construction techniques can be a source of divergences from what is observed on a national scale), the indications obtained from the brick typologies could have a wider scope, both considering their vast presence throughout the Italian territory and further factors such as the use of regular prefabricated elements.

4.2 Definition of a tool for historical masonry walls classification and mechanical characterization

4.2.1 Outcomes summary and evaluation

The experimental data collected and organized according to the criteria illustrated in the previous sections finally allow comparisons between the ranges obtained for the historical masonry walls of the Marche Region and those provided for the whole Italian context by the current INS (with

reference to the same conservation conditions, i.e. walls in poor condition and without consolidation interventions) and its previous versions.

To this end, it is important to underline how the experimental database is realized through tests and measurements prescribed by the INS itself to reach an adequate “level of knowledge” [171], [172] and carried out: (1) by licensed laboratories; (2) on a wide spectrum of historic masonries present in the regional territory. Table 25 summarizes the ranges of the compressive strength f and the elastic modulus E (considering minimum and maximum values of each sample) obtained for the historical masonries of the Marche Region (HMM) and compared with the values provided by the INS provisions considering, respectively, its current (CSLLPP n.7/2019) and previous versions (CSLLPP n.617/2009, OPCM n.3431/2005, and CSLLPP n.21745/1981).

ID – MASONRY TYPOLOGIES	f [MPa]					E [MPa]				
	HMM	C.19	C.09	O.05	C.81	HMM	C.19	C.09	O.05	C.81*
M1 – Disorganized rubble stone	0.43	1.00	1.00	0.60	0.50	257	690	690	690	132
	1.42	2.00	1.80	0.90		2000	1050	1050	1050	
M2 – Barely cut stone	0.56	2.00	2.00	1.10	-	591	1020	1020	1020	-
	1.86		3.00	1.55		1797	1440	1440	1440	
M3 – Roughly cut stone	1.15	2.60	2.60	1.50	2.00	1158	1500	1500	1500	462
	3.40	3.80	3.80	2.00		6750	1980	1980	1980	
M4 – Irregular soft stone	1.80	1.40	1.40	0.80	-	794	900	900	900	-
	2.79	2.20	2.40	1.20		2107	1260	1260	1260	
M5 – Regular soft stone	1.01	2.00	-	-	2.50	476	1200	-	-	660
	4.86	3.20				2845	1620			
M6 – Stone blocks squared	1.48	5.80	6.00	3.00	-	878	2400	2400	2340	-
	5.59	8.20	8.00	4.00		9119	3300	3200	2820	
M7 – Solid clay bricks	0.59	2.60	2.40	1.80	3.00	222	1200	1200	1800	792
	7.50	4.30	4.00	2.80		7658	1800	1800	2400	
M8 – Clay hollow bricks	0.58	5.00	5.00	3.80	-	495	3500	3500	2800	-
	2.06	8.00	8.00	5.00		8325	5600	5600	3600	
MX1 – Stone-and-brick mixed	0.72	-	-	-	-	276	-	-	-	-
	4.62					6446				
MX2 - Solid clay with rubble stone fill	0.18	-	-	-	-	1122	-	-	-	-
	1.43									
MX3 - Concrete hollow bricks	-	-	3.00 4.40	3.00 4.40	3.00	5211	-	2700 3500	2400 3520	1188

Table 25: Comparison between the ranges of compressive strength f and elastic modulus E between historical masonries in the Marche Region (HMM) and the INS provisions considering, respectively, the current (C.19) and the previous versions (C.09, O.05, C.81, where C stands for “Circolare” and O stands for “OPCM”).

In general, results show that the experimental compressive strength of the weakest stone masonry typologies (M1, M2, M3) has a good agreement with the ranges indicated by the INS, both considering its current version (as regards the maximum values) and its previous versions (minimum values). In the case of irregular soft stone masonry (M4), the range provided in the 2009 version is the closest to the values obtained for historical masonries of the Marche Region, while for regular squared stone blocks masonry (M6) and clay hollow bricks masonry (M8) the closest values are those provided in the 2005 standards.

For what concerns the elastic modulus, the shear strength, and the shear modulus, the current database is difficult to evaluate, either because of the high dispersion of the experimental ranges or the limited number of tests available.

Table 26 shows the experimental values of shear strength for diagonal cracking τ_0 measured through diagonal compression tests regulated by ASTM standards. In fact, this type of test is recommended by the INS to improve the level of knowledge of the masonry [172], [182], unlike the vertical flat-jack test which was developed more recently and currently lacks a reference standard [183]. Values for solid clay brick masonry (M7) and for stone-and-brick mixed masonry (MX1) were obtained from diagonal compression tests (superscript “a” in Table 26), while for the disorganized rubble stone masonry (M1) and the clay hollow bricks masonry (M8) from vertical flat-jacks measurements (superscript “c” in Table 26). In particular, an interesting result concerns the clay hollow bricks masonry (M8), where experimental data are comparable with the range proposed in the 2005 and 2009 standards rather than the current one.

ID – MASONRY TYPOLOGIES	τ_0 [MPa]				G [MPa]			
	HMM	C.19	C.09 O.05	C.81	HMM	C.19 C.09	O.05	C.81
<i>M1 – Disorganized rubble stone</i>	0.03^b 0.07^b	0.018 0.032	0.020 0.032	0.02	-	230 350	115 175	22
<i>M7 – Solid clay bricks</i>	0.10^a 0.12^a	0.050 0.130	0.060 0.092	0.12	397^c	400 600	300 400	132
<i>M8 – Clay hollow bricks</i>	0.55^b 0.39^b	0.08 0.17	0.24 0.32	-	-	875 1400	560 720	-
<i>MX1 – Stone-and-brick mixed</i>	0.25^a 0.26^a	-	-	-	-	-	-	-

Table 26: Comparison between the ranges of shear strength τ_0 and elastic modulus G between historical masonries in the Marche Region (HMM) and the INS provisions considering, respectively, the current (C.19) and the previous versions (C.09, O.05, C.81, where C stands for “Circolare” and O stands for “OPCM”). (^a) range based on diagonal compression test measurements (DCT); (^b) range based on vertical flat-jacks test measurements (VFJT); (^c) only value found.

Finally, Table 27 shows a rapid comparison between the values of shear strength f_{v0} (mortar joints failure) for the clay hollow bricks masonry (M8) which is the only typology for which shove tests have been found. The experimental range obtained is wider than the current INS one (in the previous versions this parameter was not included), although in line considering the maximum thresholds.

ID – MASORY TYPOLOGIES	f_{v0} [MPa]		G [MPa]	
	HMM	C.19	HMM	C.19
<i>M8 - Clay hollow bricks masonry</i>	0.05 0.44	0.20 0.36	-	875 1400

Table 27: Comparison between the ranges of shear strength τ_0 and elastic modulus G between historical masonries in the Marche Region (HMM) and the current INS provisions (C.19).

4.2.2 Results innovation and utility for practitioners

The results collected in this study provide an innovative, microscopic assessment of the historical masonry present in the Marche Region and their mechanical characterization. In particular, the fruit of this research is a book named “*Murature Storiche nella Regione Marche: Specificità Costruttive e Caratterizzazione Sperimentale*” (in Italian) [61], which concerns the development of reference tables and datasheets for the regional context thanks to a massive effort for quantitative and qualitative data collection from experimental, literature, and photographic sources. The book

represents a tool useful for practitioners and insiders to better recognize, understand, evaluate, and verify local masonry also in view of the indications provided by the Italian National Standard, who expressly encourage the Regions to «take into account the construction specificities of their territory, defining homogeneous areas to refer to», and therefore to provide indications on possible experimental values.

In particular, starting from the INS classification, reference ranges are proposed both for typologies already regulated (in order to provide comparisons between the local specificities and the national overview), and unregulated (which can also be useful for external users from the regional context, as they include widespread typologies throughout the Italian territory such as the stone-and-brick mixed masonry). Furthermore, for the first time, indications are also provided for earthen masonry typologies, which represent construction specificities with a strongly territorial character and have never been regulated by the INS. In this case, due to the absence of measurements through experimental tests in situ, estimates are retrieved from literature research and other country standards where these typologies are already regulated.

The final experimental database consists of more than 400 experimental tests on more than 10 different masonry typologies. Most of these tests are performed through double flat jacks, allowing a detailed picture to be drawn on compressive strength and elastic modulus thanks to statistical analyses (normality test and quartile-based analysis) to trace the reference ranges. Results demonstrate a better agreement for the compressive strengths, while for the elastic modulus, the comparisons are not always comparable with the INS provisions due to the great variability registered by the experimental data. However, considering the E/f ratio (evaluated with respect to their average values both on the overall sample and for each masonry typology), this work findings are very close to the INS provisions ($E/f \approx 1000$ for generic stone masonries, brick masonries, and mixed ones) and to previous literature ($E/f \approx 600$ for soft stone masonries).

4.2.3 Limitations and future aims

Besides double flat-jacks tests, measurements for estimating the shear strength and the shear modulus were also collected, but the samples in these cases are still too small to provide significant experimental reference ranges for all masonry typologies. Accordingly, for these mechanical parameters, evaluations are provided only by referring to the precise values recorded from the single tests and organizing them by type of test (i.e. diagonal compression in situ/in the laboratory, vertical flat jacks, shove tests). Future efforts should be then aimed at further increasing and diversifying the number and types of the tests (especially for what concerns shear parameters) besides the masonry typologies investigated to provide an even more extensive and varied database in terms of experimental, photographic, and literature documentation. In particular, since the proposed tool embraces a "circular logic" according to which the data collected are provided by the same subjects to whom this work is mainly aimed (i.e., professionals, laboratories, and institutions), the next steps should certainly look at the possibility of developing an automatic and collaborative tool allowing users to directly insert input and access common files, in order to also speed up their up-to-date use with respect to the most recent data.

5. Evaluating vulnerability and exposure in multi-risk HCC: spatiotemporal impact of different types of areas and users

This section is organized according to classes of KPIs introduced in the previous §3.4.3 (Public Open Space Characterization, Users' Daily Characterization, and Users' Hourly Characterization) referring to the sample of squares assessed in this work as relevant POSs (see Section §11.3.2, Appendices).

5.1 Square characterization

The square sample is mainly characterized by the presence of walkable areas (median WAp=65%) as highlighted in Figure 26A, while a non-negligible part is occupied by carriageable areas and transportation systems (median CAp=30% circa). However, considering walkable and carriageable areas as a whole (thus considering those areas that can be ideally used in case of an evacuation), they cover almost the entire area of the squares, while the remaining space is occupied by dehors, monuments, and/or private courtyards (up to about 10%).

82% of the analyzed squares are characterized by the presence of at least one special building or special use within the square (SB). Figure 26B shows that the most recurring condition regardless of the special building and use types (blue boxplot) can be described by SBn=2 as the median value. "Theatres, Museums, Religious buildings" and "Government buildings" are the most frequent special buildings and uses in the squares, being consistent also in view of the specificities of the historic cities assessed in this research, as these kinds of functions are usually hosted in historic buildings [297]. Considering the identified sensitive buildings typologies, the median area SBA is equal to 1310m² for Theatres, 940m² for Museums, 880m² for Religious Buildings, and 1770 m² for Government Buildings. As shown in Figure 26C, *indoor areas* are about 2.5 times larger than *outdoor areas* considering the median value of AIOIr.

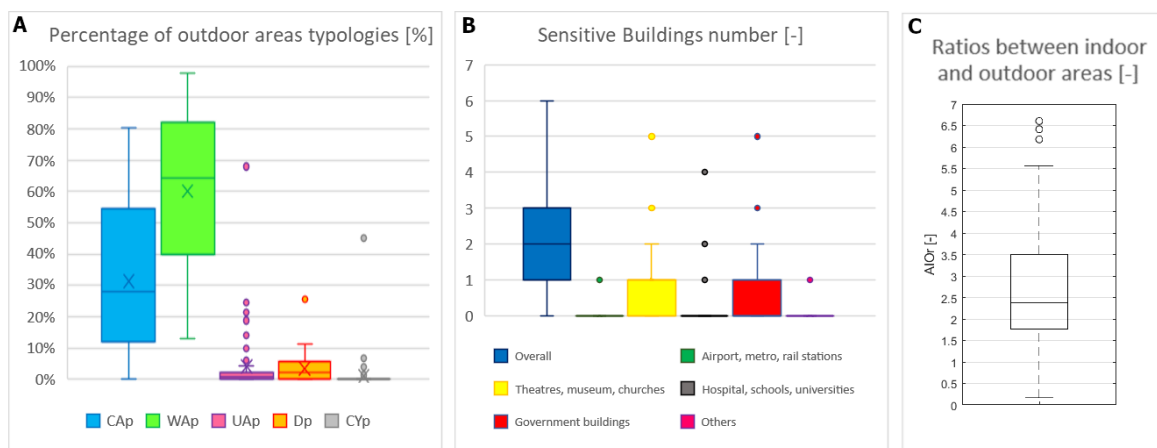


Figure 26: POSC-related KPIs - Quartile-based analysis of: (A) Percentage of outdoor areas er typology; (B) Sensitive Buildings number per square SBn; (C) Ratios between the indoor and outdoor areas (AIOIr). Outliers are shown by the dots.

5.2 Users' characterization

5.2.1 Hourly characterization

Figure 27 compares the UOod trends over the daytime for working days and holidays, as an effect of the square temporalities, for the whole sample of squares. On working days, the UOod peak appears in the morning (up to 0.75 pp/m² between 9-12 am), when all the users' typologies are active in the square areas, i.e. especially those relating to NR hosted in buildings open to the public. UOod values decrease in the afternoon (about 0.25-0.50 pp/m²) and the evening (about 0.15-0.25 pp/m²) until dropping under 0.10 pp/m² in the night hours when most of the users are only R. These general trends appear to be comparable during holidays, except for the morning hours of the holidays when UOod barely overcomes 0.50pp/m², thus suggesting a less intense use of the squares.

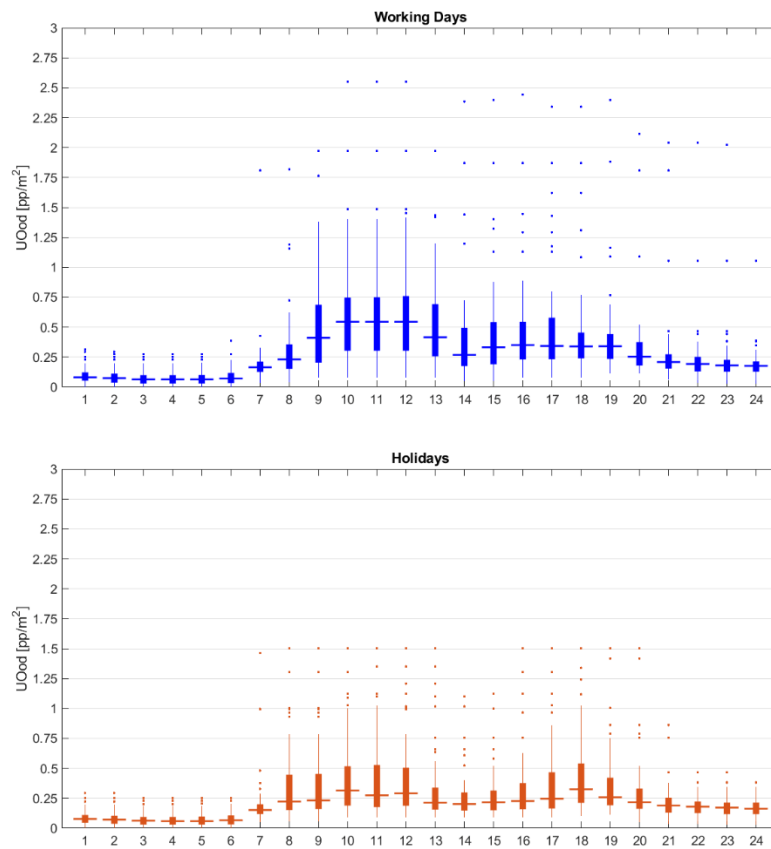


Figure 27: UHC-related KPIs - Quartile-based analysis of the Users' Overall outdoor density (UOod) on working days (in blue) and holidays (in orange). Outliers are shown by the dots.

The effects of hourly temporalities can be better displayed according to the analysis of percentages of users considering their familiarity with the square. Figure 28A shows that, for most of the day and both considering working days and holidays, the median OOp is generally less than 30% except at 7 and from 21 to 24 both for working days and holidays. However, since OO has been considered a non-time-dependent component (except during the night when they are absent), their percentage strictly depends on how other users' typologies populate the square (hence, on the dimensions of the indoor and outdoor areas and their related hourly temporalities).

As expected, PO represents the most limited part of the population, regardless of the daytime and day type, as the median POp always ranges between 0 and 5% (Figure 28B). This is due to the limited

Dp value, and so the small surface, as discussed in the previous subsection. Outliers in Figure 28B refer to non-stop activities, especially those hosted in squares without residential areas (during the evening and night-time), and for open markets (e.g. from 7 am to 7 pm), whose dimensions are considerably higher than the ones generally related to bars and restaurants with outdoor activities.

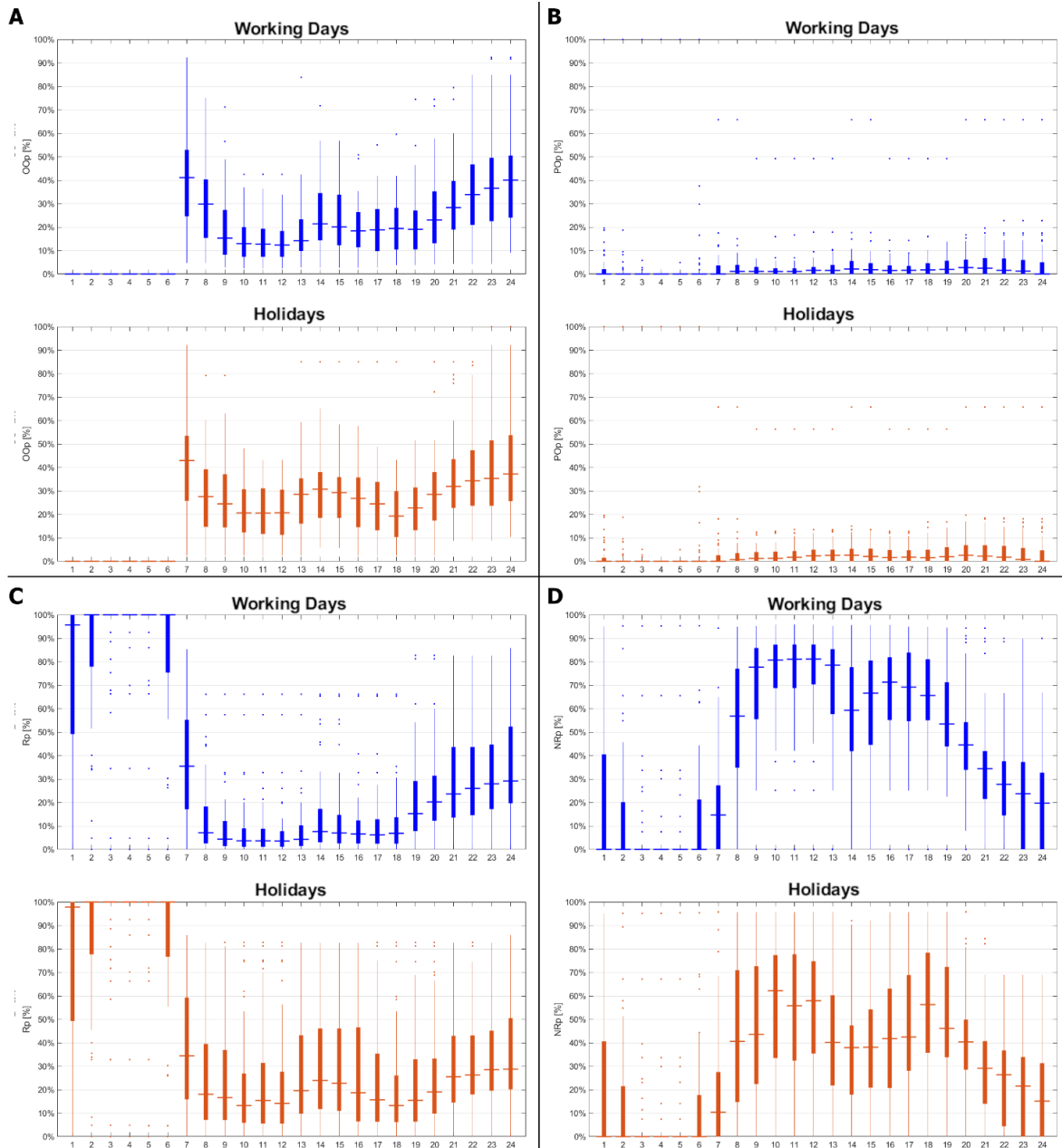


Figure 28: UHC-related KPIs – Quartile-based analysis of: (A) Only Outdoor users percentage OOp; (B) Prevalent Outdoor users percentage POP; (C) Residents users percentage Rp; (D) Non-residents percentage NRp. Working days are in blue, holidays in orange. Outliers are shown by the dots.

During the working hours of working days, i.e. from 8 am to 6 pm, R represents a small part of the population within the squares (Figure 28C), as shown by Rp, which is at most equal to 10% considering median values. This percentage increases to 10-40% (7-12 pm) in the evening, and up to 70-100% during the night (1-5 am), when OO is not accounted for, and most of the activities are closed (NR and PO). On the other hand, during holidays, R represents a larger part of the population because they are considered at home the whole day (on average, 15-35% excluding the night hours, where working days outcomes are confirmed). Both the working day and the holiday conditions point

out how the squares in the considered sample are mainly characterized as residential areas, as also remarked by the outliers that assume values near 0%.

In view of the above, Figure 28D shows how, during the working days, NRp is maximized during the working hours (8 am to 6 pm), where median NRp is always >60%, and minimized in the night-time (<30%), where non-stop activities placed indoor and hotels host most of NR. Such trends are confirmed for holidays, but data also show a significant decrease concerning attendance in the central hours of the days (about -20% with respect to the working days' trends between 8 am-8 pm). Anyway, in both conditions, outliers refer to hotels, accommodation structures, and non-stop activities.

5.2.2 Daily characterization

Figure 29 arranges the data applying the adopted quartile-based approach to extreme conditions of square use (maximum and minimum boxplot) and the recurring conditions (median boxplot), for working days and holidays. Figure 29A shows the UOod trends, thus considering all the users contemporarily in *outdoor areas*, such as in evacuation conditions. Considering the median data (gray boxplots), working days and holidays appear to be characterized by the same levels of density in outdoor (about 0.25 pp/m²). On the other hand, in peak conditions, the difference between working days and holidays appears to be significant, as values decrease by about 30/35% (blue boxplots). However, even considering the maximum subsets of data (blue boxplots) and excluding outliers (i.e. those for working days), the outdoor density is lesser than the critical value of 3.00 pp/m², which can lead to physical contact between individuals standing up, for instance, while waiting for the rescuers' access in emergency conditions excluding outliers [207].

According to Figure 29B, working days still represent more critical conditions than holidays considering UOid values, although density values are lower than those of UOod, thanks to the AIO_r>1 (compare with Figure 26B). This implies a slight impact of users outdoors on the overall conditions when particular circumstances can force them to move inside the buildings searching for safety or shelter (e.g., in case of terroristic attack outdoors; unacceptable environmental outdoor conditions related to air pollution or heatwaves).

Figure 29C shows Uid conditions according to the same quartile-based approach, thus only considering NR and R users. On working days, according to Section §5.2.1 discussion, peak conditions of each subset of data can be traced back basically to hours between 10-12 am, when most of the offices and government buildings are open to the public (i.e., the ones that can host the higher number of users because of their dimension and occupant load). In holiday scenarios, Uid values are lower, and essentially affected by the opening conditions of theatres, museums, and religious buildings, whose OL_T and dimensions are similar to those of other public buildings open on working days.

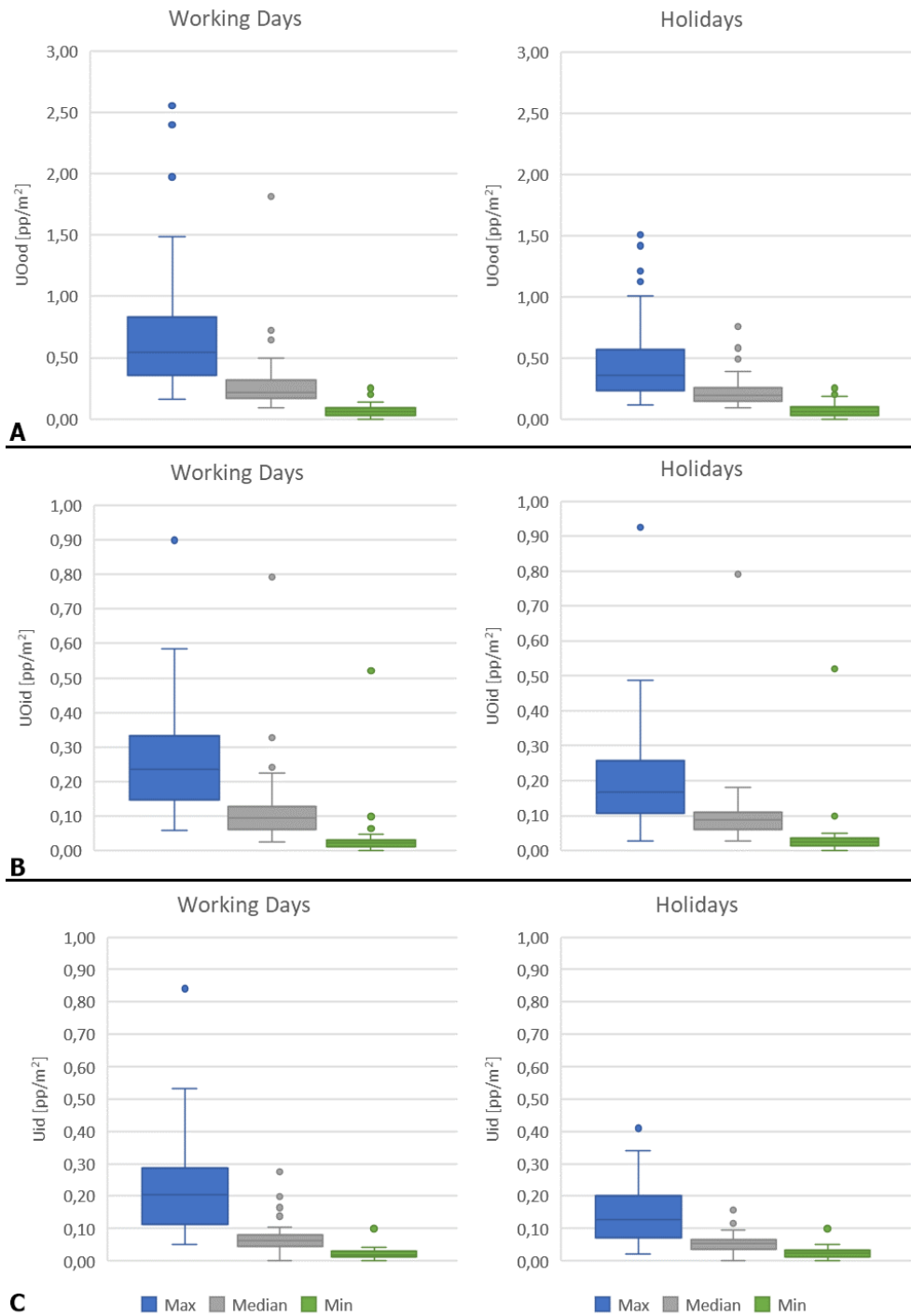


Figure 29: UDC-related KPIs - Quartile-based analysis of: (A) Users' Overall outdoor density UOod; (B) Users' Overall indoor density; (C) Users' indoor density Uid in working days and holidays. Outliers are shown by the dots.

Previous outcomes about densities find confirmation by analyzing the ratio between users populating *indoor* and *outdoor areas* of the square (Figure 30). Indeed, the median UIOr data ranges between about 2 and 5 both considering the working days and holidays scenarios (gray boxplots, quartiles 1 and 3), with maximum peak conditions up to 15, excluding outliers and data on maximum values subsets (blue boxplots). However, the median values of the minimum subset of UIOr (that is minimizing the indoor users and maximizing the outdoor users), remain around 1 (green boxplots in Figure 30), meaning that indoor and outdoor users are at least equal in both working days and holidays.

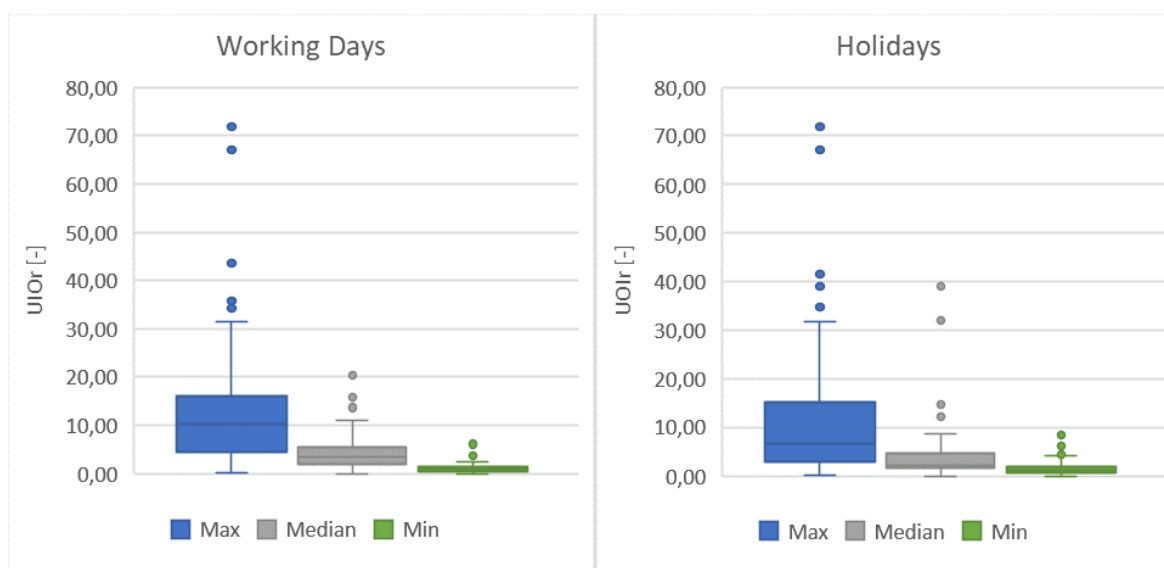


Figure 30: UDC-related KPIs - Quartile-based analysis of UIOr in working days and holidays. Outliers are shown by the dots.

The characterization of quartile-based analysis of users depending on their familiarity with the POS, considering the whole daily data derived from the same KPIs on hourly temporalities in Section §5.2.1, rapidly traces the general features of the sample of squares investigated in this work. Figure 31A shows that recurring conditions for OOp assume the range between about 10-30% of the population (gray boxplots). As also pointed out in Figure 28A, minimum values refer to the nighttime (0%), while maximum refers to (a) particular hours of the day when most of the other users' typologies are absent (e.g., early in the morning) or (b) squares without residential buildings.

Figure 31B underlines how, for both the working days and holidays, PO represents a limited part of the population also in peak condition (blue boxplots, expect outliers). Minimum data for each subset of values refer to closing time (or absent dehors areas). Outliers mainly describe covered/partially covered areas within the square, like permanent shelters for open markets (hosted during the day), whose dimensions are considerably higher than the ones generally related to bars and restaurants, as also displayed in Figure 28B.

Figure 31C and Figure 31D respectively trace the data for R and NR, during working days and holidays. As also demonstrated in Figure 28C and Figure 28D, most of the squares are mainly used for residential purposes, thus boosting the Rp values, especially during the holidays, which implies considering most of the activities for NR close to the public. Minimum data of Rp values refers to working hours, while maximum data, up to 100%, to night-time. However, in working days, considering the median subset of data for Rp and NRp (gray boxplots), it could be pointed out that NR higher affects the recurring daily conditions of the squares since they range from 35-55% (1st and 3d quartiles in Figure 31D) with respect to 10-30% referring to R (1st and 3d quartiles in Figure 31C). During holidays, such values assume an opposite trend, with slight Rp differences of about +10% with respect to working days, thanks to the limited impact of openings of public buildings (i.e. theatres, museums, religious buildings) during the daytime (i.e. compare Figure 28C and Figure 28D).

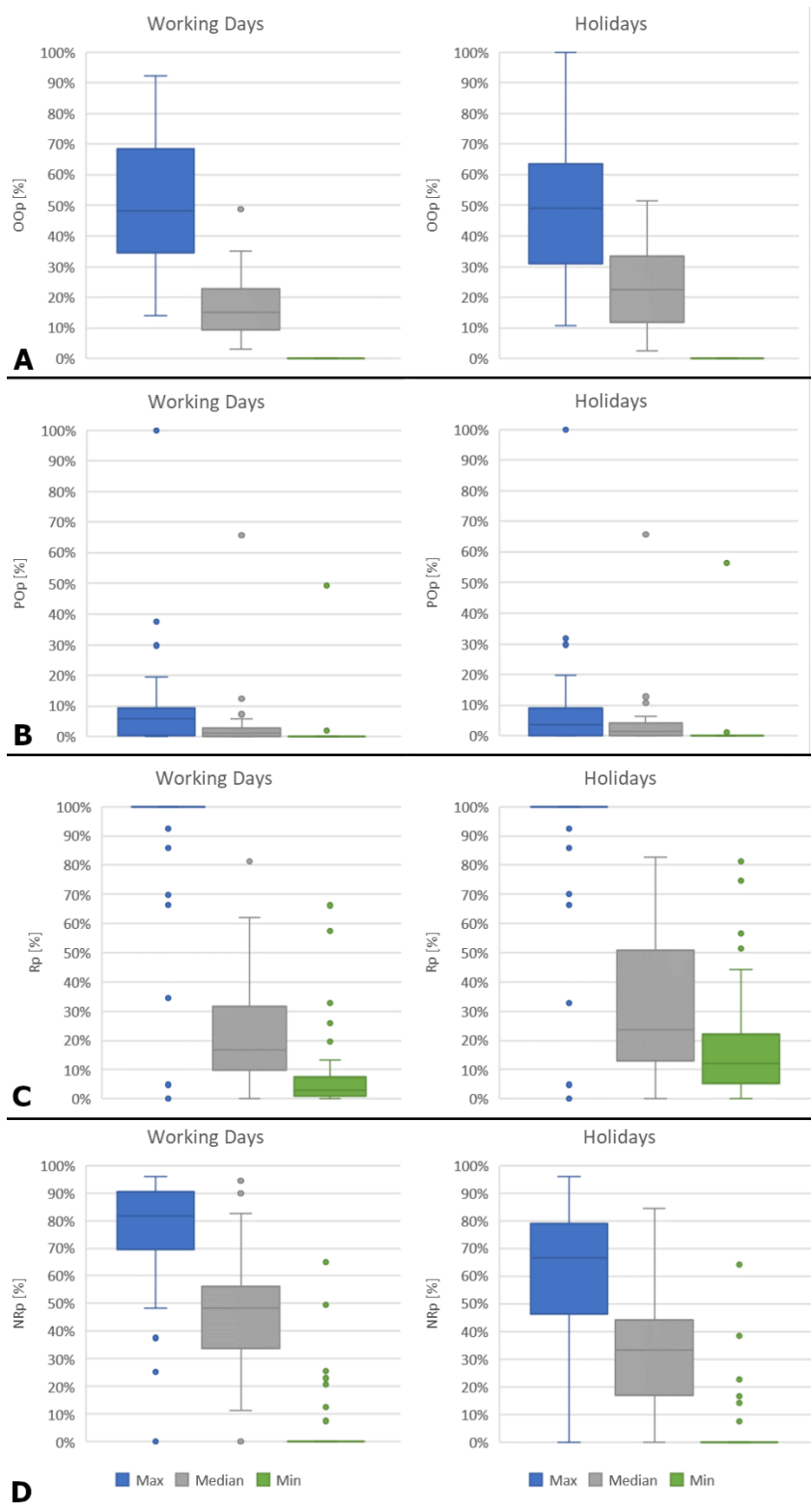


Figure 31: UDC-related KPIs - Quartile-based analysis of: (A) Only Outdoor users percentage OOp; (B) Prevalent Outdoor users percentage POp; (C) Residents users percentage Rp; (D) Non-residents percentage NRp in working days and holidays. Outliers are shown by the dots.

Figure 32 shows results on the individual vulnerabilities according to the users' age and gender, which are consistent with Italian national statistics [298], also in view of the quick data source used in this work.

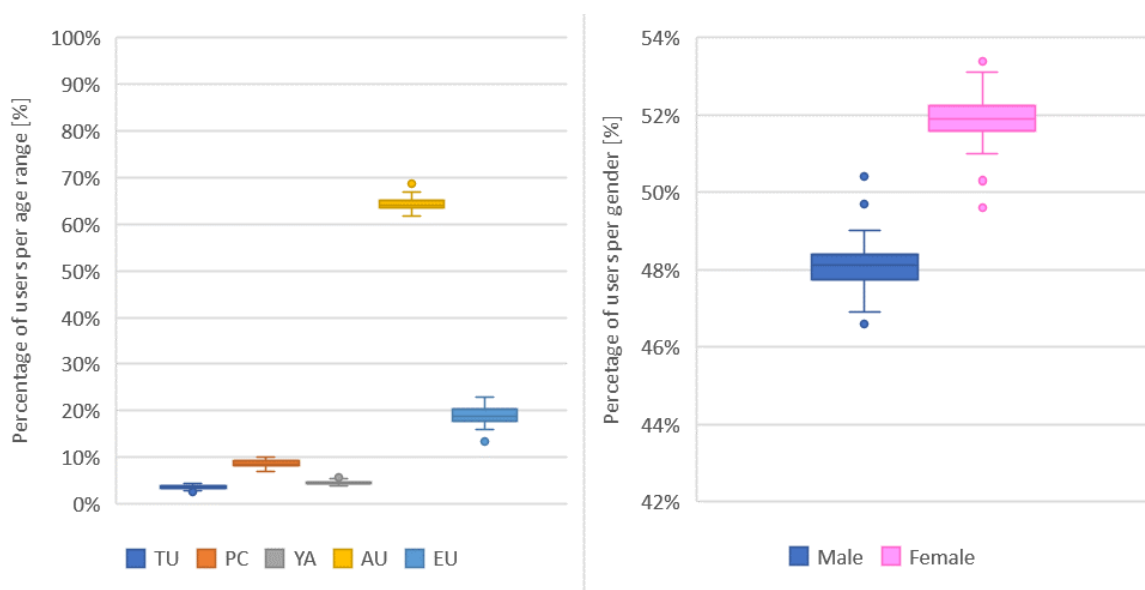


Figure 32: UDC: *Quartile-based analysis considering individual vulnerability (age and gender). Outliers are shown by the dots.*

5.3 Outcomes evaluation

Results demonstrate that this work provides an innovative and quick-to-apply methodology to collect and quantify data for the users' vulnerability and exposure characterization in POS, by both allowing deriving typological conditions and performing single case analyses (see Section §11.3.5 for an application example). In this sense, such results can be herein discussed to point out innovation, policy implications, limitations, and future aims.

5.3.1 Innovation of the results

Compared to the current state of the art, this work innovatively provides a new methodology for the typological description of a sample of POS (like squares) in cities prone to risks thanks to innovative KPIs concerning both general features of the built environment (POSC-related KPIs), and the users' temporalities affecting vulnerability and exposure issues (UHC- and UDC- related KPIs).

Considering such a typological perspective relying on the whole sample application (in this work, 56 Italian squares), the typological description firstly confirms previous works relating to POSC-related KPIs, as: (1) "Theatres, Museums, Religious buildings" and "Government buildings" are the most frequent special buildings and uses in the squares [297]; (2) the high built-up density of the considered squares (see AIO_r) is one of the fundamental markers for the characterization of historic scenarios, especially in the Italian context [13], [44], [210]; (3) a non-negligible part of such scenarios is destined to carriageable areas (see CA_p) [297].

Concerning UHC and UDC, the proposed approach to mesoscale analyses confirms how users' temporalities are fundamental to evaluating how users' exposure and vulnerability issues vary and evolve over space and time [10], [76]. In the considered case studies sample, UHC-related peak conditions of square use (compare Section 4.2) are gained between 10-12 am either on: (a) working days, when most of the functions and public office are open; and (b) holidays, because of the presence of religious building hosting a large number of users. Users in indoor areas represent the largest part of the population within the square, while outdoor users increase when activities hosting a large number of users are closed, that is early in the morning (e.g., restaurants, museums) and in the

evening (e.g., offices). Finally, users' vulnerability issues depending on age and gender are in keeping with the national percentage distributions, mainly due to the low recurrences of functions that can vary the trend in the analyzed sample (e.g., schools, nursing homes).

In view of the above, Table 28 traces the users' daily characterization through the median values of the UDC-related KPIs [180]. It is worthy of notice that Table 28 provides no time-dependent quantification of the typological scenario, but it reliably offers a quick and general overview of the POS recurring features.

KPI	Max (W : H)	Med (W : H)	Min (W : H)
UOod	0.55 : 0.36	0.22 : 0.20	0.06 : 0.06
UOid [pp/m ²]	0.24 : 0.17	0.10 : 0.09	0.02 : 0.02
Uid [pp/m ²]	0.20 : 0.13	0.06 : 0.05	0.02 : 0.02
UIOr [-]	10.26 : 6.64	3.47 : 2.15	0.94 : 1.04
OOp [%]	48 : 49	15 : 23	0 : 0
POp [%]	6 : 4	1 : 1	0 : 0
Rp [%]	100 : 100	17 : 24	3 : 12
NRp [%]	82 : 67	48 : 33	0 : 0

Table 28: Outline of the typological description of the square according to the median values of UDC-related KPIs.

5.3.2 Policy for stakeholders and practitioners

In view of the innovations listed in the previous subsection, key findings of our works can be also exploited by local administrators and their low-trained technicians (mainly, municipalities or even public event managers) for risk assessment and mitigation purposes, for application to their single case studies that could be potentially affected by different SLODs and/or SUODs. Such policy implications are connected to two main issues.

First, technicians could use very simple and quick-to-apply outputs of Table 28 to depict the general scenario of their own POS according to UDC-related KPIs, just using the POS surface as a reference to evaluate the crowding level in it. Similarly, UHC-related KPIs can be then used to deepen the users' factors trends and roughly estimate peak conditions.

Second, stakeholders could directly apply the method to their specific POS, being guided toward the users' factors assessment in a structured manner. They can take advantage of easy-to-collect variables using open-data and freely accessible databases to easily evaluate the potential impact on users of peak conditions of use of the POS. These pre-emergency data can be then combined with particular circumstances leading all users to move towards outdoor (e.g., earthquakes), or indoor (e.g., to perform sheltering-in-place for terrorist acts, especially in holidays, or to mitigate effects of SLODs like heatwaves or air pollution).

In addition to such issues, the proposed methodology can be boosted and easily adapted to consider specific elements in the POS in the presence of more detailed sources and analyses provided for instance by local authorities. In this sense, this task can be achieved by: (1) introducing specific data measuring the presence of certain users' typologies, like tourists or daily commuting; or (2) by considering the impact of seasonality that may influence the use of spaces, like weather conditions, hours of sun per day, shadow shapes, and so on). However, in view of the conservative approach proposed both for the data collection and the crowding conditions evaluation (according to the maximum occupant loads indicated by the current Italian regulations for the users' quantification),

the present methodology is also suitable for providing basic conditions for more detailed analyses, such as those related to behavioral correlation with climatic factors, or the evaluation of pre-emergency conditions in the POSs (that is excluding the contemporary presence of SLOD or SUOD events). Therefore, enabling also comparisons between different case studies and/or different usage conditions.

5.3.3 *Limitations and future aims*

The authors are aware of limitations due to some simplifications in the POS analysis assumptions, which should be solved by future works, and mainly:

- a. possible changing environmental conditions (e.g., due to seasonality, weather conditions, lightning conditions both during daytime and nighttime, and shape of the shadows during the daytime). They could highly influence the use of outdoor areas for public activities like bars and restaurants (in this work, *dehors*), as well as areas for leisure purposes and spontaneous gathering of users, so their presence, characterization, and spatiotemporal variations could be added by future efforts, by associating specific crowding indexes or use probabilities;
- b. elements that can increase (e.g., green areas, blue areas, playgrounds, benches, monuments, and sights) or decrease (e.g., air and noise pollutants) the attractiveness of the spaces. As for previous point A, future efforts could better quantify the impact of them in how (mainly) walkable outdoor areas pedestrian densities can be modified, thus overcoming the assumption of the maximum occupant load of 0.10 pp/m^2 adopted in a homogeneous way for each case study in this work, and thus for both for monumental and leisure areas;
- c. evaluate the influence that the cities' characteristics play on the POSs, including effects of touristification, daily commuting, and seasonal variations. Future efforts should be devoted to the same actions for the previous point (b) and could move towards the clustered organization of squares into more detailed sub-typologies depending on similar composition and geometrical features. To this end, the same approach of this work could be fully adopted, by increasing the sample dimension.

In view of the above, the current methodology could be easily updated for future application, such as by varying densities of some occupant loads depending on the application contexts (e.g., historical POS in several Countries) or by applying them for specific types of areas (e.g., indoor and outdoor sights that attract visitors “unfamiliar with the POS”). In this way, although the current computation only depends on the squares' geometrical features, we could still *rapidly* consider the presence of certain users' typologies regardless of aspects difficult to quantify without having particularly refined sources and analyses (e.g., touristification in a capital city is different than in smaller cities).

In addition to this, further research could improve the results of the adopted “robust-to-outliers” methodology by increasing the case-studies sample and then moving toward cluster analysis techniques [42], [45], which allow the organization of groups of squares by homogeneous classes and so the possibility to quickly identify the most probable typology of the square thanks to the KPIs combination. In this sense, some user-related KPIs proposed in this work could be selected as the most relevant ones, and the square description could combine them with morphological, functional, and physical features.

6. How hazard features can affect pedestrian evacuation: investigating behavioral patterns under different floodwater conditions

Results on behavioral patterns through video analyses are organized in four sections: firstly, the overall frequency PI/PO in relation to the overall sample is discussed (Section 6.1); then, the situational frequencies in relation to the floodwaters' depth and flow evaluated are evaluated separately (PI_d/PI and PI_f/PI) and jointly ($PI_{d,f}/PI_d$) (Section 6.2); behavioral patterns are finally traced (Section §6.3) and discussed according to their innovations, limitations, and future aims (Section §6.4). By-literature and new-noticed behaviors are discussed together.

6.1 Observed behaviors and their overall frequency

For what concerns *new-noticed* behaviors, 444 pedestrians have been observed clinging to ropes and cables during their motion and eventually holding hands to arrange “human chains” (see Figure 33), making it the second most performed behavior in terms of PI [pp]. In general, such responses allow for improving the evacuation process by mitigating problems related to human speed and body instability in the floodwaters. Although some similarities are shared with other literature behaviors, the following main differences can be respectively noticed:

- while in *attraction towards unmovable obstacles* M2 pedestrians (try to) reach supports, in this case, they can be reached by ropes and cables on site, thus avoiding further dangerous movements in floodwaters;
- differently from *social influence and group phenomena* M6, in this case, physical contacts are not only widely accepted by pedestrians, but also sought after.



Figure 33: Panel A: a group of 4 pedestrians clinging to a rope (in brown) and arranging a human chain {48}. Panel B: a group of 15 pedestrians clinging to a rope and arranging a “human chain” {17}. Jagged lines in blue indicate the waves.

Thus, this behavior will be referred to in the following as *clinging to ropes and arranging “human chains”*, and can be classified as: (1) relevant to the *motion toward the evacuation target* phase, as it concerns the actual physical movement through and out of the flooded areas; (2) *peculiar*, as it can be currently observed only for flood evacuations, at the authors' knowledge; (3) *deliberately chosen*, since it is performed as a result of a decision; (4) *protective*, since it is aimed at improving the pedestrian safety; (5) relying on *environmental elements*, as it depends on the presence of i.e. ropes

and cables (even though partially also on the direct support of rescuers or other pedestrians by means of their body within the “human chain”). In view of the following behavioral analysis, Table 29 resumes this classification according to the same layout as Table 67, while Figure 34 resumes all the behaviors considered for the following proper video analysis.

ID	Behavior and Definition	Type	Voluntariness	Human Response	Reference Elements
M9	Clinging to ropes and arranging “human chains”: pedestrians look for physical support by grabbing ropes and eventually holding hands	Peculiar	Deliberately Chosen	Protective Behavior	Environmental Elements

Table 29: New-observed behavior classified into the “Motion towards the evacuation target” phase.

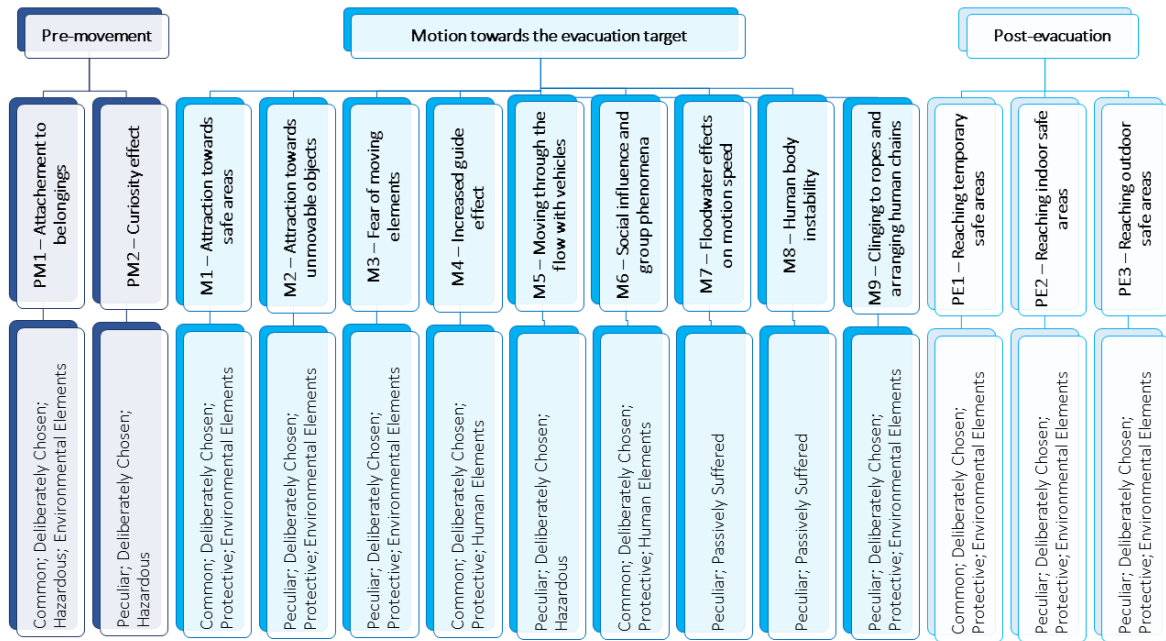


Figure 34: Final picture of all the behaviors observed in the videotapes organized per evacuation phase, which integrates literature classifications.

Figure 35 resumes the Overall frequency PI/PO [%] of the observed behaviors (right y-axis) and the reference number of People Overall PO [pp] as the sample dimension (left y-axis).

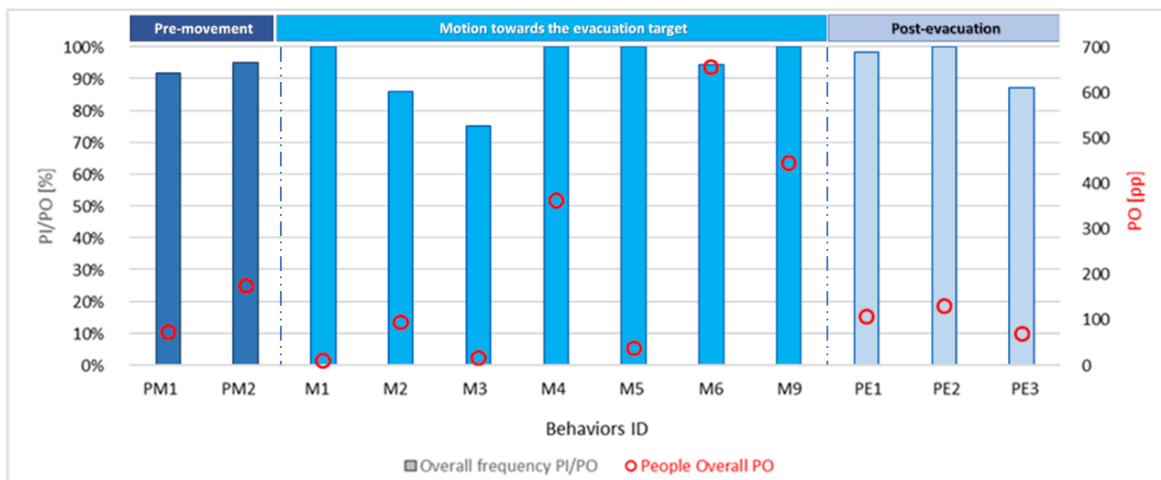


Figure 35: Overall frequency PI/PO [%] (colored bars; left y-axis) of deliberately chosen behaviors, and People Overall PO [pp] as the sample dimension (red circles; right y-axis).

For what it concerns the behaviors of the *pre-movement* phase, results confirm the tendency of people to perform *hazardous behaviors* before starting a flood evacuation [223], as PI/PO is higher than 90% both for *attachment to belongings* PM1 and “*curiosity*” effects PM2 on a sample of, respectively 72 and 173 PO.

As regards the *motion towards the evacuation target* phase, results demonstrate that the presence of evacuation leaders, rescuers, and their equipment (i.e., ropes and cables) almost always triggers behaviors like *increased guide effect* M4, *social influence and group phenomena* M6, and *clinging to ropes and arranging “human chains”* M9, as stated by PI/PO close to 100% (even if some exception may exist, for instance due to factors like the lack of trust in authorities and warnings [153], [299]). Furthermore, they also are the most observed behaviors as they rank in the top three for the highest number of people involved (PI) and people overall (PO), being both greater than 300 pp. Similarly, the other *observed behaviors* (*attraction towards safe areas* M1, *attraction towards unmovable obstacles* M2, *fear of moving elements* M3, and *moving through the water with vehicles* M5) recorded a high PI/PO, although with smaller samples.

Finally, *post-evacuation* phase results seem to point out a slight, overall preference for people in *reaching indoor safe areas* (PE2, PI/PO=100% on 139 PO) rather than *outdoor* (PE3, PI/PO=87% on 69 PO).

6.2 Statistical frequencies with respect to situational samples

Situational frequencies contextualize behavioral data with respect to the floodwater conditions in which they are observed. General results are resumed in Table 31 and Table 32. Inferential statistical outcomes are shown in Table 30, according to the Chi-squared test. For all the considered conditions, the test results prove how the performed behaviors can be considered non-independent of the floodwater situational conditions. Finally, in the following subsections behavioral patterns are organized and discussed per evacuation phase.

Parameter [pp]	CATEGORIES	DOF	Critical Chi-square $\chi^2_{(\alpha; DOF)}$	Pearson's Chi-square S
PI _d	Behaviors x Water Depth	39	54.57	645.86
PI _f	Behaviors x Water Flow	13	22.36	323.97
PI _{d,f}	Behaviors x Water Conditions	91	114.26	1459.51

Table 30: Chi-squared test outcomes. For $S > \chi^2$ the null hypothesis is rejected and provides support that the categories are related. DOF stays for Degree of Liberty. The significance level α is 0.05; p -values are < 0.00001 in all the cases.

		Post-evacuation		Motion towards the evacuation target									Post-evacuation		
		PM1	PM2	M1	M2	M3	M4	M5	M6	M7	M8	M9	PE1	PE2	PE3
PI_d/PI [%] (Figure 36)	ANKLES	32	47	33	20	0	32	75	23	29	19	20	0	2	73
	KNEES	44	53	11	43	8	25	22	46	49	31	38	95	17	7
	WAIST	14	0	56	33	92	32	0	29	16	37	38	0	66	20
	HIGHER	11	0	0	5	0	10	3	2	6	13	4	5	15	0
PI_f/PI [%] (Figure 37)	STILL	59	27	89	14	0	49	47	19	46	8	37	0	6	45
	FLOWING	41	73	11	86	100	51	53	81	54	92	63	100	94	55

Table 31: Situational frequency percentages of the observed behaviors evaluated with respect to the water depth (PI_d/PI [%]) and the water flow (PI_f/PI [%]). Behavior IDs from Figure 34.

		Post-evacuation				Motion towards the evacuation target												Post-evacuation											
		PM1		PM2		M1		M2		M3		M4		M5		M6		M7		M8		M9		PE1		PE2		PE3	
		S	F	S	F	S	F	S	F	S	F	S	F	S	F	S	F	S	F	S	F	S	F	S	F	S	F	S	F
A Figure 39		29	71	55	45	100	0	6	94	-	-	74	26	41	59	17	83	0	100	0	100	88	12	-	-	100	0	61	39
K Figure 41		72	28	2	98	0	100	12	88	0	100	55	45	75	25	20	80	71	29	2	98	30	70	0	100	0	100	0	100
W Figure 43		56	44	-	-	100	0	19	81	0	100	15	85	-	-	18	82	31	69	5	95	15	85	-	-	6	94	0	100
HW Figure 45		100	-	-	-	-	-	25	75	-	-	61	39	0	100	36	64	100	0	43	57	50	50	0	100	0	100	-	-

Table 32: Situational frequency percentages per water depth of the observed behaviors (PI_{d,f}/PI_d [%]). Behavior IDs from Figure 34, abbreviations from Figure 14.

6.2.1 Water Depth influence

Figure 36 shows the results concerning the situational frequency with respect to water depth, thus regardless of the water flow. Considering the evacuation phases, it is worthy of notice that:

- *Pre-movement* phase: the “curiosity” effect PM2 has been observed only with floodwaters lower than the knees, while *attachment to belongings* PM1 phenomena result can be noticed for all the water depth conditions;
- *Motion towards evacuation target* phase: *moving through the water with vehicles* M5 is more frequent for water depths up to the ankles ($PI_A/PI=75\%$), essentially in view of the lower perception of risk in such conditions. Behaviors (a) aimed at restoring the pedestrians’ safety (*attraction towards unmovable obstacles* M2, *increased guide effect* M4, *social influence and group phenomena* M6, *clinging to ropes and arranging “human chains”* M9) and (b) the ones producing dangerous effects on the pedestrians’ motion (*floodwaters effects on motion speed* M7 and *human body instability* M8) have a similar frequency in each condition, ranging from 20-40%, while are less frequent for water depth above the waist condition ($PI_{HW}/PI<10\%$). *Fear of moving elements* M3 is finally more frequent for water levels up to the waist, that is essentially when objects start floating and then are dragged by floodwaters (compare also Section 4.2.2) [300].
- *Post-evacuation* phase: pedestrians generally prefer *reaching outdoor safe areas* PE3 with floodwaters under the ankles ($PI_A/PI=73\%$), and *reaching indoor safe areas* PE2 with higher depth values ($PI_W/PI=66\%$). The possibility of *reaching temporary safe areas* PE1 is more frequent for water depths between the ankles and the knees. In such conditions, pedestrians are still able to move without suffering major impediments [223], [231].

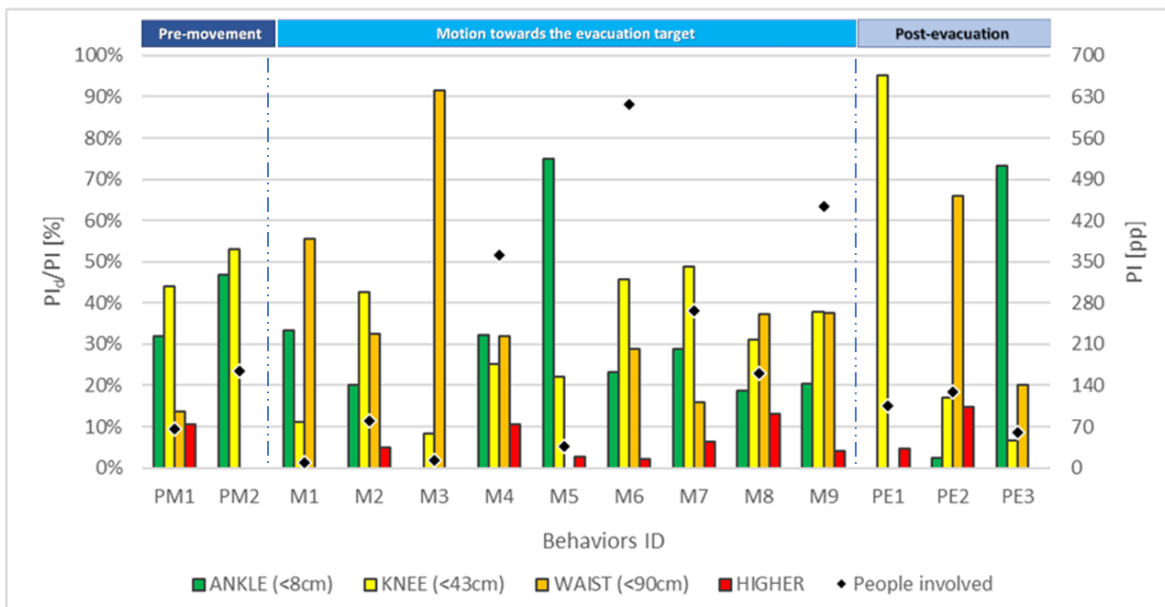


Figure 36: Situational frequency PI_d/PI [%] (colored bars; left y-axis) of the observed behaviors evaluated with respect to the water depth levels, and People Involved PI [pp] as the sample dimension (black rhombuses; right y-axis). Behaviors IDs from Figure 34.

6.2.2 Water Flow influence

Figure 37 shows the results concerning the situational frequency with respect to water flow. Considering the evacuation phases, it is worthy of notice that:

- *Pre-movement phase: attachment to belongings* PM1 is more frequent in the case of still water, essentially because of lower possible floodwater resistance against pedestrians' motion. Vice versa, results show that the "curiosity" effect PM2 seems more likely to be activated with flowing water. Thus, such insight seems to suggest that pedestrians find the water depth more dangerous than its flowing conditions, because, on the contrary, the situational frequency of this behavior decreases with the increasing severity of the event in terms of water depth (see PI_d/PI in Figure 36).
- *Motion towards evacuation target phase: protective behaviors* are more frequent with flowing water ($PI_F/PI > 80\%$) suggesting: (a) a greater sense of danger perceived by the pedestrians in such conditions (considering the increase of, e.g., *social influence and group phenomena* M6); and (b) the suffered impact of effective more severe conditions that trigger *human body instability* M8 [227] and so of the related actions to restore it (i.e., *attraction towards unmovable objects* M2 and *clinging to ropes and arranging "human chains"* M9) [134]. *Fear of moving elements* M3 is due to flowing water dragging objects ($PI_F/PI = 100\%$). Results also seem to point out that *attraction toward safe areas* M1 is more frequent in still waters, but this result could be partially affected by the small sample dimension (<10 pedestrians involved).
- *Post-evacuation phase: general outcomes* seem to highlight that *temporary* PE1 and *indoor safe areas* PE2 are mainly reached in case of flowing waters ($PI_F/PI > 90\%$), mainly because of the efforts due to moving against higher resistance of floodwaters [301], while in the case of still water pedestrians choose *outdoor safe areas* PE3 too (PI_S/PI and PI_F/PI between 45-55%).

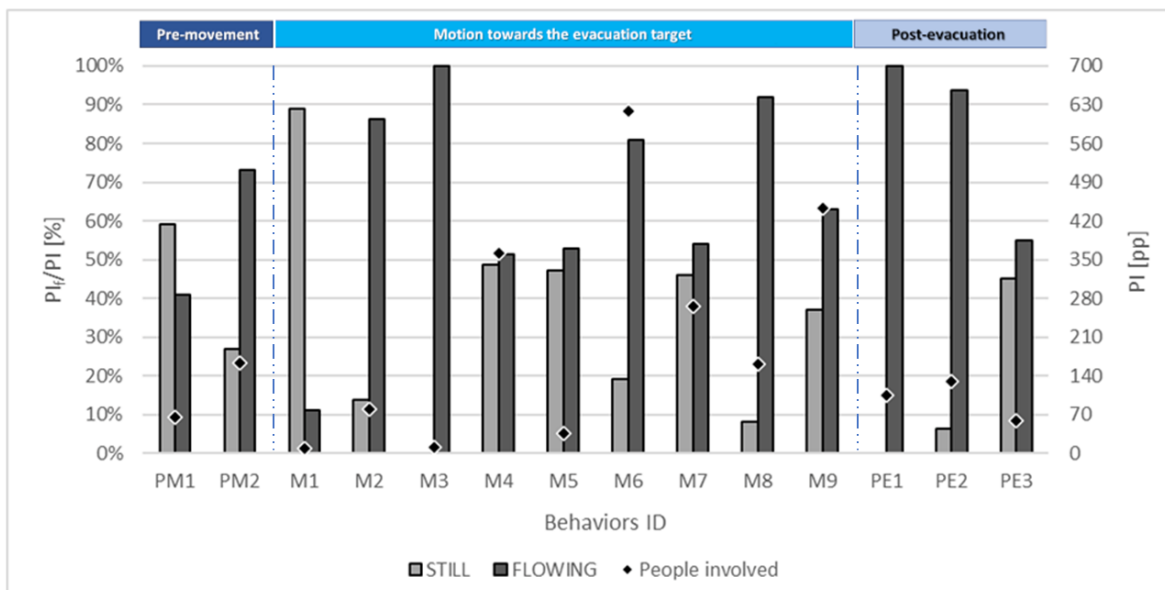


Figure 37: Situational frequency PI_f/PI [%] (colored bars; left y-axis) of the observed behaviors evaluated with respect to the water flow levels, and People Involved PI [pp] as the sample dimension (black rhombuses; right y-axis). Behaviors IDs from Figure 34.

6.2.3 Water depth equal to or up to the ankles

Figure 39 shows the results concerning the situational frequency with respect to water depth equal or up to the ankles, by distinguishing between still and flowing waters (Figure 38). Considering the evacuation phases, it is worthy of notice that:

- *Pre-movement phase: hazardous behaviors (attachment to belongings PM1 and “curiosity” effect PM2)* are noticed in both still and flowing waters conditions, although *attachment to belongings PM1* is less frequent in case of still water ($PI_{A,S}/PI_A = 29\%$), probably due to a slighter sense of danger felt by pedestrians with regards to their goods [223].
- *Motion towards evacuation target phase:* behaviors assuming motion problems are essentially activated with flowing water (i.e., for *floodwaters effects on motion speed M7*, *human body instability M8*, and *attraction toward unmovable obstacles M2*, $PI_{A,F}/PI_A > 95\%$) since the possibility to move the feet inside or outside of the water is also affected by the additional resistance of flowing waters [50], [231], [243]. Behaviors that typically involve the presence of rescuers (i.e., *increased guide effect M4* and *clinging to ropes M9*) seem to be more frequent with still water ($PI_{A,F}/PI_A > 70\%$), thus highlighting the importance of safety procedures also in less severe floodwater conditions that can still affect the safety of most vulnerable pedestrians, such as children, elderly, and pedestrians with mobility impairments. *Social influence and group phenomena M6* are more frequent with flowing water ($PI_{A,F}/PI_A = 83\%$). Videotapes involving the presence of *moving elements M3* were not found, essentially because of the limited water depth.
- *Post-evacuation phase:* pedestrians selecting *temporary safe areas PE1* were not found while *reaching outdoor safe areas PE3* appears to be a common solution both in the cases of still and flowing waters. The statistical significance of *reaching indoor safe areas PE2* could be limited in view of the sample dimension ($PI_A=3$ pp, all in the same videotape).

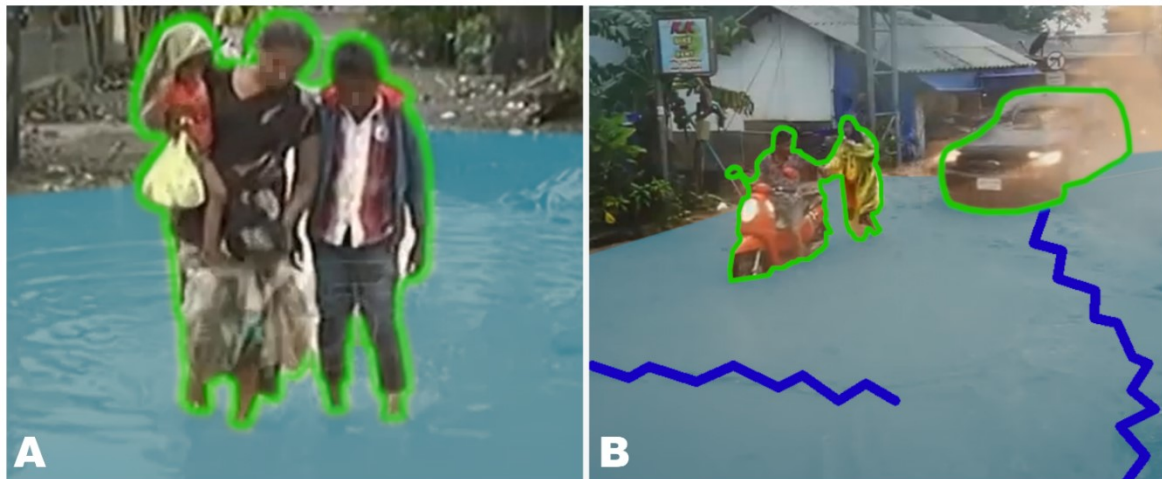


Figure 38: People dealing with water up to the ankles (outlined in green). Panel A is for still water, panel B is for flowing water and the blue jagged lines indicate the waves (reference videotapes: {70}, {119}).

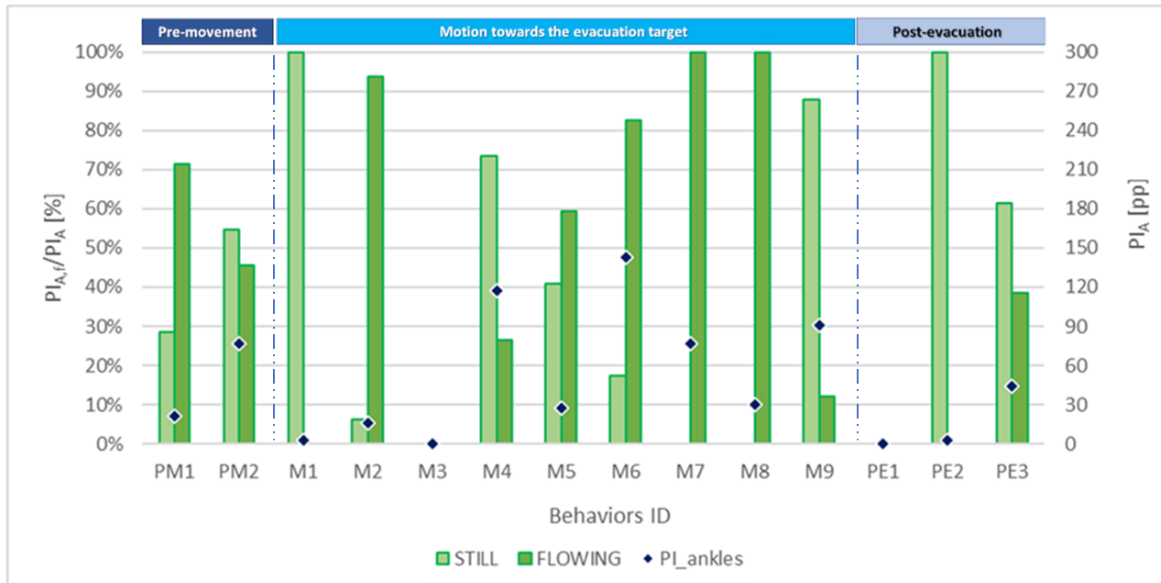


Figure 39: Situational frequency per water depth equal to or lower than the ankles $PI_{A,t}/PI_A$ [%] (colored bars; left y-axis) of the observed behaviors evaluated by comparing the water flow. The sample dimension is outlined by PI_A [pp] (black rhombuses; right y-axis). Behaviors IDs from Figure 34.

6.2.4 Water depth equal to or up to the knees

Figure 41 shows the results concerning the situational frequency with respect to water depth higher than the ankles, but equal or up to the knees, by distinguishing between still and flowing waters (Figure 40). Considering the evacuation phases, it is worthy of notice that:

- *Pre-movement* phase: differently from the ankle-related situational frequencies ($PI_{A,t}/PI_A$, Figure 39), *attachment to belongings* PM1 is more frequent in still water ($PI_{K,S}/PI_K = 72\%$), while “*curiosity*” effect PM2 in flowing conditions ($PI_{K,F}/PI_K = 98\%$).
- *Motion towards evacuation target* phase: *human body instability* M8 still can be essentially noticed in flowing water. On the contrary, *floodwater effects on motion speed* M7 seem to be more frequent in still water, thus implicitly confirming the possibility of moving in such conditions while being affected by a reduction in the evacuation speed [50], [231], [243]. The sample dimensions for these behaviors are different, and they could influence the results. However, behaviors aimed at restoring the people’s safety like *fear of moving elements* M3, *social influence and group phenomena* M6, and *clinging to ropes and arranging “human chains”* M9 are confirmed to be more frequent in flowing water ($PI_{K,F}/PI_K > 80\%$). *Moving through the flow vehicles* M5 is more frequent in still water, which implies less severe conditions in terms of floodwaters resistance against the vehicles [300].
- *Post-evacuation* phase: videotapes with pedestrians *reaching temporary* PE1, *indoor* PE2, and *outdoor safe areas* PE3 were only found with flowing waters.



Figure 40: People dealing with water up to the knees (outlined in yellow). Panel A is for still water, panel B is for flowing water and the blue jagged lines indicate the waves (reference videotapes: {76}, {42}).

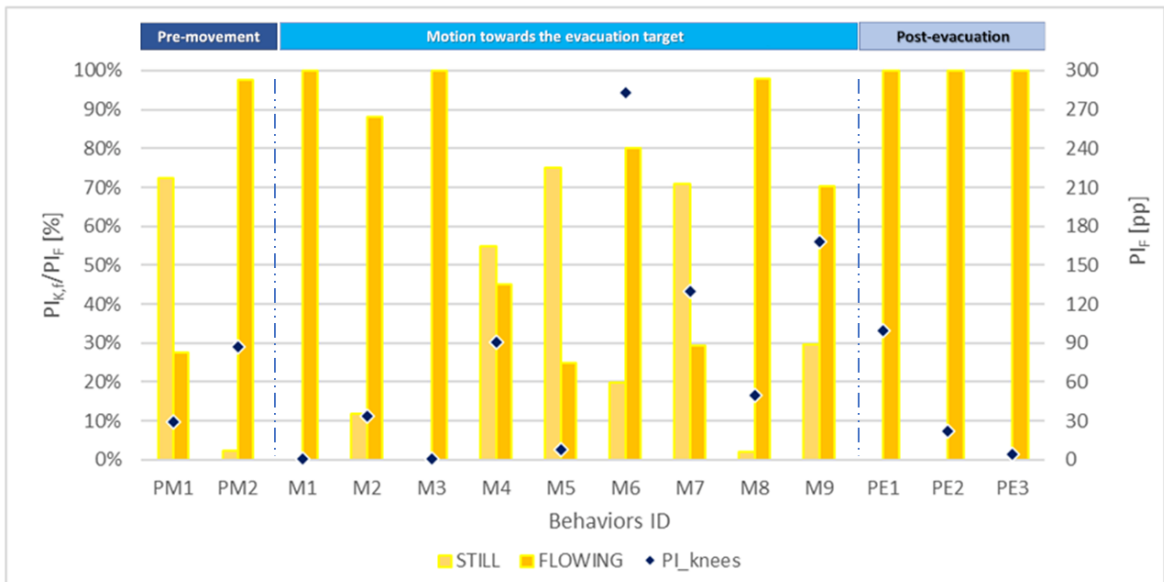


Figure 41: Situational frequency per water depth equal to or lower than the knees $PI_{k,t}/PI_k$ [%] (colored bars; left y-axis) of the observed behaviors evaluated by comparing the water flow. The sample dimension is outlined by PI_k [pp] (black rhombuses; right y-axis). Behaviors IDs from Figure 34.

6.2.5 Water depth equal to or up to the waist

Figure 43 shows the results concerning the situational frequency with respect to water depth higher than the knees, but equal or up to the waist, by distinguishing between still and flowing waters (Figure 42). Considering the evacuation phases, it is worthy of notice that:

- *Pre-movement phase: “curiosity” effect* PM2 was not found in the analyzed sample, while *attachment to belongings* PM1 has a quite similar frequency in both still and flowing waters.
- *Motion towards evacuation target phase:* general outcomes of $PI_{k,t}/PI_k$ (Figure 41) are confirmed, especially for *fear of moving elements* M3 as the number of people involved increases. *Moving through the water with vehicles* M5 was not found in the analyzed sample.

As expected [50], [227], [301], issues concerning *Floodwater effects on motion speed* M7 and *human body instability* M8 are more frequent in flowing waters.

- *Post-evacuation* phase: for what it concerns *reaching indoor safe areas* PE2 and *outdoor safe areas* and PE3, results are similar to the knees-related outcomes ($PI_{K,t}/PI_K$, Figure 41) and they are also corroborated by a greater number of people involved ($PI_{waist} = 90pp$, $PI_{knees} = 30pp$). On the other hand, *reaching temporary safe areas* PE1 was not found in the analyzed sample.

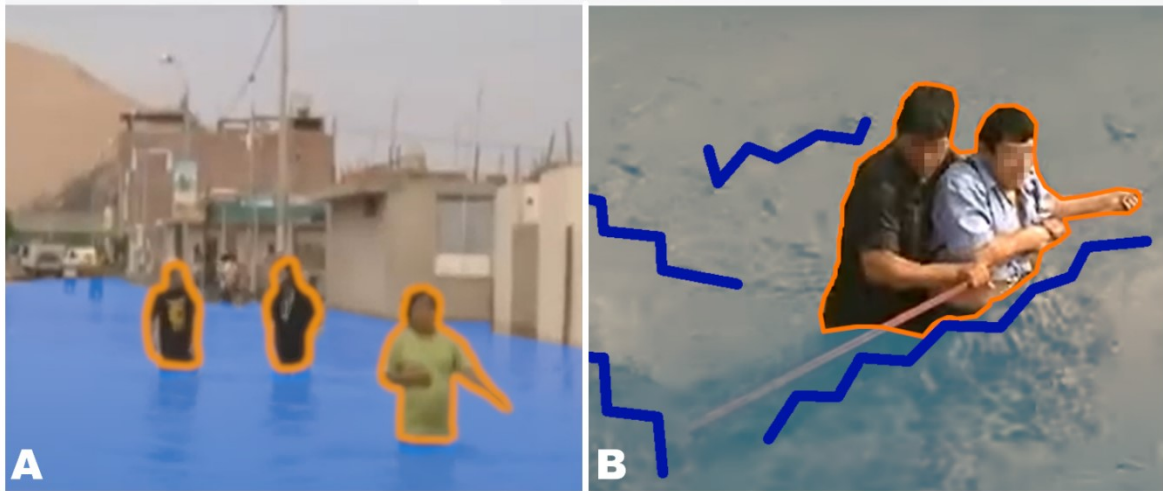


Figure 42: People dealing with water up to the waist (outlined in orange). Panel A is for still water, panel B is for flowing water and the blue jagged lines indicate the waves (reference videotapes: {100}, {84}).

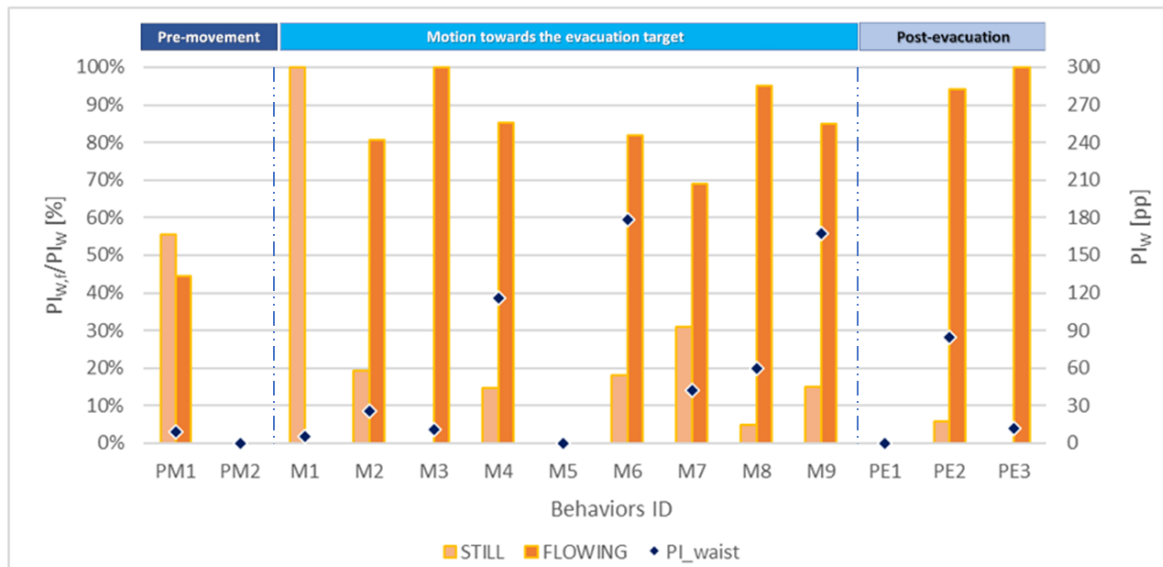


Figure 43: Situational frequency per water depth equal to or lower than the waist $PI_{w,t}/PI_w$ [%] (colored bars; left y-axis) of the observed behaviors evaluated by comparing the water flow. The sample dimension is outlined by PI_w [pp] (black rhombuses; right y-axis). Behaviors IDs from Figure 34.

6.2.6 Water depth higher than the waist

Figure 45 shows the results concerning the situational frequency with respect to water depth higher than the waist, by distinguishing between still and flowing waters (Figure 44). Considering the evacuation phases, it is worthy of notice that:

- *Pre-movement phase: attachment to belonging* PM1 is the unique noticed behavior within the analyzed sample, and only in the case of still water.
- *Motion towards evacuation target* phase: in general, analyzed people managed to perform few behaviors in such high-water depth conditions. In particular, *increased guide effect* M4 and *clinging to ropes and arranging “human chains”* M9 are the most frequent in both the water flow conditions, thus highlighting the importance of rescuers’ presence and rescue tasks in such critical situations. Compared to the previous cases (Figure 39, Figure 41, and Figure 43), *social influence and group phenomena* M6 and *human body instability* M8 become more frequent with still water ($PI_{HW,S}/PI_{HW}$ respectively up to 36% and 43%). Finally, *floodwater effects on motion speed* M7 can be observed only with still water, thus confirming that pedestrians can be able to additionally move in still floodwaters deeper than 1.20m [227].
- *Post-evacuation phase: reaching outdoor safe areas* PE3 was not found in the analyzed sample and the statistical significance of *reaching temporary safe areas* PE1 could be limited in view of the sample dimension ($PI_{HW}=5$ pp, all in the same videotape). On the other hand, the frequency of *reaching indoor safe areas* PE2 underlines the impact of critical flow conditions on pedestrians’ preferences to move far from the flooded areas reaching raised indoor positions (for *reaching indoor safe areas* PE2).

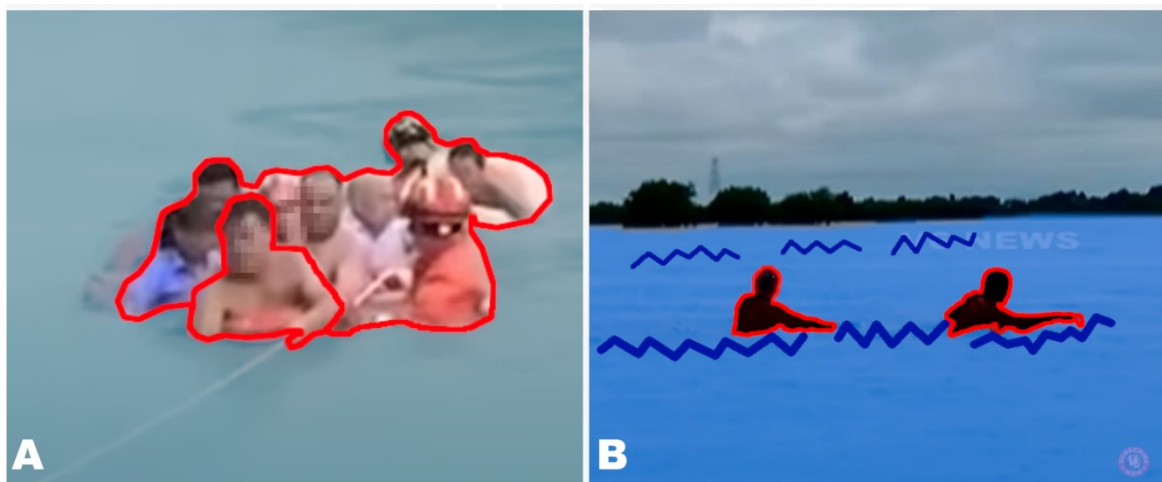


Figure 44: People dealing with water higher than the waist (outlined in red). Panel A is for still water, panel B is for flowing water and the blue jagged lines indicate the waves (reference videotapes: {25}, {55}).

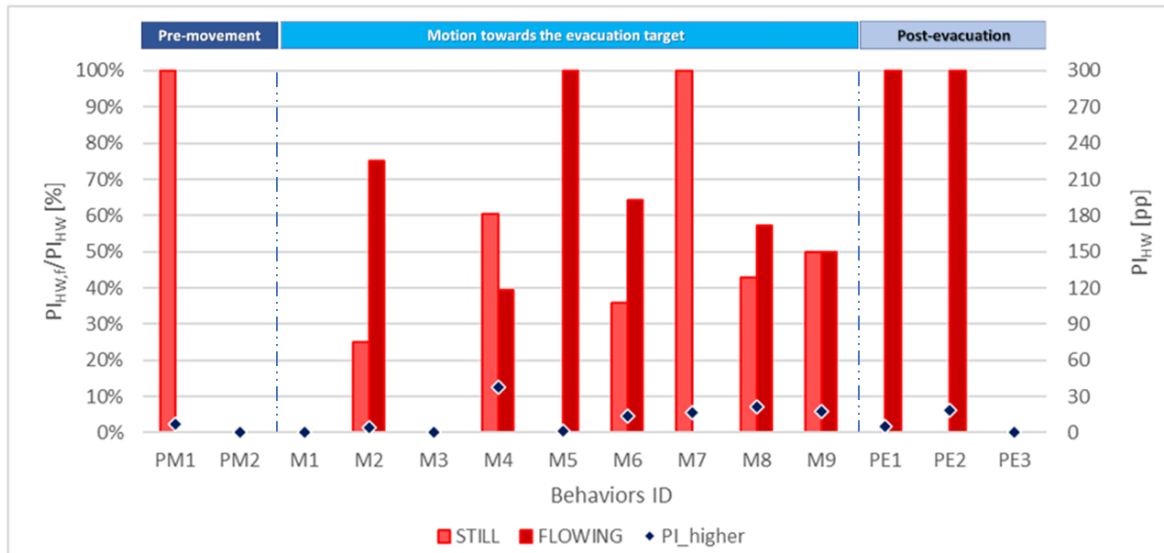


Figure 45: Situational frequency per water depth higher than the waist $PI_{HW,\epsilon}/PI_{HW}$ [%] (colored bars; left y-axis) of the observed behaviors evaluated by comparing the water flow. The sample dimension is outlined by PI_{HW} [pp] (black rhombuses; right y-axis). Behaviors IDs from Figure 34.

6.3 Most frequent floodwater conditions for behavioral patterns

The use of human body parts as references for the behavioral patterns activations pursues a quick but reliable assessment of people’s response to flood evacuation. Behavioral key findings are summarized in Table 33, which resumes the most frequent floodwater conditions in which behaviors are observed.

For what concerns the *pre-movement* phase, although the observed behaviors can be classified as *hazardous behaviors*, some interesting differences can be found. Indeed, even though both *attachment to belongings* PM1 and “*curiosity*” effect PM2 are characterized by a sort of “warning threshold” for pedestrians at the level of the knees, the latter is observed predominantly with flowing conditions, thus suggesting that pedestrians are more influenced by the water depth than its flowing conditions. This threshold decreases down to the ankle level for *moving through the water with vehicles* M5, which is comparable with previous works findings carried out through questionnaires, according to which people’s perception of the risk increases with the water depth [302], [303]. Moreover, considering its occurrence during the evacuation phases, *moving through the water with vehicles* M5 can also be associated with the *pre-movement* phase in view of the similarities with *attachment to belonging* PM1 (i.e., the vehicles), which can delay the actual evacuation on foot [304], [305]. These differences can be also traced back to the significant worsening in the walking behaviors (i.e., speed, trajectory, step frequency, lateral swaying, stability) that arise when the knee articulations are even partially submerged, thus suggesting a different acceptance of the risk depending on the context and the reference elements [50], [231].






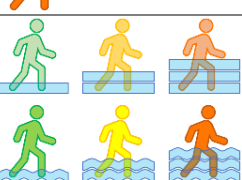




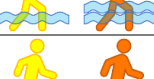



PRE MOVEMENT		
ID – Observed Behavior	Most frequent floodwater conditions	
PM1 - Attachment to belongings	Water up to the knees	
PM2 - “Curiosity” effect	Flowing water up the knees	
MOTION TOWARDS THE EVACUATION TARGET		
ID – Observed Behavior	Most frequent floodwater conditions	
M1 - Attraction towards safe areas	Still water up to the waist	
M2 - Attraction toward unmovable obstacles	Flowing water between the ankles and the waist	
M3 - Fear of moving elements	Flowing water between the knees and the waist	
M4 - Increased guide effect	Water up to the waist	
M5 - Moving through the water with vehicles	Water up to the ankles	
M6 - Social influence and group phenomena	Flowing water between the knees and the waist	
M7 - Floodwaters effects on motion speed	Water between the ankles and the knees	
M8 - Human body instability	Flowing water between the ankles and the waist	
M9 - Clinging to ropes and arranging “human chains”	Flowing water between the ankles and the waist	
POST EVACUATION		
ID – Observed Behavior	Most frequent floodwater conditions	
PE1 - Reaching temporary safe areas	Flowing water between the ankles and the knees	
PE2 - Reaching indoor safe areas	Flowing water between the knees and the waist	
PE3 - Reaching outdoor safe areas	Water up to the ankles	

Table 33: observed behaviors and frequent floodwater conditions in which they are performed.

Motion toward evacuation target behaviors strongly depend on (1) the presence of reference elements in the flooded scenarios and (2) the possibility for pedestrians to move without restrictions imposed by the water. As a consequence, behaviors like *attraction towards safe areas* M1 or *fear of moving elements* M3 only rely on a few observations (respectively, PI=9 on 3 videotapes and PI=16

on 3 videotapes). However, comparing our findings with those on human body instability and motion speed in floodwaters [50], [99], [227], [231], [306], it could be noticed that:

- *attraction towards safe areas* M1 was observed for still waters up to the waist, essentially because these conditions still avoid buoyancy problems for pedestrians, and so they allow pedestrians to move towards an evacuation target;
- *attraction towards unmovable obstacles* M2 was noticed for flowing waters between the ankles and the waist. These conditions can provoke human body instability problems thus leading pedestrians to search for physical support;
- *fear of moving elements* M3 concerns scenarios in which flowing water (that is consistent with having objects dragged by floodwater) is combined to water depth between the knees and waist (that is excluding limited and extreme interactions with floodwaters).

As expected, the main intent of *deliberately chosen* behaviors performed during the actual movement within the floodwaters is to recover from human body instability problems and speed up the restoration of safety conditions. Thus, the most frequent conditions for *passively suffered* behaviors represent a benchmark also for behaviors aimed at improving the pedestrians' mobility into the floodwaters. In this sense, *floodwater effects on motion speed* M7 can be noticed especially in water up to the knees, thus excluding conditions that impede human motion [227]. Furthermore, it is worthy of notice that this behavior was not observed at all with still water under the ankles, where pedestrians are still capable of moving without significant problems [50], [231]. Besides, *human body instability* M8 is mostly observed for flowing water between the ankles and the waist [99], [227], even if a wide number of observations were retrieved also with higher/lower water depth. As a consequence, *protective behaviors* that could involve also the presence of rescuers like *increased guide effect* M4, *clinging to ropes and arranging "human chains"* M9, and *social influence and group phenomena* M6 (which includes also pro-social actions such as trying to rescue other pedestrians) are attempted in whatever kind of condition, especially in flowing water up to the waist (basically the same conditions provoking human body instability and motion speed problems [99], [227], [239]). However, it is worthy of notice that these behaviors are the three most observed in terms of people involved (Figure 35), which confirms the importance of actions aimed at saving their own lives and those of others during flooding disasters [307].

Furthermore, *post-evacuation* behaviors highlight a trend for *reaching indoor safe areas* PE2 in case of flowing water higher between the knees and the waist, while *outdoor safe areas* PE3 in water up to the knees. This result is consistent with differences in risk perception depending on water depth and flow [308], besides the availability of outdoor areas in case of extreme events. On the other hand, *temporary safe areas* PM1 can be substantially traced back to flowing water between the ankles and knees, which can be probably considered sufficiently severe to induce pedestrians to stop during their motion to target (thus excluding still water and less deep than the ankles), but not to threaten the safety of the selected area (floodwaters above the knees can reasonably induce threat in temporary areas like vehicle roofs) [50], [227], [231].

6.4 Outcomes evaluation

Observations of real floods in outdoor BEs empirically (1) confirmed that the floodwater conditions strongly affect people's behaviors before, during, and after the evacuation, and (2) demonstrated that critical thresholds with respect to water depth and flow vary for each of the observed behaviors. In

this sense, the outcomes of this work can support the development of risk-mitigation strategies and simulation modeling approaches (subsections §6.4.1 and §6.4.2), even though some limitations need to be discussed (subsection §6.4.3).

6.4.1 Implications for modeling approaches

This work's findings can support the development and validation of simulation tools based on microscopic approaches relying on the representation of people's tasks with respect to the surrounding floodwater conditions, such as agent-based models [135], [245], [309]. These approaches can be then combined with modeling approaches to estimate pedestrians' behaviors, velocity, and paths, such as cellular automata [130] or force-based models [134]. Since this work focuses on qualitative aspects of human response, works to consolidate motion speed assessment are needed. In particular, considering *attraction towards unmovable obstacles* and *clinging to ropes and arranging "human chains"* behaviors, experiments could be conducted toward the quantification of human stability and evacuation speed improvements thanks to supporting elements like ropes and cables that were found to be widely used by evacuees and rescuers. These studies could then move towards the analysis of rescuers' operations and equipment during the evacuation in order to improve their design and use under specific hydrodynamic conditions. In this way, additional tests through evacuation simulators could be also conducted for testing new equipment for rescue tasks and their implementation within the urban layout.

6.4.2 Relations with risk-mitigation strategies

Behavioral results retrieved in the *pre-movement* phase of the emergency demonstrate that future efforts should move towards the study of risk-reduction measures to speed the (right) decision-making process and reduce the time spent performing pre-movement hazardous behaviors which can often mark the difference between surviving or not, or at least avoid that the best option becomes the "least harmful one" (e.g., to be obligated to cross deep flowing waters rather than not). Indeed, floods are disasters whose impact can locally vary depending on specific conditions of the meteorological event or of the built environment, which can be partially subject to prediction biases (e.g., in the case of flash floods). Therefore, solutions may include the provision of communication strategies, wayfinding systems, and Early Warning Systems to be implemented, for instance, in the form of reliable social-media alerts or apps for mobile devices, so as to reduce the reaction time (i.e., the overall "pre-movement" phase) to avoid floodwater interactions at all and ease the evacuation timing and path selection [248], [249], [253], [310], [311].

Similarly, qualitative findings in the *motion toward the evacuation target* phase can help local authorities and technicians in planning and designing targeted interventions in flood-prone built environments (some examples are shown in Figure 46). Possible applications could include: (1) the improvement and proper positioning of "passive" architecturally-implemented solutions such as handrails, benches, and raising floor systems, as well as traditional signage systems such as hazard signs, water heights indicators, wayfinding systems [134], [312]–[314]); (2) the implementation of "active" systems for emergency warning and wayfinding, including both visual (e.g. through variable and luminescent directional signs) and acoustic indications [246], [311]); (3) the improvement of evacuation planning with innovative and retrofitted solutions evaluated on the basis of local and/or temporary risks [119], [236]; (4) the promotion of exercises and awareness campaigns to improve the community resilience and educate people on the danger of walking and driving in floodwaters, also with the aid of innovative immersive techniques like virtual reality (VR) or

augmented reality (AR) serious games [98], [315], [316]; (5) the wide use of ropes and cables (that can be more effective than expected especially if considering their general low cost) regardless of the floods magnitude, since future events harsher than usual cannot be excluded at all in flood prone areas even in presence of specific data linked to recurring conditions.

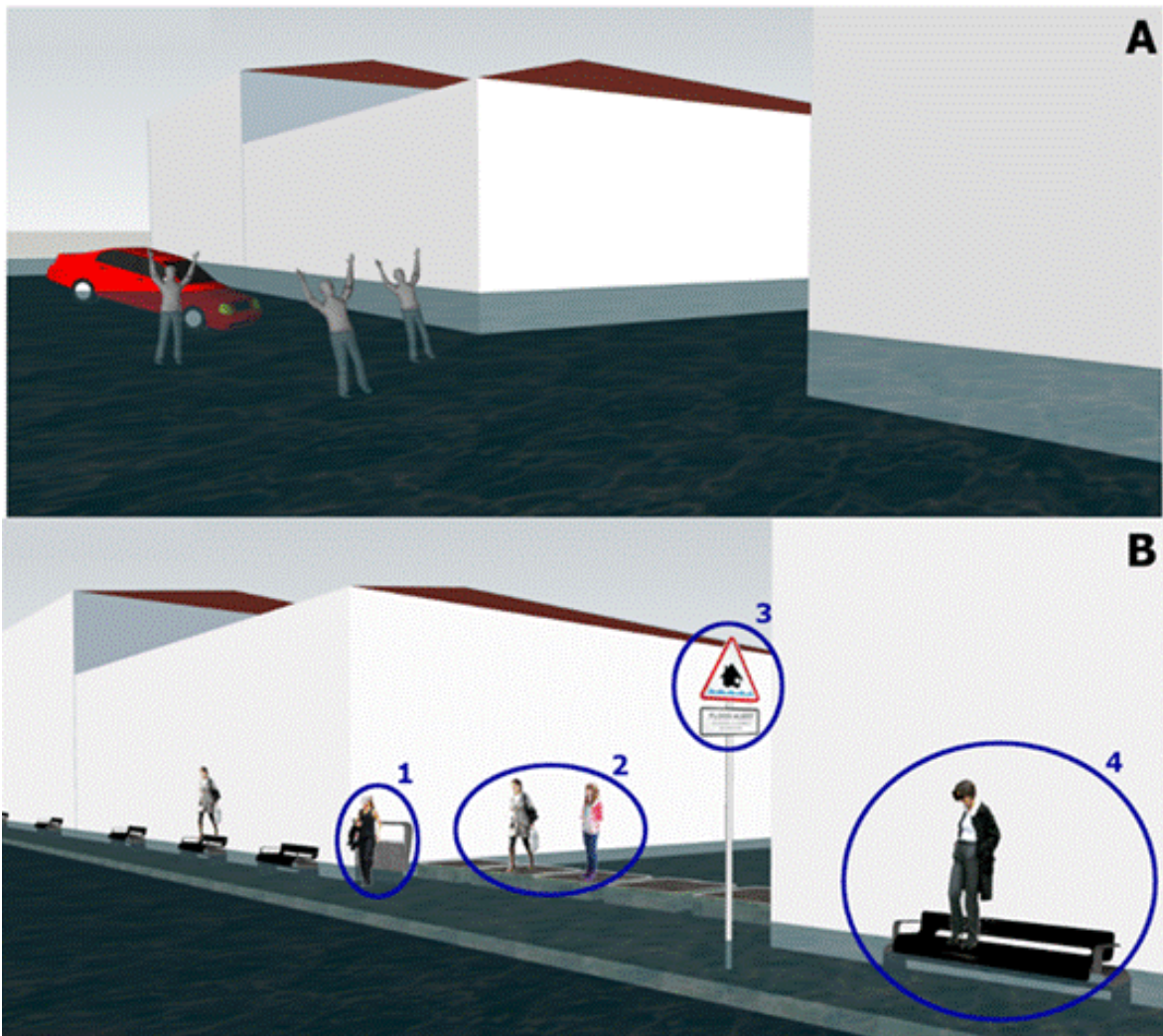


Figure 46: Example of how “passive aids” can be implemented in the outdoor BE. Scenario A lacks targeted interventions; Scenario B includes the presence of handrails (1), raised platforms (2), road signs (3), and benches (4).

In this sense, this work also supports the identification of necessities behind the selection of a certain type of safe area. Results emerging from the analysis of *post-evacuation* behaviors can be used to evaluate aspects like the safe areas’ position, dimensions (i.e., height, area, density), and type also as a function of the expected risk in a given scenario (e.g., evaluating the prearrangement of indoor areas or temporary forecast-based solutions aimed at gathering a certain number of evacuees), and so depending on the general features of the floodwater conditions in terms of water depth (with respect to the human body parts) and of the presence of still or flowing waters.

6.4.3 Limitations and future aims

Finally, it is worth noticing that the work insights are mainly affected by some limitations, which can be overcome by future works. The presence of some situations with a limited number of involved and assessed people could be overcome by enlarging the videotape database. Furthermore, results

could be influenced by additional factors such as physical (different body parts submerged under the same water depth, different weight, and so on), geographical, cultural, and risk-awareness-related features of people, which could be not directly and easily assessed by videotapes analysis. In this sense, this work considers a worldwide database as a unique sample, so as to point out “average” behavioral responses to floods in the investigated outdoor BEs, as for previous methods applied to other kinds of disasters [57], [58], [237], [238]. Similarly, results could be affected also by external factors like the presence of individuals with cameras or smartphones, who could hardly decide to film unless something is happening (see for example the lack of post-evacuation scenes). However, the approach pursued by this work allows taking advantage of unbiased sources, differently from controlled experimental tests that inevitably are influenced by simplified laboratory conditions both in terms of environmental and human factors. In this sense, future works could: (1) integrate the database enlargement with specific analysis, e.g. on geographical areas or including standard analyses through gender, age, and/or height estimation when possible by the videotapes; (2) move towards quantitative assessment of floodwater conditions, by also using image processing [252], which could reduce the quickness of the proposed approach but could also improve their reliability and the detail level of the results (e.g. measuring “how much” the individual body is submerged by the floodwaters rather than just defining general conditions based on body parts); (3) investigate recurring evacuation “storylines” so as to additionally inquire “when” each behavior is usually performed, thus identifying the recurrent order of activation of behaviors during a flood evacuation or even behavioral patterns differences over the evacuation time. At the same time, collected data could be also exploited by machine learning approaches to investigate situational influences affecting behavioral patterns [317]. In this sense, this work approach could provide simple but reliable bases for the situational features’ selection while creating structured databases in the flood context.

7. Simplified flood evacuation simulation in HCCs: preliminary comparison between custom and generic simulators

The following sections are organized to compare the outputs obtained from the generic and the custom simulators (§7.1, §7.2, and §7.3), then the comparison is extended to real-world observations (§7.4). Finally, the generic simulator fittest setup is selected and discussed (§7.5) by also considering its limitations and related future research steps (§7.6).

7.1 Evacuation curves comparison

The evacuation curves graphical comparison is shown in Figure 47. Table 34 resumes the KPIs measuring the differences of the evacuation curves obtained from each setup tested on the generic simulator computed with respect to custom simulator results. Results are shown in terms of mean and standard deviation values according to the grouping criteria shown in Figure 16. Average results per group are provided.

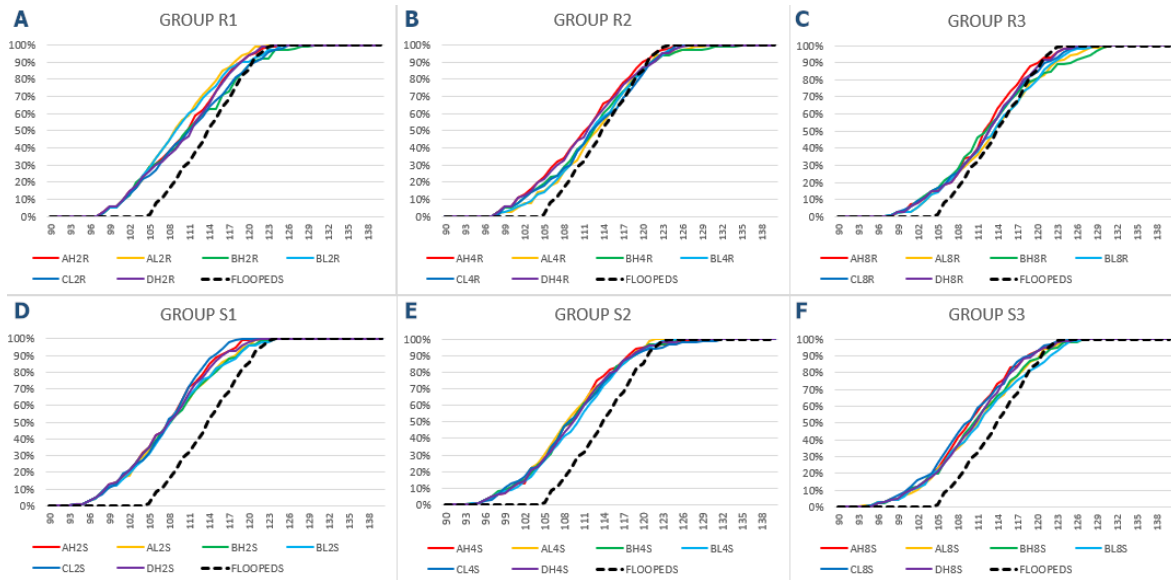


Figure 47: Comparison of the custom simulator evacuation curve (black dashed lined) and those of the generic simulator (straight lined). Generic simulator setups are grouped according to the criteria shown in Figure 16, that is considering the same entrance portals configuration, i.e., setup groups R1 to R3 are rectangular (panels A-B-C), S1 to S3 are squared (panels D-E-F). 0-90s are omitted as no pedestrians complete the evacuation in this timespan.

The results highlight that, when the “first servers” position is closer to the entrance *portals*, that is for setup groups R3 and S3, the generic simulator outputs are closer to those of the custom simulator. In fact, in these cases, *SC* increases and *ERD* decreases. As expected, *EPC* seems non to be affected by the setup, as it tends to 1 in all the cases. In general, the generic simulator seems to underestimate the safety conditions of the pedestrian who arrives first by about 30% (see, for instance, Figure 47). Anyway, the *DAUC* always assumes positive values regardless of the proposed setup, meaning that the generic simulator slightly overestimates the entire evacuation process speed, as values range from 1 to 24%.

Considering the specificities of the setup groups, R2, R3, and S3 are the only ones with *SC* > 0.8 and *ERD* < 0.2, thus improving the similarities between the evacuation curves. These groups are

characterized by smaller distances between the entrance *portals* and the *servers*. Slight differences can be noticed considering the number and positioning of the *servers* with respect to the side of the pathway, as the standard deviation values of all the KPIs point out, ranging between 0.01-0.03. On the other hand, when a pedestrian has the probability *by-literature* to select one of the “first servers”, *SC*, *ERD*, and *DAUC* improve together with the curve shape similarity (see extended results for each setup in Section §11.5.5, Appendices).

<i>Setup</i>	<i>Values</i>	<i>SC</i>	<i>ERD</i>	<i>EPC</i>	<i>DAUC</i>
R1	avg	0.777	0.170	1.038	13%
	<i>st. dev.</i>	<i>0.031</i>	<i>0.025</i>	<i>0.016</i>	<i>2%</i>
R2	Avg	0.849	0.102	1.008	7%
	<i>st. dev.</i>	<i>0.035</i>	<i>0.024</i>	<i>0.011</i>	<i>2%</i>
R3	avg	0.857	0.084	0.997	4%
	<i>st. dev.</i>	<i>0.029</i>	<i>0.011</i>	<i>0.016</i>	<i>2%</i>
S1	avg	0.710	0.260	1.073	22%
	<i>st. dev.</i>	<i>0.021</i>	<i>0.016</i>	<i>0.009</i>	<i>2%</i>
S2	avg	0.764	0.208	1.053	17%
	<i>st. dev.</i>	<i>0.032</i>	<i>0.013</i>	<i>0.005</i>	<i>1%</i>
S3	avg	0.822	0.157	1.035	12%
	<i>st. dev.</i>	<i>0.028</i>	<i>0.021</i>	<i>0.013</i>	<i>2%</i>
OVERALL	avg	0.796	0.164	1.034	13%
	<i>st. dev.</i>	<i>0.060</i>	<i>0.063</i>	<i>0.028</i>	<i>6%</i>

Table 34: KPIs measuring differences between evacuation curves obtained from each setup tested on the generic simulator and the one obtained from the custom simulator. Results are shown in terms of mean and standard deviation values according to the grouping criteria shown in Figure 16.

7.2 Comparison between D_w trend along the pathway

Table 35 resumes the analysis of the D_w trend according to the KPIs and considers the median distribution on a 3m resolution along the pathway. Results are grouped according to Figure 16 criteria, while simulation outputs for the 1st and 3rd quartile are available in Section §11.5.5 (Appendices). Average and standard deviation values per group are provided.

As for the previous section results, setup groups characterized by smaller distances between the entrance *portals* and the *servers* seem to lead to more similar results with respect to the custom simulator, as shown by the median D_w trends in Figure 48. This result is mainly remarked by the *SC* values for groups R3, S2, and S3 ranging between 0.45-0.54, which is significantly higher if compared to other setup groups, thus implying that the *server* constraint should be placed closer to the start to effectively attract pedestrians near the unmovable obstacles (i.e., to reduce the curve subtended area). In this sense, such results seem to confirm those on the evacuation curve. However, the *SC* variability between the setups in the groups demonstrates some differences in D_w trends, as standard deviation values range from 0.07 to 0.12, while they are up to 0.20 considering the overall sample. Nevertheless, it is worth noticing that a limited correspondence between all the setups and the custom simulator outputs on D_w appears according to the other KPIs, as shown by Table 35 samples.

<i>Setup</i>	<i>Values</i>	<i>SC</i>	<i>ERD</i>	<i>EPC</i>	<i>DAUC</i>
R1	avg	0.048	0.579	1.293	37%
	<i>st. dev.</i>	0.070	0.064	0.076	9%
R2	avg	0.316	0.448	1.203	27%
	<i>st. dev.</i>	0.073	0.062	0.082	10%
R3	avg	0.447	0.446	1.173	25%
	<i>st. dev.</i>	0.108	0.070	0.089	10%
S1	avg	0.170	0.510	1.278	34%
	<i>st. dev.</i>	0.096	0.060	0.067	8%
S2	avg	0.542	0.416	1.214	27%
	<i>st. dev.</i>	0.083	0.077	0.085	10%
S3	avg	0.506	0.409	1.166	23%
	<i>st. dev.</i>	0.121	0.074	0.093	11%
OVERALL	avg	0.338	0.468	1.221	29%
	<i>st. dev.</i>	0.203	0.090	0.096	11%

Table 35: KPIs measuring differences between curves tracing the D_w trend for each setup tested on the generic simulator and the one obtained from the custom simulator (2nd quartile data). Results are shown in terms of mean and standard deviation values according to the grouping criteria shown in Figure 16. Extended results for each setup are in Section §11.5.5 (Appendices).

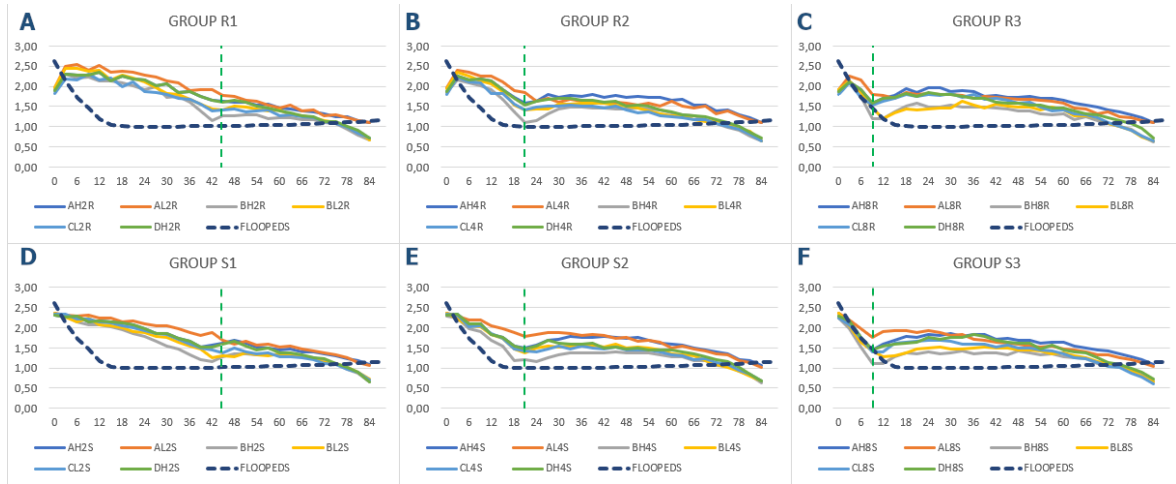


Figure 48: Comparison of 2nd quartile D_w trend for the custom simulator (blue dashed line) and those of the generic simulator (straight lines). Generic simulator setups are grouped according to the criteria shown in Figure 16, that is considering the same entrance portals configuration, i.e., setup groups R1 to R3 are rectangular (panels A-B-C), S1 to S3 are squared (panels D-E-F). The green dashed line indicates the position of the “first servers” along the pathway.

7.3 Quartile analysis of trends in pedestrians’ evacuation timing

Overall outcomes about the maximum evacuation time t_{max} (Figure 49) show similar results between the two simulators (1s difference between the custom simulator and the generic one mean value). Concerning the distinction by setup, the percentage differences range between -4% and 4% considering all the setups tested but the outliers (blue box). Differences between squared and rectangular portals seem to be negligible (<5%), even if groups ‘R’ (i.e., rectangular *entrance portals*) register slightly higher t_{max} values. This result seems to be affected by repulsion forces between pedestrians in those entrance areas, and their effects are increased by the high-density

conditions (about 3 pp/m²) in the rectangular portals. As a consequence, these conditions imply the pedestrians' trajectories are farther from the pathway sides while they are approaching the “first servers” (as shown in Figure 48).

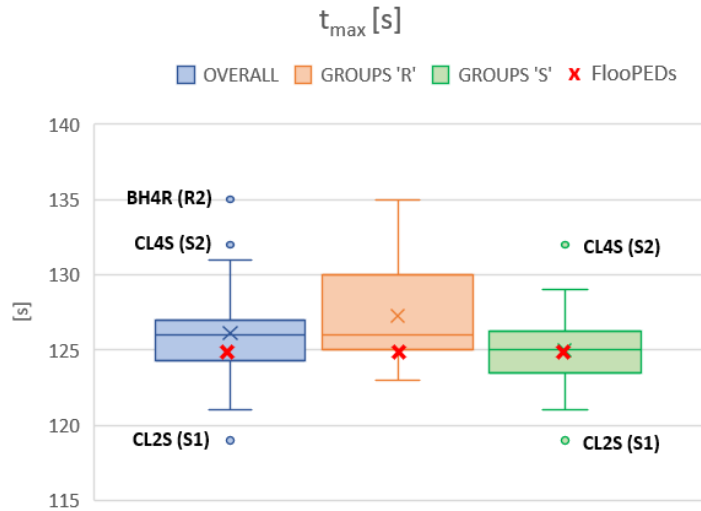


Figure 49: Comparison between the maximum evacuation time t_{max} of the custom simulator (red cross) and the generic simulator distinguishing overall (blue box) and groups data (orange and green boxes). Outlier setups are marked as follows: “Setup name (Group name)”. Extended results for each setup are resumed in Section §11.5.5 (Appendices).

In general, a queue formation trend can be noticed because all pedestrians start at the same time and place, and they are “forced” to pass by the *server*. Some pedestrians could be forced to stop the evacuation for some time. Thus, regarding the maximum waiting time percentage W , the comparison between all the setups in Figure 50 shows how pedestrians behave similarly regardless of the shape of the *entrance portals* and the *servers'* features (i.e., their position and number), as differences between maximum and minimum values are only of about 7% (blue box). Anyway, absolute waiting times are in the range of 5-15 s, which is reasonable for flood outdoor evacuations where circumstances like social attachment, group phenomena, and difficulties in motion and stability can force pedestrians to stop [22].

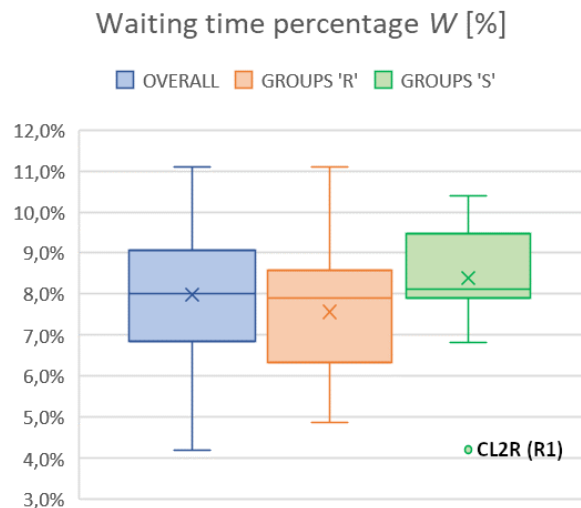


Figure 50: boxplot representation of the maximum waiting time percentage W , distinguishing overall (blue box) and group data (orange and green boxes). Outlier setups are marked as follows: “Setup name (Group name)”. Extended results for each setup are resumed in Section §11.5.5 (Appendices).

Finally, Figure 51 shows how group phenomena seem to have a greater impact in the generic software than in the custom simulator regardless of the setup tested. Indeed, the evacuation flows F are 30% smaller considering the mean values of all the setup groups, and percentage differences between setups are <5% (excluding the outliers highlighted in Figure 51). Such phenomena could be linked to the aforementioned “forced” passage by the servers.

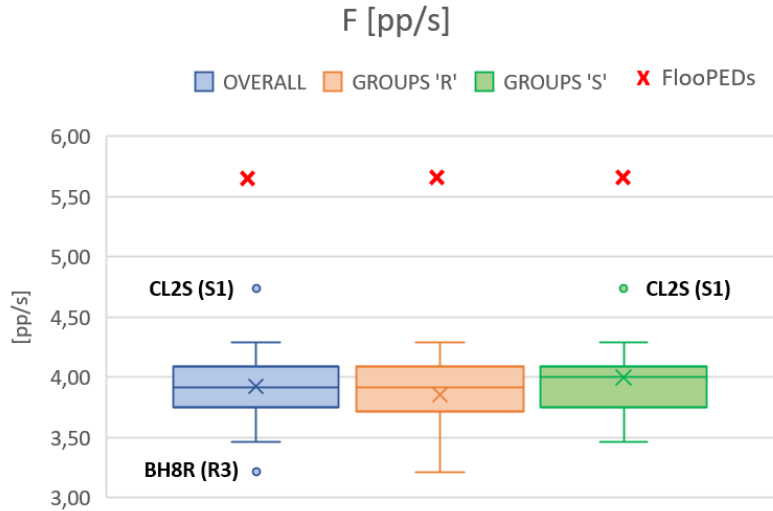


Figure 51: Comparison between the evacuation flow F values of the custom simulator (red cross) and of the generic simulator distinguishing overall (blue box) and groups data (orange and green boxes). Outlier setups are marked as follows: “Setup name (Group name)”. Extended results for each setup are resumed in Section §11.5.5 (Appendices).

7.4 Comparison with real-world observations

The positioning of “attraction” objects (i.e., the *servers*) ensures the representation of attraction phenomena towards unmovable obstacles (i.e., the *floor* edges). According to indications provided in subsection §3.5.3.4, *homogeneous* or *by-literature* setups are tested, thus representing different probabilities that a pedestrian can choose one of the “first servers”.

Table 36 compares the D_w percentage distribution of the distance between pedestrians and unmovable obstacles from the generic simulator with those obtained, respectively, from the real-world observations (as a reference for the comparison [134]), and the custom simulator. Results show non-significant differences between the setup groups, as the standard deviations range, in general, between 1-5%. On the other hand, the comparison with the custom simulator and the real-world observations from previous literature works shows more significant differences. In particular, concerning the $1 < D_w \leq 2m$ class, these differences are essentially due to the repulsive forces between pedestrians in the same group, which induce lower frequency in this class of distance (negative differences). On the other hand, $D_w > 2m$ is more frequent in the generic simulator compared to what is observed in the real world and the custom simulator (positive differences). Thus, from the behavioral modeling point of view, the generic simulator conservatively overestimates the risk condition during the evacuation, as pedestrians will travel wider trajectories in their route to safety, hence facing longer exposition to risk through longer evacuation paths. In addition to this, from a hydrodynamic point of view, the overestimation of D_w also leads to a decrement in the pedestrians’ speed and problems of instability as the streets in general behave like open channels and the water speed increases moving away from the edges [192] (compare with Equation 3.2). However, it is worth noting that we actually consider stationary conditions in this first, simple testing scenario,

which implies having the same evacuation speed v_i on each point of the floor regardless of the pedestrians' distance from the side of the buildings.

<i>Pedestrians' frequency percentage distribution and variability [%]</i>				
	$D_w \leq 1m$ [%]	$1 < D_w \leq 2m$ [%]	$D_w > 2m$ [%]	
<i>Real-world observations from the literature</i>	29	50	21	
<i>Custom simulator</i>	23	66	11	
<i>Generic simulator setup</i>				
R1	37 (L: +8; C: +14)	29 (L: -21; C: -37)	34 (L: +13; C: +23)	Avg
	4	1	4	Dev. St.
R2	38 (L: +9; C: +15)	31 (L: -19; C: -35)	31 (L: +10; C: +20)	Avg
	4	2	5	Dev. St.
R3	37 (L: +8; C: +14)	33 (L: -17; C: -33)	30 (L: +9; C: +19)	Avg
	4	2	4	Dev. St.
S1	36 (L: +7; C: +13)	29 (L: -21; C: -37)	35 (L: +14; C: +24)	Avg
	4	1	4	Dev. St.
S2	36 (L: +7; C: +13)	32 (L: -18; C: -34)	32 (L: +11; C: +21)	Avg
	4	1	4	Dev. St.
S3	36 (L: +7; C: +13)	34 (L: -16; C: -32)	30 (L: +9; C: +19)	Avg
	5	2	4	Dev. St.
OVERALL	37 (L: +8; C: +14)	31 (L: -19; C: -35)	32 (L: +11; C: +21)	Avg
	4	2	5	Dev. St.

Table 36: Pedestrians' frequency percentage distribution and variability for each distance class: comparison of the setup of the generic simulator (grouped according to the criteria shown in Figure 16) with real-world observations from literature works (L) [134] and the custom simulator data (C). Avg refers to average data, Dev. St. refers to the related standard deviation of the sample. Extended results for each setup are resumed in Section §11.5.5 (Appendices).

7.5 Best setup definition

The organization of the results in setup groups allowed for finding a key element for the modeling of the simulation environment, that is the position of the *servers*. Indeed, the positioning of these attraction points closer to the *entrance portals* seems to be the most influential option which allows having graphical outputs as similar as possible to those of the custom simulator (i.e., evacuation curves in Figure 47 and D_w trends in Figure 48, groups R3 and S3). Furthermore, this positioning also helps to obtain simulations consistent with real-world observations, as groups R3 and S3 are the ones with the closer distribution to real-world observations in the $1 < D_w \leq 2m$ class (Table 36).

However, among all the setups tested, the BL8S (group S3) is the one that produced the closest results to the custom simulator, and is characterized by the following features that support the similarities with the custom simulator:

- The condition of the *squared entrance portals*, in which pedestrians are generated with a density of about $1pp/m^2$, is similar to those of the custom simulator. The initial effect of the repulsive force between pedestrians seems to be mitigated because of their mutual distance, which is preserved along the pathway. Meanwhile, in the other configuration, the density is 3 times higher, so that pedestrians spread out at the very beginning of the pathway;

- Two “first servers” are positioned at 1/8 of the pathway length (i.e., about 10m from the start). This condition allows for increasing the attraction towards unmovable obstacles and the interaction between pedestrians. Considering the distance from the side of the pathway, the “first servers” are placed in the middle of each class of distance (i.e., *servers* at 0.5m and 1.5m from the wall), with a *by-literature* probability distribution for pedestrians to select one of them. This element of the setup seems to reduce the MassMotion trend in simulating higher pedestrian-unmovable obstacle distances. Anyway, having *servers* extremely close to the start of the pathway could represent a problem for what concerns queue phenomena, especially with very large groups of pedestrians.

Figure 52 shows the evacuation curves and the D_w trends obtained from the proposed setup (red solid lines) and the custom simulator (black dashed lines). According to the results on KPIs introduced in Table 16, the evacuation curves are similar in shape and size ($SC=0.78$, $EPC=1.01$), close to each other ($ERD=0.13$), and without significant differences in underestimating/overestimating contingencies ($DAUC=9\%$). Anyway, it is worthy of notice that the generic simulator seems to speed up the evacuation process for the first-arrived pedestrians, which can be considered as free to move in the environment and to pass by the server with a reduction of group interactions. In this sense, the custom simulator better points out the group attraction phenomena, by reducing the time gap between the first and the last arrived pedestrians. However, in view of the above, considering such risk conditions in terms of the pedestrians’ density and practicability conditions (i.e., pedestrians still manage to move in the floodwater without experiencing instability problems), the two simulators produce comparable results concerning macroscopic aspects like the over-time progression of the evacuation process (i.e., evacuation curves EC , flow F , and maximum evacuation time t_{max}).

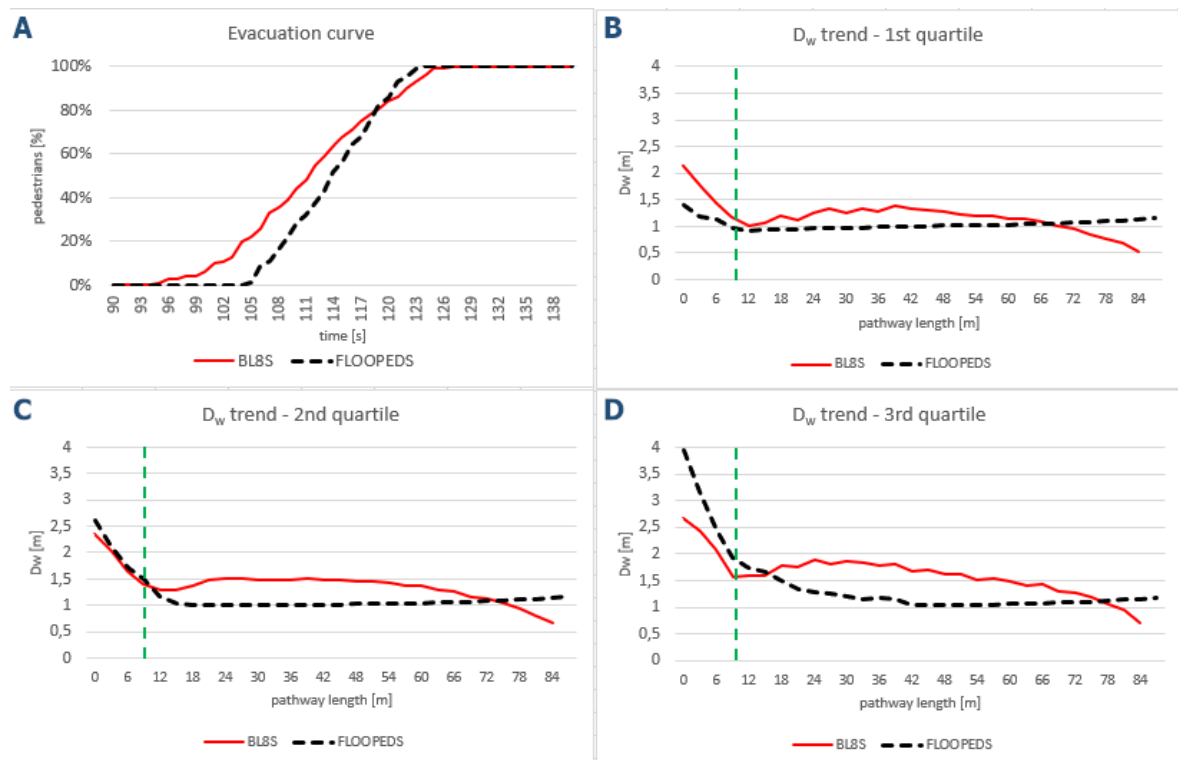


Figure 52: Comparison between the evacuation curves (panel A) and the D_w trends (panels B-C-D) obtained from the BL8S setup of the generic simulator (red solid lines) and the custom simulator (black dashed lines). The green dashed line indicates the “first servers” position along the pathway. The evacuation curves comparison considers the range between 90-140s, which is from the arrival of the first pedestrian to the exit of the last one.

On the other hand, from a microscopic point of view, differences emerge in pedestrians' trajectories, as the D_w outcomes point out. In particular, the generic simulator BL8S setup seems to overestimate the pedestrians' risk if considering their trajectories, because the setup and the model force them to travel along larger trajectories towards the evacuation target. This implies higher exposition for pedestrians to the floodwaters [192], especially after the attraction points effect (i.e., the "first server") as shown in Figure 52. Table 37 summarizes the KPIs values concerning the D_w trends comparison, showing differences in the curves' shape and overall agreement. However, considering the probability distributions in class distances (Table 38), the generic simulator setup finds good agreement with the real-world observations (differences <15%), meaning that the general trends can be considered preliminary acceptable for simulation purposes [103], [258], [259].

	<i>SC</i>	<i>ERD</i>	<i>EPC</i>	<i>DAUC</i>
1st quartile	0.53	0.36	1.10	10%
2nd quartile	0.71	0.33	1.09	14%
3rd quartile	0.65	0.35	0.99	11%

Table 37: KPIs measuring differences between curves tracing the D_w trend of the generic simulator best setup (BL8S) and the custom simulator (quartile analysis).

	<i>Dw</i> ≤1m [%]	1< <i>Dw</i> ≤2m [%]	<i>Dw</i> >2m [%]
Real-world observations from the literature	29	50	21
Custom simulator	23	66	11
BL8S setup	39	37	25

Table 38: Pedestrians' frequency percentage distribution for each distance class: comparison of the generic simulator best setup (BL8S) with the literature distributions [134] and the custom simulator distributions. Percentage differences between literature (L) and custom software (C) data are pointed out in brackets.

Finally, Table 39 shows the pedestrians' evacuation timing data concerning: (a) the maximum evacuation time t_{max} , which is almost identical between the two analyzed software, thus confirming non-particular underestimating/overestimating safety contingencies, (b) the waiting time percentage W , and (c) the evacuation flow F , whose values are by the way comparable with the generic simulator overall trend.

	t_{max} [s]	W [%]	F [pp/s]
Custom simulator	125	-	5.63
Generic simulator (median)	126	8%	3.91
BL8S setup	127 (C: 2%; G: 1%)	10% (C: -; G: 2%)	3.75 (C: -33%; G: -4%)

Table 39: Comparison of the maximum evacuation time t_{max} , the waiting time percentage W , and the evacuation flow F of the generic simulator best setup (BL8S): percentage differences between the custom simulator (C) and the generic software median data (G) are pointed out into brackets.

7.6 Limitations and future aims

Additional tests on more complex scenarios, real-world contexts, and pedestrians' features (e.g. investigating larger groups of pedestrians and/or with different physical and social features) should be performed in the future assuming the best setup of this work. To this end, the same proposed setup methodology and comparison criteria could be adopted and support researchers in such preliminary validation and verification tasks. Moreover, the next research steps should also move towards modifications to the generic software code to include SFM-related interactions to overcome current setup-based simulator limitations in describing the outdoor evacuation behaviors in complex POSs (i.e., with the effective implementation of unmovable objects like trees, walls, fences, that can have

an attractive effect on the pedestrians). Similarly, to overcome the use of (pseudo-)stationary conditions in floodwaters, the variations in floodwaters levels to represent hydrodynamics conditions could be managed by directly connecting input data from external hydrodynamic simulators, thus adapting flood inputs affecting the pedestrians' motion and decision-making. Anyway, the proposed tool could be used to preliminary assess flood evacuation risks in HCCs and to increase pedestrian safety through risk-mitigation strategies (i.e. emergency management strategies, architectural layout modifications, micro-scale re-thinking of built spaces, direct support to pedestrians by also using wayfinding and alert systems, management actions by rescuers).

8. How urban layout and pedestrian evacuation behaviors can influence the risk in HCCs: the case of fluvial floods

This section is organized to first introduce specific floodwater levels (hydrodynamic conditions) reached in the HCCs open spaces and subspaces during the flood peak time (section §8.1), then specific risk-based evaluations are provided on the basis of the values assumed by previously defined Risk Indexes and Risk Maps (section §8.2). Risk comparisons and key findings are finally discussed in section §8.3.

8.1 Floodwater levels in the HCCs

The risk without the *pedestrian evacuation behaviors* combines the effects of the fluvial flood hazard and the *physical vulnerability* of Scenarios 1 and 2, by means of the analysis of D_fV_f levels in outdoor spaces. According to the hydrodynamic simulation results, regardless of the specific POS scenario, critical D_fV_f conditions for each gauging point have been generally reached at about 45 minutes after the beginning of the flooding event. Figure 53 shows a representative example of this D_fV_f trend over time, referring to Scenario 1, and considering different gauging points along the central perpendicular street. t_{sim} is hence centered with respect to this simulation time span.

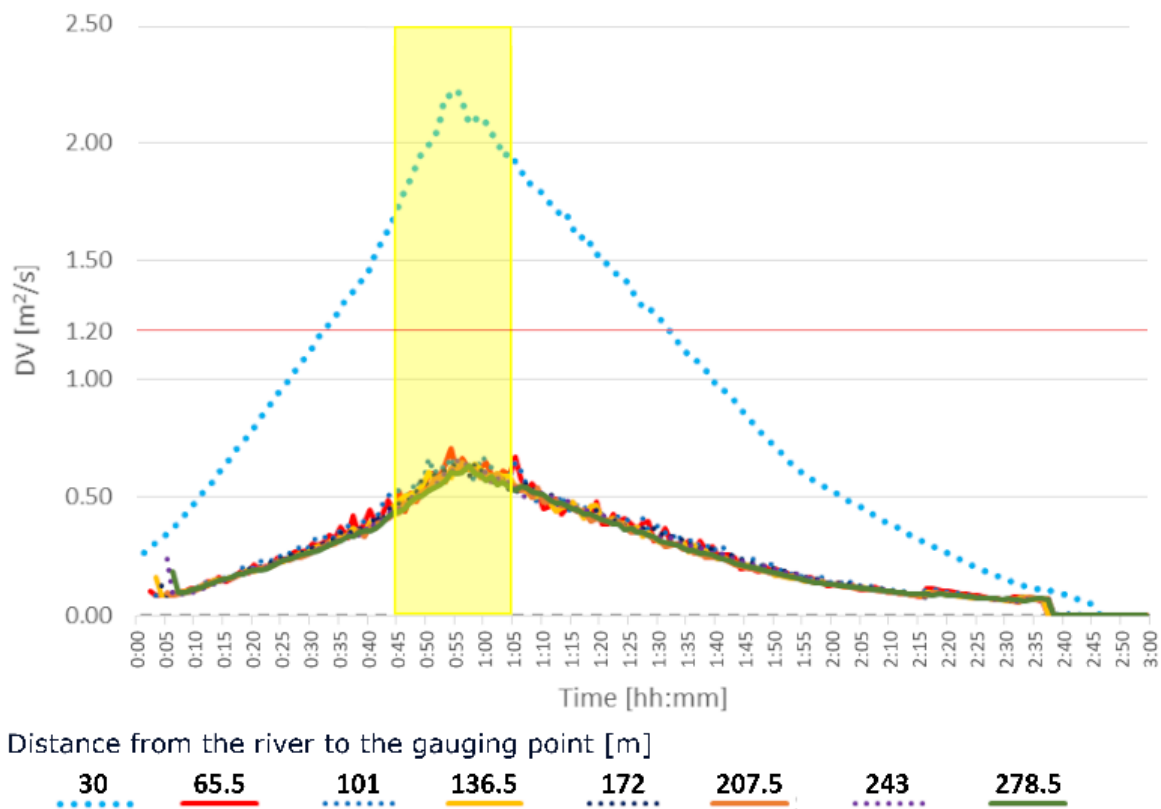


Figure 53: D_fV_f trend over time for Scenario 1 by considering the central perpendicular street and for different distances [m] from the river. Straight lines refer to gauging points inside the outdoor spaces, dashed lines refer to those inside the crossroads. The yellow area highlights the time span for the simulations. The limit condition for stability ($D_fV_f = 1.20 \text{ m}^2/\text{s}$) is also highlighted by the red continuous line.

Figure 54-A traces the overall DV_i maps for each typological POS. Such results firstly show that, in each typological POS, parallel streets have lower DV_i levels than the perpendicular ones. Therefore, low risks for stability exist, and higher v_i are allowed. The parallel street adjacent to the river has the

highest risk levels in terms of DV_i because it is immediately and continuously affected by the river overflow.

Squares seem to additionally own the lowest DV_i values, being close to 0 in some sub-spaces of *Scenario 2.A* and *Scenario 2.B*. Nevertheless, *Scenario 2.C* shows significant differences because of its layout configuration in comparison to the others. The analysis of local maximum D_fV_f values at the solving mesh scale offers the reasons for such results, as shown by the example of Figure 54-B and by the overview in Section §11.6 (Appendices).

In particular, Figure 54-B shows these data for the square of *Scenario 2.E*, which are similar to those of *Scenarios 2.A*, *2.B*, and *2.D*. The upstream parts of the square, which is just near the facing buildings, are characterized by D_fV_f close to 0 m²/s, because the square generates a beneficial effect being like a detention basin and the facing buildings constrain waterflows from the streets placed upstream. On the contrary, the square in *Scenario 2.C* is placed close to the river and directly collects waters from river overflow, thus increasing the flows on the connected streets placed downstream. These streets should discharge higher floodwater flows but they have limited widths, and so their DV_i values are sensibly higher than in all the other typological POSs. Considering the square itself, the two sub-spaces on the bottom of this outdoor space are protected by direct floodwater thanks to the building placed along it. Thus, their DV_i refer to low risk for stability conditions, as shown by the green sub-spaces of the square of *Scenario 2.C* in Figure 54-A. Meanwhile, the two sub-spaces on the top of the square are directly hit by floodwaters, thus causing extreme risk conditions for stability, as shown by the red sub-spaces of the square of *Scenario 2.C* in Figure 54-A.

In view of these microscale results, Figure 54-A also outlines the position of gathering areas in the two considered evacuation strategies. As shown by the arrow signs in Figure 54-A, the positions of the gathering areas in the “*leaving*” strategy are considered at the downstream exits of the POS streets, regardless of the DV_i conditions. On the contrary, as shown by the magenta dots in Figure 54-A, the position of the gathering areas in “*sheltering*” strategies is different in each analyzed scenario because the layout influences DV_i . They are placed in outdoor spaces and sub-spaces characterized by lower DV_i , as discussed above, so as to allow pedestrians to wait for the rescuers’ arrival in safer conditions in terms of stability.

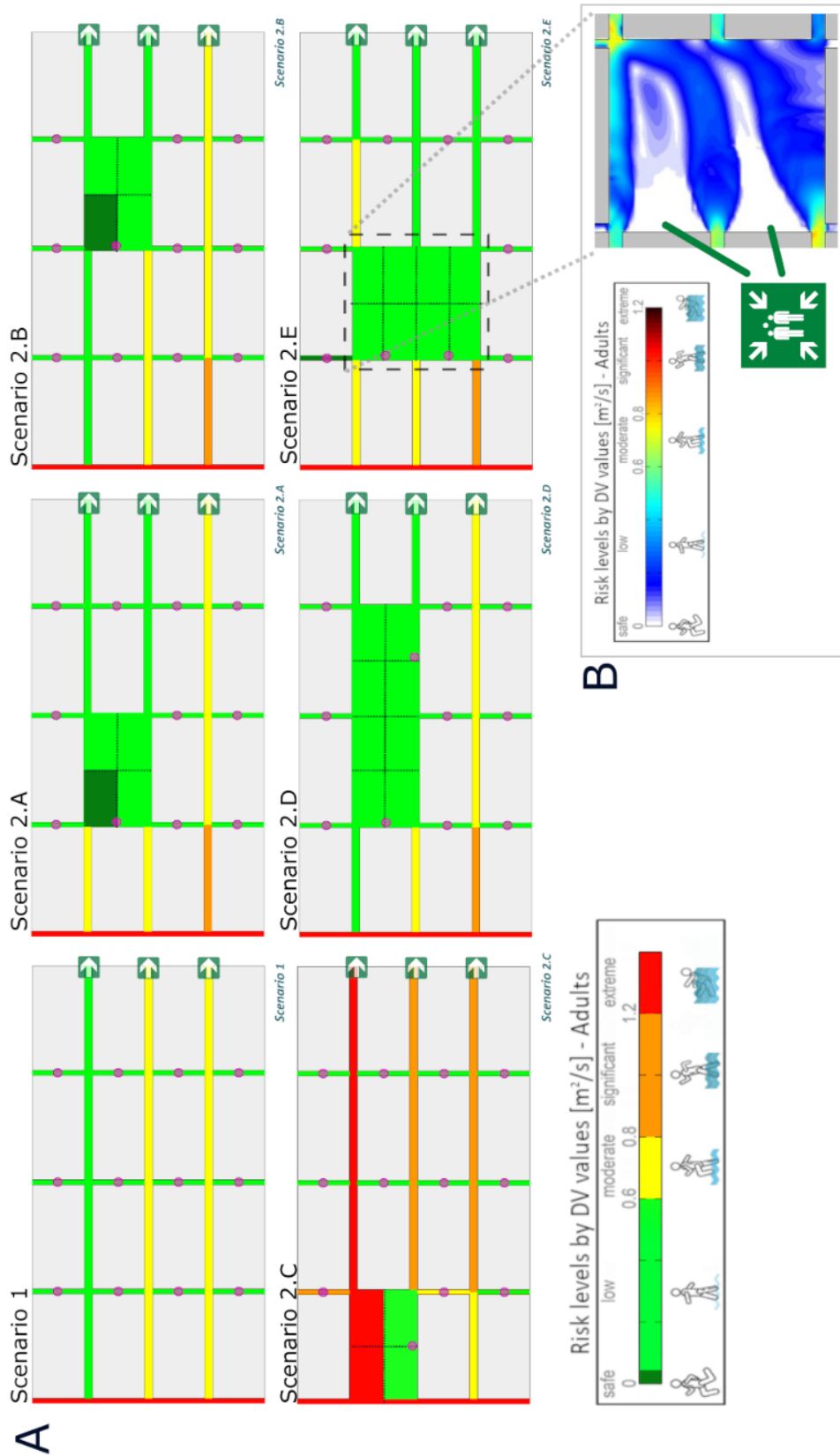


Figure 54: DV_i maps for each typological POS, with respect to adopted stability limits conditions [227], by offering: A) the conditions of each outdoor space and sub-spaces (i.e. for squares, see the dotted lines) and the localization of gathering areas in “sheltering” (magenta dots) and “leaving” (arrow signs) evacuation strategies; B) an example (Scenario 2.E) of local DV_i conditions in the main square according to the 1m x 1m solving mesh, by including the gathering areas posting according to the “sheltering” strategy. For each panel, the scale representation of DV_i values is offered.

From a mesoscale standpoint, Table 40 summarizes the values $DV_{a,M}$ and IDV_{M} (that is equal to $RI_{POS,M}$). Results show that the typological POSs in *Scenarios 2* are generally characterized by lower $DV_{a,M}$ values in comparison to *Scenario 1*. As a consequence, the microscale effects of the floodwater spreading into the outdoor spaces in the POS are confirmed. Nevertheless, as pointed out above, *Scenario 2.C* shows the highest risk level from a macroscopic standpoint because of the square position in the aligned layout. Furthermore, typological POSs with wider squares not just behind the river, that are *Scenarios 2.D* and *2.E*, seem to be less risky than the others, thanking the possibility of a positive impact of such “detention” basins. No significant difference emerges by changing the direction of the major axis.

Typological POS	$DV_{a,M}$ [-]	$IDV_{M} = RI_{POS,M}$ [-]
Scenario 1	0.65	0.54
Scenario 2.A	0.49	0.41
Scenario 2.B	0.50	0.42
Scenario 2.C	0.98	0.82
Scenario 2.D	0.42	0.35
Scenario 2.E	0.41	0.34

Table 40: $DV_{a,M}$ and IDV_{M} values for each typical POS as graphically described in Figure 10.

8.2 HCCs flood risk with and without pedestrian evacuation behaviors

Table 41 summarizes the KPI and RI values for the typological POSs, with and without the *pedestrian evacuation behaviors*, and by including the specific evacuation strategies, according to the mesoscale standpoint. Evacuation simulation results are reported in Section §11.6 (Appendices).

TYPOLOGICAL POS		KEY PERFORMANCE INDICATORS					RISK INDEX		RI _{evac,M} Reduction [%]
Scenario	Strategy	T _{e,M} [-]	D _{t,M} [-]	N _{a,M} [-]	F _{e,M} [-]	IDV _M [-]	RI _{POS,M}	RI _{evac,M}	
1	Leaving	0.38	1.00	0.00	0.75	0.54	0.54	0.45	-
	Sheltering	0.11	0.30	0.00	0.15	0.54	0.54	0.34	-24%
2.A	Leaving	0.36	1.00	0.00	0.73	0.41	0.41	0.39	-
	Sheltering	0.11	0.30	0.00	0.07	0.41	0.41	0.26	-33%
2.B	Leaving	0.37	0.99	0.00	0.73	0.42	0.42	0.39	-
	Sheltering	0.11	0.29	0.00	0.07	0.42	0.42	0.27	-33%
2.C	Leaving	1.00	0.95	0.65	0.91	0.82	0.82	0.76	-
	Sheltering	1.00	0.30	0.39	0.50	0.82	0.82	0.59	-21%
2.D	Leaving	0.34	0.99	0.00	0.71	0.35	0.35	0.37	-
	Sheltering	0.11	0.29	0.00	0.00	0.35	0.35	0.23	-38%
2.E	Leaving	0.35	0.99	0.00	0.69	0.34	0.34	0.36	-
	Sheltering	0.11	0.30	0.00	0.06	0.34	0.34	0.22	-39%

Table 41: summary of the KPIs and values of risk indexes with ($RI_{evac,M}$) and without ($RI_{POS,M}$) pedestrian evacuation behaviors, and depending on the evacuation management strategies. The $RI_{evac,M}$ Reduction is calculated in percentage terms with respect to the $RI_{evac,M}$ in “leaving” strategy.

In general terms, the effects of accounting or not the *pedestrian evacuation behaviors* have no relevant effects at the mesoscale, as shown by Table 41. In fact, higher $RI_{POS,M}$ values correspond to higher $RI_{evac,M}$ values, essentially because of the impact of IDV_{M} on both the risk indexes. Nevertheless, $RI_{evac,M}$ varies depending on the evacuation management strategies and the last column of Table 41 highlights how the “*sheltering*” strategy always decreases the risk. Considering the KPIs based on the *pedestrian evacuation behaviors*, *Scenario 2.C* highlights the most critical risk

conditions in both the emergency management strategies. The main impact is due to $T_{e,M}$ and $N_{a,M}$, which consider how pedestrians can be trapped during the evacuation process, essentially because of their position with respect to the square. In fact, in *Scenario 2.C*, trapped pedestrians are initially pedestrians placed upstream and near the square, thus suffering higher DV levels that both: (1) slow down their motion, as shown by $T_{e,M}$; and (2) can provoke the loss of stability, as shown by $N_{a,M}$.

The microscale standpoint confirms the same trends. For each outdoor space and sub-space, Figure 55 and Figure 56 resume $RI_{POS,m}$ (panel A) and $RI_{evac,m}$ (panel B for “leaving” and panel C for “sheltering”). $RI_{POS,m}$ -related maps do not change with the evacuation strategy, since the index is based on KPIs representing the POS geometry and morphology through $D_{r,m}$ and the event’s magnitude through $I_{DV,m}$. On the contrary, $RI_{evac,m}$ includes the effects of *pedestrian evacuation behaviors* since it includes $N_{a,m}$ indeed.

According to Figure 55 and Figure 56, apart from *Scenario 2.C*, the squares are characterized by a lower risk than the streets that link them to the river, thanking the aforementioned “detention basin”-like effect. This result confirms the outcomes of section §8.1.

The *pedestrian evacuation behaviors* exalt the risks in the squares sub-spaces in which the floodwaters enter from/exit towards the linked streets. In view of this phenomenon, streets placed downstream with respect to the squares³² generally present equal or worse conditions than the squares themselves, because they are drain elements for them. When trapped pedestrians along these paths are present, $RI_{evac,m}$ is higher than $RI_{POS,m}$ by evidencing the streets where pedestrians could not end the motion process, in view of the abovementioned $N_{a,m}$ contribution.

On the contrary, the outdoor spaces placed further from the river are characterized by $RI_{evac,m} < RI_{POS,m}$ since the simulation results point out how the pedestrians could still move along them and reach a safe area or leave the flood-affected area without additional threats, such as being trapped. This case is reported, for instance, in:

1. the squares of *Scenario 2.B* and *Scenario 2.E*, due to the positive effects of these squares as detection basins;
2. most of the perpendicular streets of *Scenario 1*;
3. the perpendicular streets in *Scenario 2.C* in the bottom right part of the POS, as an effect on pedestrians’ motion due to the lower $RI_{POS,m}$ in comparison to the ones closer to the river.

In this sense, the sub-space of the square in *Scenario 2.C* offers a valuable difference due to $N_{a,m}$ with respect to the two proposed strategies, as pointed out by the comparison between Figure 56-B and Figure 56-C. $RI_{evac,m}$ is lower than $RI_{POS,m}$ of about 15% in “leaving”, while of about 30% in “sheltering”.

Finally, in percentage terms, differences between $RI_{evac,m}$ and $RI_{POS,m}$ for the considered spaces vary by about 15% in absolute terms.

³² In this case, higher risks are related to the linked streets having a lower altitude in respect to the upstream part of the square.

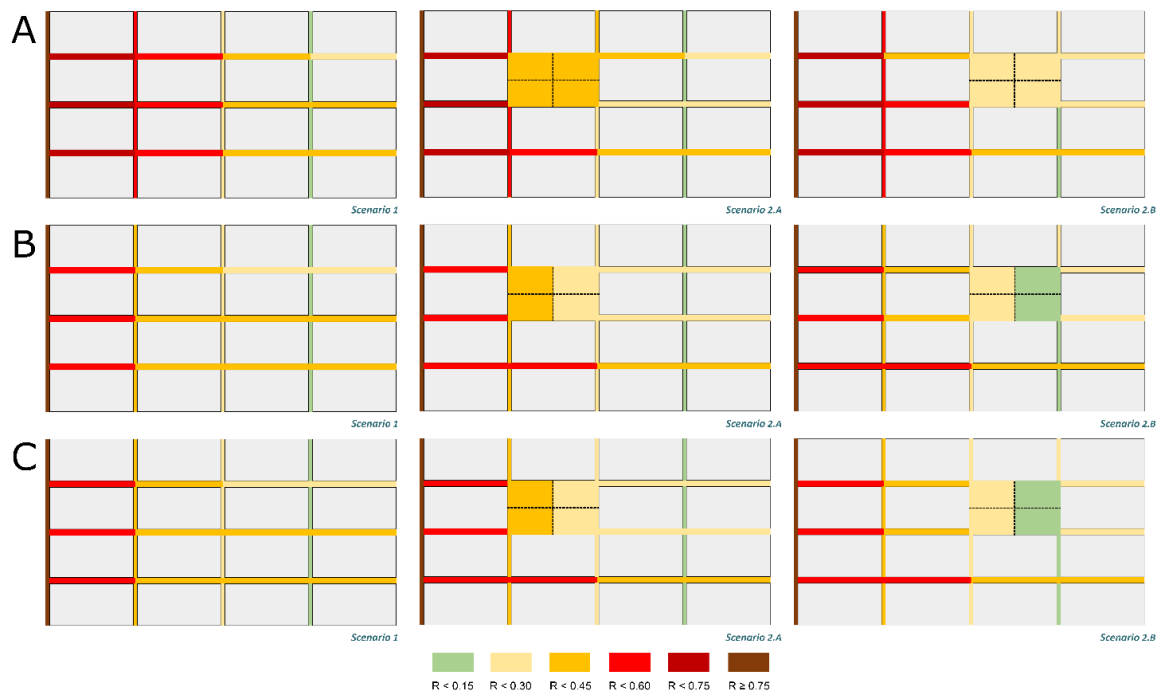


Figure 55: RI maps at the microscale level by considering Scenario 1, 2.A, and 2.B: A) without pedestrian evacuation behaviors; B) with pedestrian evacuation behaviors in “leaving” strategy; C) with pedestrian evacuation behaviors in “sheltering” strategy.

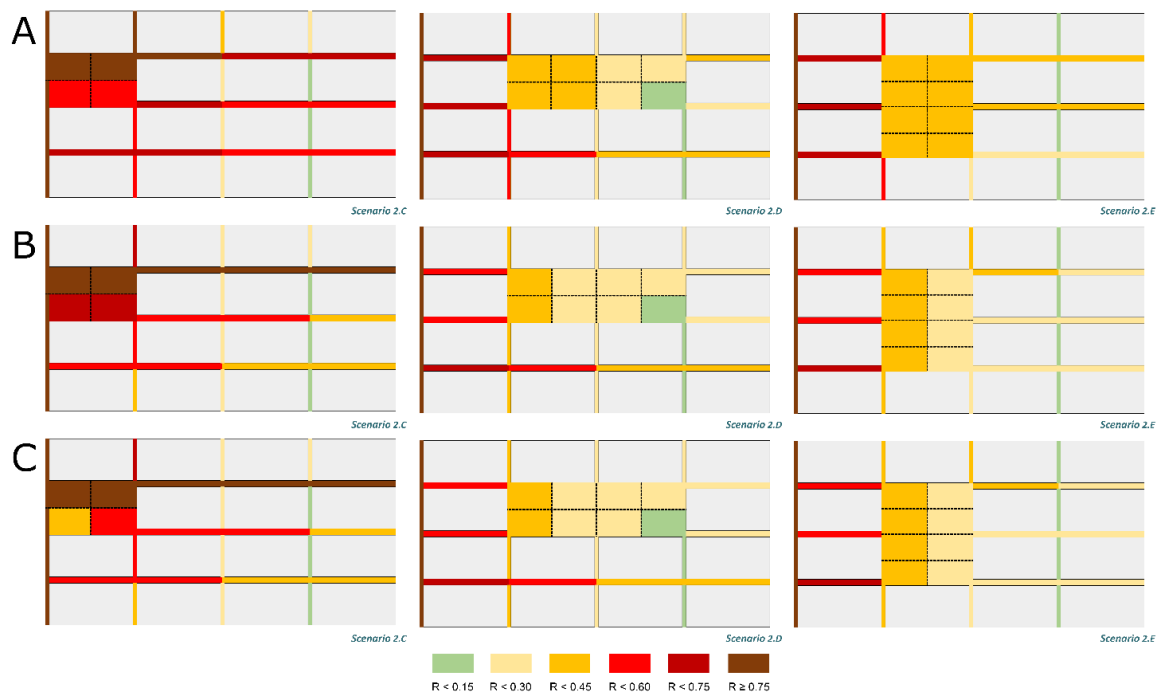


Figure 56: RI maps at the microscale level by considering Scenario 2.C, 2.D, and 2.E: A) without pedestrian evacuation behaviors; B) with pedestrian evacuation behaviors in “leaving” strategy; C) with pedestrian evacuation behaviors in “sheltering” strategy.

8.3 Outcomes evaluation

8.4.1 Typological HCC risk comparison

Microscale and mesoscale results provide some general considerations about the tested typological riverine POSs, which can be categorized as different variations of an aligned layout configuration. These considerations can be also related to risk assessment with or without the *pedestrian evacuation behaviors*, thus demonstrating the capabilities of the novel approach in solving the research assumptions in section §3.5.4.1. Anyway, it is worth noticing that the following remarks do not want to move towards universal rules regarding the POS and they are strictly related to the modeled flood and to the considered case studies to define the tested layout. However, they surely represent the first attempt to be done in that direction.

First, regardless of accounting or not *pedestrian evacuation behaviors*, in each typological POS, the risk levels of the outdoor spaces decrease with the distance from the river. The street adjacent to the river is always characterized by the extreme risk level, because of the effects of floodwaters flow entrance due to the river overflow. Considering the assumed time span for the simulations, D_fV_f conditions do not allow the positioning of gathering areas in these outdoor spaces, while physical retains and supports for evacuation motions (e.g. handrails or raised platforms) can have a limited impact too. These outcomes underline the importance of technological systems to prevent or slow down the river overflow, as well as the importance of early warning systems to improve safety, especially for the POS areas closer to the river [32], [36], [311].

Considering risk assessment without the *pedestrian evacuation behaviors*, higher risk levels are related to more compact POSs, such as: (1) *Scenario 1*, where the compact layout forces the floodwater motion towards the downstream exits of the POS; (2) *Scenario 2.C*, where the presence of a square adjacent to the river may amplify the effects of floodwater spreading in the other outdoor spaces, since the square firstly collects and then pours larger volumes of water towards the linked streets placed downstream.

Lower risks are related to the typological POSs with a non-adjacent square placed. In fact, according to Table 40, $RI_{POS,M}$ values in *Scenarios 2.A, 2.B, 2.D, and 2.E* are almost the same (variations lower than 23% with respect to minimum $RI_{POS,M}$). In these cases, the higher the square dimension, the lower the risk of the spaces, both from microscale and mesoscale standpoints. Furthermore, from a microscale standpoint, the streets parallel to the river are characterized by a lower risk than the perpendicular ones, regardless of the typological POS layout. This result is due to the abovementioned effects of floodwater spreading downstream, that is far from the river.

Although differences considering RI without *pedestrian evacuation behaviors* exist, similar trends are also seen for risk assessment with *pedestrian evacuation behaviors*. The final outcomes depend on the considered emergency management strategies. From the mesoscale standpoint, in all the considered typological POSs, “*sheltering*” seems to be more efficient than “*leaving*”. In fact, $RI_{evac,M}$ is reduced up to 40%, essentially because interferences between the pedestrians and the floodwaters are limited in terms of path length and motion timing. The presence of trapped pedestrians occurs only in *Scenario 2.C*, but their number is lower in “*sheltering*” strategies in comparison to “*leaving*”.

Reasons for the improvement under the “*sheltering*” strategies are linked to the microscale D_fV_f assessment, which quickly suggests where to place the gathering areas, as shown in section §8.2. From a general point of view, it could be considered that gathering areas could be placed along the

parallel streets and the upstream part of the squares, close to the buildings. Such positions can take advantage of the protection from direct floodwater impact due to the buildings themselves, as also shown by Figure 54-B and Figure C1 in Section §11.6 (Appendices). In such parts, safety planners could implement signage systems and, eventually, raised platforms where to gather, so as to avoid further threats over time [120], [134]. A widespread implementation of these gathering areas can ensure a reduction of the pedestrians' threats while moving, because the evacuation path is quite short for each pedestrian.

Anyway, evacuation simulations can test different quantities of such gathering areas. Thus, the optimization of their number can be pursued with respect to their benefits, according to the provided KPIs and RI accounting for *pedestrian evacuation behaviors*.

In each typological POS, simulation outcomes additionally suggest how evacuation systems support pedestrians' motion and stability in floodwater, such as handrails where hanging on [134], should be generally implemented along the streets parallel to the river, especially for those placed nearer to the river. Along these streets, handrails can be integrated in the building façade as well as by means of urban furniture. Handrails should be also installed in the square of *Scenario 2.C*, so as to help pedestrians move towards the gathering area in the square itself. In the square, such handrails can be included in the urban furniture placed inside the outdoor space itself, being also combined with architecturally integrated raised platforms. In this sense, heritage preservation issues should be also evaluated from an aesthetic point of view. In view of the above, quick planning of emergency areas could be easily reached for the whole POS, thus speeding up local authority's actions to this end in a sustainability perspective.

8.4.2 Key findings, work novelties, and future aims

Four main issues demonstrate the key findings of this research, its novelties, and the future works to be carried out by adopting the proposed approach.

First, this research is a first attempt to compare how accounting or not *pedestrian evacuation behaviors* can affect the flood risk assessment in POSs. As shown in the results section, differences between $RI_{POS,m}$ and $RI_{evac,m}$ are noticed in all the typological POSs and can lead to discrepancies in the definition of risk-mitigation strategies for the immediate flood response phase and the evacuation process. In this sense, the proposed approach can support existing methodologies for the assessment of emergency actions and related mobility for the rescuers and the population [34], [124], [135].

Second, according to a sustainability perspective in the methodology application, an easy-to-use simulation model for evacuation simulation is provided, which is based on a quick setup of commercial generic software. The simulator can be ideally used by low-trained and non-expert technicians, such as the ones of local authorities. The model can simulate man-environment interactions at a microscopic level since the model assigns emergency evacuation rules to each of the simulated agents. Considering previous works on evacuation simulation models and applications [124], [134], this approach can:

1. provide a more rapid application of the simulator also in real-world environments, because of the simpler setup of the behavioral and motion quantities with respect to microscopic models;
2. improve the reliability of simulation with respect to simplified macroscopic models, such as the fluid-dynamics ones.

As for the quick evacuation simulation approach, the proposed KPIs could support rapid evaluations since they are based on a few simple parameters concerning the simulation outputs. Anyway, it is worth noting that this approach considers average and homogeneous *pedestrian evacuation behaviors* and pedestrian features. Some simplifications are hence assumed, including those on neglected factors such as mobility, age, and gender (i.e., users' vulnerability), as well as the effective familiarity with the urban layout and the emergency strategies [124]. Future works should try to include such issues. If commercial tools will not be able to quickly include such issues, custom and more complex tools can be used, according to the same microscopic evacuation simulation modeling, and without changing the overall evaluation methodology.

Third, the research is innovatively oriented towards flood-prone HCC contexts, and, in particular, focuses on the public open spaces as key elements for risk assessment due to their paramount role in the evacuation process. Here, the impact of emergency evacuation strategies can be investigated at a double scale (thus overcoming the general limitations of previous approaches [124], [135], [221]) by including or not *pedestrian evacuation behaviors* in the risk assessment. The mesoscale assessment allows for comparing and ranking the overall risk of a specific POS. The microscale assessment allows comparing the risk into specific parts in the POS, with the final aim of providing data on where and how to introduce interventions for risk mitigation and support pedestrians in emergency conditions.

Fourth, in view of the previous novelty, this application is also one of the first attempts to compare the effectiveness of emergency management strategies based on “*leaving*” the flood-affected area and on “*sheltering*” inside it. This comparison has been not provided by previous works, which generally focus on simple evacuation strategies organizations, such as gathering in safe areas or moving upstairs in buildings [124]. In this perspective, future efforts should investigate possible variations in each of these strategies, by investigating the effects in the quantities of evacuation paths and gathering areas as well as the combination of these strategies indeed.

In this process, the *pedestrian evacuation behaviors* in flood are also assessed for risk assessment purposes, for the first time. It is clear that the results hold inside the adopted physical parameters and the considered hazard. On the contrary, the methodology can be applied to other POSs far from the considered ones, as well as in non-HCC context, and can also assess the impact of other flood typologies [274]. The simulation results and related risk assessment outcomes can be considered as valid for HCCs having such typical analyzed scenarios, as well as non-HCCs having the same features, under the riverine contexts and the overflow of the river. Furthermore, future works should be aimed at including further POS-characterizing factors, such as the vulnerability of buildings in view of flood-induced damages or the surface description.

9. Optimizing pedestrian evacuation strategies in flooded HCCs according to a behavioral-based approach

9.1 How many, where, how, and which gathering areas and evacuation routes are needed in the HCC-related POS

In the following sections, the proposed risk index $RI_{i,M}$ is used to identify the best evacuation strategy in terms of gathering areas' optimal number (*how many*, section §9.1.1) and position (*where*, section §9.1.2), optimal evacuation routes (*which*, section §9.1.3), and resulting evacuation units (*how*, section §9.1.4) derived according to the selection of routes. The best evacuation strategy is then identified (§9.1.5) and finally adopted for comparison purposes with the microscopic simulator previously defined (§9.1.6)

9.1.1 Gathering areas optimal number

The optimal number of gathering areas to be provided in the POS can be evaluated according to the values assumed by $RI_{i,M}$, which are organized in Figure 57 in three different trends according to the approaches for the evacuation route choice.

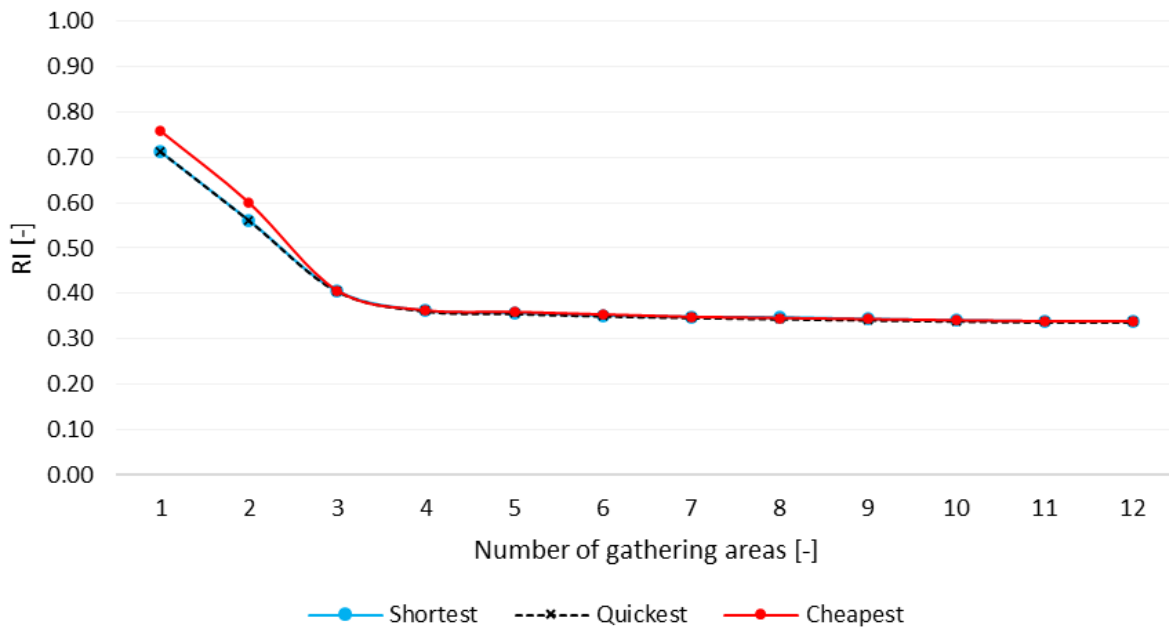


Figure 57: $RI_{i,M}$ values depending on the approach for the path choice “ i ” (shortest, quickest, or cheapest) and the number of gathering areas available “ M ”. “Shortest” and “quickest” trends are overlapped.

For evacuation strategies with one and two available gathering areas, the “cheapest” approach registers the highest values of risk ($RI_{c,1}$ and $RI_{c,2}$), since pedestrians have to travel greater evacuation lengths and times to obtain benefits in terms of effort, thus increasing the overall risk. On the other hand, with these configurations, the trends for the “shortest” and the “quickest” approaches have lower risk and are overlapped ($RI_{s,M}$ and $RI_{q,M}$), meaning that, for this specific case study, these approaches have the same level of risk.

By placing three available gathering areas, the three trends of strategies i converge ($RI_{i,3} = 0.40$), thus identifying a threshold beyond which $RI_{i,M}$ no longer varies although the gathering areas' positions are differentiated between the solutions (meaning that, for this specific case study, they can be

considered at the same level of risk). In addition, with four (or more) gathering areas available and regardless of the strategy i , $RI_{i,M}$ does not significantly decrease (i.e., $RI_{i,M}$ drops by less than 5%) as the number of available gathering areas increases ($RI_{i,4} = 0.36$). This outcome can help evaluate the number of gathering areas to be prepared according to further possible criteria, such as the gathering areas' available surfaces [m^2] in relation to the expected number of pedestrians to accommodate, and the gathering area density [pp/m^2] to avoid physical contacts between pedestrians and flow problems [318].

Furthermore, it is worth noticing that all three approaches produce indifferently the same number $Z_{(i,M)}$ of pedestrians who cannot complete the evacuation due to their starting position in deadly points (i.e., areas where $D \geq 1.20m$, $V \geq 3.00m/s$, or $D_f V_f \geq 1.20m^2/s$), that is up to 123 with $M = 1$, and 88 with $M > 1$. All the values of the evacuation parameters and the following KPIs and Ris are resumed in Section §11.6 (Appendices).

9.1.2 Gathering areas optimal position

This section shows and discusses the results only with respect to the optimal configuration in the number of gathering areas (equal to 4), which is provided in the previous subsection.

The positioning of these gathering areas is shown in Figure 58. All the tested approaches for the route choice unanimously select gathering areas A , D , G , and K , highlighting how a modular criterion for the positioning of the gathering areas is required to reduce the risk, and it basically depends on the distance from the source of hazard, i.e. the river. Except for the gathering area provided in the square (A), the other gathering areas (D , G , K) have to be placed along the streets parallel to the river (therefore every 66m) to advantage of the shielding of the building blocks. In this way, each pedestrian has to travel, at most, along only one building block until reach safety, thus avoiding passing through crossroads where the confluence of multiple floodwater flows may provoke more severe conditions for the pedestrians' safety [151]. Additional insights relating to non-optimal solutions ($M < 4$) seem to suggest how to organize the gathering area hierarchy and position to prevent, for example, problems in case one (or more) of them becomes impracticable or reaches capacity limits. As shown by Table 42, decreasing the number of available gathering areas implies that the optimal solutions are always those that provide at least one gathering area in the street furthest from the hazard (K or L , as they manage to collect the maximum number of pedestrians), and eventually one in the square (A). In particular, gathering area A is the only gathering area that can effectively reduce the number $Z_{(i,M)}$ of pedestrians who cannot complete the evacuation. In fact, the environmental conditions at the exit nodes from the square prevent the evacuation towards gathering areas displaced in the streets (i.e., outside of the square).

Approach i	$M=4$ ($RI_{i,4} = 0.36$)	$M=3$ ($RI_{i,3} = 0.43$)	$M=2$ ($RI_{i,2} \approx 0.70$)	$M=1$ ($RI_{i,1} > 0.80$)
Shortest (min S; $i=s$)	K ; A ; G ; D	K ; A ; G	K ; A	K
Quickest (min T; $i=q$)	K ; A ; G ; D	K ; A ; G	K ; A	K
Cheapest (min DVS; $i=c$)	K ; A ; G ; D	K ; A ; G	L ; A	L

Table 42: Gathering areas selection depending on the approach for the path choice "i" and the number of gathering areas available "M" (by considering only strategies with $M \leq 4$). The map with the gathering areas' position is shown in Figure 58.

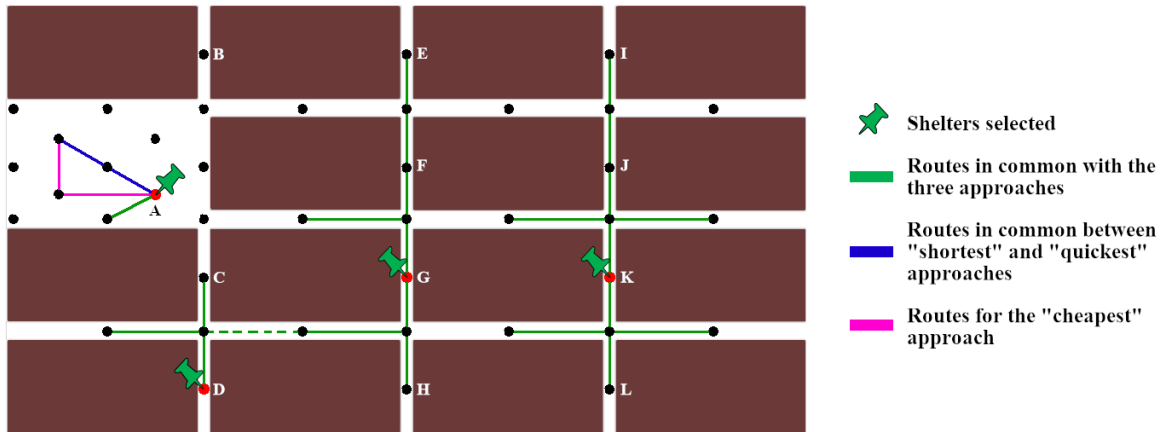


Figure 58: Gathering areas selection and evacuation routes to reach them in the case of $M=4$. For $M = 3$, pedestrians collected in node D should reach node G by traveling the dashed green link. Isolated nodes (non-linked) are deadly points.

9.1.3 Optimal evacuation routes

Once the optimal number ($M=4$) and position (K , A , G , and D) of gathering areas are determined, the evacuation routes to reach them must be defined. In this section, the evacuation routes obtained from the three tested approaches (“shortest”, “quickest”, and “cheapest”) are compared for $M=4$. In Figure 58, isolated black nodes are deadly points, while pinned red nodes indicate the gathering areas selected between those available (which are those named with a letter).

Concerning the evacuation routes, all the approaches are correlated to the same evacuation routes if considering the gathering areas located along the streets (i.e., K , G , and D), as shown by the solid green lines in Figure 58. Furthermore, the green dashed line points out the evacuation route that pedestrians should use in the case only three gathering areas are available (basically, pedestrians allocated to D go instead of G). On the other hand, for pedestrians displaced in the square (gathering area A), the three tested approaches provide two different evacuation routes. As shown in Figure 58, the “shortest” and the “quickest” approach share the same route, as shown by the blue lines, while the “cheapest” approach is traced by the magenta line. Nevertheless, all the approaches are characterized by the same level of risk ($RI_{i,4} = 0.36$).

9.1.4 Optimal evacuation units

According to the results obtained in the previous sections, Figure 59 traces the four outgoing evacuation units for the urban area, each of which includes the gathering areas and the full evacuation routes for pedestrians (starting node to ending node). In this way, the evacuation units subdivide the urban area into basic sectors according to their distance from the source of danger and to the shielding guaranteed by the building blocks.

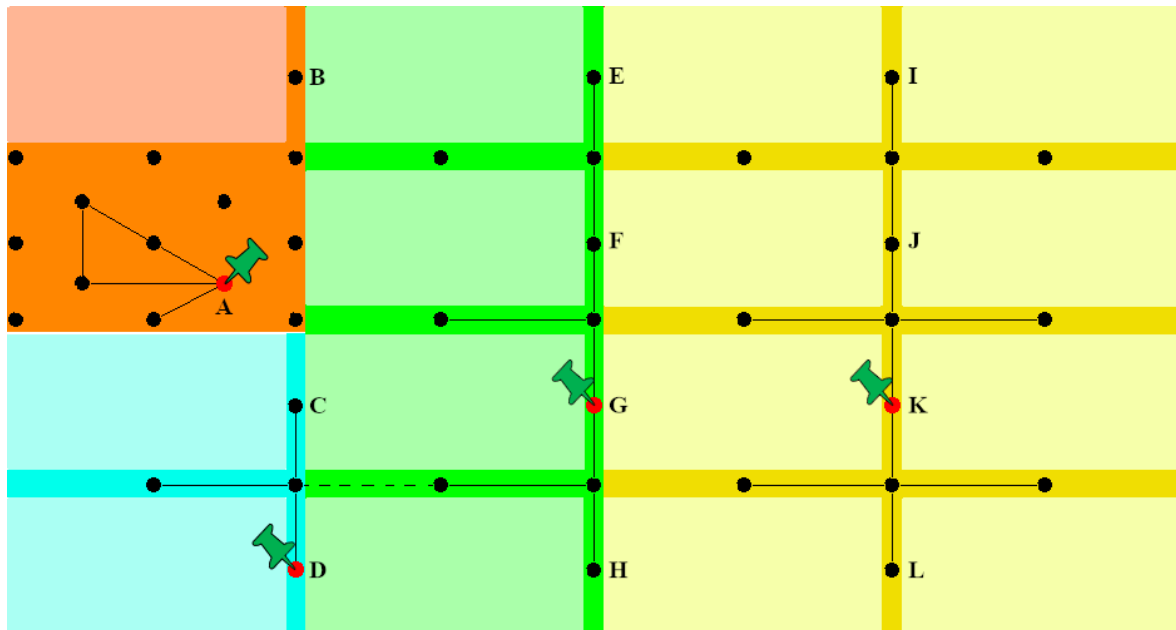


Figure 59: Evacuation units with $M=4$. For $M=3$, the blue unit can be linked to the green one through the dashed link.

Table 43 shows the number of pedestrians present in each evacuation unit and the number of pedestrians expected to be allocated, which is evaluated excluding the number $Z_{(i, M)}$ of pedestrians (88 pp) who are unable to complete the evacuation due to their starting position in deadly nodes. It is worth noticing $Z_{(i, M)}$ cannot be decreased because of the hydrodynamic conditions within the urban area, and it is always the same when $M>1$, indifferently from the approach for the route choice, as shown in detail in Section §11.7.3. In particular, the deadly nodes are displaced in most downstream areas of the case study and in the square, as highlighted by the isolated nodes in Figure 59. The blue evacuation unit is the only one in which 100% of pedestrians manage to reach safety since no deadly nodes are herein included. As a result, the only possible strategy to improve such an outcome is evacuating the urban area before the event reaches its peak time.

Gathering area	Evacuation unit	N° of pedestrians' present	N° of pedestrians to be allocated
K	Yellow	82	60
G	Green	49	38
D	Blue	19	19
A	Orange	90	35
ALL	ALL	240	152

Table 43: number of pedestrians present in each evacuation unit, and to be allocated to each gathering area. The differences between those quantities are the number $Z_{(i, M)}$ of pedestrians unable to complete the evacuation in each evacuation unit.

9.1.5 Identification of the best evacuation strategy

The typological POS tested should be made safe through an optimal solution unanimously identified by the three tested approaches for the route choice, namely “shortest”, “quickest”, and “cheapest”. In fact, considering the peculiarities of the urban area and of the flood event, the minimization of the evacuation length, time, and effort provides the same level of risk for pedestrians. In particular, the identification of the best evacuation strategy supplied the following optimal configuration:

- Four gathering areas (A , K , G , and D) should be foreseen, being the minimum number and configuration of gathering areas beyond which the risk does not decrease, and their selection

is able to cover all the four main areas of the case study (i.e., the square and the three streets parallel to the river);

- The evacuation routes to be traveled are pointed out in Figure 59.

The urban area is hence subdivided into four evacuation units, each of which is characterized by one gathering area and the entire development of the evacuation routes to get there (hence, by a given number of pedestrians that could be allocated as a function of the starting nodes included in the units). In this way, when the flood occurs³³, pedestrians displaced in a certain area of the case study (identified by a given color in the map shown in Figure 59), should be able to complete the evacuation by only moving within their evacuation unit.

9.1.6 Comparisons between macroscopic and microscopic modeling approaches

Comparisons between macroscopic and microscopic modeling approaches are herein discussed on the basis of the RI_i values resumed in Table 44 by only considering the best evacuation strategy configuration (which is discussed in the previous subsection §9.1.5).

Evac. Strategy	$N_{a(i)}$	n_a	$S_{AVG(i)}$	s_i	$T_{AVG }$	t_i	$DVS_{AVG(i)}$	dvs_i	RI_i
Macro	88	0.37	42	0.37	66	0.37	19	0.31	0.36
Micro	103	0.43	33	0.29	52	0.29	21	0.34	0.38
Percentage differences	+6%*	+6%*	-21%	-22%	-21%	-22%	+10%	+10%	+6%

*Table 44: RI_i values for each evacuation strategy i tested, distinguishing the values for the KPIs. Since the tested evacuation strategy is characterized by the same configuration of evacuation paths and gathering areas regardless of the route choice behavior (i.e., shortest, quickest, and cheapest), macroscopic approach outcomes are considered a unique optimal solution. *: the difference is calculated with respect to the overall initial number of pedestrians (240 pp).*

In particular, focusing on the KPI_i values:

- The missing pedestrians' ratio (n_a) is higher in the microscopic approach, where 15 pedestrians did not manage to complete the evacuation, which in percentage terms is about 6% of the total population taking part in the evacuation (value comparable with the acceptability thresholds of 15% generally prescribed in the relevant literature for differences due to the modeling logics at both macroscale and microscale [258]);
- The normalized average evacuation length (s_i) is noticeably lower in the microscopic approach, where pedestrians who manage to complete the evacuation on average travel 9m less (-21%) than in the macroscopic approach to reach the gathering areas. This is reasonably due to the totally random displacement of pedestrians within the scenario in the microscopic approach (starting areas), differently from the macroscopic one where the starting points have fixed coordinates;
- The normalized average evacuation time (t_i) follows the same trend, since in the microscopic approach pedestrians who manage to complete the evacuation on average take 14s less (-21%) than the macroscopic approach to reach the gathering areas;

³³ As stated in Section 2, the evacuation strategies discussed in this research are referred to the event peak time, therefore they could change by varying the reference timespan.

- The normalized average evacuation effort (dvs_i) is slightly higher in the microscopic approach, meaning that on average pedestrians make a little bit more effort to reach the gathering areas than in the macroscopic approach ($2m^2/s$, which is about +10%).

These differences seem to suggest that the microscopic approach can be more conservative than the macroscopic one, but the overall risk measured by RI_i is nonetheless comparable since the microscopic approach is about 6% higher than the macroscopic one. While the microscopic approach tends to overestimate the risk for the single pedestrian, by computing higher distances and times to reach the shelters, the macroscopic approach tends to overestimate the risk for the group by computing a higher number of pedestrians unable to complete the evacuation.

9.2 Outcomes evaluation

The results shown in section §9.1 offer interesting insights to discuss general key findings in terms of innovations (§9.2.1), following implications for decisions-makers (§9.2.2) as well as related limitations to overcome for future improvements (§9.2.3).

9.2.1 Innovation of the results

The proposed approach introduces several novelties in the field of emergency management applied to flood disasters, with particular attention to risk-reduction measures to improve the preparation and response phases. From a methodological perspective, previous studies investigated optimization and districting issues for emergency management, but present relevant differences as they consider other types of disaster (e.g., earthquakes) [319], evacuations by vehicles [266], [320], or pre-determined districts considering logistic constraints and resources (budget, number of ambulances, number emergency teams) [321], [322]. This part of the thesis seems to overcome their limitations by more clearly addressing the problem of optimizing flood evacuation strategies (number and location of gathering areas, evacuation routes depending on different approaches, districting evacuation units) while (a) taking into account evacuation by foot, thus considering pedestrian behaviors in floodwater, and (b) defining unifying assessment criteria which can be exploited also in other contexts and disasters conditions, thanks to quick but reliable and general-purpose KPIs and Risk Index focused on pedestrian-related issues. Furthermore, significant differences emerge from the closest studies investigating the location of the gathering areas and the evacuation planning problem relying on a multi-objective approach [321], [322], as they seem to ignore the number of victims as an optimization criterion (which is instead the essential target of the proposed hierarchical method). Furthermore, the multi-objective framework entails the solution of two separate models: a preliminary flow model for generating the limited set of selectable evacuation routes, and a subsequent location model that incorporates these routes.

In this sense, the analysis of gathering areas and evacuation routes provides fundamental information to avoid survivorship bias-like phenomena, especially in deadly areas where pedestrians are unable to move safely due to particularly adverse environmental conditions (e.g., in this case study, the isolated nodes in Figure 59). To this end, the results obtained by applying this tool also enhance evaluations for the implementation in the urban area of adequate gathering areas (i.e., sufficiently spacious and raised), urban furniture (e.g., handrails, raised platforms, sidewalks to improve pedestrians' speed and stability), wayfinding systems (including communication through portable devices), and road signs to improve pedestrians' communication and allocation toward the gathering areas preferably even before the actual disaster occurrence [186], [246], [311], [313].

9.2.2 Policy implications for decision-makers

Districting the urban area into evacuation units is useful to solve possible logistic issues, such as planning how many emergency teams are needed for rescuers' operations (i.e., by assigning each evacuation unit to a squad composed of a certain number of rescuers, especially in the unwalkable areas), or how pedestrians could be re-allocated (i.e., redirected) if accidentally during the evacuation process, one of the planned gathering areas becomes impracticable. For instance, with respect to the last issue, Figure 59 shows how pedestrians initially allocated to gathering area *D* could be reallocated to gathering area *G* by only traveling the dashed link (which is equivalent to connecting the blue unit to the green one). Although the definition of a set of gathering areas maximally robust with respect to scenarios where pedestrians must be dynamically reallocated due to the gathering areas' inaccessibility is a different mathematical problem, the solutions we obtain contain basic information useful to evaluate the dimensions of the areas on the basis of the number of pedestrians eventually expected from other evacuation units and therefore to implement real-time reallocation strategies.

In view of the above, the proposed methodology also relies on sustainability, flexibility, versatility, and application quickness criteria, being useful to support testing, assessment, and/or comparison of different evacuation strategies under different scenarios and conditions. Decision-makers and local administrators could hence exploit the methodology to evaluate *how many* and *where* gathering areas should be provided, *which* evacuation routes should be traveled to reach them, and *how* the urban area should be districted into evacuation units (within which the evacuation can be entirely developed). The capabilities demonstration in the selected case study could point out general critical issues in urban areas characterized by similar conditions and thus could support the design and evaluation of standard solutions and mitigation strategies fundamental to anticipate/improve evacuation, also before the event peak-time. In this sense, the general typological-based assessment can be then tailored to specific real-world contexts [186]. Furthermore, easy comparisons between different solutions and scenarios are possible thanks to additional customization of the Risk Index on the basis of physical parameters that depend on the features of the event, the urban area, and the pedestrians. To this end, one of the main advantages introduced is the possibility to test solutions and variations thanks to simple updates of the main features of the case study, including its users (e.g., considering pedestrians with reduced motion capabilities like elderlies, disabled, and children).

9.2.3 Limitations and future aims

The tested scenario has been investigated thanks to its typological value as a representative experimentally-based archetype of riverine urban areas in historical contexts [186], [236]. Although this scenario can hence represent a reference scenario for flood evacuation simulation and strategies comparisons, it is worth noticing that some results could be influenced by the low complexity of the case study, e.g. the street network does not consider factors such as differences in width, slope, and direction of the streets, the paving materials, or the presence of sewer systems and green areas. Such assumptions might explain the almost absolute concordance between the three tested approaches for the route choice. Indeed, even considering a slightly more complex portion of the graph, like that representing the square, different evacuation routes are computed to reach the same shelter (i.e., *A*).

In future research steps, both the idealized case study and the risk index can be improved to consider further aspects that may respectively influence the overall urban layout and the risks for the pedestrians, such as the presence of budget limitations or urban constraints (e.g., cultural heritages

where it would be impossible implementing shelters). In particular, the proposed Risk Index could be refined also by considering such issues with the help of multicriteria decision-making techniques like the Analytic Hierarchy Process, which allows assigning priorities and evaluating the impact of each parameter by assigning them different weights.

Furthermore, an interesting line of investigation, also in view of possible future applications for computational modeling on evacuation simulation software, is how to improve the proposed methodology in order to address the single pedestrian behaviors in terms of preferences and interactions with each other and with the surrounding environment. For this purpose, traffic models relying on constrained optimal systems or tolerance-based dynamic users could be evaluated for accounting for the evacuee's selfishness while keeping the computational viability of the approach (compare, e.g., with [128]). Such kind of analysis could be also very helpful for a future implementation of the graph-solving algorithm into custom or generic software [323] with the aim of providing a complete simulator for flood evacuation, which would represent an increasing innovation in the field.

10. Conclusions and future works

Historic City Centers (HCCs) and their inhabitants are constantly threatened by multiple types of risks that can unfold every day without warning. For this reason, it is essential to resort to adequate mitigation and preparation strategies calibrated according to the specific needs of historic centers and the behaviors of the people who populate them. Current strategies are influenced by a schematic and deterministic approach. Often, in fact, risks are assessed in a “reductionist” manner, i.e., by separately evaluating the individual factors (vulnerability, exposure, and hazard) without considering their interaction within a broader vision. In addition to this, such analyses often require large computational, economic, and proficiency efforts which significantly slow down their development and therefore their impact. Similar problems are noticed at both “microscopic” (squares, streets) and “mesoscopic” (Public Open Spaces, as combinations of squares and streets) scales. Hence, this study aims to promote innovative methodologies and tools for holistic risk assessment in HCCs according to expeditious approaches that can be easily used also by low-trained and non-expert technicians of local authorities and policymakers. The main conclusions of this research are offered below by listing key findings and related future works, respecting the same order as the previous sections with respect to the various phases of the thesis work.

The first area of investigation of this thesis work concerned the evaluation of the *physical vulnerability* of existing masonry buildings according to a *microscopic approach* to improving their performance and safety. In this sense, the execution of numerous and detailed in-situ tests on historic buildings would be essential for their mechanical characterization, but there are often issues of executive, economic, and conservation nature that hinder or prevent their execution. Furthermore, the great variety of materials and techniques employed along the Italian territory can represent an additional source of uncertainty. Therefore, starting from the suggestions of the Italian National Standards itself (INS) about the opportunity for the Regions to independently identify reference parameters for local specificities, the first part of the research concerned the realization of a database collecting experimental campaigns performed by licensed laboratories in the Marche region. Then, specific results provide a detailed overview of the mechanical characterization of historical masonry in the regional context. The reference database includes a sample of over 400 experimental tests on more than 10 different masonry typologies, encompassing those already regulated by the Italian National Standard (INS) and newly introduced ones. The majority of these tests involve double flat-jack investigations, allowing for a detailed framework on compressive strength parameters and elastic modulus, as well as facilitating comparisons with the INS, and with measurements collected from literature works. Such comparisons are facilitated by statistical analyses (normality test and quartile-based analysis), which identify, for each type, the ranges of variation for the aforementioned parameters. Tests for estimating shear strength and shear modulus have been collected too, although the sample size still needs to be increased compared to the previous one. Following the INS suggestions, for the first time, reference values are provided for local specificities and not, including typologies never regulated by the INS, such as raw earth masonries. In conclusion, this research succeeds in providing effective technical support to local (and non-local) professionals coping with the *mitigation phase* of disaster risk management, by means of a tool useful for consulting, evaluating, and comparing the construction and mechanical characteristics of both historically significant masonry (as also encouraged by regulations) and more common and recurring types throughout the national context. In particular, such results are useful both for the mechanical characterization of masonry typologies already regulated by the INS (hence for comparison purposes,

or as an incentive to update old values), as well as for masonry typologies still unregulated, thus providing assistance to local and non-local professionals. However, future efforts must certainly be addressed at updating the current database by including new tests and developing an automatic and collaborative tool allowing users to directly insert input and access common files according to a "circular logic" in which the data collected are provided by the same subjects to whom this tool is mainly aimed (i.e., professionals, laboratories, and institutions). To this end, possible solutions could be the use of web-based platforms offering standard surveys and modules to input basic data (similar to the one adopted in this research), entry-level big data analytics tools that simplify the analysis of large datasets providing rapid risk insights, simple machine learning applications that automate repetitive tasks providing quick insights from available data.

Exposure and vulnerability assessment in the **mitigation phase** can also be carried out according to **mesoscale approaches** that delve into specific features of building complexes, Public Open Spaces (i.e., streets, squares), and their combinations. This is of particular importance, especially in reference to **pre-emergency conditions and patterns**, and considering POSs placed in HCCs prone to risk and multi-risk. From this perspective, the evaluation of users' temporalities (i.e., how specific features vary over space and time) is fundamental to evaluating how and when things are taking place and estimating the possible consequences related to risks. However, temporalities are still limitedly considered for risk analyses and should be exploited especially at the mesoscale, as it is detailed enough to discuss interactions between the built environment and the users' daily activities that could have implications for HCCs resilience. Therefore, an innovative methodology is provided to quickly and easily collect data on relevant vulnerability and exposure features identified in literature studies (i.e., users' familiarity with spaces and emergency procedures, motion abilities in relation to age, and presence of sensitive buildings). Common simple tools and data sources are exploited to investigate Italian HCC-related POSs. In order to facilitate replicability, adaptability, and comparability of the analyses, new synthetic criteria are introduced (Key Performance Indicators) to be applied to single case studies (to depict specific POS conditions), as well as to derive typological, statically recurring conditions (such as in this study). Results ensure daily or hourly overviews, as well as identifying peak (critical) usage conditions. Furthermore, they could be exploited for future simulation-based analyses to identify priority scenarios to be deeply investigated by safety designers. In this sense, the next steps in the research can combine the retrieved typological scenarios with typological hazards and vulnerabilities, depending on the specific risks in the city or the combination between them, from a multi-risk standpoint. BIM software with pre-designed templates for the rapid creation of 3D models, allowing for quick risk analysis and simulation could be exploited. Additional local databases and in-situ surveys can also integrate data from open-access and quick-to-apply repositories used in this work, thus increasing the reliability of collected data and their analysis. Finally, results firstly encourage future efforts to broaden the current analyses to a greater number of POSs prone to multi-risk, so as to improve the statistical significance of typological scenarios definition. Moreover, future research could easily apply this methodology to any urban POSs, (e.g. non historic ones; characterized by other main land uses) and Countries.

After focusing on pre-emergency conditions dealing with the mitigation phase of disaster risk management, the thesis delves into **specific emergency conditions** for the proposal of tools and methodologies applicable in the **preparation phase**. In particular, the selected case study concerns **flood risk**. Flood risk in riverine HCCs depends on the correlation between its **physical vulnerability** and the severity and frequency of **hazard**, as well as on the immediate response of hosted communities, in view of their **exposure** and **pedestrian evacuation behaviors**. To this end,

comprehending decision-making processes and reasons behind human behaviors in flood emergencies is fundamental for the development of risk assessment tools and risk-reduction strategies. Floodwater-human evacuation interactions are deeply influenced by the event features and the people's perception of surrounding conditions and related risks. A large number of previous studies already define flood-related behaviors and evacuation physical quantities, but the relationship between frequent behaviors and floodwater conditions is not yet really clarified from this point of view. Therefore, a reference behavioral database has been organized in relation to the evacuation phases and the main literature classifications, including also new-noticed behaviors to enlarge the reference database (more than 1000 people involved in flood evacuation were considered, representing the largest set in the field of video analysis for human behaviors). The behavioral patterns have been defined according to statistical frequencies innovatively evaluated through the number of people performing and that could actually perform the behaviors. Collected qualitative data have been organized according to the floodwaters' conditions (distinguished by the water depth and flow) in which the behaviors were observed. Such a significant overview of flood evacuation behaviors can find application in different fields of risk management and assessment, spacing from supporting safety planners in designing evacuation plans and installations for resilient built environments, to the employment for the development and validation of dedicated simulation tools.

In fact, the following step of the thesis work was the implementation of an outdoor flood evacuation model in a generic evacuation simulation software (MassMotion) to ease and speed up the risk assessment analyses by using a quick no-code modification approach. Different setups are tested to describe the pedestrians-floodwaters interactions during a flood evacuation given previous findings in the thesis as well as in the literature. As a benchmark, a previously developed and tested custom flood evacuation simulator based on the same *microscopic modeling approach* is selected, that is FlooPEDs (Flooding Pedestrians' Evacuation Dynamics Simulator). Stationary flood conditions (i.e., still water) and compact groups of 10 pedestrians are considered in the comparison, which is consistent with basic conditions in outdoor evacuation after the peak of the event, but sufficiently detailed to represent a valid preliminary test. Considering the best setup, the comparison of the results shows slight differences between the two software. Indeed, from a macroscopic point of view, the generic simulator manages to represent the main effects of the flood evacuation as proved by outcomes in terms of evacuation timing. On the other hand, considering microscopic aspects such as the pedestrian trajectories along the pathway, the best setup shows better agreement with the real-world observations. However, to overcome the use of (pseudo-)stationary conditions in floodwaters, the next research steps should also move towards directly connecting input data from external hydrodynamic simulators to compute the dynamic variations in floodwater levels. Anyway, the proposed tool could be used by low-trained technicians and Local Authorities to preliminary assess evacuation risks in HCCs and propose risk-mitigation strategies (i.e. architectural layout modifications, micro-scale re-thinking of built spaces, direct support to pedestrians by also using wayfinding and alert systems).

Based on the behavioral-based simulation methodology thus developed, the following research steps investigated how differences in HCCs layout and pedestrian evacuation behaviors in risk assessment could lead to differences in flood risk evaluations. Parametric configurations of typological POSs are then defined on the basis of recurring features of riverine Italian HCCs affected by floods in recent years. The previously developed evacuation simulator is then coupled with an existing tool to evaluate the hydrodynamic conditions established in the typological POS scenarios by a flooding event with a return period of 100 years that actually occurred in Italy. Risk Indexes and Risk Maps

are developed to evaluate the risk: 1) at the mesoscale (which is considering the whole POSs) and at the microscale (which is considering single streets and squares); 2) without considering pedestrians evacuation behaviors, and considering two different evacuation emergency strategies (i.e., leaving the affected area of sheltering in pre-arranged gathering areas). According to the proposed Risk Indexes and considering the typological POS scenarios tested in this work, mesoscale trends are similar. On the contrary, differences are more relevant at the microscale level, where some streets and squares could reach deadly conditions for pedestrians. Considering the risk assessment without pedestrian evacuation behaviors, the risk seems to be overestimated in streets and squares where pedestrians can safely move and/or gather indeed, while the risk seems to be underestimated where pedestrians can be trapped because they do not have enough time to reach a gathering area. At the same time, the magnitude of overestimations/underestimations depends on the specific conditions of the POS layout, thus remarking the impact of such flood-affecting factors in risk assessment. Furthermore, the proposed risk maps (organized on the basis of the aforementioned risk indexes) represent easy-to-apply tools for the support of safety designers, local authorities, and Civil Protection Bodies. These stakeholders can identify priority areas for risk-mitigation strategies, arrange suitable and sustainable evacuation management plans, and put in place support systems for pedestrians (e.g. gathering areas, also hosted by raised platforms; handrails to have support while moving in critical floodwaters). According to this application perspective, the proposed assessment and comparison methodology could be applied to compare: (1) different POS layouts, by varying the *physical vulnerability* modeling; (2) different flood events, by varying the *hazard* modeling; and (3) different emergency plans, by varying the *exposure* modeling.

However, although such efforts succeed in considering and comparing differences in modeling, there are still gaps to overlay with respect to optimization problems of evacuation strategies (i.e., optimal number and position of gathering areas, evacuation routes to travel). In fact, when floodwater spreads within urban areas pedestrians can experience difficulty in choosing or performing the right evacuation strategy. Therefore, operational decisions and procedures should be evaluated in the preparation phase. The last part of the thesis proposes a novel methodology to assess the effectiveness of evacuation strategies differentiated by the number and position of gathering areas, the evacuation routes to reach them, and the type of behaviors adopted by pedestrians to evacuate the flooded areas. The testing scenario is the riskiest one between the typological POSs previously defined. Different evacuation strategies are investigated by varying the behavioral criterion adopted by pedestrians for the choice of the evacuation route (three approaches are tested, namely the shortest, the quickest, and the cheapest route to safety), and the number of available potential gathering-areas in the case study. Differently from the previous cases, a *macroscopic modeling approach* is adopted for the simulations, which consists of an Integer Linear Program (ILP) solving an optimization flow problem on a graph representing the POS street network. The number of casualties (pedestrians who cannot complete the evacuation) is minimized together with the length, time, and effort to travel the evacuation routes. In this process, the group behaviors and dynamics have been preferred to those of the single pedestrian (i.e., ILP minimizes the evacuation routes with respect to the total number of initial pedestrians). Finally, the optimal solutions obtained are assessed and compared through a Risk index, which adopts a holistic, behavioral-based, and systematic approach to dealing with disaster management, and combines KPIs on specific metrics descriptive of the urban layout (*physical vulnerability*), the event intensity (*hazard*), and the pedestrian behaviors (*exposure*). Results allow (1) identifying the optimal number and position of the gathering areas together with the evacuation routes to reach them, and (2) districting the affected area into evacuation units to allocate pedestrians

depending on their position. This type of analysis is propaedeutic at the implementation of retrofitting strategies and solutions to ensure the safety of the HCC and its inhabitants (e.g., how and where rescue squads should be implied, how to dimension gathering areas and evacuation routes, how and where to provide urban furniture, etc.) but can be useful also for the assessment of logistic issues (e.g., how to imply the budget granted by administrations, how to allocate pedestrians to avoid overcrowding and bottlenecks issues, etc.). Furthermore, they could pave the way for more refined tools aimed at increasing communities' engagement, such as mobile apps for emergencies fostering quick and effective communication on real-time updates and Augmented Reality (AR) applications offering realistic simulations to visualize potential risks in real-world environments.

Comparisons between the macroscopic and the microscopic simulation-based evacuation models are finally provided. Once again, the risk evaluation and the results comparison are performed through a Risk Index which adopts a holistic perspective since it comprehends KPIs about pedestrian behaviors, flood hazard, and physical vulnerability of the usual testing scenario. Results show an overall good agreement between the two models. In particular, the microscopic one provides slightly more conservative outcomes in terms of the number of casualties, thus it can serve as a lower bound for the estimation of the risk, while the general reliability of the macroscopic approach counterbalances the lower complexity and time-consuming application. To better exploit the potential of this promising methodology, future applications should explore real-world case studies as well as more complex idealized scenarios characterized by non-geometrical features and logistic constraints that can affect the risk (e.g., the presence of sewer systems, the differences in the paving, the budget granted by the administrations, the rescuers' intervention, the presence of cultural heritages unsuitable to be used as shelters or that can obstruct safety operations). The promising results obtained encourage future efforts addressed also at including specific pedestrian features and interactions within the macroscopic solving algorithm, for instance by including factors that consider the possibility that some pedestrians could autonomously decide to adopt different evacuation strategies from those indicated (e.g., on the basis of their knowledge of the HCC, or to personal evaluation of the risk, or to motion capabilities related to age and disabilities).

Finally, starting from tips offered by this part of the thesis work, the very next research steps could surely regard the implementation of the static routing algorithm used to solve the graph directly in the microscopic simulator. In this way, with a unique tool, it would be possible to tackle optimization problems and consider the pedestrians' interaction with the surrounding environment at a microscopic scale. Such a tool, beyond representing an innovation in the field (no pedestrian simulation software for flood evacuation is currently in commerce), would be also easy to use for technicians of local authorities, which could speed up preliminary assessments of the evacuation risks in HCCs to propose tailored risk-mitigation strategies.

11. Appendices

11.1 Physical vulnerability at the microscale

11.1.1. Italian National Standard indication: Tables C8.5.I and C8.5.II

MASONRY TYPOLOGIES	f [MPa]	E [MPa]	τ_0 [MPa]	f_{v0} [MPa]	G [MPa]
Disorganized rubble stone	1.0	690	0.018	-	230
	2.0	1050	0.032	-	350
Barely cut stone	2.0	1020	0.035	-	340
		1440	0.051	-	480
Roughly cut stone masonry with good texture	2.6	1500	0.056	-	500
	3.8	1980	0.074	-	660
Irregular soft stone masonry (tuff, limestone, etc.)	1.4	900	0.028	-	300
	2.2	1260	0.042	-	420
Regular soft stone masonry (tuff, limestone, etc.)	2.0	1200	0.04	0.10	400
	3.2	1620	0.08	0.19	500
Stone blocks squared	5.8	2400	0.09	0.18	800
	8.2	3300	0.12	0.28	1100
Solid clay bricks and lime mortar	2.6	1200	0.05	0.13	400
	4.3	1800	0.13	0.27	600
Clay hollow bricks with cement-based mortar (holes \leq 40%)	5.0	3500	0.08	0.20	875
	8.0	5600	0.17	0.36	1400

Table 45: Masonry typologies included in the INS and reference ranges of mechanical parameters considering unreinforced panels (Tab. C8.5.I), being: f = compressive strength; E = elastic modulus, τ_0 = shear strength (from diagonal compression, to be used for irregular masonry), f_{v0} = shear strength (frictional strength at unit-mortar interface without compression, to be used for regular and irregular masonry), G = shear modulus [171], [172].

MASONRY TYPOLOGIES	Conditions			Strengthening Interventions			
	Good Mortar	Stringcourses or edging	Transversal connection	injections	jacketing	Reinforced joints sealing	Total maximum coefficient
Disorganized rubble stone	1.5	1.3	1.5	2	2.5	1.6	3.5
Barely cut stone	1.4	1.2	1.5	1.7	2.0	1.5	3.0
Roughly cut stone masonry with good texture	1.3	1.1	1.3	1.5	1.5	1.4	2.4
Irregular soft stone masonry (tuff, limestone, etc.)	1.5	1.2	1.3	1.4	1.7	1.1	2.0
Regular soft stone masonry (tuff, limestone, etc.)	1.6	-	1.2	1.2	1.5	1.2	1.8
Stone blocks squared	1.2	-	1.2	1.2	1.2	-	1.4
Solid clay bricks and lime mortar	$f_m^{0.35}$ (*)	-	1.3	1.2	1.5	1.2	1.8
Clay hollow bricks with cement-based mortar (holes \leq 40%)	1.2	-	-	-	1.3	-	1.3

Table 46: Improvement coefficients provided by the INS (Tab. C8.5.II) to be applied to the standard values of the mechanical parameters (Tab C8.5.I) in the event of better conditions or strengthening interventions [171], [172].

11.1.2. Masonry walls texture, façade, and sections

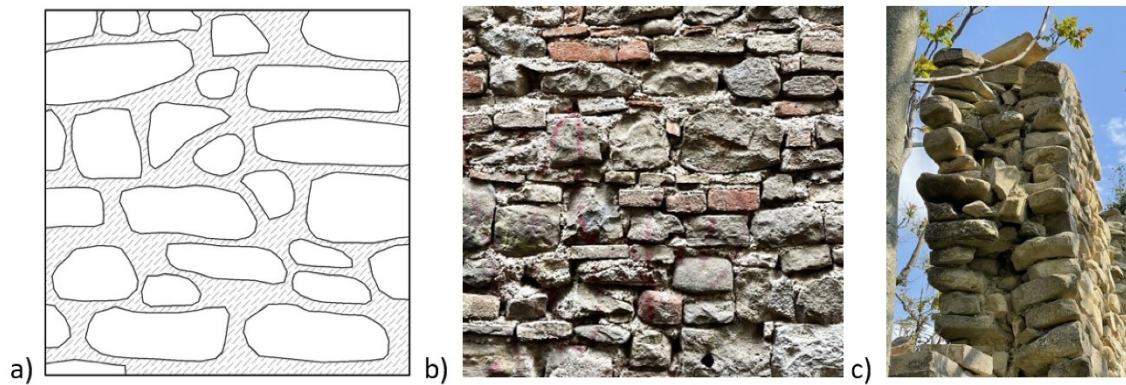


Figure 60: Disorganized rubble stone masonry (M1) – a) Graphic reconstruction of the wall texture type (1m x 1m); b) Wall façade example, photo taken in Arquata del Tronto (AP); c) Wall section example, photo taken in Treia (MC).

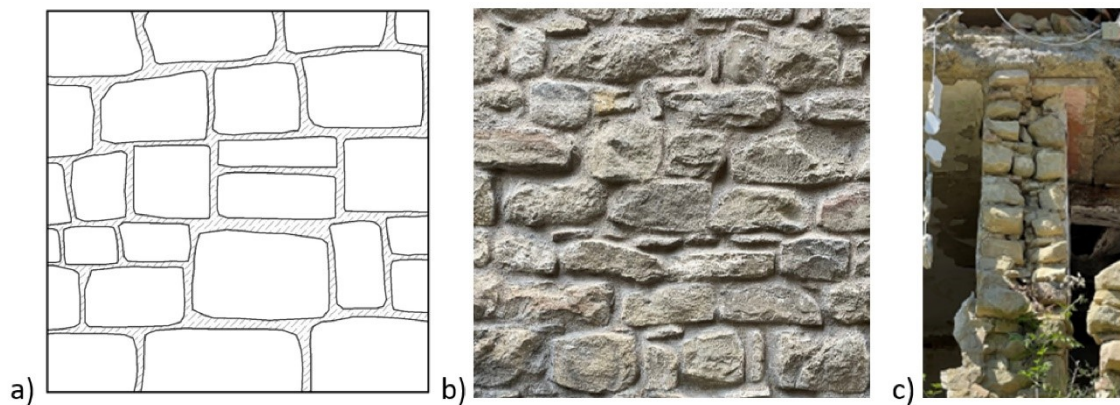


Figure 61: Barely cut stone masonry (M2) – a) Graphic reconstruction of the wall texture type (1mx1m); b) Wall façade example, photo taken in Castelsantangelo sul Nera (MC); c) Wall section example, photo taken in San Ginesio (MC).



Figure 62: Roughly cut stone with good texture (M3) – a) Graphic reconstruction of the wall texture type (1mx1m); b) Wall façade example, photo taken in Castelsantangelo sul Nera (MC); c) Wall façade example, photo taken in Cingoli (MC).

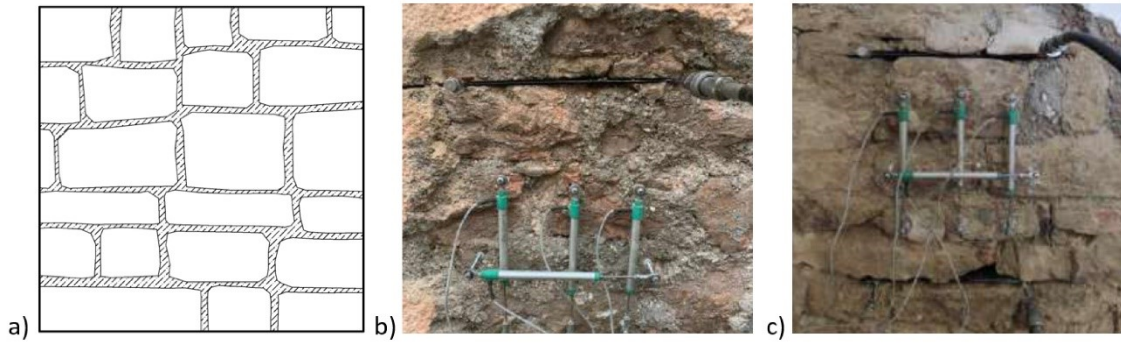


Figure 63: Irregular soft stone masonry (M4) – a) Graphic reconstruction of the wall texture type (1m x 1m); b) Double flat-jack test execution, photo taken in Fiastra (MC) [credits: LA.TE.MA srl]; c) Double flat-jack test execution, photo taken in Monte San Martino (MC) [credits: LA.TE.MA srl].

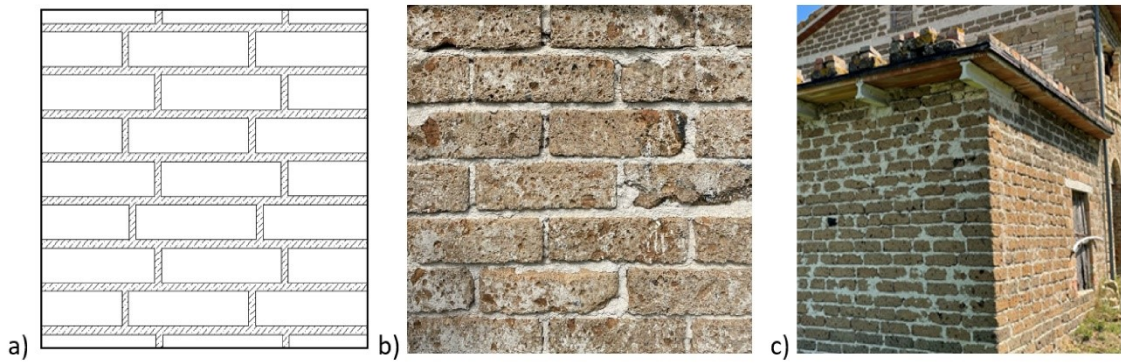


Figure 64: Regular soft stone masonry (M5) – a) Graphic reconstruction of the wall texture type (1m x 1m); b) Wall façade example, photo taken in Treia (MC); c) Typical tuff masonry building example, photo taken in San Ginesio (MC).



Figure 65: Stone blocks squared (M6) – a) Graphic reconstruction of the wall texture type (1m x 1m); b) Wall façade example, photo taken in Cingoli (MC); c) Wall façade example, photo taken in Muccia (MC).

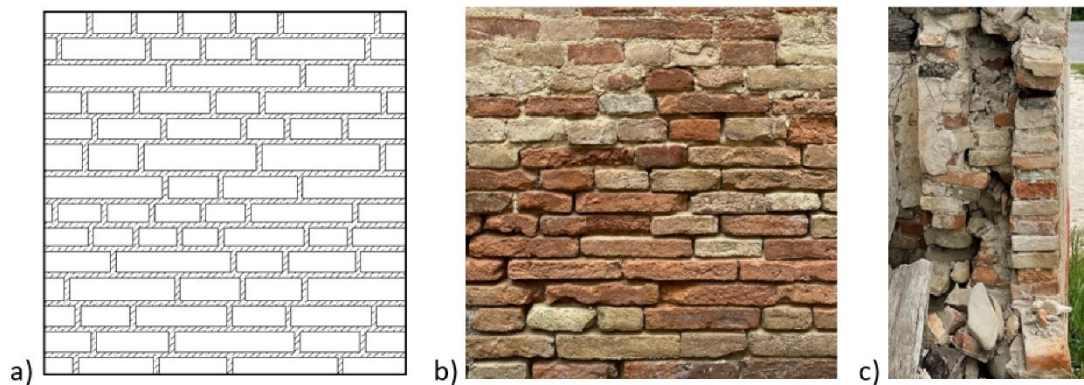


Figure 66: Solid clay brick and lime mortar (M7) – a) Graphic reconstruction of the wall texture type (1mx1m); b) Wall façade example, photo taken in Filottrano (AN); c) Wall section example, photo taken in Castelfidardo (AN).

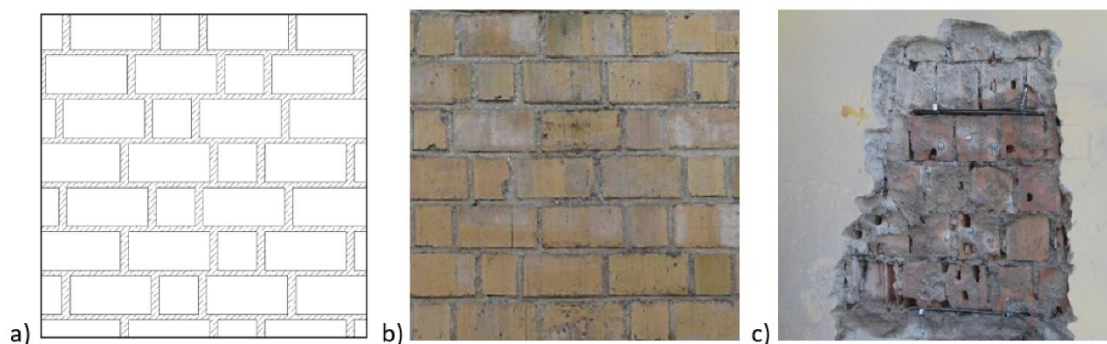


Figure 67: Clay hollow bricks with cement-based mortar (M8) – a) Graphic reconstruction of the wall texture type (1mx1m); b) Wall façade example of masonry panel with “good mortar”, photo taken in Cingoli (MC) [credits: CAP Studio]; c) Double flat-jack test execution on a masonry panel in “standard conditions”, photo taken in Frontino (PU) [credits: CAP Studio].

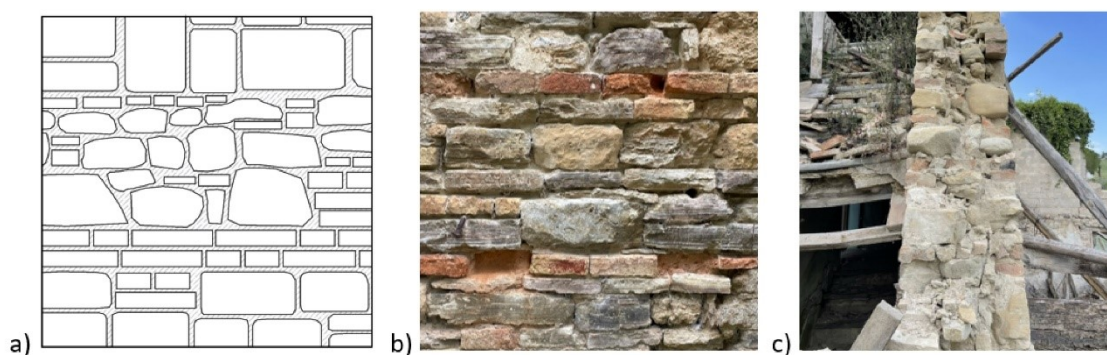


Figure 68: Stone-and-brick mixed (MX1) – a) Graphic reconstruction of the wall texture type (1mx1m); b) Wall façade example, photo taken in Camporotondo di Fiastrone (MC); c) Wall section example, photo taken in and Treia (MC).

11.1.3. Earthen masonry typologies recurrent in the Marche Region

Earthen masonries were widely widespread in some areas of the Italian territory, even though never actually permitted by the national standards. In particular, they were particularly common in areas characterized by clayey soils which provided the raw material to build constructions of poor social classes (such as rural buildings with a maximum of two floors) thanks to their cost-effectiveness combined with the good performance offered by a thermal and acoustic point of view. As regards the construction methods, there are three main 3 categories present in the Marche region [285], [324]:

- the Cob (or bauge, or “*massone*” in Italian), was made by piling up and beating large cylindrical blocks of earth mixed with straw and water, to form very thick walls with a monolithic section streamlined at the top. Figure 69 illustrates the procedure for the construction of buildings with this technique [325]: 1) manual preparation of the *massoni*; 2) *massoni* storage; 3) installation and trimming of the wall by the master;



Figure 69: Three main phases for the construction of Cob masonry buildings [61].

- the Rammed earth masonry buildings were made by compressing the slightly moist raw earth into wooden formwork to avoid cracking during the drying phase. Figure 70 illustrates the procedure which consists of [325]: 1) digging and screening of the earth; 2) filling of the formwork; 3) compaction using the "ram", dismantling and moving the formwork.



Figure 70: Three main phases for the construction of Rammed earth masonry buildings [61].

- The Adobe is an out-and-out brick made of earth, sand, and gravel dried in the sun, with the use of clay as a binder. Figure 71 illustrates the procedure for the construction of buildings with this technique [325]: 1) the earth with water and straw is mixed with the shovel and feet; 2) the composition of the mixture which is then inserted into a wooden brick mold; 3) the raw earth bricks (adobe) are extracted from the mold and placed to dry in a vertical position, before finishing with a billhook and subsequent installation.



Figure 71: Three main phases for the construction of Adobe masonry buildings [61].

Figure 72 shows the main aspect that characterizes each of these typologies, i.e. the typical arrangement of *massoni* of the Cob (in the image down on the left), the stratification and compaction operations for the creation of the Rammed earth walls, and the regular arrangement of the bricks as regards the Adobe (in the image up on the left). Figure 73 shows some case studies relating to their presence in the Region, and in particular in the village of Villa Ficana (MC): at the top left there is an example of the *massoni* used for the Cob, at the bottom left there is an example of an Adobe brick, while the two images on the right show examples of buildings made in Rammed earth.

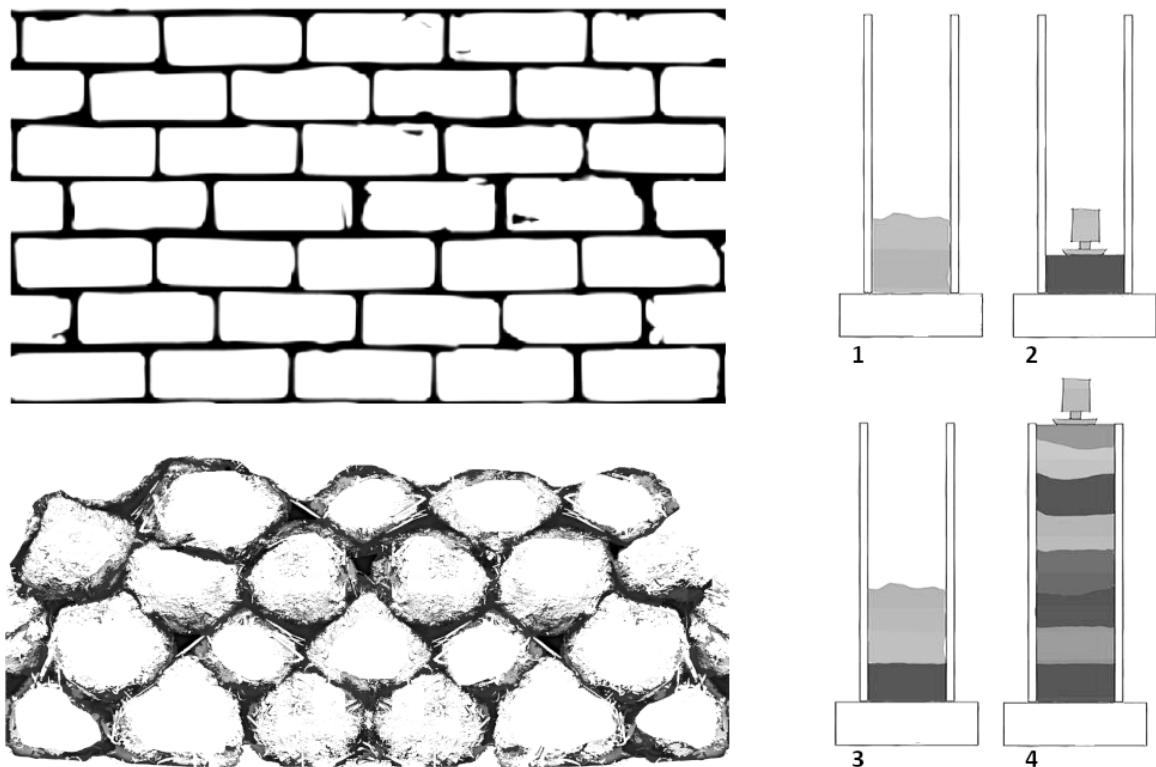


Figure 72: Graphic representation of the arrangement of Adobe bricks (top left); Cob blocks (bottom left); Layering typical of the Rammed earth (odd phases: stratification; even phases: compaction).



Figure 73: Examples of the three earthen masonry typologies considered: the Cob at the top left, the Adobe at the bottom left, and the Ramed earth in the two buildings on the right. Photos taken at the Ecomuseum of Villa Ficana (MC).

Figure 74 shows the mapping of the municipalities in which there are earthen masonries updated at a 2005 survey by the Regional Directorate for Cultural and Landscape Heritage of the Marche [287].

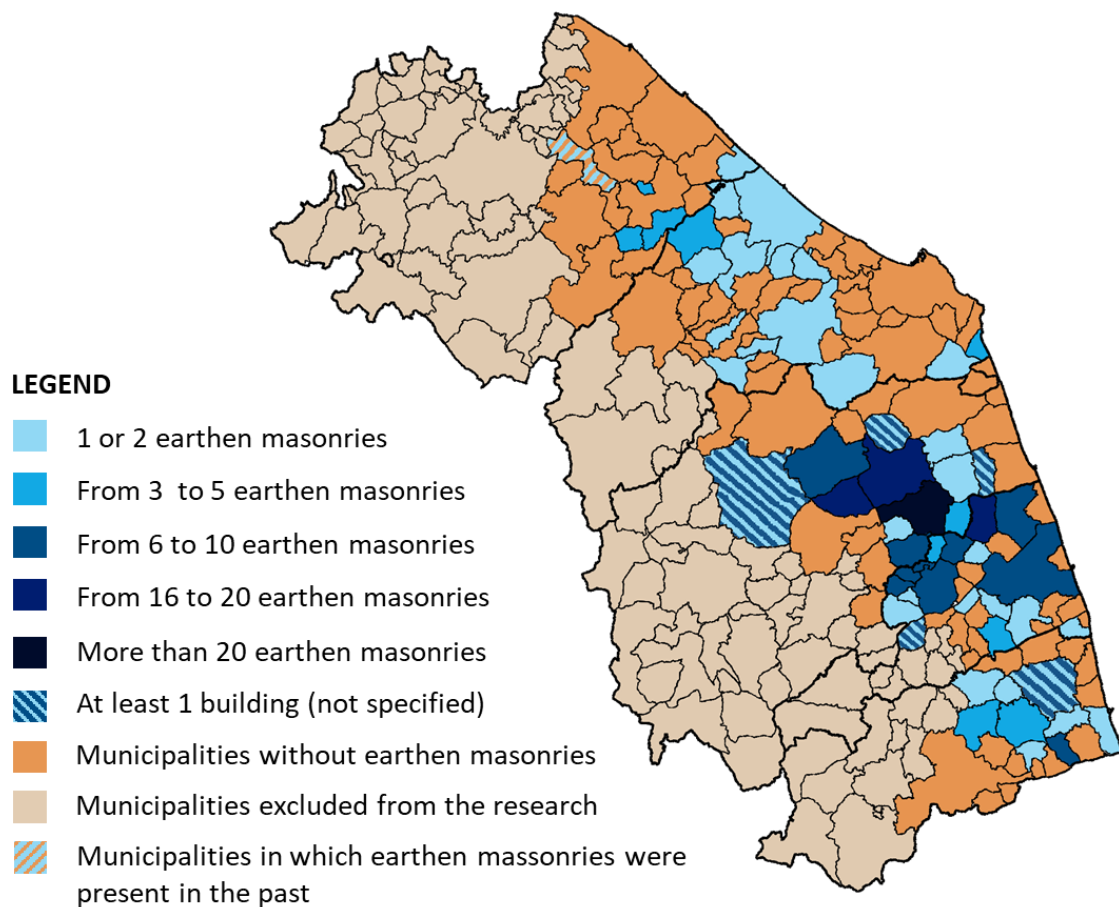


Figure 74: Map of the municipalities in the Marche Region in which the presence of earthen masonry buildings is demonstrated. Data from: "Architettura di terra nelle Marche, Catalogo a cura della Direzione Regionale per i Beni Culturali e Paesaggistici delle Marche" (2005) [287]; "Case di Terra e Paglia delle Marche" (2003) [326].

11.1.4. Literature database

Reference	MASONRY TYPOLOGY ID	Location of the tests	E [MPa]
Croce et al. (2018) [327]	M7	-	1926; 2235; 1137; 1195; 1494; 2709; 1569; 1187; 1607; 3284; 2517; 1874; 2287; 2087; 1863; 2938; 3532; 2386; 4891; 3672; 3107; 1951
	M1	-	1562; 1262; 1134; 2862; 2864; 915; 1131; 578; 2087; 1137; 1137; 2938; 2938; 2254; 1655; 1528; 2156; 2961; 1320; 2627; 2617; 1166; 2438; 1622; 1630; 3972; 2669
Alecci et al. 2019 [328]	M5	Arezzo (AR)	1143; 1143; 1088; 1028
Armanasco and Foppoli (2020) [183]	M7	Stuffione (MO)	1389; 2064; 2500; 1167; 556; 4000
Alecci et al. (2019) [328]	M7	Arezzo (AR)	2506; 2506; 2387; 2030

Table 47: list of double flat-jack tests (ASTM C1197 [175]) and relative measurements from literature studies, organized per masonry typology (M1 = rubble stone masonry, M5 = regular soft stone masonry, M7 = solid clay bricks masonry [171], [172]).

References	MASONRY TYPOLOGY ID	E/f ratio[-]
Marcari et al. (2017) [293]	M5	630
Prota et al. (2006) [329]	M5	300
Marcari et al. (2010) [294]	M5	600 (tuff, single leaf)
		715 (tuff, multi-leaf)
		330 (calcarenite, single leaf)
		1450 (calcarenite, multi-leaf)
Faella et al. (1991) [330]	M5	800
Augenti and Parisi (2009) [295]	M5	560
Calderoni et al. (2009) [331]	M4	280; 340
Grande and Romano A. (2012) [332]	M5	400

Table 48: E/f ratio values from literature studies, organized per masonry typology (M4 = irregular soft stone masonry, M5 = regular soft stone masonry [171], [172]).

Reference	Geographic area	f [MPa]	E [MPa]
Quagliarini et al. (2009) [285]	Italy (Ancona)	1.20; 0.77	40; 26
Miccoli, et al. (2014) [333]	Germany	3.28	803
Lan et al. (2020) [334]	China	0.74; 2.33	-
Mahdad, et al. (2021) [335]	Algeria	1.90; 2.00; 2.00	350; 360; 360
Röhlen et al. (2010) [336]	Germany	2.15	315
Vicente and Torrealva (2016) [337]	Peru	0.42; 0.6; 0.39; 0.58; 0.76;	104; 95; 94; 48; 49; 75;
		0.47; 0.48; 0.44	60; 106
Lan et al. (2023) [338]	China	0.71; 0.56; 0.53; 0.94; 0.79; 0.72; 1.80; 1.34; 1.15	63; 48; 43; 16; 116; 85; 91; 75; 68
Delgado and Guerrero (2006) [283]	Spain	1.20	-
Meli, via [339]	Mexico	1.32	245
San Bartolomè and Pehovaz, via [339]	Peru	0.86	-

Reference	Geographic area	f [MPa]	E [MPa]
Torrealva and Acero, via [339]	Peru	0.85	432
Yamin et al., via [339]	Colombia	1.10	98
Wu et al. [340]	China	0.94	34
Silveira et al. [341]	Portugal	0.33	757
Illampas et al. [342]	Cyprus	0.88; 1.73	15.5; 22

Table 49: compressive strength f and elastic modulus E evaluations from literature studies on Adobe masonry.

References	Geographic area	f [Mpa]	E [MPa]
Quagliarini et al. (2010) [343]	Italy (Ancona)	0,24; 0,37; 0,40; 0,26; 0,25; 0,26	40
Quagliarini and Maracchini (2018) [324]	Italy (Ancona)	1,05; 1,12; 1,17; 1,13; 1,35; 0,74.	16,9; 15,51; 15,08; 16,17; 14,68; 17,56; 16,56; 16,42; 17,75; 21,47; 30,21.
Miccoli et al. (2014) [333]	Germany	1,59	651
C. Ziegert (2003) [344]	Germany	0,45; 1,40	170; 335
Houben and Guillard (1994), via [345]	-	0.10	-
Saxton (1995) [346], via [345]	-	0.35; 1.75	-
Coventry (2004), via [345]	-	0.48; 1.24	170; 335
Keefe (2005), via [345]	-	0.60; 1.40	-
Akinkurole et al. (2006) [347], via [345]	Nigeria	0.60; 2.20	-
Weismann et al. (2006), via [345]	-	0.77	-
Pullen and Scholz (2011) [348], via [345]	Oregon	0.45; 0.89	11; 69
Minke (2012), via [345]	-	0.50	-
Rizza and Bottger (2015), via [345]	-	0.60	71.5
Brunello et al. (2018), via [345]	-	0.71; 0.87	-
Vinceslas et al. 2020) [349], via [345]	-	0.50; 0.76	110; 350
Wright (2019) via [345]	-	1.22; 1.53; 0.77; 2.45	-
Jimenez Rios and O'Dwyer (2020) [350]	Ireland, UK, France	0.70	143

Table 50: compressive strength f and elastic modulus E evaluations from literature studies on Cob masonry.

References	Geographic area	f [Mpa]	E [MPa]
Miccoli et al. (2014) [333]	Germany	2.40; 3.00; 1.00; 1.50; 4.00; 0.75; 1.46; 1.80; 2.00; 0.60; 0.70; 3.88; 2.46; 0.62; 0.97; 3.73	650; 90; 105; 750; 60; 205; 160; 60; 70
Jaquin et al. (2007) [351]	India	0.60-0.70	60
Romanazzi et al. (2019) [352]	Portugal	1.50	471
Q-B. Bui et al. (2014) [353]	France	1.00	90-105
T.-T. Bui et al. (2014) [354]	France	1.90	500
Hall et al. (2014) [355]	UK	0.75-1.46	-
Sabbà et al. (2021) [356]	Italy	1.30; 3.73; 1.50; 0.60;	300; 471; 67
Araki et al. (2010), via [339]	Japan	2.80; 4.20	-
Bui (2008), via [339]	France	1.95; 1.75; 1.95; 1.90; 1.22	-
Champire et al. (2016) [357]	France	4.8; 4.1; 3.2	-
Ciancio et al. (2013) [358]	Australia	0.30; 0.56; 0.34; 0.42; 0.54	-
Hall e Djerbib (2004) [355]	-	0.90; 1.00; 0.77; 1.10; 1.40; 1.37; 1.45; 1.15; 1.35; 1.10	-
Maniatidis et al (2008) [359], via [360]	-	0.81; 1.90; 2.46	65; 160
T.T. Bui et al. (2014), via [361]	France	1.00	100
Liu e Tong (2017) [362], via [360]	China	1.04	103
Tripura et Singh. (2015) [363], via [360]	-	1.10	1050
El Nabouch (2017) [360], via [364]	-	1.15; 2.00	365; 763
Silva et al. (2014) [365]	Portugal	1.26	1034
T.T. Bui et al. (2016) [366]	France	1.30	500
Arrigoni et al (2017) [367], via [360]	Australia	1.40	-
Pakand e Toufigh (2017) [368], via [360]	Iran	1.77	-
Kosarimovahhed e Toufigh (2020) [369], via [360]	Iran	1.85	34
Lilley e Robinson (1995) [370], via [360]	-	1.90	-
Toufigh e Kianfar (2019) [371]	Iran	2.23	143

Table 51: compressive strength f and elastic modulus E evaluations from literature studies on Rammed earth masonry.

11.2 Case studies characterization and typological HCCs definition

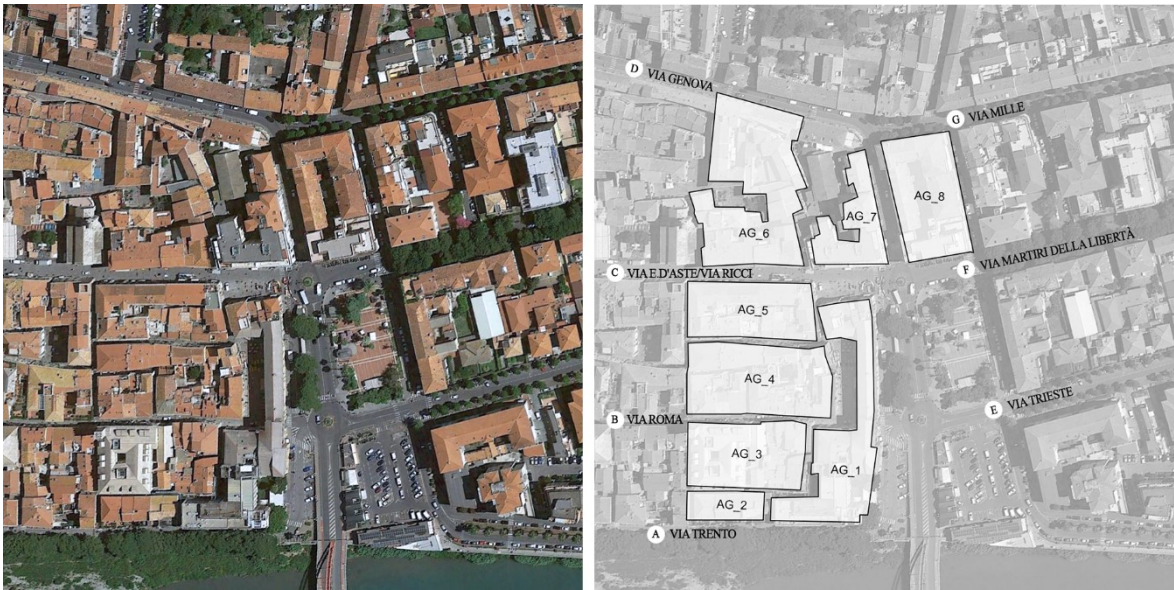


Figure 75: POS “Piazza del Popolo” area in Albenga – streets and building blocks included in the case study.

Streets parallel to the river	Average width [m]	Average slope [%]
Via Trento	11.6	+0.56
Via Roma	4.7	/
Via D’Aste/Via Ricci	9.5	/
Via Genova	10.7	-0.41
Via Trieste	20.1	+0.33
Via Martiri della Libertà	18.0	-0.07
Via Mille	12.0	0.65

Streets parallel to the river	Average width [m]	Average slope [%]
Via Milite Ignoto	8.8	+1.98
Strada Provinciale n.39	9.8	/
Via Gian Maria Oddo	3.3	-1.26

Table 52: Streets data (Albenga case study)



Figure 76: POS “Piazza Alberica” area in Carrara – streets and building blocks included in the case study.

Streets parallel to the river	Average width [m]	Average slope [%]
Via Carriona	6.7	+1.6
Via Ghibellina	3.5	+4.9
Via Beccheria	5.5	+3.1
Via A. Pisano	4.0	+3.8

Streets parallel to the river	Average width [m]	Average slope [%]
Via Ponte Baroncino	6.4	-2.0
Vicolo Olivo	5.4	+6.0
Via Ponte delle Lacrime	4.3	+8.0

Table 53: Streets data (Carrara case study)



Figure 77: POS “Piazza Garibaldi” area in Colorno – streets and building blocks included in the case study.

Streets parallel to the river	Average width [m]	Average slope [%]
Via Ferdinando Galli Bibbiena	3.9	/
Via Cairoli	4.0	/

Streets parallel to the river	Average width [m]	Average slope [%]
Via Cavour	18.2	+1.48
Via Edmondo de Amicis	6.9	-4.20
Via Giuseppe Mazzini	5.7	/

Table 54: Streets data (Colorno case study)



Figure 78: POS “Historical City Center” area in Montevarchi – streets and building blocks included in the case study.

Streets parallel to the river	Average width [m]	Average slope [%]
Via Madre M. T. Scrilli	4.7	+0.6
Vicolo Sacconi	2.5	+0.9
Vicolo Martini	2.8	+0.5
Vicolo Ramacci	2.3	+1.6

Streets parallel to the river	Average width [m]	Average slope [%]
Via del lungo/ Via poggio Bracciolini	6.7	-1.1
Via Roma	10.6	-1.1
Via Cennano	7.4	+0.7

Table 55: Streets data (Montevarchi case study)

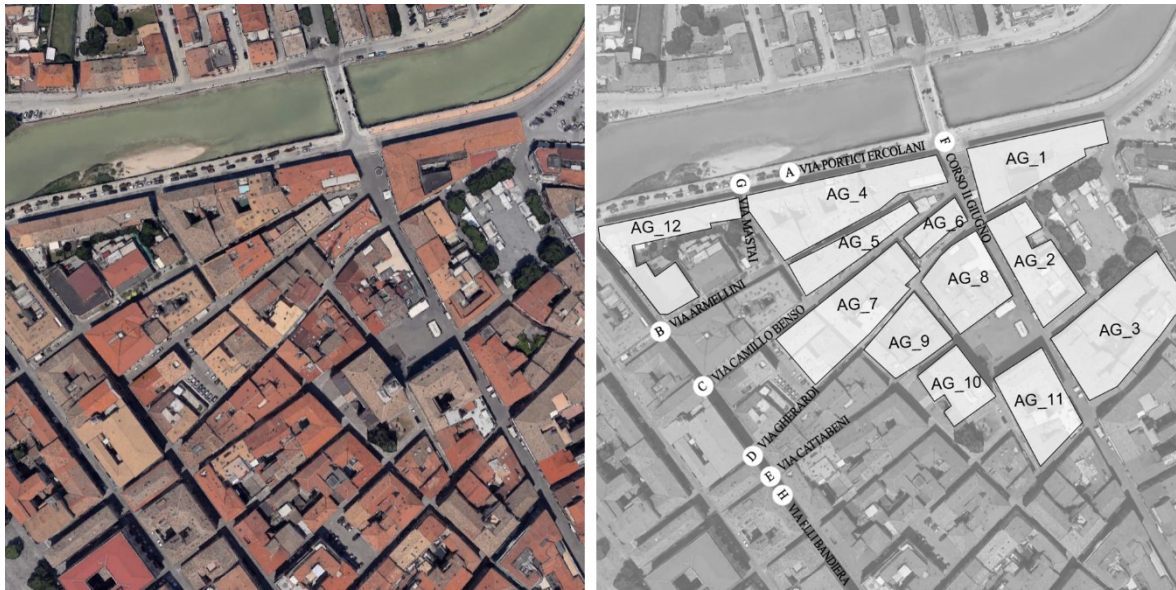


Figure 79: POS “Portici Ercolani” area in Senigallia – streets and building blocks included in the case study.

Streets parallel to the river	Average width [m]	Average slope [%]
Via Portici Ercolani	13.9	+0.6
Via Armellini	5.5	+0.6
Via Camillo Benso	6.6	+0.6
Via Gherardi	4.7	+0.7
Via Cattabeni	3.6	+0.7

Streets parallel to the river	Average width [m]	Average slope [%]
Corso II Giugno	9.3	+0.9
Via Mastai	4.0	-0.4
Via Fratelli Bandiera	5.45.0	+0.8

Table 56: Streets data (Senigallia case study)

b/l	Albenga	Carrara	Colorno	Montevarchi	Senigallia
AG_1	0.3	3.3	2.8	0.5	2.8
AG_2	2.7	12.6	1.1	0.4	0.4
AG_3	1.8	5.6	2.0	0.7	1.9
AG_4	2.1	0.5	0.5	0.5	4.1
AG_5	2.4	0.6	4.4	0.7	5.5
AG_6	0.5	0.4	1.3	0.7	2.7
AG_7	0.5	0.3	2.7	0.9	2.9
AG_8	0.5	0.3	-	0.7	0.9
AG_9	-	1.9	-	0.6	1.4
AG_10	-	2.4	-	0.6	0.8
AG_11	-	-	-	-	0.6
AG_12	-	-	-	-	5.7

Table 57: Building block data (all the case studies)

City	Paved	Area [m²]	Distance from the river [m]	Number of streets linked [-]	Direction of the square major axis
Albenga	Yes	9235	0-100	8	Perpendicular to the river
Carrara	Yes	3510	0-100	6	Perpendicular to the river
Colorno	Yes	4559	0-100	4	Perpendicular to the river
Montevarchi	Yes	1820	200-300	5	Parallel to the river
Senigallia	Yes	1264	100-200	6	Parallel to the river

Table 58: Squares data (all the case studies)

11.3 Exposure and vulnerability in pre-emergency conditions

11.3.1. Symbols and acronyms

Symbols and Acronyms	Unit of Measure	Meaning	Note
AIO_r	-	(Accessible) Indoor-outdoor area ratio	Ratio between the indoor area and the outdoor area
AP_a	[%]	Users' age percentage	Age percentage distribution of the a-th age range
AU	-	Adults	Users from 20 to 69 years
AUn	pp	Adults number	-
AUp	%	Adults percentage	Percentage value with respect to UOn
CA	m ²	Carriageable areas	Outdoor areas primarily occupied by vehicles, e.g. carriageway, parking lots
CAp	%	Carriageable areas percentage	Percentage value with respect to the overall outdoor areas
cp	[-]	Presence coefficient	Equal to 1 if users are present, to 0 if users are absent, and to the local percentage of unemployed users to consider their presence at home
CY	m ²	Private courtyards areas	Outdoor areas generally inaccessible to the public like fenced courtyards of dwellings
CYp	%	Private courtyard areas percentage	Percentage value with respect to the overall outdoor areas
D	m ²	Dehors areas	Outdoor areas intended for open-air terraces of restaurants, bars, open markets, and other outdoor areas hosting a specific intended use or connected to a specific building, placed at the ground levels, and including both temporary (removable) and permanent structures
Dp	%	Dehors areas percentage	Percentage value with respect to the overall outdoor areas
EU	-	Elderlies	Users from 70 years onwards
EUn	pp	Elderlies number	-
EUp	%	Elderlies percentage	Percentage value with respect to UOn
Fp	%	Female users percentage	Percentage value with respect to UOn
H	-	Holidays	Sundays and other national holidays
IQR	-	InterQuartile Range	Difference between 3 rd and 1 st quartiles
KPI	-	Key Performance Indicator	-
Mp	%	Male users percentage	Percentage value with respect to UOn
NR	-	Non-residents	Users that occupy the private/public services and institutions
NRn	pp	Non-residents number	-
NRp	%	Non-residents percentage	Percentage value with respect to Uon
NU	[pp]	Maximum number of users	Sum of all the users considered within the POS
OL_i	pp/m ²	Occupant load	Occupant load of the i-th type of area
OO	-	Only outdoor users	Users that populate the walkable areas WA
OO_n	pp	Only outdoor users number	-
OO_p	%	Only outdoor users percentage	Percentage value with respect to Uon
PC	-	Parents-assisted children	Users from 5 to 14 years
PC_n	pp	Parents-assisted children number	-

Symbols and Acronyms	Unit of Measure	Meaning	Note
PCp	%	Parents-assisted children percentage	Percentage value with respect to UOn
PO	-	Prevalent outdoor users	Users that populate the dehors D
POn	pp	Prevalent outdoor users number	-
POp	%	Prevalent outdoor users percentage	Percentage value with respect to Uon
POS	-	Public Open Space	e.g., squares, streets, districts
POSC	-	Public Open Space Characterization	-
R	-	Residents	Users that occupy the residential buildings
Rn	pp	Residents number	-
Rp	%	Residents percentage	Percentage value with respect to Uon
SB	Boolean	Presence or not of special buildings or uses	-
SBA	m ²	Special buildings/uses area	-
SBn	number of items	Number of special buildings or uses per square	-
SLOD	-	Slow Onset Disaster	e.g., heatwaves, pollution, pandemic
SU_i	[m ²]	Effective surface	Effective surface of the i-th type of area
SUOD	-	Sudden Onset Disaster	e.g., earthquake, flood, fire
TU	-	Toddlers	Users from 0 to 4 years
TUn	pp	Toddlers number	-
TUp	%	Toddlers percentage	Percentage value with respect to UOn
UA	m ²	Unwalkable areas	Outdoor areas occupied by monuments, fountains, and fenced areas including greeneries
UAp	%	Unwalkable areas percentage	Percentage value with respect to the overall outdoor areas
UDC	-	Users' Daily Characterization	-
UHC	-	Users' Hourly Characterization	-
UId	pp/m ²	Users' indoor density	Ratio between the indoor users (as the sum of R+NR) and the indoor area
Ulod	pp/m ²	Users' overall indoor density	Ratio between UOn and the indoor area
UIOr	-	Indoor-outdoor users ratio	Ratio between users in indoor areas (R+NR) and users in outdoor areas (OO+PO)
UOn	pp	Users' overall number	-
UOod	pp/m ²	Users' overall outdoor density	Ratio between UOn and the outdoor area (as the sum of WA, D, and CA)
W	-	Working days	Monday to Saturday
WA	m ²	Walkable areas	Outdoor areas accessible by pedestrians
WAp	%	Walkable areas percentage	Percentage value with respect to the overall outdoor areas
YA	-	Young autonomous	Users from 15 to 19 years
YAn	pp	Young autonomous number	-
YAp	%	Young autonomous percentage	Percentage value with respect to UOn

Table 59: Symbols and acronyms explanation

11.3.2. List of case studies

City	Square	Link
Arezzo	Piazza Grande	https://goo.gl/maps/ae5dbepkaczRkosaA
Bari	Piazza Umberto I	https://goo.gl/maps/EURAUfoE9jb4mqHc9
Brindisi	Piazza Duomo	https://goo.gl/maps/wEDLsQAmDv5jiH7e8
Caldarola	Piazza Vittorio Emanuele	https://goo.gl/maps/M4Whe432J8h597H47
Carpi	Piazza Martiri	https://goo.gl/maps/pCFkm2UKKPos7qGA7
Carrara	Piazza Alberica	https://goo.gl/maps/RqzQigFeujdj4kUM7
Catania	Piazza Università	https://goo.gl/maps/n4TbZCTT3NYTF1Vb8
Cesena	Piazza del Popolo	https://goo.gl/maps/brGubNHGV69t1jET8
Cosenza	Piazza Duomo	https://goo.gl/maps/UQ7xegwSJ6umAvpRA
Crotone	Piazza Duomo	https://goo.gl/maps/NQb2yhpJDhUA6bgL9
Cuneo	Piazza Tancredi Galimberti	https://goo.gl/maps/CQnpMNTRsx7oW4ZD9
Fermo	Piazza del Popolo	https://goo.gl/maps/wyAy1L7JuG8GdFzZ6
Forlì	Piazza Aurelio Saffi	https://goo.gl/maps/rQPnXoSQgUBv97Yj6
Gorizia	Piazza della Vittoria	https://goo.gl/maps/z1wMAYTxCzLdsTxHA
Iglesias	Piazza Municipio	https://goo.gl/maps/JXU43keJv9itf1Ux8
Imperia	Piazza San Giovanni	https://goo.gl/maps/mdCsKgrkgxny8vZq9
Lodi	Piazza della Vittoria	https://goo.gl/maps/meTUapY56YazZmHSA
Lucca	Piazza dell' Anfiteatro	https://goo.gl/maps/BUUPfzVG5htibLbw6
Manfredonia	Piazza del Popolo	https://goo.gl/maps/4efwMtLeAfSoDwsT9
Mantova	Piazza Sordello	https://goo.gl/maps/gydun7svSSQJHdHs7
Messina	Piazza Duomo	https://goo.gl/maps/ysXJGQ5hDjDxbddMA
Milano	Piazza Emilia	https://goo.gl/maps/qhNzWJCRpXwBTpUS9
Milano	Piazza Fratelli Bandiera	https://goo.gl/maps/HAchC4nSWzoXV2Ev8
Modena	Piazza Grande	https://goo.gl/maps/LTA1u77TixoRP7KA6
Monza	Piazza Trento e Trieste	https://goo.gl/maps/wEb5pNQEz4SRyVzC7
Narni	Piazza dei Priori	https://goo.gl/maps/Gg9aD43aTfyWg4gE9
Padova	Piazza delle Erbe	https://goo.gl/maps/E96JV1Nu3ipM9yzL6
Pesaro	Piazza del Popolo	https://goo.gl/maps/hrn9oyME1s4i3ELq5
Pescara	Piazza della Rinascita	https://goo.gl/maps/Zm84L7yWYEcx7yiC6
Pisa	Piazza dei Cavalieri	https://goo.gl/maps/hfD2LV5NBG8EMjv8A
Pisa	Piazza XX Settembre	https://goo.gl/maps/fvtCLcLrSg1TMieq6
Prato	Piazza del Comune	https://goo.gl/maps/CkQ7LX7fKJipfbV87
Ravenna	Piazza del Popolo	https://goo.gl/maps/HzUGvRdQhUFwM1JM9
Reggio Calabria	Piazza Duomo	https://goo.gl/maps/vioURxSbSTfKXdnr8
Reggio Emilia	Piazza Camillo Prampolini	https://goo.gl/maps/9iXH88oc55rnoR3Z7
Rimini	Piazza Cavour	https://goo.gl/maps/Tpm9jxP1DdALDWNy6
Roma	Piazza della Pigna	https://goo.gl/maps/EjuqTzp4kQkHRmdYA
Roma	Piazza Lancellotti	https://goo.gl/maps/pKc8iAykigUS42Tm7
Rovigo	Piazza Vittorio Emanuele	https://goo.gl/maps/cgE1NzqFXEd6s2yUA
San Gemini	Piazza San Francesco	https://goo.gl/maps/6dwjeoK4xQBihXdcA
San Giovanni in Persiceto	Piazza del Popolo	https://goo.gl/maps/dsDwkuEieYwafHue8
Savona	Piazza Sisto IV	https://goo.gl/maps/tEAFtUyTgKbD8yyF8
Siena	Piazza d'Ovile	https://goo.gl/maps/aBjSwkbXFmm3xkyu6
Siracusa	Piazza Minerva	https://goo.gl/maps/jyAExRHTD4Jw5eU6

City	Square	Link
Sondrio	Piazza Garibaldi	https://goo.gl/maps/XEVHrK9EQ2bXbHF3A
Taranto	Piazza del Duomo	https://goo.gl/maps/yjussdG3KtH3z8x28
Torino	Piazza del San Carlo	https://goo.gl/maps/3Fqpvx28AKKKhESN9
Torino	Piazza Vittorio Veneto	https://goo.gl/maps/dJznvKhkpMVfYTUR7
Trapani	Piazza Lucatelli	https://goo.gl/maps/skbyZKYrxsgeoGLU7
Udine	Piazza Matteotti	https://goo.gl/maps/BcUzsnhsgJYm922U8
Varese	Piazza San Vittore	https://goo.gl/maps/xumkYe5MGDqR2Yvq9
Venezia	Campo Sant' Aponal	https://goo.gl/maps/4pf9YXQrY1oKk5GYA
Vercelli	Piazza Cavour	https://goo.gl/maps/8PzHEvYYsKBL2Hd58
Verona	Piazza dei Signori	https://goo.gl/maps/SisVkhQivZsE9GzN8
Vibo Valentia	Piazza Armando Diaz	https://goo.gl/maps/Pj9tAHwNno5wXd7S6
Viterbo	Piazza del Plebiscito	https://goo.gl/maps/Hjn1k5qvcRtUDwbk7

Table 60: List of case studies and their geo-localization

11.3.3. Intended uses full table

Intended use <i>T</i>	<i>OL_T</i> and notes	References : Italian regulations
Residential buildings	Occupants loads approach: 0.05 pp/m ² (assumed according to regulations)	DM 3/8/2015
Institutional buildings including architectural and historic ones used as offices, administrative/government offices/buildings, police stations/military bases	Occupants loads approach: closed to the public, 0.1 pp/m ² ; open to the public, 0.4 pp/m ² ; gathering areas open to the public, 0.7 pp/m ² . As an alternative, the certified number of occupants (e.g. workers) plus 25% rounded to the upper bound.	DM 10/3/1998, DM 3/8/2015; for historical buildings: DM 20/5/1992, DPR 30/6/1995; for other public buildings used for cultural events: DM 19/8/1996, DM 6/3/2001, DM 3/8/2015
Religious buildings	Occupants loads approach: 0.7 pp/m ² applied to the available area extension. As an alternative, the number of seats plus the number of standing places	Adopted referring to entertainment and public exhibition places: DM 19/08/1996, DM 6/3/2001, DM 18/12/2012
Hospital and healthcare buildings	Occupants loads approach: Ambulatory and similar, 0.1 pp/m ² ; Spaces for visitors, 0.4 pp/m ² . As an alternative, the number of in-service personnel plus the average number of visitors referring to at least three typical days	Adopted referring to working places: DM 10/3/1998
Educational buildings	Occupant loads approach: During lesson hours, 0.4 pp/m ² applied to the available area extension. As an alternative, a maximum of 26 individuals in each classroom and annex (e.g., refectory, gym) plus 4% of the people in the buildings for teachers and personnel. During non-lesson hours: 0.1 pp/m ² , as for Offices closed to the public	DM 26/8/1992, DM 12/5/2016, DM 3/8/2015
Cultural and entertainment buildings (public exhibitions such as museums, art galleries, theatres and cinemas, and sports facilities)	Occupant load approach: 3 pp/m ² applied to the available area extension. As an alternative, for theatres and cinemas, the number of seats for the public plus 20% for the personnel; for museums and art galleries, data provided by tourism organizations and/or infields survey on the daily influx	DM 18/3/1996, DM 6/6/2005, DM 19/8/1996, DM 18/12/2012
Commercial buildings	Occupant load approach: 0.4 pp/m ² applied to the available area extension	DM 27/7/2010, DM 3/8/2015
Accommodation facilities	Occupant load approach: 0.4 pp/m ² applied to the available area extension. As an alternative, the number of beds plus 20% for the personnel	DM 27/7/2010, DM 3/8/2015
Public shops such as restaurants bars and cafes	Occupant loads approach: Indoor, 0.7 pp/m ² applied to the available area extension; Outdoor (i.e., see <i>Dehors</i>) 0.4 pp/m ²	Adopted referring to: DM 19/8/1996, DM 6/3/2001, DM 18/12/2012; from a general point of view: DM 3/8/2015
Metro / train / bus stations	Occupants loads approach: common areas for travelers' passage, waiting, and other activities 0.2 pp/m ² , as a minimum value for precautionary evaluations, and extended to all the building area.	Assumed according to the draft document of the fire safety code for train stations ³⁴

Table 61: Quick *OL_i* values for different indoor areas' intended uses according to the Italian fire safety codes and methodologies, and previous works [41].

³⁴ https://www.cni.it/images/bozza_RTV_stazioni_ferroviarie_CCTS.pdf (last access: 14/07/2021)

11.3.4. Users' temporalities full table

Users' age ranges	Only Outdoor users (OO)	Prevalent Outdoor users (PO) – opening time	Resident users (R)	Non-Resident users (NR)					
				Educational buildings: primary and secondary schools		All the uses (excluding primary and secondary educational buildings)			
				Lesson time (depending on the educational stage system, e.g., 8 am to 1 pm)	Normal closure to scholars, that is out of lessons time	Intended use open to the public (excluding universities) – opening time	Universities (depending on the lesson time, e.g., 8 am to 8 pm) – opening time	Intended use close to the public - opening time	Religious buildings
Toddlers (TU)	W, H: equal to OOn [pp] * TUp [%] from 7 to 24; elsewhere 0 [pp]	W, H: equal to POn [pp] for the considered outdoor area use * TUp [%]	W, H: equal to Rn [pp] * TUp [%]	W, H: 0 [pp]	W, H: 0 [pp]	W, H: equal to NRn [pp] for the considered building * TUp [%]	W, H: 0 [pp]	W, H: 0 [pp]	W: 0 H: equal to NRn [pp] for the considered building * TUp [%]
Parent-assisted Children (PC)	W, H: equal to OOn [pp] * PCp [%] from 7 to 24; elsewhere 0 [pp]	W, H: equal to POn [pp] for the considered outdoor area use * PCp [%]	W: equal to 0 [pp] from 8am to 1pm; elsewhere Rn [pp] * PCp [%] H: equal to Rn [pp] * PCp [%]	W: considering 0.4pp/m ² , all the users are PC in the case of primary schools H: 0 [pp]	W, H: 0 [pp]	W, H: equal to NRn [pp] for the considered building * PCp [%]	W, H: 0 [pp]	W, H: 0 [pp]	W: 0 H: equal to NRn [pp] for the considered building * PCp [%]
Young Autonomous users (YA)	W, H: equal to OOn [pp] * YAp [%] from 7 to 24; elsewhere 0 [pp]	W, H: equal to POn [pp] for the considered outdoor area use * YAp [%]	W: equal to 0 [pp] from 8am to 1pm; elsewhere Rn [pp] * YAp [%] H: equal to Rn [pp] * YAp [%]	W: considering 0.4pp/m ² , all the users are YA in the case of secondary schools H: 0 [pp]	W, H: 0 [pp]	W, H: equal to NRn [pp] for the considered building * YAp [%]	W, H: 0 [pp]	W, H: 0 [pp]	W: 0 H: equal to NRn [pp] for the considered building * YAp [%]
Adults (AU)	W, H: equal to OOn [pp] * AUp [%] from 7 to 24; elsewhere 0 [pp]	W, H: equal to POn [pp] for the considered outdoor area use * AUp [%]	W: equal to Rn [pp] * AUp [%] * 0.09 ^(B) from 8am to 6pm; elsewhere Rn [pp] * AUp [%] H: equal to Rn [pp] * AUp [%]	W: 4% of the users in the building, derived from PC or YA (primary schools / secondary schools) ^A H: 0 [pp]	W: considering 0.1pp/m ² , all the users are AU H: 0 [pp]	W, H: equal to NRn [pp] for the considered building * AUp [%]	W: considering 0.4pp/m ² , all the users are AU H: 0 [pp]	W: considering 0.1pp/m ² , all the users are AU H: 0 [pp]	W: 0 [pp] H: equal to NRn [pp] for the considered building * AUp [%]
Elderly (EU)	W, H: equal to OOn [pp] * EUp [%] from 7 to 24; elsewhere 0 [pp]	W, H: equal to POn [pp] for the considered outdoor area use * EUp [%]	W, H: equal to Rn [pp] * EUp [%]	W, H: 0 [pp]	W, H: 0 [pp]	W, H: equal to NRn [pp] for the considered building * EUp [%]	W, H: 0 [pp]	W, H: 0 [pp]	W: 0 [pp] H: equal to NRn [pp] for the considered building * EUp [%]

Table 62: Users' temporalities considering their age ranges (rows), and familiarity with areas occupied (super-columns), by including specific uses and opening times to the public both on working days (W) and Holidays (H) (sub-columns). ^A : 4% relates to at least 1 teacher over 26 students (see §11.3.3). The number of classes will have YA=0.4pp/m²*1000m²=400pp; AU=400*4%=16pp. ^B : 9% relates to the percentage of unemployed users in Italy when the research was carried out.

11.3.5. Guide for application

This section is dedicated to the application of the proposed methodology to a single case study, and then to the comparison with the typological conditions retrieved in section §5. The selected POS selected for this purpose is Piazza del Popolo in Manfredonia. Figure 80 shows its aerial view. The outdoor areas are composed of 25% of carriageable areas (CA, in yellow), 71% of walkable areas (W, in red), 3% of dehors (D, blue rectangles), and 1% of unwalkable areas (UA, black circles). No private courtyards (CY) are present. The indoor areas (in orange) are composed of 47% of residential uses (mainly on the upper floors of the buildings), and 53% of non-residential uses, among which: the Church (S1), the Municipality (S2), and some commercial activities on the ground floors.



Figure 80: Aerial view of Piazza del Popolo, Manfredonia (IT). Yellow areas are Carriageable Areas (CA), red areas are Walkable Areas (WA), blue rectangles indicate Dehors (D), black circles indicate Unwalkable Areas (UA), and orange areas indicate the indoor areas considered. Special buildings are signed with the letter “S”.

The layout of the given POS, together with the users’ age range percentages (Table 63) and their daily and hourly temporalities within the intended uses (see Sections §11.3.3 and §11.3.4), provide the data necessary for the KPIs calculus, therefore to quantify the users’ vulnerability and exposure in the given case study. In particular, the main temporalities timetables are resumed in the following³⁵: (1) the Church is occupied by users only during the Sunday services, that is between 8-10, and 18-20 of the Holiday scenario; (2) the Municipality is closed in the Holiday scenario; (3) most of the commercial uses’ opening time range between 9-13 both on Working Days and Holidays.

Users’ typology	Age range	AP _a [%]
T - TODDLERS	0-4	3,6%
PC - PARENT-ASSISTED CHILDREN	5-14	9,7%
YA - YOUNG ADULTS	15-19	5,5%
AU - ADULTS USERS	20-69	64,7%
EU - ELDERLY USERS	70+	16,5%

Table 63: Users’ age distribution of the a-th age range AP_a [%] in the city of Crotona.

³⁵ Data retrieved from <https://www.google.it/maps/?hl=it> (last access on 25/07/2021)

POSC-related KPIs are summarized in Table 64, which shows how the configuration of the outdoor areas of the case study (median values) is comparable with the typological description derived from the recurring conditions [180]. In particular, the largest percentage is occupied by walkable areas (WAp), then by carriageable ones (CAp), and there is a limited presence of unwalkable areas (UAp) and dehors (Dp). Furthermore, the ratio between indoor and outdoor areas (AOIr) is slightly lower than the same KPI's median value, and closer to the 1st quartile value (1.80). Finally, the most recurring condition concerning the number (and type) of special buildings is confirmed (SBn=2), and in the case of Manfredonia, they are represented by a religious building and a government building.

KPI	Typological scenario : Manfredonia	KPI	Typological scenario : Manfredonia
CAp [%]	28 : 25	SBn [-]	2 : 2
WAp [%]	64 : 71	AIOr [-]	2.38 : 1.66
UAp [%]	1 : 1		
Dp [%]	2 : 3		
CYp [%]	0 : 0		

Table 64: POSC-related KPIs comparison between the typological scenario (see Section §5.1) and the case study of Manfredonia.

As a result, also UDC-related KPIs are comparable with the recurring conditions traced by the median values (Table 65), especially for what it concerns density parameters (i.e., UOod, UOid, Uid) that straightly depend on the square geometrical features (as well as n users' temporalities). It can also be noticed how, similarly to what is shown by the previous KPIs, indoor areas have a lower impact than the typological scenario, as the ratio between users in indoor and outdoor areas is closer to the 1st quartile ("Min" column) both on working day and holidays. As a result, outdoor users' percentages (OOp and POp) in the case of Manfredonia are higher than the median values.

KPI	Max (W : H)	Med (W : H)	Min (W : H)	Manfredonia (W : H)
UOod	0.55 : 0.36	0.22 : 0.20	0.06 : 0.06	0.19 : 0.16
UOid [pp/m ²]	0.24 : 0.17	0.10 : 0.09	0.02 : 0.02	0.11 : 0.10
Uid [pp/m ²]	0.20 : 0.13	0.06 : 0.05	0.02 : 0.02	0.07 : 0.05
UIOr [-]	10.26 : 6.64	3.47 : 2.15	0.94 : 1.04	1.99 : 1.53
OOp [%]	48 : 49	15 : 23	0 : 0	25 : 27
POp [%]	6 : 4	1 : 1	0 : 0	4 : 0
Rp [%]	100 : 100	17 : 24	3 : 12	16 : 25
NRp [%]	82 : 67	48 : 33	0 : 0	44 : 31

Table 65: Comparison between the typological scenario (see Section §5.2.2) and the case study of Manfredonia according to the median values of UDC-related KPIs. W stands for Working Days, H for Holidays.

However, it is worthy of notice that Table 65 provides no time-dependent quantification of the typological scenario, although it reliably offers a quick and general overview of the POS recurring conditions. Therefore, a more detailed picture can be obtained by analyzing hourly temporalities through UHC-relate KPIs. The comparisons between the case study of Manfredonia and the most recurring conditions are shown in Figure 81 (in terms of users' densities) and Figure 82 (in terms of users' percentages).

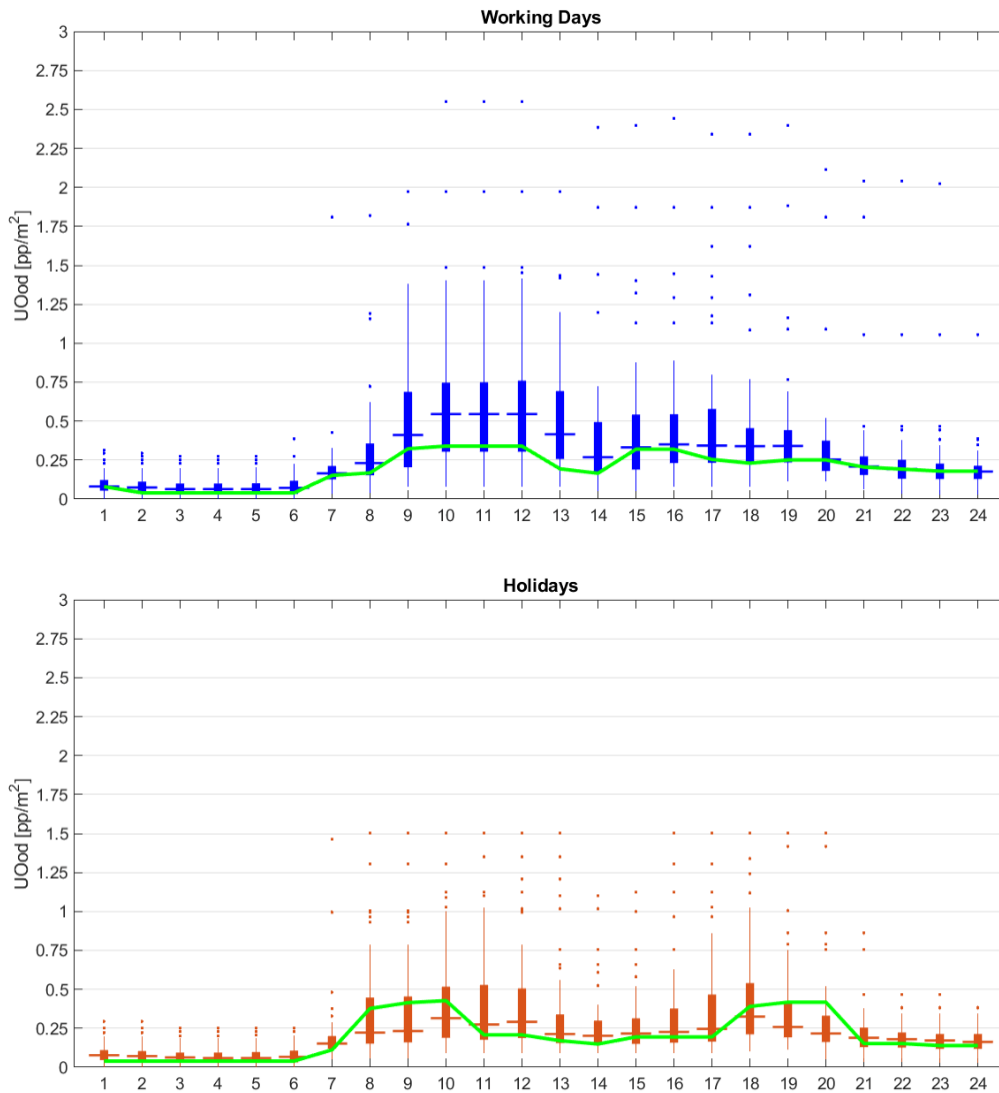


Figure 81: UHC-related KPIs – Comparison between Piazza del Popolo in Manfredonia (in green) and the quartile-based analysis of the Users' Overall outdoor density (UOod) on working days (in blue) and holidays (in orange). Outliers are shown by the dots.

The main results highlight how:

- On working days:
 - UOod is comparable with the median values during the night and the afternoon, while in the morning hours (i.e., between 9-14) the level of crowding is slightly lower and settles around the 1st quartile values;
 - With respect to the recurring conditions, in the morning hours, OOp increases (close 3rd quartile) and NRp decreases (close 1st quartile) as a result of the limited presence of commercial activities; on the other hand, Rp and POP are comparable with the median values.
- On Holidays:
 - UOod is comparable with the median values basically during all the day, except for the Sunday service hours (that is between 8-10 and 18-20), as the Church is characterized by a larger surface and a higher occupant load than the other intended uses;

- As a result of the previous point, in the aforementioned hours, NRp settles around the 3rd quartile, as well as OOp in the rest of the day, while Rp and POp are comparable with the median values.

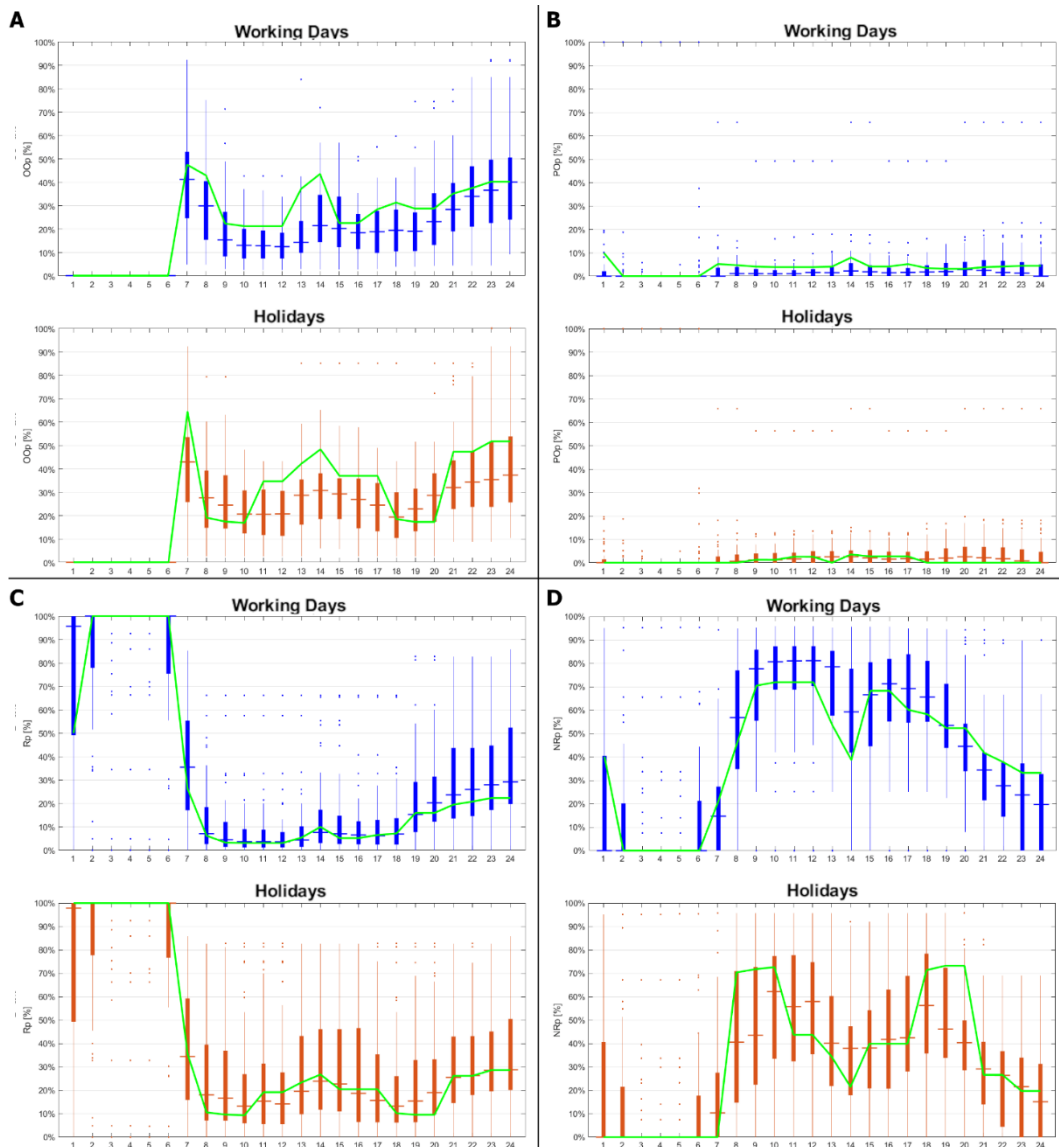


Figure 82: UHC-related KPIs – Comparison between Piazza del Popolo in Manfredonia (in green) and the quartile-based analysis of: (A) Only Outdoor users' percentage OOp; (B) Prevalent Outdoor users percentage POp; (C) Residents users percentage Rp; (D) Non-residents percentage NRp. Working days are in blue, holidays in orange. Outliers are shown by the dots.

11.4 Video-analyses on pedestrian evacuation behaviors

11.4.1. Evacuation behaviors codified and classified in literature

Previous literature identifies several factors leading or forcing people to take part in a flood evacuation (by foot or vehicle, that is pedestrians or drivers), thus exposing them to potentially dangerous (deadly) interactions with the floodwaters. Such interactions can be *deliberately chosen* or *passively suffered* by people [246]. The voluntariness to come in contact with floodwaters as a result of a decision can be traced back to human factors [244], involving people's physical, psychological, cognitive, motivational, and social features. The main factors refer to: (a) the experience with previous floods [308], [372]; (b) the preparedness to cope with similar emergencies [372], [373]; (c) the familiarity with the environment and the eventual knowledge of safe evacuation plans/sites [372], [373]; (d) the perception of risk, as well as the trust and attitude towards public authorities and rescuers [153], [374], [375]; (e) the expected personal impact basing on self-confidence, "heroism", and personal skills (e.g., swimming, escaping, requesting help) [153], [314]; (f) people's age, gender, health, foot size, height, body shape, mass, abilities/impairments, geographical area, cultural background, education level, socio-economic status, and occupational duty [55], [245], [376]–[378].

On the other hand, *environmental factors* can impose additional risks when the floodwater conditions are such to prevent people from performing the desired behaviors [244], [379]. Correlations between floodwater conditions and walking behaviors and quantities (e.g., speed, trajectory, step frequency, lateral swaying, instability thresholds) generally highlight how the increase in water depth and speed: (a) slows down pedestrians' desired evacuation speed [50], [231], [243], [380]; and (b) triggers the main mechanism of instability, namely sliding (that is more frequent with high speed above the knees waters), and toppling (that is more common when the water depth approaches the height of the waist) [239], [241], [306], [381].

Table 66, Table 67, and Table 68 resume the most relevant and frequent *by-literature* behaviors according to the evacuation phase in which they are observed. To properly focus on evacuation tasks, the collected behaviors refer to the ones of people exposed to flood, by excluding mandatory behaviors due to occupational duty, such as the ones of rescuers [246], and by indifferently including both flash floods and slow-onset floods regardless of their cause or source [307]. Behaviors are listed in alphabetical order, and they are associated with identification codes (ID in Table 66, Table 67, and Table 68) composed by the main reference to the related evacuation phase (that are: PM for *pre-movement*; M for *motion towards the evacuation target*; and PE for *post-evacuation*) and a number. For each behavior, when possible, Table 66, Table 67, and Table 68 also provide:

- the type of emergency in which they are noticed, distinguishing between *peculiar behaviors* when they are characteristic only of the flood evacuation, or *common behaviors* and when they are noticeable also in other emergency conditions [223];
- the voluntariness in performing the behavior as a result of a decision, as *deliberately chosen* or *passively suffered* [246];
- the people's response against the hazard, in terms of *protective behavior* directly aimed at saving their own and/or other's lives, or *hazardous behavior* [247];
- the required presence of *reference elements* for people to activate the behavior, such as *environmental elements* (e.g., obstacles, debris, urban furniture, tools furnished by rescuers), or *human elements* (i.e., other evacuees or rescuers) [223].

ID	Behavior and Definition	Type	Voluntariness	Human Response	Reference Elements	Ref.
PM1	<i>Attachment to belongings</i> : before starting the evacuation pedestrians try to save personal belongings (including animals, vehicles, and excluding other individuals) once they are aware of the hazard in terms of floodwater conditions and damages	Common	Deliberately Chosen	Hazardous Behavior	Environmental Elements	[223], [246], [382]
PM2	<i>“Curiosity” effect (“flood tourism”)</i> : pedestrians delay the evacuation start since they spend time looking at floodwater conditions and recording with smartphones or cameras	Peculiar	Deliberately Chosen	Hazardous Behavior	-	[223], [246], [382]

Table 66: List of frequent by-literature human behaviors observed in the “pre-movement” phase, and their classification according to type, voluntariness, human response, and reference elements.

ID	Behavior and Definition	Type	Voluntariness	Human Response	Reference Elements	Ref.
M1	<i>Attraction towards safe areas</i> : pedestrians (try to) move towards safe areas, or considered as such, to restore adequate safety conditions (e.g., areas with lower levels of damage, lower floodwater depth)	Common	Deliberately Chosen	Protective Behavior	Environmental Elements	[223], [382]
M2	<i>Attraction towards unmovable obstacles</i> : pedestrians prefer to move towards (and along) elements that cannot be dragged by the floodwaters, looking for physical support (e.g., walls, street signals, trees, fences)	Peculiar	Deliberately Chosen	Protective Behavior	Environmental Elements	[223]
M3	<i>Fear of moving elements</i> : pedestrians prefer to move far from floating objects dragged by the floodwaters (e.g., debris, vehicles, bins)	Peculiar	Deliberately Chosen	Protective Behavior	Environmental Elements	[223]
M4	<i>Increased guide effect</i> : pedestrians benefit from the presence of rescuers and/or evacuation leaders thus improving the evacuation process (e.g.: choosing appropriate behaviors and evacuation directions, increasing motion speeds)	Common	Deliberately Chosen	Protective Behavior	Human Elements	[223]
M5	<i>Moving through the water with vehicles</i> : drivers prefer still moving through the floodwaters with vehicles (including cars, motorcycles, buses, bikes, and excluding fire trucks) rather than moving on foot	Peculiar	Deliberately Chosen	Hazardous Behavior	-	[246], [304], [305], [382]
M6*	<i>Social influence and group phenomena</i> : pedestrians move in groups, activate herding behaviors, share information, and perform pro-social actions (e.g., try to rescue other individuals)	Common	Deliberately Chosen	Protective Behavior	Human Elements	[223], [246]
M7*	<i>Floodwaters effects on motion speed</i> : pedestrians are slowed down by floodwaters depending on the water depth and flow	Peculiar	Passively Suffered	-	-	[223], [227], [301]
M8*	<i>Human body instability</i> : pedestrians experience instability problems due to the water depth and flow	Peculiar	Passively Suffered	-	-	[99], [223], [227]

**Although the marked behaviors can be generally observed during all the evacuation phases, previous works' evidence shows significant relevance for what concerns the “motion towards evacuation target” phase [223]. However, these findings were also confirmed during preliminary video observations made early in this study.*

Table 67: List of frequent by-literature human behaviors observed in the “motion towards the evacuation target” phase, and their classification according to type, voluntariness, human response, and reference elements.

ID	Behavior and Definition	Type	Voluntariness	Human Response	Reference Elements	Ref.
PE1	<i>Reaching temporary safe areas:</i> pedestrians reach temporary safety in spontaneous areas waiting for rescuers (e.g., vehicle roofs, trees) and eventually restart the evacuation motion	Common	Deliberately Chosen	Protective Behavior	Environmental Elements	[223], [382]
PE2	<i>Reaching indoor safe areas:</i> pedestrians reach safety at the upper levels of buildings, including non-strictly indoor areas like building roofs, terraces, and balconies to be reached by rescuers.	Peculiar	Deliberately Chosen	Protective Behavior	Environmental Elements	[382], [383]
PE3	<i>Reaching outdoor safe areas:</i> pedestrians reach safety on raised areas and street furniture (e.g., benches, sidewalks, raised platforms)	Peculiar	Deliberately Chosen	Protective Behavior	Environmental Elements	[223]

Table 68: List of frequent by-literature human behaviors observed in the “post-evacuation” phase, and their classification according to type, voluntariness, human response, and reference elements.

The proposed behavioral database from Table 66, Table 67, and Table 68 have been used as a reference for the video analysis introduced in Section §3.4.2.1.

11.4.2. Symbols and acronyms explanation

Symbols	Meaning
BE	Built Environment
PM	“Pre-Movement” phase
PM1	Pre-Movement Behavior #1: Attachment to belongings
PM2	Pre-Movement Behavior #2: “Curiosity” effect (“flood tourism”)
M	“Motion towards the evacuation target” phase
M1	Motion towards the evacuation target Behavior #1: Attraction towards safe areas
M2	Motion towards the evacuation target Behavior #2: Attraction towards unmovable obstacles
M3	Motion towards the evacuation target Behavior #3: Fear of moving elements
M4	Motion towards the evacuation target Behavior #4: Increased guide effect
M5	Motion towards the evacuation target Behavior #5: Moving through the water with vehicles
M6	Motion towards the evacuation target Behavior #6: Social influence and group phenomena
M7	Motion towards the evacuation target Behavior #7: Floodwaters effects on motion speed
M8	Motion towards the evacuation target Behavior #8: Human body instability
M9	Motion towards the evacuation target Behavior #9: Clinging to ropes and arranging “human chains”
PE	“Post-Evacuation” phase
PE1	Post-Evacuation Behavior #1: Reaching temporary safe areas
PE2	Post-Evacuation Behavior #2: Reaching indoor safe areas
PE3	Post-Evacuation Behavior #3: Reaching outdoor safe areas
A	Water up to the ankles
K	Water up to the knees
W	Water up to the waist
HW	Water higher than the waist
S	Still water
F	Flowing water
PO [pp]	People overall
PI [pp]	People involved
PI _a [pp]	People involved per water depth

Symbols	Meaning
PI_f [pp]	People involved per water flow
PI_{d,r} [pp]	People involved per floodwater conditions
PI/PO*100 [%]	Overall frequency
PI_d/PI*100 [%]	Situational frequency (with respect to the water depth)
PI_f/PI*100 [%]	Situational frequency (with respect to the water flow)
PI_{d,r}/PI_d*100 [%]	Situational frequency per water depth (with respect to the water flow given the same water depth)

Table 69: List of abbreviations

11.5 Specifications on evacuation simulators

11.5.1. Modeling logic

FloPEDS is used as the custom reference simulator [134] since it includes all the main criteria provided by section §3.5.3.2. FloPEDS combines a module to simulate flood hydrodynamics based on Nonlinear Shallow Water Equations (NSWE) [222], [384], and a module to simulate pedestrians' evacuation based on the SFM approach, thus pursuing a microscopic approach. The NSWE and the SFM-based modules of FloPEDS work in series, with no back interaction of pedestrians on the water flows. Since, in this work, the core of the comparison with the generic software concerns the pedestrians' evacuation model, the hydrodynamic one is ignored here.

MassMotion 10.6³⁶ is used as the generic simulator to be modified according to section §3.5.3.2 criteria. In general terms, the two models consider that the simulated pedestrians (in MassMotion, *agents*) move in 2-D planes, from an initial position to reach intermediate and final evacuation targets (in MassMotion, *portals* represent both the entrances into the simulation and the pedestrians' destinations). The planes can be divided into one or more areas (in MassMotion, they are the *floors*), depending on the specific D_f and V_f local conditions (hence v_i , as discussed in section §3.5.3.2 and Equation 3.2). As for FloPEDS, MassMotion adopts the SFM approach to simulate the microscopic pedestrians' movement [255]. The calculation of the evacuation velocity $\overrightarrow{v_i(t)}$ [m/s] (as a vector) for each pedestrian involved in the simulation depends on the sum of repulsive and attractive forces on the pedestrian, according to Equation 15.1:

$$m_i \frac{d\overrightarrow{v_i(t)}}{dt} = \overrightarrow{O_g(t)} + \sum \overrightarrow{F_{rep,i}(t)} + \sum \overrightarrow{F_{rep,w}(t)} + \sum \overrightarrow{F_{attr,i}(t)} + \sum \overrightarrow{F_{attr,w}(t)} \quad (15.1)$$

where m_i [kg] is the body mass of the pedestrian, dt [s] is the time between two consecutive calculation iterations, $\overrightarrow{O_g(t)}$ [N] is the drive-to-target force depending on the target direction, and the current and desired pedestrian's velocity (and so, it depends on v_i). In Equation 15.1, the pedestrian is affected by attractive (subscript *attr*) and repulsive (subscript *rep*) forces [N] with the surrounding pedestrians i and with the surrounding obstacles w . The main difference between the two simulators' logic relies on the attractive force between the individual and the unmovable obstacles $\overrightarrow{F_{attr,w}(t)}$. FloPEDS, unlike the generic simulator, also includes this phenomenon, considering the attraction of elements placed at a distance equal to or lower than 3m [143]. In particular, the attraction force modulus in FloPEDS is equal to 300N, according to verifications with real-world observations [134]. The adopted values for the other specific SFM parameters in FloPEDS simulations are reported by the original verification work [134].

In view of the criteria shown in section §3.5.3.2, this work considers stationary floodwater conditions for both the application of FloPEDS and MassMotion, assuming that D_f and V_f do not change over the simulation time. A unique area in terms of D_f and V_f is simulated, thus creating a unique v_i value in the setup process. Maximum (e.g. capped) motion speeds v_i are calculated according to Equation 3.2 (see section §3.5.3.2) so as to adopt a conservative approach in the motion speed estimation and in the evacuation timing assessment. As for most of the evacuation simulators, differences between v_i are assigned in a rapid manner using a v_i distribution, and so they could be used to additionally

³⁶ Tests (randomly selected within the list of the validation scenarios in Figure 16, Section §3.5.3.4) are additionally carried out with MassMotion 9.5.2.2 to compare results with the previous version and no differences are found.

consider different pedestrian typologies. According to the reference work [134], v_i in the range 0.85 ± 0.05 m/s (Gaussian distribution) is herein assigned to describe low-medium floodwater levels, e.g. being $(D_f \cdot V_f^2)/g + D_f^2/2 \approx 0.01 \text{m}^3/\text{m}$.

Non-critical conditions for human body stability are assumed in this work. Indeed, it is considered that the motion-process for a safe evacuation should be carried out by avoiding possible major threats due to floodwater [263]. Thus, all the pedestrians can arrive in a safe area in the simulated scenario, and tests can focus on the motion tasks.

Finally, in the MassMotion setup, the simulated pedestrians are assumed to move along linear paths alongside the building walls/fences, thanks to the use of *servers* [254]. The *servers* are elements already present within MassMotion, and they are useful to model queues and, more in general, to vehiculate pedestrians' movements and behaviors. Using *servers* to model the pedestrian-unmovable obstacles attraction could introduce some simplifications according to Equation 15.1, i.e. does not consider possible variations in their trajectory due to extraordinary conditions related, for instance, to the presence of floating obstacles or impracticable areas.

11.5.2. *MassMotion specific configuration*

In this section the specific software configuration terms are provided, underlining MassMotion options in italics, and in square brackets, where needed. Three main elements compose the MassMotion testing scenario [254]: (1) the *floor*, simulating the linear pathway where *agents* (i.e. pedestrians) move; (2) the *portals*, representing both the entrances into the simulation and the *agents'* destinations; and (3) the *servers*, used in this work to reproduce the attraction of the *agents* (i.e. pedestrians) towards unmovable obstacles (i.e. buildings).

Entrance only and *destination portals* (respectively, where *agents* enter and exit the simulation *floor*) are placed close to the later *floor* limit, to reproduce the ideal maximum distance among pedestrians and buildings according to the considered real-world observations [134]. An *entrance only portal* (whose dimensions depend on the setup tested) and a *destination portal* are placed on each *floor* side.

The *servers* are introduced to increase the attraction behavior towards unmovable obstacles, that are the pathway sides. The start points of the *servers* (whose number depends on the setup tested) are placed on each *floor* lateral side. With respect to the pathway length, the *servers* are tested in three different positions: halfway, a quarter, and an eighth of the *floor*. Thus, the first part of the pathways is intended to replicate the pedestrians' organization alongside the pathway side, being the *agents* attracted by the *servers* start points [134]. Concerning these start points' distances from the *floor* lateral edge, multiple setups are also tested in order to represent the classes of distance by literature [134]. Moreover, *servers* are connected through a single internal connection, the *dispatch*, to a single endpoint (placed near the end of the pathway, at the *destination portal*). In this way, the configuration tries to force the *agents* to move near the *floor* edge by reproducing the maximum attraction phenomena for building-pedestrians distances of about 2m [134].

The *agents'* motion is configured so as to link them towards the *servers* placed on the same generation *floor* side, and then towards the final *destination portal*. In particular, the *agents* are divided between the elements of the *server* according to two distributions: homogeneous, where agents have the same probability in choosing the related *server*, and by-literature, according to the real-world observations about the frequency for each class of distance from unmovable obstacles. The *dispatches* also increase the possibility of motion interaction between *agents* moving from the

two start points to the unique endpoint. The *servers*' configuration also includes the following features:

1. *agents* are initially generated at the *entrance only portal*, and then directly move towards the exits [*approach: standard walk to target; Target: server exit*]. Each *server* influences the *agents*' motion as a waypoint for the evacuation motion, only because of its position (the *server* length is not relevant);
2. no limitations in the exit flows are considered [*Processors: unlimited; Capacity: infinite; Contact time: disabled*]. The impact of queueing phenomena on the *server* motion steps and at the exit can be reduced by combining these setup strategies with previous point 1.
3. the correct evacuation direction is identified uniquely to avoid coming-and-going behaviors and street-crossing behaviors along the *floor*, which are not noticed in flood evacuation conditions [*Dispatch objects* are configured to directly connect the *servers* along the evacuation motion direction.

Each simulated *agent* moving on *floor* is characterized by a unique profile according to the *Agent Behavior Tab* setup interface. Compact groups are simulated by considering no pre-movement time delay [*Population: arrival -> instant*]. The *agents*' maximum (e.g. capped) motion speed v_i is assigned through the *floor* properties (maximum speed allowed on the floor). The default speed-density relation is adopted since no current advances in literature on these aspects are provided for the flood evacuation case. The *agents*' queue spacing is similarly set up according to the default normal distribution (minimum=0m, maximum=1m, mode=0.25m, standard deviation 0.125m) for the same reason. The selected *direction bias* is "none" to avoid influencing the overtaking of other *agents*. Besides the configuration of *portals* and *servers*, the minimization of *floor*-crossing probability is also assigned to each *agent* [*assigned goal -> grouped: lowest cost*] hence representing an improved attraction behavior towards the *floor* limits where they are generated.

11.5.3. Setup symbols and properties

	A-B-C-D	H-L	2-4-8	R-S
Setup	Servers' distance from the wall: "first servers" * // second server [m]	Probability a pedestrian can choose one of the "first servers" * [%]	First servers' distance from the start of the pathway [m]	Entrance portals configuration: width; length; distance from the wall [m]
AH2R	1; 2 // 1	50; 50	43.5	3; 1; 0
AL2R	1; 2 // 1	29; 71	43.5	3; 1; 0
BH2R	0.5; 1.5 // 0.5	50; 50	43.5	3; 1; 0
BL2R	0.5; 1.5 // 0.5	29; 71	43.5	3; 1; 0
CL2R	0.5; 1.5; 2.5 // 0.5	29; 50; 21	43.5	3; 1; 0
DH2R	1; 2 // 0.5	50; 50	43.5	3; 1; 0
AH4R	1; 2 // 1	50; 50	21.75	3; 1; 0
AL4R	1; 2 // 1	29; 71	21.75	3; 1; 0
BH4R	0.5; 1.5 // 0.5	50; 50	21.75	3; 1; 0
BL4R	0.5; 1.5 // 0.5	29; 71	21.75	3; 1; 0
CL4R	0.5; 1.5; 2.5 // 0.5	29; 50; 21	21.75	3; 1; 0
DH4R	1; 2 // 0.5	50; 50	21.75	3; 1; 0
AH8R	1; 2 // 1	50; 50	10.87	3; 1; 0
AL8R	1; 2 // 1	29; 71	10.87	3; 1; 0
BH8R	0.5; 1.5 // 0.5	50; 50	10.87	3; 1; 0
BL8R	0.5; 1.5 // 0.5	29; 71	10.87	3; 1; 0
CL8R	0.5; 1.5; 2.5 // 0.5	29; 50; 21	10.87	3; 1; 0
DH8R	1; 2 // 0.5	50; 50	10.87	3; 1; 0
AH2S	1; 2 // 1	50; 50	43.5	3; 3; 1
AL2S	1; 2 // 1	29; 71	43.5	3; 3; 1
BH2S	0.5; 1.5 // 0.5	50; 50	43.5	3; 3; 1
BL2S	0.5; 1.5 // 0.5	29; 71	43.5	3; 3; 1
CL2S	0.5; 1.5; 2.5 // 0.5	29; 50; 21	43.5	3; 3; 1
DH2S	1; 2 // 0.5	50; 50	43.5	3; 3; 1
AH4S	1; 2 // 1	50; 50	21.75	3; 3; 1
AL4S	1; 2 // 1	29; 71	21.75	3; 3; 1
BH4S	0.5; 1.5 // 0.5	50; 50	21.75	3; 3; 1
BL4S	0.5; 1.5 // 0.5	29; 71	21.75	3; 3; 1
CL4S	0.5; 1.5; 2.5 // 0.5	29; 50; 21	21.75	3; 3; 1
DH4S	1; 2 // 0.5	50; 50	21.75	3; 3; 1
AH8S	1; 2 // 1	50; 50	10.87	3; 3; 1
AL8S	1; 2 // 1	29; 71	10.87	3; 3; 1
BH8S	0.5; 1.5 // 0.5	50; 50	10.87	3; 3; 1
BL8S	0.5; 1.5 // 0.5	29; 71	10.87	3; 3; 1
CL8S	0.5; 1.5; 2.5 // 0.5	29; 50; 21	10.87	3; 3; 1
DH8S	1; 2 // 0.5	50; 50	10.87	3; 3; 1

Table 70: Each setup (first column) is based on four properties coded by four symbols, and the properties characterization is discussed in each of the columns, as also shown in Table 14. Best setup in italics. Notes: * Each "first servers" group can be composed of two or three servers according to section §3.5.3.4 criteria, so the semicolon separates the value for each of them.

11.5.4. Symbols and acronyms

Symbol	Meaning	Reference
v_i	Evacuation speed	Equation 3.2
D_f	Floodwater depth	Equation 3.2
v_f	Floodwater speed	Equation 3.2
m_i	Pedestrian body mass	Equation 15.1
d_t	Time between two consecutive calculation iterations	Equation 15.1
$O_g(t)$	Drive-to-target force	Equation 15.1
$F_{rep,i}$	Repulsive force with surrounding pedestrians	Equation 15.1
$F_{rep,w}$	Repulsive force with surrounding obstacles	Equation 15.1
$F_{attr,i}$	Attractive force with surrounding pedestrians	Equation 15.1
$F_{attr,w}$	Attractive force with surrounding obstacles	Equation 15.1
R1, R2, R3	Setup groups having rectangular <i>portals</i>	Figure 16
S1, S2, S3	Setup groups having squared <i>portals</i>	Figure 16
A, B, C, D	Server position with respect to the wall	Figure 16 and Table 14
H, L	Probability a pedestrian can choose a server	Figure 16
2, 4, 8	Server position with respect to the start	Figure 16
R, S	Shape of the entrance portal	Figure 16
EC	Evacuation curves	Table 15
D_w	Pedestrian - side of the building distance during the evacuation	Table 15
t_{max}	Maximum evacuation time	Table 15
W	Waiting time percentage	Table 15
F	Evacuation flow	Table 15
SC	Secant cosine	Table 16
ERD	Euclidean relative difference	Table 16
EPC	Euclidean projection coefficient	Table 16
DAUC	Difference between the graphic Areas Under the Curves	Table 16

Table 71: List of notations and references to their detailed explanation

11.5.5. Detailed KPIs and simulation results

<i>Setup</i>	<i>Secant Cosine [-]</i>	<i>Euclidean Relative Difference [-]</i>	<i>Euclidean Projection Coefficient [-]</i>	<i>Difference between the graphics Area Under the Curve [%]</i>
AH2R	0.780	0.166	1.044	14%
AL2R	0.802	0.208	1.061	17%
BH2R	0.722	0.151	1.015	10%
BL2R	0.752	0.199	1.047	15%
CL2R	0.789	0.143	1.022	10%
DH2R	0.816	0.155	1.042	13%
AH4R	0.826	0.138	1.028	11%
AL4R	0.832	0.072	0.999	4%
BH4R	0.883	0.100	0.998	6%
BL4R	0.901	0.079	1.005	5%
CL4R	0.855	0.093	1.001	6%
DH4R	0.799	0.130	1.016	9%
AH8R	0.841	0.092	1.021	7%
AL8R	0.871	0.074	0.979	1%
BH8R	0.803	0.104	0.981	4%
BL8R	0.895	0.073	0.986	2%
CL8R	0.858	0.083	1.005	5%
DH8R	0.874	0.078	1.011	5%
AH2S	0.711	0.278	1.081	24%
AL2S	0.751	0.246	1.066	21%
BH2S	0.695	0.245	1.063	21%
BL2S	0.694	0.242	1.063	20%
CL2S	0.688	0.282	1.087	24%
DH2S	0.717	0.266	1.076	23%
AH4S	0.725	0.219	1.056	18%
AL4S	0.774	0.223	1.060	19%
BH4S	0.770	0.206	1.053	17%
BL4S	0.823	0.183	1.048	15%
CL4S	0.762	0.210	1.045	17%
DH4S	0.731	0.205	1.053	17%
AH8S	0.843	0.180	1.049	15%
AL8S	0.829	0.136	1.028	11%
BH8S	0.858	0.148	1.028	11%
<i>BL8S</i>	<i>0.783</i>	<i>0.135</i>	<i>1.013</i>	<i>9%</i>
CL8S	0.785	0.190	1.050	9%
DH8S	0.830	0.155	1.041	13%

Table 72: KPIs measuring differences between the evacuation curves obtained from each setup tested on the generic simulator and the one from the custom simulator. Best setup in italics.

<i>1st quartile</i>					
<i>Setup</i>	<i>Values</i>	<i>Secant Cosine [-]</i>	<i>Euclidean Relative Difference [-]</i>	<i>Euclidean Projection Coefficient [-]</i>	<i>Difference between the graphics Area Under the Curve [%]</i>
R1	avg	0.040	0.462	1.197	22%
	<i>st. dev.</i>	<i>0.128</i>	<i>0.033</i>	<i>0.064</i>	<i>7%</i>
R2	avg	0.179	0.374	1.124	14%
	<i>st. dev.</i>	<i>0.136</i>	<i>0.042</i>	<i>0.079</i>	<i>8%</i>
R3	avg	0.494	0.363	1.127	14%
	<i>st. dev.</i>	<i>0.108</i>	<i>0.051</i>	<i>0.098</i>	<i>10%</i>
S1	avg	-0.039	0.539	1.262	28%
	<i>st. dev.</i>	<i>0.125</i>	<i>0.046</i>	<i>0.098</i>	<i>10%</i>
S2	avg	0.104	0.438	1.204	21%
	<i>st. dev.</i>	<i>0.130</i>	<i>0.032</i>	<i>0.067</i>	<i>7%</i>
S3	avg	0.562	0.377	1.149	15%
	<i>st. dev.</i>	<i>0.134</i>	<i>0.043</i>	<i>0.082</i>	<i>8%</i>
OVERALL	avg	0.224	0.425	1.177	19%
	<i>st. dev.</i>	<i>0.260</i>	<i>0.075</i>	<i>0.096</i>	<i>10%</i>
<i>3rd quartile</i>					
<i>Setup</i>	<i>Values</i>	<i>Secant Cosine [-]</i>	<i>Euclidean Relative Difference [-]</i>	<i>Euclidean Projection Coefficient [-]</i>	<i>Difference between the graphics Area Under the Curve [%]</i>
R1	avg	0.066	0.569	1.246	39%
	<i>st. dev.</i>	<i>0.094</i>	<i>0.053</i>	<i>0.057</i>	<i>8%</i>
R2	avg	0.309	0.432	1.126	26%
	<i>st. dev.</i>	<i>0.084</i>	<i>0.066</i>	<i>0.068</i>	<i>10%</i>
R3	avg	0.634	0.428	1.070	22%
	<i>st. dev.</i>	<i>0.014</i>	<i>0.035</i>	<i>0.053</i>	<i>7%</i>
S1	avg	0.267	0.442	1.157	29%
	<i>st. dev.</i>	<i>0.058</i>	<i>0.058</i>	<i>0.055</i>	<i>8%</i>
S2	avg	0.396	0.380	1.086	21%
	<i>st. dev.</i>	<i>0.086</i>	<i>0.064</i>	<i>0.069</i>	<i>10%</i>
S3	avg	0.634	0.400	1.050	19%
	<i>st. dev.</i>	<i>0.047</i>	<i>0.043</i>	<i>0.064</i>	<i>8%</i>
OVERALL	avg	0.384	0.442	1.123	26%
	<i>st. dev.</i>	<i>0.214</i>	<i>0.081</i>	<i>0.090</i>	<i>11%</i>

Table 73: KPIs measuring differences between curves tracing the D_w trend for each setup tested on the generic simulator and the one obtained from the custom simulator (1st and 3rd quartile data). Results are shown in terms of mean and standard deviation values according to the grouping criteria shown in section §3.5.3.4. Graphical trends are shown in Figure 83 and Figure 84.

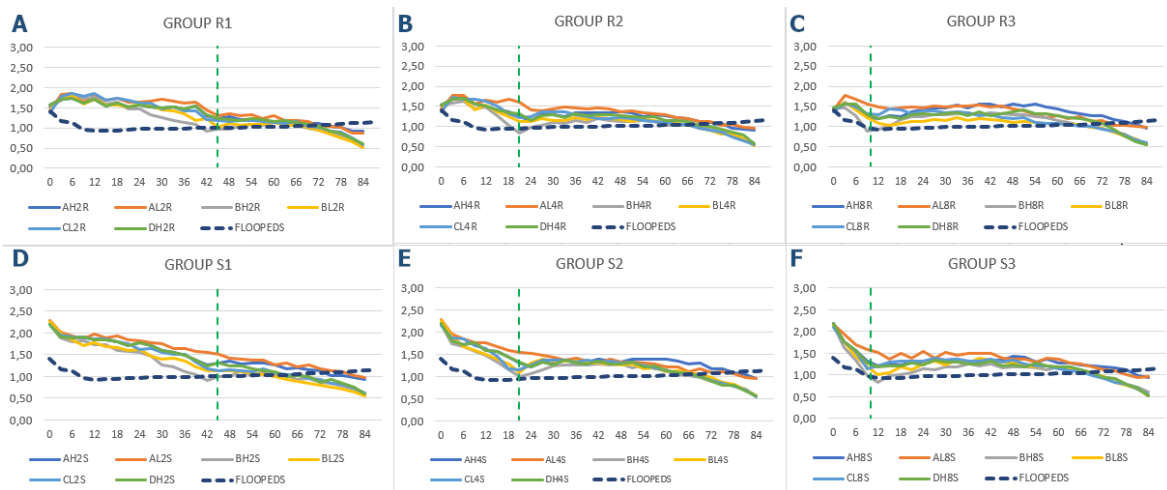


Figure 83: Custom simulator 1st quartile D_w trend (dashed line) compared to those of the generic simulator grouped according to the criteria shown in section §3.5.3.4 (straight lines), that is considering the same entrance portals configuration, i.e., setup groups R1 to R3 are rectangular (panels A-B-C), S1 to S3 are squared (panels D-E-F). The green dashed line indicates the position of the “first servers”.

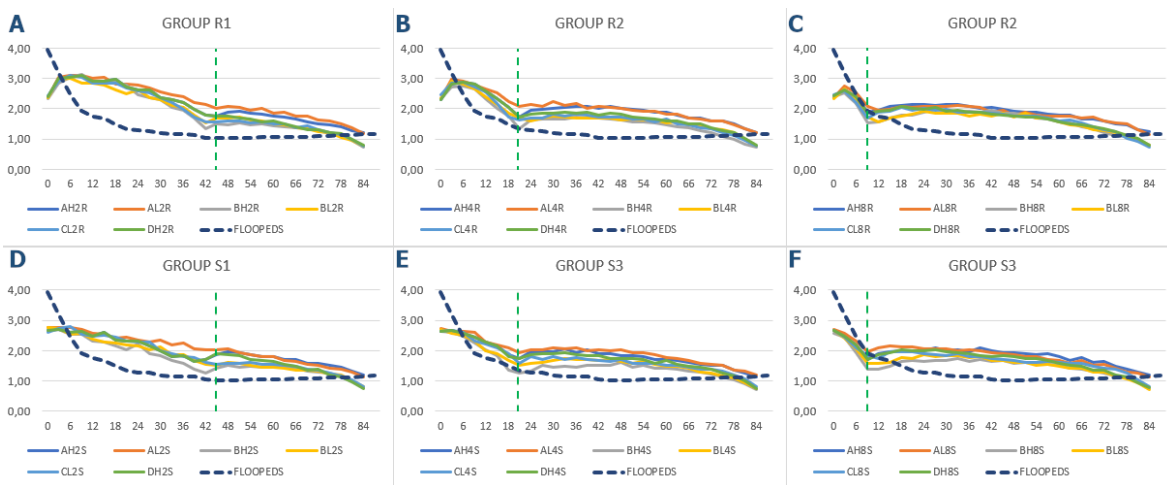


Figure 84: Custom simulator 3rd quartile D_w trend (dashed line) compared to those of the generic simulator grouped according to the criteria shown in section §3.5.3.4 (straight lines), that is considering the same entrance portals configuration, i.e., setup groups R1 to R3 are rectangular (panels A-B-C), S1 to S3 are squared (panels D-E-F). The green dashed line indicates the position of the “first servers”.

1st quartile				
<i>Setup</i>	<i>Secant Cosine [-]</i>	<i>Euclidean Relative Difference [-]</i>	<i>Euclidean Projection Coefficient [-]</i>	<i>Difference between the graphics Area Under the Curve [%]</i>
AH2R	0.066	0.442	1.233	25%
AL2R	0.208	0.519	1.298	32%
BH2R	-0.084	0.420	1.102	12%
BL2R	0.188	0.443	1.136	16%
CL2R	-0.136	0.491	1.210	23%
DH2R	-0.001	0.457	1.205	23%
AH4R	0.243	0.367	1.181	19%
AL4R	0.308	0.451	1.259	28%
BH4R	0.167	0.316	1.018	3%
BL4R	0.298	0.347	1.057	7%
CL4R	-0.097	0.395	1.101	12%
DH4R	0.157	0.370	1.129	14%
AH8R	0.615	0.417	1.261	28%
AL8R	0.383	0.434	1.251	27%
BH8R	0.656	0.319	1.044	6%
BL8R	0.498	0.289	1.003	1%
CL8R	0.376	0.356	1.083	10%
DH8R	0.439	0.362	1.121	14%
AH2S	-0.128	0.549	1.338	35%
AL2S	-0.016	0.618	1.424	44%
BH2S	-0.068	0.469	1.137	15%
BL2S	0.224	0.502	1.163	17%
CL2S	-0.087	0.541	1.242	26%
DH2S	-0.157	0.554	1.265	28%
AH4S	-0.063	0.445	1.285	29%
AL4S	0.175	0.491	1.302	31%
BH4S	0.173	0.383	1.115	12%
BL4S	0.209	0.423	1.169	18%
CL4S	0.221	0.443	1.179	19%
DH4S	-0.092	0.443	1.176	19%
AH8S	0.645	0.377	1.223	23%
AL8S	0.288	0.459	1.289	30%
BH8S	0.690	0.312	1.041	4%
<i>BL8S</i>	<i>0.532</i>	<i>0.360</i>	<i>1.098</i>	<i>10%</i>
CL8S	0.656	0.383	1.125	13%
DH8S	0.564	0.369	1.121	13%

Table 74: KPIs measuring differences between curves tracing the D_w trend for each setup tested on the generic simulator and the one obtained from the custom simulator (1st quartile data). Best setup in italics.

2nd quartile				
<i>Setup</i>	<i>Secant Cosine [-]</i>	<i>Euclidean Relative Difference [-]</i>	<i>Euclidean Projection Coefficient [-]</i>	<i>Difference between the graphics Area Under the Curve [%]</i>
AH2R	0.025	0.602	1.341	44%
AL2R	-0.041	0.690	1.422	52%
BH2R	0.171	0.495	1.194	26%
BL2R	0.108	0.573	1.286	36%
CL2R	0.019	0.516	1.215	29%
DH2R	0.006	0.599	1.301	39%
AH4R	0.271	0.534	1.314	40%
AL4R	0.219	0.515	1.305	38%
BH4R	0.331	0.367	1.102	15%
BL4R	0.351	0.414	1.167	22%
CL4R	0.448	0.392	1.123	18%
DH4R	0.274	0.465	1.208	28%
AH8R	0.321	0.542	1.288	39%
AL8R	0.489	0.495	1.270	36%
BH8R	0.510	0.350	1.049	11%
BL8R	0.631	0.358	1.081	14%
CL8R	0.393	0.467	1.155	24%
DH8R	0.339	0.465	1.193	28%
AH2S	0.086	0.538	1.329	40%
AL2S	0.088	0.610	1.390	47%
BH2S	0.275	0.423	1.185	23%
BL2S	0.265	0.463	1.227	28%
CL2S	0.255	0.495	1.250	31%
DH2S	0.051	0.531	1.285	35%
AH4S	0.646	0.483	1.302	37%
AL4S	0.387	0.542	1.343	42%
BH4S	0.599	0.302	1.091	12%
BL4S	0.495	0.389	1.175	22%
CL4S	0.559	0.372	1.166	21%
DH4S	0.564	0.411	1.209	26%
AH8S	0.457	0.493	1.275	36%
AL8S	0.327	0.490	1.280	36%
BH8S	0.601	0.298	1.029	7%
<i>BL8S</i>	<i>0.711</i>	<i>0.332</i>	<i>1.092</i>	<i>14%</i>
CL8S	0.464	0.398	1.128	19%
DH8S	0.477	0.442	1.193	26%

Table 75: KPIs measuring differences between curves tracing the D_w trend for each setup tested on the generic simulator and the one obtained from the custom simulator (2nd quartile data). Best setup in italics.

3rd quartile				
<i>Setup</i>	<i>Secant Cosine [-]</i>	<i>Euclidean Relative Difference [-]</i>	<i>Euclidean Projection Coefficient [-]</i>	<i>Difference between the graphics Area Under the Curve [%]</i>
AH2R	0.086	0.601	1.291	46%
AL2R	0.058	0.668	1.346	54%
BH2R	-0.071	0.522	1.187	31%
BL2R	0.238	0.514	1.193	32%
CL2R	0.005	0.535	1.213	34%
DH2R	0.079	0.575	1.244	39%
AH4R	0.227	0.507	1.197	37%
AL4R	0.378	0.531	1.230	40%
BH4R	0.273	0.359	1.032	13%
BL4R	0.460	0.377	1.080	19%
CL4R	0.283	0.387	1.094	21%
DH4R	0.230	0.434	1.126	26%
AH8R	0.630	0.485	1.142	32%
AL8R	0.622	0.468	1.138	31%
BH8R	0.661	0.407	1.011	15%
BL8R	0.644	0.390	1.015	15%
CL8R	0.626	0.413	1.049	19%
DH8R	0.621	0.407	1.064	20%
AH2S	0.235	0.482	1.200	36%
AL2S	0.197	0.533	1.247	41%
BH2S	0.318	0.357	1.076	18%
BL2S	0.353	0.391	1.117	23%
CL2S	0.292	0.436	1.147	27%
DH2S	0.205	0.454	1.155	29%
AH4S	0.402	0.436	1.147	30%
AL4S	0.230	0.478	1.186	35%
BH4S	0.507	0.289	0.979	6%
BL4S	0.444	0.331	1.033	14%
CL4S	0.431	0.353	1.071	18%
DH4S	0.364	0.395	1.101	23%
AH8S	0.585	0.463	1.119	29%
AL8S	0.639	0.444	1.131	29%
BH8S	0.725	0.348	0.952	7%
<i>BL8S</i>	<i>0.647</i>	<i>0.355</i>	<i>0.990</i>	<i>11%</i>
CL8S	0.617	0.382	1.049	18%
DH8S	0.588	0.405	1.058	20%

Table 76: KPIs measuring differences between curves tracing the D_w trend for each setup tested on the generic simulator and the one obtained from the custom simulator (3rd quartile data). Best setup in italics.

<i>Setup</i>	<i>t_{max} [s]</i>	<i>Setup</i>	<i>t_{max} [s]</i>	<i>Setup</i>	<i>t_{max} [s]</i>
AH2R	125	AH4R	125	AH8R	126
AL2R	123	AL4R	130	AL8R	131
BH2R	130	BH4R	135	BH8R	131
BL2R	125	BL4R	126	BL8R	129
CL2R	126	CL4R	125	CL8R	127
DH2R	124	DH4R	127	DH8R	126
AH2S	121	AH2S	129	AH8S	126
AL2S	124	AL2S	122	AL8S	125
BH2S	124	BH2S	126	BH8S	127
BL2S	124	BL2S	125	<i>BL8S</i>	<i>127</i>
CL2S	119	CL2S	132	CL8S	125
DH2S	122	DH2S	126	DH8S	126

Table 77: Maximum evacuation time t_{max} for each setup tested. Best setup in italics.

<i>Setup</i>	<i>W [%]</i>	<i>Setup</i>	<i>W [%]</i>	<i>Setup</i>	<i>W [%]</i>
AH2R	5.6	AH4R	6.4	AH8R	7.9
AL2R	4.9	AL4R	8.5	AL8R	9.2
BH2R	6.9	BH4R	11.1	BH8R	9.9
BL2R	6.4	BL4R	8.7	BL8R	8.5
CL2R	6.3	CL4R	8.0	CL8R	7.9
DH2R	5.6	DH4R	6.3	DH8R	7.9
AH2S	9.1	AH2S	7.8	AH8S	9.5
AL2S	8.1	AL2S	8.2	AL8S	10.4
BH2S	8.9	BH2S	7.1	BH8S	9.4
BL2S	8.1	BL2S	8.0	<i>BL8S</i>	<i>10.2</i>
CL2S	4.2	CL2S	6.8	CL8S	8.0
DH2S	9.0	DH2S	7.9	DH8S	10.3

Table 78: Waiting time percentage W for each setup tested. Best setup in italics.

	<i>Dw</i> ≤1	1< <i>Dw</i> ≤2	<i>Dw</i> >2
<i>Literature data</i>	29	50	21
<i>Custom simulator</i>	23 (L: -6)	66 (L: +16)	11 (L: -10)
<i>Generic simulator setup</i>			
AH2R	34 (L: +5; C: +11)	30 (L: -20; C: -36)	36 (L: +15; C: +25)
AL2R	31 (L: +2; C: +8)	30 (L: -20; C: -36)	40 (L: +19; C: +29)
BH2R	42 (L: +13; C: +19)	29 (L: -21; C: -37)	29 (L: +8; C: +18)
BL2R	39 (L: +10; C: +16)	30 (L: -20; C: -37)	31 (L: +10; C: +20)
CL2R	40 (L: +11; C: +17)	28 (L: -22; C: -38)	32 (L: +11; C: +21)
DH2R	37 (L: +8; C: +14)	29 (L: -21; C: -37)	34 (L: +13; C: +23)
AH4R	34 (L: +5; C: +11)	30 (L: -20; C: -36)	36 (L: +15; C: +25)
AL4R	32 (L: +3; C: +9)	30 (L: -20; C: -36)	38 (L: +17; C: +27)
BH4R	43 (L: +14; C: +20)	32 (L: -18; C: -34)	25 (L: +4; C: +14)
BL4R	42 (L: +13; C: +19)	30 (L: -20; C: -36)	28 (L: +7; C: +17)
CL4R	38 (L: +9; C: +15)	34 (L: -16; C: -32)	27 (L: +6; C: +16)
DH4R	39 (L: +10; C: +16)	30 (L: -20; C: -32)	31 (L: +10; C: +20)
AH8R	34 (L: +5; C: +11)	31 (L: -19; C: -35)	35 (L: +14; C: +24)
AL8R	29 (L: 0; C: +6)	36 (L: -14; C: -30)	35 (L: +14; C: +24)
BH8R	42 (L: +13; C: +19)	33 (L: -17; C: -33)	25 (L: +4; C: 14)
BL8R	40 (L: +11; C: +17)	35 (L: -15; C: -31)	25 (L: +4; C: +14)
CL8R	39 (L: +10; C: +16)	33 (L: -17; C: -33)	28 (L: +7; C: +17)
DH8R	39 (L: +10; C: +16)	31 (L: -19; C: -35)	30 (L: +9; C: +19)
AH2S	32 (L: +3; C: +9)	29 (L: -21; C: -37)	39 (L: +18; C: +28)
AL2S	28 (L: -1; C: +5)	30 (L: -20; C: -36)	42 (L: +21; C: +31)
BH2S	42 (L: +13; C: +19)	29 (L: -21; C: -37)	29 (L: +8; C: +18)
BL2S	37 (L: +8; C: +14)	32 (L: -18; C: -34)	31 (L: +10; C: +20)
CL2S	37 (L: +8; C: +14)	29 (L: -21; C: -37)	34 (L: +13; C: +23)
DH2S	36 (L: +7; C: +13)	28 (L: -22; C: -38)	36 (L: +15; C: +25)
AH4S	32 (L: +3; C: +9)	34 (L: -16; C: -32)	35 (L: +14; C: +24)
AL4S	29 (L: 0; C: +6)	31 (L: -19; C: -35)	40 (L: +19; C: +29)
BH4S	41 (L: +12; C: +18)	32 (L: -18; C: -34)	26 (L: +5; C: +15)
BL4S	39 (L: +10; C: +16)	31 (L: -19; C: -35)	29 (L: +8; C: +18)
CL4S	39 (L: +10; C: +16)	31 (L: -19; C: -35)	30 (L: +9; C: +19)
DH4S	37 (L: +8; C: +14)	31 (L: -19; C: -35)	32 (L: +11; C: +21)
AH8S	31 (L: +2; C: +8)	33 (L: -17; C: -33)	35 (L: +14; C: +24)
AL8S	28 (L: -1; C: +5)	37 (L: -13; C: -29)	35 (L: +14; C: +24)
BH8S	43 (L: +14; C: +20)	32 (L: -18; C: -34)	25 (L: +4; C: +14)
<i>BL8S</i>	<i>39 (L: +10; C: +16)</i>	<i>37 (L: -13; C: -29)</i>	<i>25 (L: +4; C: +14)</i>
CL8S	38 (L: +9; C: +15)	32 (L: -18; C: -34)	30 (L: +9; C: +19)
DH8S	37 (L: +8; C: +14)	31 (L: -19; C: -35)	31 (L: +10; C: +20)

Table 79: Pedestrians' frequency percentage distribution for each distance class: comparison of the setup tested with the generic simulator with the literature distributions (L) [134] and the custom simulator distributions (C). Best setup in italics.

11.6 Detailed flood simulation outputs

11.6.1. Flood risk maps

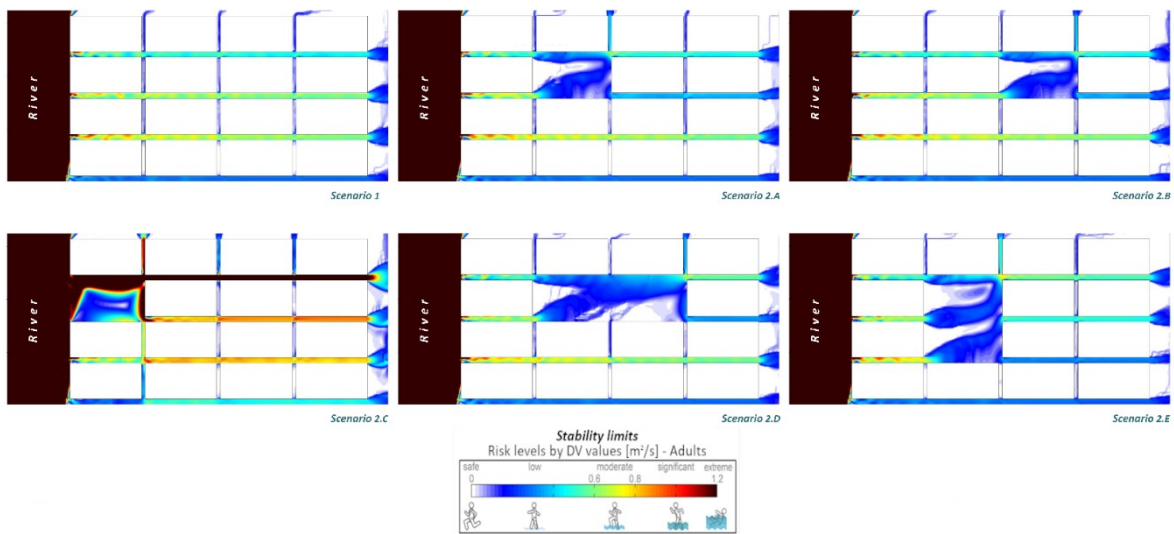


Figure 85: Local D_fV_f conditions in the outdoor spaces for each typological POS, affecting stability. Data are shown according to the $1\text{ m} \times 1\text{ m}$ solving mesh, by including the continuous scale representation of D_fV_f values (on the bottom).

CASE STUDY		OUTPUTS			
Scenario	Strategy	$t_{\max, \text{evac}}$ [s]	d_{\max} [m]	n_a [pp]	f_{e95} [pp/s]
1	Leaving	460	278.37	0	0.53
	Sheltering	131	82.56	0	1.82
2.A	Leaving	436	277.85	0	0.57
	Sheltering	128	82.44	0	1.98
2.B	Leaving	440	276.43	0	0.57
	Sheltering	128	80.59	0	1.98
2.C	Leaving	1200	265.79	156	0.18
	Sheltering	1200	82.45	93	1.07
2.D	Leaving	413	276.44	0	0.62
	Sheltering	127	79.95	0	2.14
2.E	Leaving	422	276.26	0	0.67
	Sheltering	126	83.88	0	2.00

Table 80: results from evacuation simulations.

11.6.2. Symbols and acronyms

Notation	Unit of measure	Macroscopic (M) or microscopic (m)	Definition
A_i	$[\text{m}^2]$	m	area of a specific outdoor space i
b	[m]	n.a.	parallel (with respect to the river) base of the building blocks based on a rectangular shape representation and perpendicular length l [m]
D	[m]	n.a.	floodwater depth
d_{\max}	[m]	M	longest evacuation path according to the evacuation simulation results
$d_r, d_{r, \text{MAX}}$	[m]	m	the Euclidean distance between the river axis and the barycentre of the outdoor space or sub-space, and the related maximum value considering the outdoor spaces in the POS

Notation	Unit of measure	Macroscopic (M) or microscopic (m)	Definition
$D_{r,m}$	[-]	m	normalized distance from the outdoor space to the river
$D_{t,M}$	[-]	M	normalized traveled distance based on the evacuation simulation results
DV	[m ² /s]	n.a.	multiplication between the floodwater depth D and speed V
$DV_{a,M}$	[m ² /s]	M	average DV value weighted by the outdoor space areas
DV_i	[m ² /s]	m	DV value suffered by the pedestrians in the considered outdoor space i
$DV_{max,i}$	[m ² /s]	M	maximum value of DV during the simulation time, for all the outdoor spaces i
f_{e95} , $f_{e95,MAX}$	[pp/s]	M	pedestrian flow at the gathering areas calculated considering the 5 th to 95 th percentiles of pedestrians, and related maximum value
$F_{e,M}$	[-]	M	normalized pedestrian flow based on the evacuation simulation results
POS	acr	acr	Public Open Space
IDV_M	[-]	M	stability index for the whole POS
IDV_m	[-]	m	stability index for each outdoor area
l	[m]	n.a.	perpendicular (with respect to the river) length of the building blocks based on a rectangular shape representation
KPI	acr	acr	Key Performance Indicator
M	[m ³ /m]	m	floodwater flow specific force for width unit
n_a	[pp]	M	number of pedestrians unable to arrive in a gathering area
$N_{a,M}$	[-]	M	percentage of non-arrived pedestrians based on the evacuation simulation results
$N_{a,m}$	[Boolean]	m	presence of trapped pedestrians in a given outdoor space based on the evacuation simulation results
P	[pp]	M	whole number of simulated pedestrians
RI	[-]	n.a.	generic Risk Index
$RI_{evac,M}$	[-]	M	mesoscale RI without pedestrian evacuation behaviors
$RI_{evac,m}$	[-]	m	microscale RI without pedestrian evacuation behaviors
$RI_{POS,M}$	[-]	M	mesoscale RI with pedestrian evacuation behaviors
$RI_{POS,m}$	[-]	m	microscale RI with pedestrian evacuation behaviors
$T_{e,M}$	[-]	M	normalized evacuation time based on the evacuation simulation results
$t_{max,evac}$	[s]	M	maximum evacuation time according to the evacuation simulation results
t_{sim}	[s]	M	overall simulation time
V	[m/s]	n.a.	floodwater speed
V_p, V_{p_i}	[m/s]	m	general pedestrian evacuation speed, and speed depending on DV_i
w_k	[-]	n.a.	weight of each parameter in RI calculation according to the Analytical Hierarchy Process

Table 81: list of symbols and Acronyms used in the main text of this work, including the application to macroscopic or microscopic assessment purposes. "acr" is used for acronyms while "n.a." in the macroscopic/microscopic column implies that no assignment can be done to the variable.

11.7 Mathematical methods for evacuation plan optimization

11.7.1. A minimum cost flow-based Integer Linear Program

Integer Linear Programs consist of three components: 1) a set of integer decision variables codifying the quantitative features of decision strategies; 2) a linear objective function indicating the optimization criteria for evaluating solution quality; 3) a set of linear constraints defining the feasible region, i.e., the variables' values that describe allowed decision strategy.

On the basis of the classical linear formulation of the minimum cost flow problem, i.e., the problem of sending the flow supplied from a given set of source nodes of a network G to a given set of sink nodes of G at the minimum cost, an Integer Linear Program (ILP) for solving the optimal evacuation problem is presented in this section. Under the classical assumptions of time-constant and conservative flows -the former states that the network is in a stationary state and the latter that the total amount of flow entering each node u , including the quantity $p_u > 0$ supplied from outside, must be equal to the total amount of flow leaving the node including the quantity $p_u < 0$ absorbed from the outside- we study the evacuation problem modeling the routes of pedestrians as a flow throughout a given network. In our case, the network $G = (V, E)$, where V is the set of nodes and E is the set of links, is uncapacitated and oriented, i.e. each link (u,v) has a capacity u_{uv} unbounded (which is consistent with the number of simulated pedestrians) and can be crossed only by a flow from u to v and not vice-versa.

The optimal evacuation problem can be stated as: “given a street network, locate at most M gathering areas, and find the pedestrians' evacuation routes of the minimum total cost”. Graph G is the representation of the street network of the typological POS (see sections §3.3.3 and §3.5.5.2), where the set V of nodes are the pedestrians' starting points (every node in the map) and $V_s \subseteq V$ are the subset of potential gathering areas (nodes circled in red).

Nodes in V are associated with reference points of the streets and of the square. Links in E (in green) model both the segments of streets and elementary routes in the square. Due to the considered application, directed links model the possible directions of the pedestrian evacuation, which generally are from the source of risk and cannot be upstream [134], [186]. It follows that the streets parallel to the river, which therefore can be traveled in both directions, are represented by bidirectional links (or equivalently by non-oriented links). On the other hand, perpendicular and oblique streets induce oriented links in the graph moving away from the river, with the only exception for the “dead-end” streets furthest from the river that can only be left by moving upstream to remain within the boundaries. The cost c_{uv} of each link (u,v) is computed according to the pedestrian speed, stability, and effort on the flooded streets by considering the hydrodynamic conditions of the floodwater spreading within the urban area as indicated in sections §3.6 (flood modeling criteria), and §8.1 (following results).

According to the case study description, the instance of the graph considered presents $|V| = 41$ starting points, $|E| = 130$ links, and $|P| = 240$ pedestrians that, before the event, have been randomly distributed among the starting points. As a result, 86 pedestrians have been allocated to the square, 11 pedestrians to each street perpendicular to the river, and 4 pedestrians to each street parallel to the river [186].

Moreover, $|V_s| = 12$, i.e., 12 nodes of G are potential gathering areas, basically corresponding to (quasi-)dry areas (i.e., $D_f V_f \approx 0 \text{ m}^3/\text{s}$), chosen according to the hydrodynamic conditions reported in

a recent previous study [186]. In particular, potential gathering areas located in the midpoints of the parallel streets simulate the entrance to indoor safe areas, while those in the square simulate an outdoor safe area.

Dummy nodes and connections are added to V and E in order to formulate the optimal evacuation problem on G in terms of a particular minimum cost network flow problem on a new graph G' . Given the graph G in Figure 86(a), which is a subgraph of the street network associated with the urban area, Figure 86(b) depicts the graph G' obtained by adding the blue nodes and the dotted links. In details:

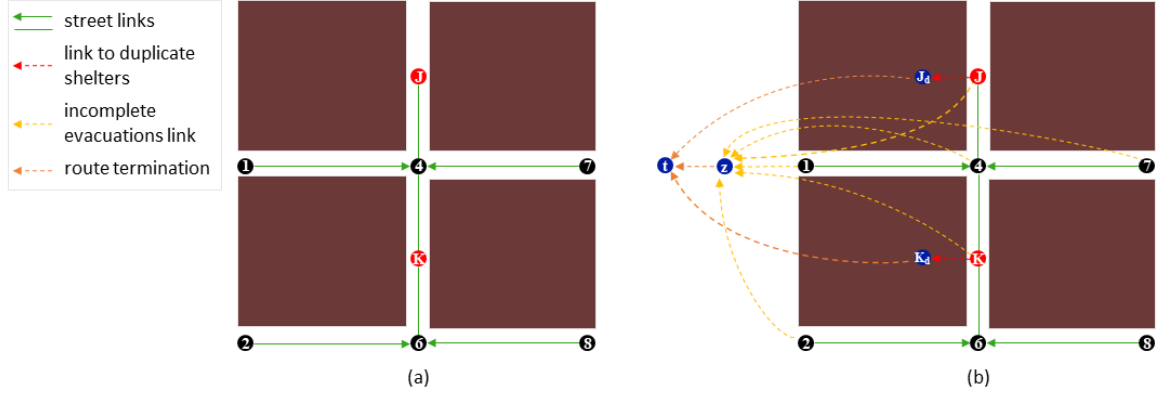


Figure 86: (a) subgraph of the street network; (b) subgraph obtained considering the dummy nodes (in blue) and related link (dotted). Legend on the left (orientated links are the green arrows, non-orientated links are the green lines).

- For each potential gathering area $u \in V_s$, a new node w with $p_w = 0$ is introduced, along with an oriented link (u, w) with $c_{uw} = 0$ (dotted red links in Figure 86(b)). The set V_d , indeed a duplicate of V_s , allows the incoming flow at node $u \in V_s$ to exit the network from the same node u at zero cost, i.e., it allows the pedestrians whose starting point is also a potential gathering area to select that gathering area without moving.
- A new node z with $p_z = 0$ is added and then linked at cost $c_{uz} = C$ (dotted ochre links in Figure 86(b)) to each starting node $u \in V \setminus V_d$. The node z is needed to balance the flow of pedestrians who cannot complete the evacuation. The constant C is sufficiently large to ensure that, in any optimal solution, a pedestrian chooses the destination z if and only if (s)he cannot reach any potential gathering area.
- A sink node t with $p_t = -|P|$ is added and connected by oriented links (u, t) of cost $c_{ut} = 0$ to all the nodes in $V_d \cup \{z\}$ (dotted orange links in Figure 86(b)). The sink t is used to balance the whole incoming/outgoing flow in the network since it absorbs, at no cost, all the $|P|$ units of flow coming from either the nodes in V_d (successful evacuations) or from node z (uncompleted evacuations).

In summary, the extended graph G' of the urban area has $|V| = 55$, $|V_d| = 12$, and $|E| = 130$ and, given its size, we do not explicitly report it. On the other hand, the notation used in this section is reported in the next subsection.

$$V_s \subseteq V p_u^k p_u = \sum_{k \in P} p_u^k p_t = -|P| f_{uv}^k \begin{cases} = 1 \\ = 0 \end{cases} y_u \begin{cases} = 1 \\ = 0 \end{cases}$$

The parameter p_u^k is set to one if the node u is the starting point of the pedestrian k , and 0 otherwise. Thus, $p_u = \sum_{k \in I} p_u^k$ is the total amount of pedestrians starting the evacuation from node u .

Moreover, we recall that M is the maximum number of nodes of V_s that can be selected as gathering areas.

The model is defined on the vectors of decision variables $\mathbf{f} \in \{0,1\}^{|P| \times |E|}$ and $\mathbf{y} \in \{0,1\}^{|V_d|}$: $f_{uv}^k = 1$ if and only if the pedestrian k walks the link (u,v) , whereas $y_u = 1$ if and only if the node u is selected as gathering area (actually, y_u refers to the node in V_d which is the duplicate of the node u in V_s).

About the ILP constraints, the classical flow-balancing equalities of the minimum cost flow problem read as:

$$\sum_{\substack{v \in V: \\ (v,u) \in E}} f_{vu}^k + p_u^k = \sum_{\substack{v \in V: \\ (u,v) \in E}} f_{uv}^k \quad \forall k \in P, u \in V \quad (17.1)$$

Enforcing the network to be conservative, the constraint ensures that a pedestrian k enters a node $u \in V$, because starting from it ($p_u^k = 1$) or arriving from an incoming link (v, u) , must leave it through one of the outgoing links (u, v) . Since the sink node t has no outgoing links, we can sum up the pedestrians and obtain:

$$\sum_{k \in P} \sum_{u \in V_d \cup \{z\}} f_{ut}^k = -p_t \quad (17.2)$$

which imposes, by recalling that $p_t = -|P|$, all the pedestrians to reach the sink.

Further inequalities are required to control the gathering areas' selecting variables \mathbf{y} :

$$\sum_{k \in P} \sum_{\substack{v \in V: \\ (v,u) \in E}} f_{vu}^k \leq |P| \cdot y_u \quad \forall u \in V_d \quad (17.3)$$

If any pedestrian k reaches the gathering area located at node u (actually at its duplicated node in V_d), then the gathering area u must be selected ($y_u = 1$). In that case, i.e., when $y_u = 1$, the constraint does not restrict the capacity of the gathering area, being $|P|$ an upper bound to the number of pedestrians that can reach the node u . If otherwise $y_u = 0$, then the evacuation from the gathering area u is not allowed.

The last constraint just bounds from above the number of selected gathering areas to M :

$$\sum_{u \in V_d} y_u \leq M \quad (17.4)$$

A minimum total cost flow on G' describes an optimal evacuation plan. Then, the objective function is given by:

$$\min \sum_{k \in P} \sum_{(u,v) \in E} c_{uv} f_{uv}^k \quad (17.5)$$

The above ILP models the case where a single decision-maker (the coordinator of the evacuation operations) computes evacuation routes in a centralized fashion and assigns them to pedestrians. Moreover, minimizing the sum of costs, the objective function (6) assumes a collaborative dynamic of groups where a single pedestrian could accept a difficult evacuation route if this choice helps many other pedestrians. However, alternative objective functions, e.g., minimizing the cost of the most difficult pedestrian's path, could be implemented in order to equally rescue all the pedestrians.

The above single objective function actually implements a hierarchical optimization between two objectives: minimizing the number Z of the pedestrians unable to complete the evacuation and, for the same Z , minimizing the total cost of the successful evacuations. Such a hierarchy is obtained by choosing the cost C of the links (u, z) large enough. Other than prioritizing the intrinsic value of life, the above hierarchical optimization avoids typical drawbacks of the multi-objective optimization [227] such as the extensive computation of the optimal Pareto frontier, or the sensitivity analysis on weights associated with the convex combination of terms.

If G is a strongly connected and uncapacitated network, the problem boils down to the optimal selection of gathering areas, which in any case is not trivial since $|P| \gg M$ in general. Indeed, given a selection \bar{y} of gathering areas, each pedestrian has a feasible evacuation route (G strongly connected), and such route corresponds to the minimum cost route (e.g., the shortest path) from the pedestrian starting point to t (G uncapacitated). Therefore, for a given selection \bar{y} of gathering areas, the optimal solution is simply the collection of the pedestrians' shortest routes. Nevertheless, this work considers that G is only weakly connected. Thus, not all the selections \bar{y} of gathering areas, or even none of them, guarantee a successful evacuation route for each pedestrian. Indeed, as discussed in Section 3, optimal solutions of the case study have $Z > 0$.

Clearly, the shortest evacuation routes are non-longer independent of each other in the case of capacitated networks due to the presence of saturated links that may force one or more pedestrians to deviate from their own optimal route. This naturally increases the total cost of solutions, both by augmenting the cost of completed evacuations and the occurrences of uncompleted evacuations.

The proposed ILP is solved through the commercial package IBM-CPLEX³⁷. The experiments aimed to identify the optimal solutions according to three different link costs c_{uv} , evaluated in combination with a range of values for the gathering area availability M .

For $I \hat{=} \{s, q, c\}$, Table 82 reports the details specifying the behavioral approach for the route choice leading to the settings of the link costs: the first approach chooses the *shortest* routes to minimize the evacuation length, the second one looks at the *quickest* routes to reduce the evacuation time, the third one minimizes the evacuation effort through *cheapest* routes.

i	Route choice behaviors	Criteria for the optimal solution calculation	Link Cost c
s	Shortest	Minimization of the evacuation length	S [m]
q	Quickest	Minimization of the evacuation time	T [s]
c	Cheapest	Minimization of the evacuation effort	$DfV_f \cdot S$ [m ³ /s]

Table 82: Definition of the behavioral approaches for the path choice and their computation method depending on the link cost. Links with $D \geq 1.20m$, $V \geq 3.00m/s$, or $DfV_f \geq 1.20m^2/s$ cannot be traveled [227]. The time T is evaluated as the ratio between S and v_l in each link.

As a result, 36 scenarios (i, M) are defined by combining the link cost type $i \hat{=} \{s, q, c\}$ and the number of available gathering areas $M \hat{=} \{1, 2, \dots, 12\}$. An optimal solution $[\mathbf{f}^*, \mathbf{y}^*]_{(i,M)}$ has been computed for each scenario (i, M) , where $Z_{(i,M)}$ is the minimum number of pedestrians unable to complete the evacuation, and $C_{(i,M)}$ is the total cost given by Eq. (6). The optimal solution describes the selection $\mathbf{y}^*_{(i,M)}$ of gathering areas, the evacuation route $\mathbf{f}^*_{(i,M)}$ from the starting node to the gathering areas of each pedestrian, the number $Z_{(i,M)}$ of pedestrians unable to complete the evacuation, and an array

³⁷ <https://www.ibm.com/it-it/analytics/cplex-optimizer> (last access: 03/01/2023)

$C_{AVG(i,M)} = [S_{AVG}; T_{AVG}; DfV_f S_{AVG}]_{(i,M)}$ listing the mean cost values restricted to the $|P| - Z_{(i,M)}$ successful evacuation routes.

11.7.2. Symbols and abbreviations

PARAMETERS	MEANING
$V = \{1, \dots, V \}$	set of nodes, including the dummy nodes t, z , and the dummy nodes in V_d
$V_s \subseteq V$	subset of potential gathering area nodes
$E = \{1, \dots, E \}$	set of links
$P = \{1, \dots, P \}$	set of pedestrians
p_u^k	= 1 if the pedestrian k starts the evacuation from the node u and = 0 otherwise
$p_u = \sum_{k \in P} p_u^k$	total number of pedestrians starting evacuation from node $u \neq t$
$p_t = - P $	total flow absorbed by sink node t
c_{uv}	cost of the link (u,v) between nodes u and v
C	upper bound to the costs c_{uz} with $u \in V \setminus V_d$
M	maximum number of evacuation points

Table 83: ILP model – notation

11.7.3. KPIs and RI detailed results

M	$S_{AVG(i,M)}$	$T_{AVG(i,M)}$	$DV S_{AVG(i,M)}$	$Z_{(i,M)}$	$d_{(i,M)}$	$t_{(i,M)}$	$dvs_{(i,M)}$	$mp_{(i,M)}$	RI _(i,M)
1	97	156	62	123	0.86	0.88	1.00	0.51	0.71
2	80	128	50	88	0.71	0.72	0.80	0.37	0.56
3	52	82	26	88	0.46	0.46	0.43	0.37	0.40
4	42	66	19	88	0.37	0.37	0.31	0.37	0.36
5	40	63	19	88	0.36	0.36	0.31	0.37	0.35
6	38	60	19	88	0.34	0.34	0.31	0.37	0.35
7	37	59	19	88	0.33	0.33	0.30	0.37	0.35
8	36	58	19	88	0.32	0.32	0.31	0.37	0.35
9	35	56	19	88	0.31	0.32	0.30	0.37	0.34
10	34	54	18	88	0.30	0.31	0.30	0.37	0.34
11	33	53	18	88	0.29	0.30	0.30	0.37	0.34
12	33	53	18	88	0.29	0.30	0.30	0.37	0.34

Table 84: evacuation parameters, Key Performance Indicators, and Risk Index values for $i=s$ (Approach for the route choice: “shortest”; minimization of S_{AVG}). Values in bold indicate overall maximums for normalization purposes (see Table 22).

M	$S_{AVG(2,M)}$	$T_{AVG(2,M)}$	$DVS_{AVG(2,M)}$	$Z_{(2,M)}$	$d_{(2,M)}$	$t_{(2,M)}$	$dvs_{(2,M)}$	$mp_{(2,M)}$	$RI_{(2,M)}$
1	97	156	62	123	0.86	0.88	1.00	0.51	0.71
2	80	128	50	88	0.71	0.72	0.80	0.37	0.56
3	52	82	26	88	0.46	0.46	0.43	0.37	0.40
4	42	66	19	88	0.37	0.37	0.31	0.37	0.36
5	40	63	19	88	0.36	0.36	0.31	0.37	0.35
6	38	60	19	88	0.34	0.34	0.31	0.37	0.35
7	37	58	18	88	0.33	0.33	0.30	0.37	0.35
8	36	57	18	88	0.32	0.32	0.29	0.37	0.35
9	35	55	18	88	0.31	0.31	0.29	0.37	0.34
10	34	54	18	88	0.30	0.30	0.29	0.37	0.34
11	33	52	18	88	0.29	0.29	0.29	0.37	0.34
12	33	52	18	88	0.29	0.29	0.29	0.37	0.34

Table 85: evacuation parameters, Key Performance Indicators, and Risk Index values for $i=q$ (Approach for the route choice: “quickest”; minimization of T_{AVG}). Values in bold indicate overall maximums for normalization purposes (see Table 22).

M	$S_{AVG(3,M)}$	$T_{AVG(3,M)}$	$DVS_{AVG(3,M)}$	$Z_{(3,M)}$	$d_{(3,M)}$	$t_{(3,M)}$	$dvs_{(3,M)}$	$mp_{(3,M)}$	$RI_{(3,M)}$
1	113	178	62	123	1.00	1.00	1.00	0.51	0.76
2	93	146	49	88	0.82	0.82	0.80	0.37	0.60
3	53	83	26	88	0.47	0.47	0.43	0.37	0.41
4	43	67	19	88	0.38	0.38	0.31	0.37	0.36
5	42	66	19	88	0.37	0.37	0.30	0.37	0.35
6	40	63	18	88	0.35	0.35	0.30	0.37	0.35
7	38	60	18	88	0.34	0.34	0.29	0.37	0.35
8	37	58	18	88	0.33	0.33	0.29	0.37	0.35
9	36	57	18	88	0.32	0.32	0.29	0.37	0.34
10	35	55	18	88	0.31	0.31	0.29	0.37	0.34
11	34	54	18	88	0.30	0.30	0.29	0.37	0.34
12	34	54	18	88	0.30	0.30	0.29	0.37	0.34

Table 86: evacuation parameters, Key Performance Indicators, and Risk Index values for $i=c$ (Approach for the route choice: “cheapest”; minimization of DfV_jS_{AVG}). Values in bold indicate overall maximums for normalization purposes (see Table 22).

11.8 Characterization of the flood event

The hydrodynamic simulation is based on the flood event registered in 18/11/1975 at Moie (AN) station in the Esino River, whose maximum measured flow rate was $Q_{MEAS} = 442 \text{ m}^3/\text{s}$, as shown in Figure 87 (gray line). This event has been introduced in the hazard modeling for the POSs scenarios, by deriving the maximum flow rate of the studied river cross-section $Q_{SECTION} [\text{m}^3/\text{s}]$ as in Eq. 18.1:

$$Q_{SECTION} = k_s A R_h^{2/3} \sqrt{i} \tag{Eq. 18.1}$$

In which:

- $k_s [\text{m}^{1/3}/\text{s}]$ is the Strickler hydraulic roughness of the riverbed material, assumed equal to $33 \text{ m}^{1/3}/\text{s}$;
- $A [\text{m}^2]$ is the cross-sectional area of flow;
- $R_h [\text{m}]$ is the hydraulic radius, which is the ratio between the cross-sectional area of flow and the wetted perimeter;
- $i [\%]$ is the riverbed slope, which is equal to 0.3%.

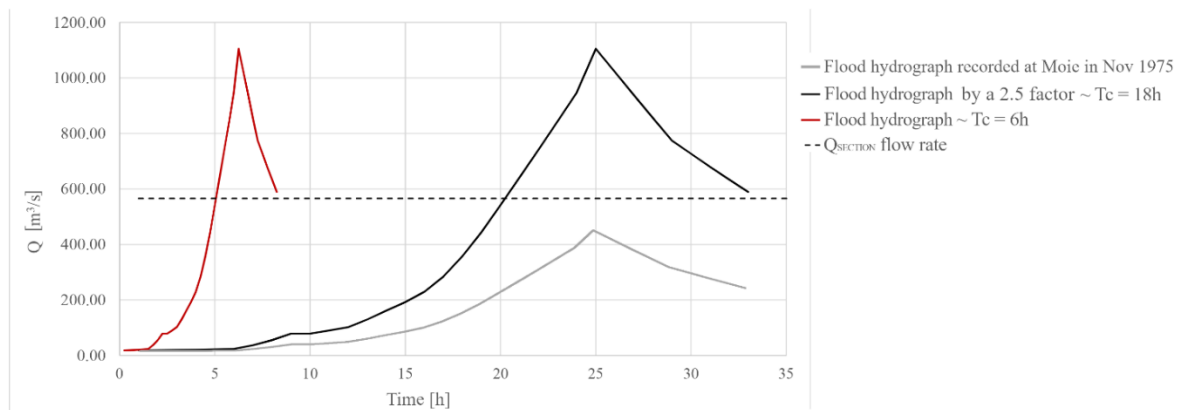


Figure 87: Flood hydrographs comparison with respect to $Q_{SECTION}$ (dashed line): measured data, by the gray curve [275], data incremented by a 2.5 factor (concentration of 18 hours), by the black curve, data used in the POS simulation (concentration of 6 hours), by the red line.

Since $Q_{SECTION}$ ($566 \text{ m}^3/\text{s}$) resulted higher than Q_{MEAS} ($442 \text{ m}^3/\text{s}$), this configuration could not imply any floods in the given area. To this end, a new flood hydrograph is obtained by multiplying the original one (relating to Q_{MEAS}) with an amplification factor equal to 2.5. As shown in Table 87, applying the theory of Giandotti [276], we obtain a 100-yr maximum flow rate of $1148 \text{ m}^3/\text{s}$, which is consistent with previous estimations for the case study [275]. The Moie River gauge was operative until 1978 and, until now, no event with a comparable peak flow rate has been measured.

Return Time	20 years	50 years	100 years	200 years	300 years	500 years
$Q [\text{m}^3/\text{s}]$	894	1039	1148	1256	1320	1399

Table 87: Flow rate values for different return times for Esino River, Moie section.

Due to the excessive duration of the time of concentration (18 hours), the final hydrograph has been modified by considering a time of concentration of 6 hours. This choice allows for reducing the time span able to influence the evacuation process by inducing critical motion conditions for pedestrians. In this way, the overflow determined by the flood event is condensed into three hours, with almost an hour necessary to reach the maximum flow rate from its beginning. Figure 87 compares the flood hydrographs for the aforementioned considered conditions, by showing the one adopted in POS-related simulations by the red curve.

Acknowledgements

My academic journey has been a rollercoaster, fluctuating between highs and some deep lows, feeling appreciated while sometimes betrayed by my own homeland. Until I moved to UNIVPM, where I finally found my own dimension, and to whom I really owe a lot to for giving me the chance to prove someone wrong. Not me though. I have never really doubted about myself, honestly.

I am deeply grateful to Professor Enrico Quagliarini for having trusted me, helping me to bring out my best, and for giving me the opportunity to interact with different researchers and research areas, as well as the freedom to delve into them without constraints. And last but not least, for allowing me to travel thanks to the results of our efforts.

Deepest thanks to Professor Marco D’Orazio who introduced me to the topics covered in this thesis since my first approach to the world of research during my master’s degree thesis, and which I had the opportunity to explore in depth in this work.

Special thanks also to my co-supervisors. Gabriele Bernardini, for guiding me in the “transition” from student to PhD candidate like an older brother, for spoiling me some “tricks of the trade”, and for doing so in the most informal and colloquial manner. Professor Giuseppe Pace, for rewarding our collaboration with the publication of a book, of which I am honored to be a co-author. To me, it is gratifying to have contributed to the development of a valuable resource for insiders and practitioners, made possible also by the support of the regional engineering association.

I would also like to express my gratitude to Professor Fabrizio Marinelli for his willingness to collaborate giving credit to my proposals, and for sharing his expertise despite operating in different research areas. I would be happy to delve deeper into what has been done in this thesis in the future.

Finally, thanks to everyone who had the opportunity to collaborate and/or share their time with me over these years, and in particular to each member of the DICEA department, present and past, who have enriched me as a person and as a colleague.

It really means a lot to me.

I hope it was as fun for you as it was for me.

Dedication

Non ho mai dato troppo peso ai traguardi che ho raggiunto in passato perché in realtà non ci ho mai trovato niente di straordinario. Dopotutto ho sempre e solo fatto ciò che gli altri si aspettavano da me, ciò che avrei dovuto fare. Ed è proprio per questo che non ho mai speso dediche e parole dolci per nessuno: in verità per delle persone straordinarie avrei voluto qualcosa di, appunto, straordinario.

A dirla tutta nemmeno questa volta credo di esserci riuscito, è cambiata però la prospettiva con cui guardo le cose. Mi sono reso conto che non è detto che avrò occasioni migliori, che non tutti diamo lo stesso peso alle cose, e soprattutto che il peso di una dedica assume valore in base a chi la riceve e non a chi la fa.

Chi si aspettava di leggere dei nomi in queste righe probabilmente rimarrà deluso. Invece i destinatari non hanno bisogno di leggerli perché sanno che sono rivolte a loro. E che una dedica su un foglio di carta non ha nulla di straordinario rispetto a quanto lo sono loro per me.

List of Tables

Table 1: survey form for the data collection. Mechanical parameters symbology: f = compressive strength; E = elastic modulus, τ_0 = shear strength (from diagonal compression, to be used for irregular masonry), f_{v0} = shear strength (frictional strength at unit-mortar interface without compression, to be used for regular and irregular masonry), G = shear modulus.	24
Table 2: experimental database sample composition organized by masonry typology and mechanical parameter measured (compressive strength f and elastic modulus E through double flat-jack tests). ID = M indicates masonry typologies included in the INS, and ID = MX indicates non-included typologies. *Non-normal distributions are indicated in italics. DFJT = double flat-jack tests. Masonry typologies translation from Boschi et al. (2018) [165].	26
Table 3: experimental database sample composition organized by masonry typology and mechanical parameter measured (shear strength τ_0 and f_{v0} , distinguished according to the INS failure mode, namely for diagonal compression or for mortar joint failure). Only one shear modulus value (G) has been registered for the masonry typology M7. ID = M indicates masonry typologies included in the INS, and ID = MX indicates non-included typologies. DCT = diagonal compression tests; VFJT = vertical flat-jack tests; ST = shove tests. Masonry typologies translation from Boschi et al. (2018) [165].	27
Table 4: Case studies selected for the creation of the typological HCC.	29
Table 5: Results from statistical analyses of case studies to define base features of the base typological POSs as in Figure 10-A (Scenario 1).	33
Table 6: Description of Scenarios 2 as in Figure 10-B, by defining the square characterization. Mode parameters are assumed for the POSs, as in Table 5.	34
Table 7: Summary of the users' temporalities according to the types of areas. W is for Working days, H is for Holidays (full list of abbreviations in Section §11.3.1, Appendices).	38
Table 8: Summary of the users' temporalities according to the age range and familiarity with the POS. W is for Working days, H is for Holidays (full list of abbreviations in Sections §11.3.1, Appendices).	39
Table 9: POSC-related KPIs.	40
Table 10: UHC-related KPIs.	41
Table 11: UDC-related KPIs.	41
Table 12: Parameters to quantify the number of people [pp] featured in the videotapes.	48
Table 13: Statistical frequencies of behaviors (and their meaning), evaluated with respect to the number of people (according to Table 12) and the floodwater conditions (in terms of water depth and flow).	49
Table 14: Setup code for the servers' position by considering their number and distance with respect to the side of the floor (i.e., the walls of the buildings).	53
Table 15: List of parameters for the comparison between the generic and the custom simulator.	54
Table 16: KPIs to perform the comparison between the graphical outputs (evacuation curves EC and D_w trends) and their meaning [155], [162].	54
Table 17: Numerical outputs comparison criteria: as the custom simulator does not consider deadlocks in the building attraction, W outputs are discussed independently to evaluate the impact of the queuing phenomena on the evacuation timing in the generic simulator.	55
Table 18: KPIs for the microscale and mesoscale risk assessment concerning physical vulnerability and hazard.	58
Table 19: KPIs for the mesoscale and microscale risk assessment concerning pedestrian evacuation behaviors.	59
Table 20: weights W_k for RI with pedestrian evacuation behaviors obtained via Analytic Hierarchy Process.	60
Table 21: Definition of the approaches for the path choice and their calculation method depending on the link cost. Links with $D \geq 1.20\text{m}$, $V \geq 3.00\text{m/s}$, or $D_f V_f \geq 1.20\text{m}^2/\text{s}$ cannot be traveled [227]. The time T is evaluated as the ratio between S and v_i in each link.	63
Table 22. Key Performance Indicators calculation method and definition.	64
Table 23: Comparison between the river basin of the selected case studies (§3.3) and the one adopted for hazard modeling.	65
Table 24: E/f ratios [-] singularly evaluated for each masonry typology and on average, considering: the overall sample (AVG), the stone masonries sample (STO, that include typologies from M1 to M6), and the brick masonries sample (BR, that include typologies M7, M8-sc, and M8-gm). "sc" stands for standard conditions, "gm" stands for good mortar.	76

Table 25: Comparison between the ranges of compressive strength f and elastic modulus E between historical masonries in the Marche Region (HMM) and the INS provisions considering, respectively, the current (C.19) and the previous versions (C.09, O.05, C.81, where C stands for “Circolare” and O stands for “OPCM”).	77
Table 26: Comparison between the ranges of shear strength τ_0 and elastic modulus G between historical masonries in the Marche Region (HMM) and the INS provisions considering, respectively, the current (C.19) and the previous versions (C.09, O.05, C.81, where C stands for “Circolare” and O stands for “OPCM”). (a) range based on diagonal compression test measurements (DCT); (b) range based on vertical flat-jacks test measurements (VFJT); (c) only value found.	78
Table 27: Comparison between the ranges of shear strength τ_0 and elastic modulus G between historical masonries in the Marche Region (HMM) and the current INS provisions (C.19).	78
Table 28: Outline of the typological description of the square according to the median values of UDC-related KPIs.	88
Table 29: New-observed behavior classified into the “Motion towards the evacuation target” phase.	91
Table 30: Chi-squared test outcomes. For $S > \chi^2$ the null hypothesis is rejected and provides support that the categories are related. DOF stands for Degree of Liberty. The significance level α is 0.05; p-values are < 0.00001 in all the cases.	92
Table 31: Situational frequency percentages of the observed behaviors evaluated with respect to the water depth (PI_d/PI [%]) and the water flow (PI_f/PI [%]). Behavior IDs from Figure 34.	93
Table 32: Situational frequency percentages per water depth of the observed behaviors ($PI_{d,f}/PI_d$ [%]). Behavior IDs from Figure 34, abbreviations from Figure 14.	93
Table 33: observed behaviors and frequent floodwater conditions in which they are performed.	102
Table 34: KPIs measuring differences between evacuation curves obtained from each setup tested on the generic simulator and the one obtained from the custom simulator. Results are shown in terms of mean and standard deviation values according to the grouping criteria shown in Figure 16.	108
Table 35: KPIs measuring differences between curves tracing the D_w trend for each setup tested on the generic simulator and the one obtained from the custom simulator (2 nd quartile data). Results are shown in terms of mean and standard deviation values according to the grouping criteria shown in Figure 16. Extended results for each setup are in Section §11.5.5 (Appendices).	109
Table 36: Pedestrians’ frequency percentage distribution and variability for each distance class: comparison of the setup of the generic simulator (grouped according to the criteria shown in Figure 16) with real-world observations from literature works (L) [134] and the custom simulator data (C). Avg refers to average data, Dev. St. refers to the related standard deviation of the sample. Extended results for each setup are resumed in Section §11.5.5 (Appendices).	112
Table 37: KPIs measuring differences between curves tracing the D_w trend of the generic simulator best setup (BL8S) and the custom simulator (quartile analysis).	114
Table 38: Pedestrians’ frequency percentage distribution for each distance class: comparison of the generic simulator best setup (BL8S) with the literature distributions [134] and the custom simulator distributions. Percentage differences between literature (L) and custom software (C) data are pointed out in brackets.	114
Table 39: Comparison of the maximum evacuation time t_{max} , the waiting time percentage W , and the evacuation flow F of the generic simulator best setup (BL8S): percentage differences between the custom simulator (C) and the generic software median data (G) are pointed out into brackets.	114
Table 40: $DV_{a,M}$ and $IDV_{v,M}$ values for each typical POS as graphically described in Figure 10.	119
Table 41: summary of the KPIs and values of risk indexes with ($RI_{evac,M}$) and without ($RI_{POS,M}$) pedestrian evacuation behaviors, and depending on the evacuation management strategies. The $RI_{evac,M}$ Reduction is calculated in percentage terms with respect to the $RI_{evac,M}$ in “leaving” strategy.	119
Table 42: Gathering areas selection depending on the approach for the path choice “i” and the number of gathering areas available “M” (by considering only strategies with $M \leq 4$). The map with the gathering areas’ position is shown in Figure 58.	126
Table 43: number of pedestrians present in each evacuation unit, and to be allocated to each gathering area. The differences between those quantities are the number $Z_{(i,M)}$ of pedestrians unable to complete the evacuation in each evacuation unit.	128
Table 44: RI_i values for each evacuation strategy i tested, distinguishing the values for the KPIs. Since the tested evacuation strategy is characterized by the same configuration of evacuation paths and gathering areas regardless of the route choice behavior (i.e., shortest, quickest, and cheapest), macroscopic approach outcomes are considered a unique optimal solution. *: the difference is calculated with respect to the overall initial number of pedestrians (240 pp).	129
Table 45: Masonry typologies included in the INS and reference ranges of mechanical parameters considering unreinforced panels (Tab. C8.5.I), being: f = compressive strength; E = elastic modulus, τ_0 = shear strength (from diagonal compression, to be used for irregular masonry), f_{v0} = shear strength (frictional strength at unit-mortar interface without compression, to be used for regular and irregular masonry), G = shear modulus [171], [172].	138

Table 46: Improvement coefficients provided by the INS (Tab. C8.5.II) to be applied to the standard values of the mechanical parameters (Tab C8.5.I) in the event of better conditions or strengthening interventions [171], [172]...	138
Table 47: list of double flat-jack tests (ASTM C1197 [175]) and relative measurements from literature studies, organized per masonry typology (M1 = rubble stone masonry, M5 = regular soft stone masonry, M7 = solid clay bricks masonry [171], [172]).....	145
Table 48: E/f ratio values from literature studies, organized per masonry typology (M4 = irregular soft stone masonry, M5 = regular soft stone masonry [171], [172]).	145
Table 49: compressive strength f and elastic modulus E evaluations from literature studies on Adobe masonry.....	146
Table 50: compressive strength f and elastic modulus E evaluations from literature studies on Cob masonry.....	146
Table 51: compressive strength f and elastic modulus E evaluations from literature studies on Rammed earth masonry.....	147
Table 52: Streets data (Albenga case study).....	148
Table 53: Streets data (Carrara case study).....	149
Table 54: Streets data (Colorno case study).....	150
Table 55: Streets data (Montevarchi case study).....	151
Table 56: Streets data (Senigallia case study).....	152
Table 57: Building block data (all the case studies).....	153
Table 58: Squares data (all the case studies).....	153
Table 59: Symbols and acronyms explanation.....	155
Table 60: List of case studies and their geo-localization.....	157
Table 61: Quick OLi values for different indoor areas' intended uses according to the Italian fire safety codes and methodologies, and previous works [41].	158
Table 62: Users' temporalities considering their age ranges (rows), and familiarity with areas occupied (super-columns), by including specific uses and opening times to the public both on working days (W) and Holidays (H) (sub-columns). ^A : 4% relates to at least 1 teacher over 26 students (see §11.3.3). The number of classes will have $YA=0.4pp/m^2*1000m^2=400pp$; $AU=400*4\%=16pp$. ^B : 9% relates to the percentage of unemployed users in Italy when the research was carried out.	159
Table 63: Users' age distribution of the a-th age range APa [%] in the city of Crotona.	160
Table 64: POSC-related KPIs comparison between the typological scenario (see Section §5.1) and the case study of Manfredonia.....	161
Table 65: Comparison between the typological scenario (see Section §5.2.2) and the case study of Manfredonia according to the median values of UDC-related KPIs. W stands for Working Days, H for Holidays.	161
Table 66: List of frequent by-literature human behaviors observed in the “pre-movement” phase, and their classification according to type, voluntariness, human response, and reference elements.....	165
Table 67: List of frequent by-literature human behaviors observed in the “motion towards the evacuation target” phase, and their classification according to type, voluntariness, human response, and reference elements.....	165
Table 68: List of frequent by-literature human behaviors observed in the “post-evacuation” phase, and their classification according to type, voluntariness, human response, and reference elements.....	166
Table 69: List of abbreviations.....	167
Table 70: Each setup (first column) is based on four properties coded by four symbols, and the properties characterization is discussed in each of the columns, as also shown in Table 14. Best setup in italics. Notes: * Each “first servers” group can be composed of two or three servers according to section §3.5.3.4 criteria, so the semicolon separates the value for each of them.....	171
Table 71: List of notations and references to their detailed explanation.....	172
Table 72: KPIs measuring differences between the evacuation curves obtained from each setup tested on the generic simulator and the one from the custom simulator. Best setup in italics.	173
Table 73: KPIs measuring differences between curves tracing the D_w trend for each setup tested on the generic simulator and the one obtained from the custom simulator (1 st and 3 rd quartile data). Results are shown in terms of mean and standard deviation values according to the grouping criteria shown in section §3.5.3.4. Graphical trends are shown in Figure 83 and Figure 84.....	174

Table 74: KPIs measuring differences between curves tracing the D_w trend for each setup tested on the generic simulator and the one obtained from the custom simulator (1 st quartile data). Best setup in italics.....	176
Table 75: KPIs measuring differences between curves tracing the D_w trend for each setup tested on the generic simulator and the one obtained from the custom simulator (2 nd quartile data). Best setup in italics.	177
Table 76: KPIs measuring differences between curves tracing the D_w trend for each setup tested on the generic simulator and the one obtained from the custom simulator (3 rd quartile data). Best setup in italics.	178
Table 77: Maximum evacuation time t_{max} for each setup tested. Best setup in italics.	179
Table 78: Waiting time percentage W for each setup tested. Best setup in italics.....	179
Table 79: Pedestrians' frequency percentage distribution for each distance class: comparison of the setup tested with the generic simulator with the literature distributions (L) [134] and the custom simulator distributions (C). Best setup in italics.....	180
Table 80: results from evacuation simulations.	181
Table 81: list of symbols and Acronyms used in the main text of this work, including the application to macroscopic or microscopic assessment purposes. "acr" is used for acronyms while "n.a." in the macroscopic/microscopic column implies that no assignment can be done to the variable.	182
Table 82: Definition of the behavioral approaches for the path choice and their computation method depending on the link cost. Links with $D \geq 1.20m$, $V \geq 3.00m/s$, or $D_f V_f \geq 1.20m^2/s$ cannot be traveled [227]. The time T is evaluated as the ratio between S and v_l in each link.....	186
Table 83: ILP model – notation.....	187
Table 84: evacuation parameters, Key Performance Indicators, and Risk Index values for $i=s$ (Approach for the route choice: "shortest"; minimization of S_{AVG}). Values in bold indicate overall maximums for normalization purposes (see Table 22).....	187
Table 85: evacuation parameters, Key Performance Indicators, and Risk Index values for $i=q$ (Approach for the route choice: "quickest"; minimization of T_{AVG}). Values in bold indicate overall maximums for normalization purposes (see Table 22).....	188
Table 86: evacuation parameters, Key Performance Indicators, and Risk Index values for $i=c$ (Approach for the route choice: "cheapest"; minimization of $D_f V_f S_{AVG}$). Values in bold indicate overall maximums for normalization purposes (see Table 22).	188
Table 87: Flow rate values for different return times for Esino River, Moie section.	189

List of Figures

Figure 1: Graphical illustration of the four phases of the disaster risk management: mitigation, preparation, response, and recovery.	3
Figure 2: Graphical illustration of the three pillars defining the disaster risk: vulnerability, exposure, and hazard.	12
Figure 3: Conceptual framework illustrating the thesis contents and organization.	21
Figure 4: On the right: map of the tests by cities included or not in the database and the following percentage distribution by provinces. On the left: database distribution organized by masonry typology and type of experimental tests. Abbreviations are shown in Table 2 and Table 3. M7 typology (solid clay brick) is shown separately due to the sample size.	28
Figure 5: POS “Portici Ercolani” in Senigallia – streets and building blocks included in the case study.	30
Figure 6: POS “Portici Ercolani” in Senigallia – streets width and direction data collection.	31
Figure 7: POS “Portici Ercolani” in Senigallia – streets slope data collection.	32
Figure 8: POS “Portici Ercolani” in Senigallia – building blocks dimension data collection.	32
Figure 9: POS “Portici Ercolani” in Senigallia – square features data collection.	33
Figure 10: Typological POSs considered in this work: A) compact layout (namely Scenario 1); B) typological POSs layouts including the square (namely, Scenarios 2), having the same basic profile section as for Scenario 1.; c) the basic profile section (ground elevation) according to section lines S1 and S2 in panel A (vertical exaggeration scale: 10x) and metric scale for plan view for all the panels. In each panel, the riverbed is represented between the two gray lines on the left, the arrow points out the river flow direction, and the full-colored gray areas are building blocks.	34
Figure 11: Specific framework for this section - from data sources to statistical analyses.	36
Figure 12: Identification of Public Open Space areas for the case study of Piazza Duomo in Reggio Calabria (see Section §11.2) by: A) distinguishing between outdoor (in orange) and indoor (in yellow) areas; B) recognizing outdoor areas types as carriageable - CA (in blue), walkable - WA (in magenta), unwalkable - UA (in gray), dehors - D (in yellow), and private courtyard – CY (in green); C) identifying the POS in the urban fabric.	37
Figure 13: videotapes general features in percentages terms according to: (A) the floodwater conditions (water depth and flow); (B) the geographic area; (C) the groups’ dimensions.	46
Figure 14: Illustration of all the floodwater conditions organized per water depth (rows) and water flow (columns), including related acronyms for subsample creation. Numerical values are referred to adults [231].	47
Figure 15: Example of 2 pedestrians (on the left) performing attraction towards unmovable obstacles M2, while the pedestrian on the right is moving away from the fence (the white arrow indicates his direction). The following parameters are considered in this scene: PO=3, PI=2, PI _w =2, PI _{w,s} =2 (reference videotape: {95}).	48
Figure 16: Organization of the setup groups depending on the entrance portals’ shape (columns) and the “first servers” position along the pathway (rows). The setup code is composed of four characters: the number and position of the servers with respect to the wall (A-B-C-D) as in Table 14, the probability a pedestrian can choose a server (H-L), the server position with respect to the start (2-4-8), and the shape of the entrance portal (R-S). Entrance portals are in yellow, exit portals in red, first servers in magenta, and buildings walls in orange.	53
Figure 17: Typological POSs as testing scenarios (A: compact layout; B: layouts including a square). More details at §3.3.	56
Figure 18: Illustration of the graph that models the street network. Blue dots are starting points; red dots can be both starting points and/or potential shelters. Links are marked in green: those parallel to the river can be traveled in both directions, the others only away from the river.	62
Figure 19: Scheme of gauging points positions (blue dots) and sub-spaces areas (divided by the dashed lines) in a typical square of the typological POSs for simulation purposes (example dimension equal to 1 module).	66
Figure 20: Compressive strength graphical comparison between the experimental data (boxplots and black markers), and the INS provisions (blue areas).	69
Figure 21: Elastic modulus graphical comparison between the experimental data (boxplots and black markers), and the INS provisions (green areas).	71
Figure 22: Shear strength graphical comparison between the experimental data and the INS provisions. Blue areas and blue markers indicate τ_0 , red areas and red markers indicate f_{v0}	73
Figure 23: Adobe masonry – Graphical comparison in terms of compressive strength f (on the left) and elastic modulus (on the right) between literature ranges (gray boxplots), the Spanish standard (orange area), and the values obtained from literature studies on regional case studies (blue markers). Outliers are indicated by the gray crosses.	74

Figure 24: Cob masonry – Graphical comparison in terms of compressive strength f (on the left) and elastic modulus E (on the right) between literature ranges (gray boxplots) and the values obtained from literature studies on regional case studies (blue markers). Outliers are indicated by the gray crosses.	74
Figure 25: Rammed earth masonry - Graphical comparison in terms of compressive strength f (on the left) and elastic modulus (on the right) between literature ranges (gray boxplots) and the Australian, Zimbabwean, Spanish, New Zealand, and US (New Mexico) standards. Outliers are indicated by the gray crosses.	75
Figure 26: POSC-related KPIs - Quartile-based analysis of: (A) Percentage of outdoor areas er typology; (B) Sensitive Buildings number per square SBn; (C) Ratios between the indoor and outdoor areas (AIOr). Outliers are shown by the dots.	80
Figure 27: UHC-related KPIs - Quartile-based analysis of the Users’ Overall outdoor density (UOod) on working days (in blue) and holidays (in orange). Outliers are shown by the dots.	81
Figure 28: UHC-related KPIs – Quartile-based analysis of: (A) Only Outdoor users percentage OOp; (B) Prevalent Outdoor users percentage POp; (C) Residents users percentage Rp; (D) Non-residents percentage NRp. Working days are in blue, holidays in orange. Outliers are shown by the dots.	82
Figure 29: UDC-related KPIs - Quartile-based analysis of: (A) Users’ Overall outdoor density UOod; (B) Users’ Overall indoor density; (C) Users’ indoor density Uid in working days and holidays. Outliers are shown by the dots.	84
Figure 30: UDC-related KPIs - Quartile-based analysis of UIOr in working days and holidays. Outliers are shown by the dots.	85
Figure 31: UDC-related KPIs - Quartile-based analysis of: (A) Only Outdoor users percentage OOp; (B) Prevalent Outdoor users percentage POp; (C) Residents users percentage Rp; (D) Non-residents percentage NRp in working days and holidays. Outliers are shown by the dots.	86
Figure 32: UDC: Quartile-based analysis considering individual vulnerability (age and gender). Outliers are shown by the dots.	87
Figure 33: Panel A: a group of 4 pedestrians clinging to a rope (in brown) and arranging a human chain {48}. Panel B: a group of 15 pedestrians clinging to a rope and arranging a “human chain” {17}. Jagged lines in blue indicate the waves.	90
Figure 34: Final picture of all the behaviors observed in the videotapes organized per evacuation phase, which integrates literature classifications.	91
Figure 35: Overall frequency PI/PO [%] (colored bars; left y-axis) of deliberately chosen behaviors, and People Overall PO [pp] as the sample dimension (red circles; right y-axis).	91
Figure 36: Situational frequency PId/PI [%] (colored bars; left y-axis) of the observed behaviors evaluated with respect to the water depth levels, and People Involved PI [pp] as the sample dimension (black rhombuses; right y-axis). Behaviors IDs from Figure 34.	94
Figure 37: Situational frequency PIf/PI [%] (colored bars; left y-axis) of the observed behaviors evaluated with respect to the water flow levels, and People Involved PI [pp] as the sample dimension (black rhombuses; right y-axis). Behaviors IDs from Figure 34.	95
Figure 38: People dealing with water up to the ankles (outlined in green). Panel A is for still water, panel B is for flowing water and the blue jagged lines indicate the waves (reference videotapes: {70}, {119}).	96
Figure 39: Situational frequency per water depth equal to or lower than the ankles $PI_{A,i}/PI_A$ [%] (colored bars; left y-axis) of the observed behaviors evaluated by comparing the water flow. The sample dimension is outlined by PI_A [pp] (black rhombuses; right y-axis). Behaviors IDs from Figure 34.	97
Figure 40: People dealing with water up to the knees (outlined in yellow). Panel A is for still water, panel B is for flowing water and the blue jagged lines indicate the waves (reference videotapes: {76}, {42}).	98
Figure 41: Situational frequency per water depth equal to or lower than the knees $PI_{K,i}/PI_K$ [%] (colored bars; left y-axis) of the observed behaviors evaluated by comparing the water flow. The sample dimension is outlined by PI_K [pp] (black rhombuses; right y-axis). Behaviors IDs from Figure 34.	98
Figure 42: People dealing with water up to the waist (outlined in orange). Panel A is for still water, panel B is for flowing water and the blue jagged lines indicate the waves (reference videotapes: {100}, {84}).	99
Figure 43: Situational frequency per water depth equal to or lower than the waist $PI_{W,i}/PI_W$ [%] (colored bars; left y-axis) of the observed behaviors evaluated by comparing the water flow. The sample dimension is outlined by PI_W [pp] (black rhombuses; right y-axis). Behaviors IDs from Figure 34.	99
Figure 44: People dealing with water higher than the waist (outlined in red). Panel A is for still water, panel B is for flowing water and the blue jagged lines indicate the waves (reference videotapes: {25}, {55}).	100

Figure 45: Situational frequency per water depth higher than the waist $PI_{HW,t}/PI_{HW}$ [%] (colored bars; left y-axis) of the observed behaviors evaluated by comparing the water flow. The sample dimension is outlined by PI_{HW} [pp] (black rhombuses; right y-axis). Behaviors IDs from Figure 34. 101

Figure 46: Example of how “passive aids” can be implemented in the outdoor BE. Scenario A lacks targeted interventions; Scenario B includes the presence of handrails (1), raised platforms (2), road signs (3), and benches (4). 105

Figure 47: Comparison of the custom simulator evacuation curve (black dashed lined) and those of the generic simulator (straight lines). Generic simulator setups are grouped according to the criteria shown in Figure 16, that is considering the same entrance portals configuration, i.e., setup groups R1 to R3 are rectangular (panels A-B-C), S1 to S3 are squared (panels D-E-F). 0-90s are omitted as no pedestrians complete the evacuation in this timespan. 107

Figure 48: Comparison of 2nd quartile D_w trend for the custom simulator (blue dashed line) and those of the generic simulator (straight lines). Generic simulator setups are grouped according to the criteria shown in Figure 16, that is considering the same entrance portals configuration, i.e., setup groups R1 to R3 are rectangular (panels A-B-C), S1 to S3 are squared (panels D-E-F). The green dashed line indicates the position of the “first servers” along the pathway. 109

Figure 49: Comparison between the maximum evacuation time t_{max} of the custom simulator (red cross) and the generic simulator distinguishing overall (blue box) and groups data (orange and green boxes). Outlier setups are marked as follows: “Setup name (Group name)”. Extended results for each setup are resumed in Section §11.5.5 (Appendices). 110

Figure 50: boxplot representation of the maximum waiting time percentage W , distinguishing overall (blue box) and group data (orange and green boxes). Outlier setups are marked as follows: “Setup name (Group name)”. Extended results for each setup are resumed in Section §11.5.5 (Appendices). 110

Figure 51: Comparison between the evacuation flow F values of the custom simulator (red cross) and of the generic simulator distinguishing overall (blue box) and groups data (orange and green boxes). Outlier setups are marked as follows: “Setup name (Group name)”. Extended results for each setup are resumed in Section §11.5.5 (Appendices). 111

Figure 52: Comparison between the evacuation curves (panel A) and the D_w trends (panels B-C-D) obtained from the BL&S setup of the generic simulator (red solid lines) and the custom simulator (black dashed lines). The green dashed line indicates the “first servers” position along the pathway. The evacuation curves comparison considers the range between 90-140s, which is from the arrival of the first pedestrian to the exit of the last one. 113

Figure 53: D_rV_f trend over time for Scenario 1 by considering the central perpendicular street and for different distances [m] from the river. Straight lines refer to gauging points inside the outdoor spaces, dashed lines refer to those inside the crossroads. The yellow area highlights the time span for the simulations. The limit condition for stability ($D_rV_f = 1.20m^2/s$) is also highlighted by the red continuous line. 116

Figure 54: DV_i maps for each typological POS, with respect to adopted stability limits conditions [227], by offering: A) the conditions of each outdoor space and sub-spaces (i.e. for squares, see the dotted lines) and the localization of gathering areas in “sheltering” (magenta dots) and “leaving” (arrow signs) evacuation strategies; B) an example (Scenario 2.E) of local D_rV_f conditions in the main square according to the 1m x 1m solving mesh, by including the gathering areas posting according to the “sheltering” strategy. For each panel, the scale representation of D_rV_f values is offered. 118

Figure 55: RI maps at the microscale level by considering Scenario 1, 2.A, and 2.B: A) without pedestrian evacuation behaviors; B) with pedestrian evacuation behaviors in “leaving” strategy; C) with pedestrian evacuation behaviors in “sheltering” strategy. 121

Figure 56: RI maps at the microscale level by considering Scenario 2.C, 2.D, and 2.E: A) without pedestrian evacuation behaviors; B) with pedestrian evacuation behaviors in “leaving” strategy; C) with pedestrian evacuation behaviors in “sheltering” strategy. 121

Figure 57: $RI_{i,M}$ values depending on the approach for the path choice “i” (shortest, quickest, or cheapest) and the number of gathering areas available “M”. “Shortest” and “quickest” trends are overlapped. 125

Figure 58: Gathering areas selection and evacuation routes to reach them in the case of $M=4$. For $M = 3$, pedestrians collected in node D should reach node G by traveling the dashed green link. Isolated nodes (non-linked) are deadly points. 127

Figure 59: Evacuation units with $M=4$. For $M=3$, the blue unit can be linked to the green one through the dashed link. 128

Figure 60: Disorganized rubble stone masonry (M1) – a) Graphic reconstruction of the wall texture type (1m x 1m); b) Wall façade example, photo taken in Arquata del Tronto (AP); c) Wall section example, photo taken in Treia (MC). 139

Figure 61: Barely cut stone masonry (M2) – a) Graphic reconstruction of the wall texture type (1mx1m); b) Wall façade example, photo taken in Castelsantangelo sul Nera (MC); c) Wall section example, photo taken in San Ginesio (MC). 139

Figure 62: Roughly cut stone with good texture (M3) – a) Graphic reconstruction of the wall texture type (1mx1m); b) Wall façade example, photo taken in Castelsantangelo sul Nera (MC); c) Wall façade example, photo taken in Cingoli (MC).	139
Figure 63: Irregular soft stone masonry (M4) – a) Graphic reconstruction of the wall texture type (1mx1m); b) Double flat-jack test execution, photo taken in Fiastra (MC) [credits: LA.TE.MA srl]; c) Double flat-jack test execution, photo taken in Monte San Martino (MC) [credits: LA.TE.MA srl].	140
Figure 64: Regular soft stone masonry (M5) – a) Graphic reconstruction of the wall texture type (1mx1m); b) Wall façade example, photo taken in Treia (MC); c) Typical tuff masonry building example, photo taken in San Ginesio (MC).	140
Figure 65: Stone blocks squared (M6) – a) Graphic reconstruction of the wall texture type (1mx1m); b) Wall façade example, photo taken in Cingoli (MC); c) Wall façade example, photo taken in Muccia (MC).	140
Figure 66: Solid clay brick and lime mortar (M7) – a) Graphic reconstruction of the wall texture type (1mx1m); b) Wall façade example, photo taken in Filottrano (AN); c) Wall section example, photo taken in Castelfidardo (AN).	141
Figure 67: Clay hollow bricks with cement-based mortar (M8) – a) Graphic reconstruction of the wall texture type (1mx1m); b) Wall façade example of masonry panel with “good mortar”, photo taken in Cingoli (MC) [credits: CAP Studio]; c) Double flat-jack test execution on a masonry panel in “standard conditions”, photo taken in Frontino (PU) [credits: CAP Studio].	141
Figure 68: Stone-and-brick mixed (MX1) – a) Graphic reconstruction of the wall texture type (1mx1m); b) Wall façade example, photo taken in Camporotondo di Fiastrone (MC); c) Wall section example, photo taken in and Treia (MC).	141
Figure 69: Three main phases for the construction of Cob masonry buildings [61].	142
Figure 70: Three main phases for the construction of Rammed earth masonry buildings [61].	142
Figure 71: Three main phases for the construction of Adobe masonry buildings [61].	143
Figure 72: Graphic representation of the arrangement of Adobe bricks (top left); Cob blocks (bottom left); Layering typical of the Rammed earth (odd phases: stratification; even phases: compaction).	143
Figure 73: Examples of the three earthen masonry typologies considered: the Cob at the top left, the Adobe at the bottom left, and the Ramed earth in the two buildings on the right. Photos taken at the Ecomuseum of Villa Ficana (MC).	144
Figure 74: Map of the municipalities in the Marche Region in which the presence of earthen masonry buildings is demonstrated. Data from: “Architettura di terra nelle Marche, Catalogo a cura della Direzione Regionale per i Beni Culturali e Paesaggistici delle Marche” (2005) [287]; “Case di Terra e Paglia delle Marche” (2003) [326].	144
Figure 75: POS “Piazza del Popolo” area in Albenga – streets and building blocks included in the case study.	148
Figure 76: POS “Piazza Alberica” area in Carrara – streets and building blocks included in the case study.	149
Figure 77: POS “Piazza Garibaldi” area in Colorno – streets and building blocks included in the case study.	150
Figure 78: POS “Historical City Center” area in Montevarchi – streets and building blocks included in the case study.	151
Figure 79: POS “Portici Ercolani” area in Senigallia – streets and building blocks included in the case study.	152
Figure 80: Aerial view of Piazza del Popolo, Manfredonia (IT). Yellow areas are Carriageable Areas (CA), red areas are Walkable Areas (WA), blue rectangles indicate Dehors (D), black circles indicate Unwalkable Areas (UA), and orange areas indicate the indoor areas considered. Special buildings are signed with the letter “S”.	160
Figure 81: UHC-related KPIs – Comparison between Piazza del Popolo in Manfredonia (in green) and the quartile-based analysis of the Users’ Overall outdoor density (UOod) on working days (in blue) and holidays (in orange). Outliers are shown by the dots.	162
Figure 82: UHC-related KPIs – Comparison between Piazza del Popolo in Manfredonia (in green) and the quartile-based analysis of: (A) Only Outdoor users’ percentage OOp; (B) Prevalent Outdoor users percentage POP; (C) Residents users percentage Rp; (D) Non-residents percentage NRp. Working days are in blue, holidays in orange. Outliers are shown by the dots.	163
Figure 83: Custom simulator 1 st quartile D_w trend (dashed line) compared to those of the generic simulator grouped according to the criteria shown in section §3.5.3.4 (straight lines), that is considering the same entrance portals configuration, i.e., setup groups R1 to R3 are rectangular (panels A-B-C), S1 to S3 are squared (panels D-E-F). The green dashed line indicates the position of the “first servers”.	175
Figure 84: Custom simulator 3 rd quartile D_w trend (dashed line) compared to those of the generic simulator grouped according to the criteria shown in section §3.5.3.4 (straight lines), that is considering the same entrance portals configuration, i.e., setup groups R1 to R3 are rectangular (panels A-B-C), S1 to S3 are squared (panels D-E-F). The green dashed line indicates the position of the “first servers”.	175

Figure 85: Local DfV_f conditions in the outdoor spaces for each typological POS, affecting stability. Data are shown according to the 1 m x 1 m solving mesh, by including the continuous scale representation of DfV_f values (on the bottom). 181

Figure 86: (a) subgraph of the street network; (b) subgraph obtained considering the dummy nodes (in blue) and related link (dotted). Legend on the left (orientated links are the green arrows, non-orientated links are the green lines). ... 184

Figure 87: Flood hydrographs comparison with respect to $Q_{SECTION}$ (dashed line): measured data, by the gray curve [275], data incremented by a 2.5 factor (concentration of 18 hours), by the black curve, data used in the POS simulation (concentration of 6 hours), by the red line. 189

Bibliography

- [1] A. F. Young e J. A. Jorge Papini, «How can scenarios on flood disaster risk support urban response? A case study in Campinas Metropolitan Area (São Paulo, Brazil)», *Sustain. Cities Soc.*, vol. 61, pag. 102253, ott. 2020, doi: 10.1016/j.scs.2020.102253.
- [2] D. Gu, «Exposure and vulnerability to natural disasters for world's cities. United Nations, Department of Economics and Social Affairs, Population Division, Technical Paper No. 4.», 2019. [In linea]. Available at: <https://www.un.org/en/development/desa/population/publications/pdf/technical/TP2019-4.pdf>.
- [3] E. Quagliarini, E. Currà, F. Fatiguso, G. Mochi, e G. Salvalai, *Resilient and User-Centered Solutions for a Safer Built Environment Against Sudden and Slow Onset Disasters: The BE S²ECURe Project*, vol. 203. 2021.
- [4] F. Rosso *et al.*, «Urban morphology parameters towards multi-risk scenarios for squares in the historical centers: Analyses and definition of square typologies and application to the Italian context», *J. Cult. Herit.*, vol. 56, pagg. 167–182, 2022, doi: 10.1016/j.culher.2022.06.012.
- [5] European Commission, «Overview of natural and man-made disaster risks in the European Union may face», 2017. doi: doi:10.2795/861482.
- [6] H. Q. Nguyen *et al.*, «Evaluation of retrofitting responses to urban flood risk in Ho Chi Minh City using the Motivation and Ability (MOTA) framework», *Sustain. Cities Soc.*, vol. 47, pag. 101465, mag. 2019, doi: 10.1016/j.scs.2019.101465.
- [7] United Nations, «World Urbanization Prospects», 2018. <https://www.un.org/development/desa/publications/2018-revision-of-world-urbanization-prospects.html> (consultato apr. 21, 2020).
- [8] I. Y. Jian, E. H. W. Chan, Y. Xu, e E. K. Owusu, «Inclusive public open space for all: Spatial justice with health considerations», *Habitat Int.*, vol. 118, pag. 102457, dic. 2021, doi: 10.1016/j.habitatint.2021.102457.
- [9] C. Garau e A. Annunziata, «Public Open Spaces: connecting people, squares and streets by measuring the usability through the Villanova district in Cagliari, Italy», *Transp. Res. Procedia*, vol. 60, pagg. 314–321, 2022, doi: 10.1016/j.trpro.2021.12.041.
- [10] A. Sharifi, «Urban form resilience: A meso-scale analysis», *Cities*, vol. 93, pagg. 238–252, ott. 2019, doi: 10.1016/j.cities.2019.05.010.
- [11] D. Cherfaoui e N. Djelal, «Change in Use and Development of Public Squares Considering Daily Temporalities.: The Case of Emir Abd El Kader Square in Algiers», *Artic. – Rev. Sci. Hum.*, 2018, doi: 10.4000/articulo.3809.
- [12] D. Apró, R. Tóth, M. Orova, I. Kiss, e D. András Reith, «Can Smart City Tools Support Historical Cities Become More Resilient and Regenerative?», 2016.
- [13] E. Micelli e P. Pellegrini, «Wasting heritage. The slow abandonment of the Italian Historic Centers», *J. Cult. Herit.*, vol. 31, pagg. 180–188, mag. 2018, doi: 10.1016/j.culher.2017.11.011.
- [14] C. Pasquinelli, M. Trunfio, N. Bellini, e S. Rossi, «Reimagining urban destinations: Adaptive and transformative city brand attributes and values in the pandemic crisis», *Cities*, vol. 124, pag. 103621, 2022, doi: <https://doi.org/10.1016/j.cities.2022.103621>.
- [15] M. Loda, S. Bonati, e M. Puttilli, «History to eat. The foodification of the historic centre of Florence», *Cities*, vol. 103, pag. 102746, ago. 2020, doi: 10.1016/j.cities.2020.102746.

- [16] M. Angelidou, «Smart city policies: A spatial approach», *Cities*, vol. 41, pagg. S3–S11, lug. 2014, doi: 10.1016/j.cities.2014.06.007.
- [17] M. Angelosanti *et al.*, «Towards a Multi-risk Assessment of Open Spaces and Its Users: A Rapid Survey Form to Collect and Manage Risk Factors BT - Sustainability in Energy and Buildings 2021», 2022, pagg. 209–218.
- [18] L. Bernabei, G. Mochi, G. Bernardini, e E. Quagliarini, «Seismic risk of Open Spaces in Historic Built Environments: A matrix-based approach for emergency management and disaster response», *Int. J. Disaster Risk Reduct.*, vol. 65, pag. 102552, nov. 2021, doi: 10.1016/j.ijdrr.2021.102552.
- [19] J. L. P. Aguado, T. M. Ferreira, e P. B. Lourenço, «The Use of a Large-Scale Seismic Vulnerability Assessment Approach for Masonry Façade Walls as an Effective Tool for Evaluating, Managing and Mitigating Seismic Risk in Historical Centers», *Int. J. Archit. Herit.*, vol. 12, n. 7–8, pagg. 1259–1275, 2018, doi: 10.1080/15583058.2018.1503366.
- [20] F. Romis, S. Caprili, W. Salvatore, T. M. Ferreira, e P. B. Lourenço, «An improved seismic vulnerability assessment approach for historical urban centres: The case study of campi alto di norcia, Italy», *Appl. Sci.*, vol. 11, n. 2, pagg. 1–27, 2021, doi: 10.3390/app11020849.
- [21] F. N. Miranda e T. M. Ferreira, «A simplified approach for flood vulnerability assessment of historic sites», *Nat. Hazards*, n. January, 2019, doi: 10.1007/s11069-018-03565-1.
- [22] G. Bernardini, E. Quagliarini, e M. D’Orazio, «Investigating Exposure in Historical Scenarios: How People Behave in Fires, Earthquakes and Floods», in *RILEM Bookseries*, 2019.
- [23] A. Arriazu-Ramos, M. Bes-Rastrollo, A. Sánchez-Ostiz Gutiérrez, e A. Monge-Barrio, «Building parameters that influence overheating of apartment buildings in a temperate climate in Southern Europe», *Build. Environ.*, vol. 228, 2023, doi: 10.1016/j.buildenv.2022.109899.
- [24] L. Quesada-Ganuza, L. Garmendia, I. Alvarez, e E. Roji, «Vulnerability assessment and categorization against heat waves for the Bilbao historic area», *Sustain. Cities Soc.*, vol. 98, 2023, doi: 10.1016/j.scs.2023.104805.
- [25] F. Fatiguso *et al.*, «Built Environments Prone to Sudden and Slow Onset Disasters: From Taxonomy Towards Approaches for Pervasive Training of Users», in *Lecture Notes in Computer Science (including subseries Lecture Notes in Artificial Intelligence and Lecture Notes in Bioinformatics)*, 2021, vol. 12956 LNCS, pagg. 125–139, doi: 10.1007/978-3-030-87010-2_9.
- [26] F. Vidal, R. Vicente, J. Mendes Silva, D. Dias, N. Pina, e O. Tchepel, «Air pollution impacts on traditional building materials: From sample exposure testing to an urban scale assessment», in *REHABEND*, 2020, pagg. 2622–2630, [In linea]. Available at: <https://www.scopus.com/inward/record.uri?eid=2-s2.0-85100411634&partnerID=40&md5=f85488eca2c23bd2d41ab9f548df99e5>.
- [27] R. Ortiz, P. Ortiz, M. A. Vázquez, e J. M. Martín, «Integration of georeferenced informed system and digital image analysis to asses the effect of cars pollution on historical buildings», *Constr. Build. Mater.*, vol. 139, pagg. 320–333, 2017, doi: 10.1016/j.conbuildmat.2017.02.030.
- [28] E. Quagliarini, F. Fatiguso, M. Lucesoli, G. Bernardini, e E. Cantatore, «Risk reduction strategies against terrorist acts in urban built environments: Towards sustainable and human-centred challenges», *Sustain.*, vol. 13, n. 2, 2021, doi: 10.3390/su13020901.

- [29] G. Bernardini, M. D'orazio, e E. Quagliarini, «Coupled Multi-risk Mitigation in Historical Urban Outdoor Built Environment: Preliminary Strategies Evaluation Through Typological Scenarios», in *RILEM Bookseries*, vol. 46, 2024, pagg. 1212–1226.
- [30] T. M. Ferreira e P. P. Santos, «An Integrated Approach for Assessing Flood Risk in Historic City Centres», *Water*, vol. 12, n. 6, pag. 1648, giu. 2020, doi: 10.3390/w12061648.
- [31] R. Ortiz, P. Ortiz, J. M. Martín, e M. A. Vázquez, «A new approach to the assessment of flooding and dampness hazards in cultural heritage, applied to the historic centre of Seville (Spain)», *Sci. Total Environ.*, 2016, doi: 10.1016/j.scitotenv.2016.01.207.
- [32] J. J. Wang, «Flood risk maps to cultural heritage: Measures and process», *J. Cult. Herit.*, 2015, doi: 10.1016/j.culher.2014.03.002.
- [33] S. G. Lanza, «Flood hazard threat on cultural heritage in the town of Genoa (Italy)», *J. Cult. Herit.*, 2003, doi: 10.1016/S1296-2074(03)00042-6.
- [34] O. M. Rezende, F. M. Miranda, A. N. Haddad, e M. G. Miguez, «A Framework to Evaluate Urban Flood Resilience of Design Alternatives for Flood Defence Considering Future Adverse Scenarios», *Water*, vol. 11, n. 7, pag. 1485, lug. 2019, doi: 10.3390/w11071485.
- [35] C. Arrighi, M. Brugioni, F. Castelli, S. Franceschini, e B. Mazzanti, «Urban micro-scale flood risk estimation with parsimonious hydraulic modelling and census data», *Nat. Hazards Earth Syst. Sci.*, 2013, doi: 10.5194/nhess-13-1375-2013.
- [36] D. La Rosa e V. Pappalardo, «Planning for spatial equity - A performance based approach for sustainable urban drainage systems», *Sustain. Cities Soc.*, vol. 53, pag. 101885, feb. 2020, doi: 10.1016/j.scs.2019.101885.
- [37] O. M. Rezende, L. F. Guimarães, F. M. Miranda, A. N. Haddad, e M. G. Miguez, «A time-integrated index for flood risk to resistance capacity», *Water (Switzerland)*, 2019, doi: 10.3390/w11071321.
- [38] J. A. Bullock, G. D. Haddow, e D. P. Coppola, «Mitigation, Prevention, and Preparedness.», *Introduction to Homeland Security*. pagg. 435–494, 2013, doi: 10.1016/B978-0-12-415802-3.00010-5.
- [39] UNDRR, «Sendai Framework Terminology», 2024. <https://www.undrr.org/drr-glossary/terminology> (consultato feb. 22, 2024).
- [40] PreventionWeb - UNDRR, «PreventionWeb - UNDRR», 2021. <https://www.preventionweb.net/understanding-disaster-risk/component-risk/disaster-risk> (consultato dic. 27, 2024).
- [41] E. Quagliarini, M. Lucesoli, e G. Bernardini, «How to create seismic risk scenarios in historic built environment using rapid data collection and managing», *J. Cult. Herit.*, vol. 48, pagg. 93–105, feb. 2021, doi: 10.1016/j.culher.2020.12.007.
- [42] J. Dibble *et al.*, «On the origin of spaces: Morphometric foundations of urban form evolution», *Environ. Plan. B Urban Anal. City Sci.*, vol. 46, n. 4, pagg. 707–730, 2019, doi: 10.1177/2399808317725075.
- [43] C. Santos, T. M. Ferreira, R. Vicente, e J. a R. Mendes da Silva, «Building typologies identification to support risk mitigation at the urban scale - Case study of the old city centre of Seixal, Portugal», *J. Cult. Herit.*, vol. 14, n. 6, pagg. 449–463, 2013, doi: 10.1016/j.culher.2012.11.001.
- [44] Q. He, P. Larkham, e J. Wu, «Evaluating historic preservation zoning using a landscape approach», *Land use policy*, vol. 109, pag. 105737, ott. 2021, doi: 10.1016/j.landusepol.2021.105737.

- [45] A. D'amico *et al.*, «Built environment typologies prone to risk: A cluster analysis of open spaces in Italian cities», *Sustain.*, vol. 13, n. 16, 2021, doi: 10.3390/su13169457.
- [46] S. Granda e T. M. Ferreira, «Assessing Vulnerability and Fire Risk in Old Urban Areas: Application to the Historical Centre of Guimarães», *Fire Technol.*, vol. 55, n. 1, pagg. 105–127, 2019, doi: 10.1007/s10694-018-0778-z.
- [47] M. A. Soltane, M. Mimoune, e A. Guettiche, «Earthquake-induced impact scenario assessment for the historical center of Skikda, Algeria», *Bull. Earthq. Eng.*, vol. 20, n. 11, pagg. 5677–5719, 2022, doi: 10.1007/s10518-022-01437-5.
- [48] A. Zlateski, M. Lucesoli, G. Bernardini, e T. M. Ferreira, «Integrating human behaviour and building vulnerability for the assessment and mitigation of seismic risk in historic centres: Proposal of a holistic human-centred simulation-based approach», *Int. J. Disaster Risk Reduct.*, vol. 43, pag. 101392, feb. 2020, doi: 10.1016/j.ijdr.2019.101392.
- [49] E. Quagliarini, G. Bernardini, S. Santarelli, e M. Lucesoli, «Evacuation paths in historic city centres: A holistic methodology for assessing their seismic risk», *Int. J. Disaster Risk Reduct.*, vol. 31, n. July, pagg. 698–710, 2018, doi: 10.1016/j.ijdr.2018.07.010.
- [50] G. Bernardini, E. Quagliarini, M. D'Orazio, e M. Brocchini, «Towards the simulation of flood evacuation in urban scenarios: Experiments to estimate human motion speed in floodwaters», *Saf. Sci.*, 2020, doi: 10.1016/j.ssci.2019.104563.
- [51] G. Bernardini, M. Postacchini, E. Quagliarini, M. D'Orazio, e M. Brocchini, «Flooding Pedestrians' Evacuation in Historical Urban Scenario: A Tool for Risk Assessment Including Human Behaviors», in *RILEM Bookseries*, 2019.
- [52] J. D. Blanco Cadena, G. Salvalai, G. Bernardini, e E. Quagliarini, «Determining behavioural-based risk to SLODs of urban public open spaces: Key performance indicators definition and application on established built environment typological scenarios», *Sustain. Cities Soc.*, vol. 95, 2023, doi: 10.1016/j.scs.2023.104580.
- [53] S. V. Shivaprasad Sharma, P. S. Roy, V. Chakravarthi, e G. Srinivasa Rao, «Flood risk assessment using multi-criteria analysis: A case study from Kopili river basin, Assam, India», *Geomatics, Nat. Hazards Risk*, vol. 5705, 2018, doi: 10.1080/19475705.2017.1408705.
- [54] R. Hassanzadeh, «Earthquake population loss estimation using spatial modelling and survey data: The Bam earthquake, 2003, Iran», *Soil Dyn. Earthq. Eng.*, vol. 116, pagg. 421–435, gen. 2019, doi: 10.1016/j.soildyn.2018.09.023.
- [55] J. Mallick *et al.*, «Assessing factors affecting drought, earthquake, and flood risk perception: empirical evidence from Bangladesh», *Nat. Hazards*, 2022, doi: 10.1007/s11069-022-05242-w.
- [56] J. Wu, M. Ye, X. Wang, e E. Koks, «Building Asset Value Mapping in Support of Flood Risk Assessments: A Case Study of Shanghai, China», *Sustainability*, vol. 11, n. 4, pag. 971, feb. 2019, doi: 10.3390/su11040971.
- [57] C. N. van der Wal, M. A. Robinson, W. Bruine de Bruin, S. Gwynne, W. B. de Bruin, e S. Gwynne, «Evacuation behaviors and emergency communications: An analysis of real-world incident videos», *Saf. Sci.*, vol. 136, pag. 105121, apr. 2021, doi: 10.1016/J.SSCI.2020.105121.
- [58] G. Bernardini e E. Quagliarini, «Terrorist acts and pedestrians' behaviours: First insights on European contexts for evacuation modelling», *Saf. Sci.*, vol. 143, pag. 105405, 2021, doi: 10.1016/J.SSCI.2021.105405.

- [59] S. G. Arce, C. Jeanneret, J. Gales, D. Antonellis, e S. Vaiciulyte, «Human behaviour in informal settlement fires in Costa Rica», *Saf. Sci.*, vol. 142, pag. 105384, 2021, doi: 10.1016/J.SSCI.2021.105384.
- [60] G. Bernardini, E. Quagliarini, e M. D’Orazio, «Towards creating a combined database for earthquake pedestrians’ evacuation models», *Saf. Sci.*, vol. 82, pagg. 77–94, 2016, doi: 10.1016/J.SSCI.2015.09.001.
- [61] E. Quagliarini, G. Pace, e G. Romano, *Murature storiche nella regione Marche: Specificità costruttive e caratterizzazione meccanica sperimentale*. Monfalcone (GO), Italy, 2023.
- [62] UNDRR, «A/RES/71/276 Report of the open-ended intergovernmental expert working group on indicators and terminology relating to disaster risk reduction», 2016.
- [63] N. Chieffo, T. M. Ferreira, R. da Silva Vicente, P. B. Lourenço, e A. Formisano, «A Simplified Approach to Estimate Seismic Vulnerability and Damage Scenarios Including Site Effects. Application to the Historical Centre of Horta, Azores, Portugal», *J. Earthq. Eng.*, 2023, doi: 10.1080/13632469.2023.2254399.
- [64] M. Xofi *et al.*, «Exposure and physical vulnerability indicators to assess seismic risk in urban areas: a step towards a multi-hazard risk analysis», *Geomatics, Nat. Hazards Risk*, vol. 13, n. 1, pagg. 1154–1177, 2022, doi: 10.1080/19475705.2022.2068457.
- [65] M.-C. Marulanda Fraume, O.-D. Cardona A, P. Marulanda Fraume, M.-L. Carreño T, e A. H. Barbat, «Evaluating risk from a holistic perspective to improve resilience: The United Nations evaluation at global level», *Saf. Sci.*, vol. 127, 2020, doi: 10.1016/j.ssci.2020.104739.
- [66] S. Jeong, B. J. Kim, Y.-J. Lee, J.-B. Chung, e S.-H. Sim, «Individual Disaster Assistance For Socially Vulnerable People: Lessons Learned From the Pohang Earthquake in the Republic of Korea», *Risk Anal.*, vol. 40, n. 11, pagg. 2373–2389, 2020, doi: 10.1111/risa.13554.
- [67] Y. Ebrahimian Ghajari, A. A. Alesheikh, M. Modiri, R. Hosnavi, M. Abbasi, e A. Sharifi, «Urban vulnerability under various blast loading scenarios: Analysis using GIS-based multi-criteria decision analysis techniques», *Cities*, vol. 72, pagg. 102–114, feb. 2018, doi: 10.1016/j.cities.2017.08.006.
- [68] S. De Angeli, B. D. Malamud, L. Rossi, F. E. Taylor, E. Trasforini, e R. Rudari, «A multi-hazard framework for spatial-temporal impact analysis», *Int. J. Disaster Risk Reduct.*, vol. 73, pag. 102829, apr. 2022, doi: 10.1016/j.ijdr.2022.102829.
- [69] A. Booth, K. Chmutina, e L. Boshier, «Protecting crowded places: Challenges and drivers to implementing protective security measures in the built environment», *Cities*, vol. 107, 2020, doi: 10.1016/j.cities.2020.102891.
- [70] G. Bernardini, M. D’Orazio, e E. Quagliarini, «Towards a “behavioural design” approach for seismic risk reduction strategies of buildings and their environment», *Saf. Sci.*, 2016, doi: 10.1016/j.ssci.2016.03.010.
- [71] E. E. Koks, B. Jongman, T. G. Husby, e W. J. W. Botzen, «Combining hazard, exposure and social vulnerability to provide lessons for flood risk management», *Environ. Sci. Policy*, vol. 47, pagg. 42–52, mar. 2015, doi: 10.1016/j.envsci.2014.10.013.
- [72] O. D. Cardona *et al.*, «Determinants of risk: Exposure and vulnerability», *Manag. Risks Extrem. Events Disasters to Adv. Clim. Chang. Adapt. Spec. Rep. Intergov. Panel Clim. Chang.*, vol. 9781107025, pagg. 65–108, 2012, doi: 10.1017/CBO9781139177245.005.
- [73] J. C. Villagràn De León, «Vulnerability: A conceptual and methodological review», 2006.
- [74] C. Wang *et al.*, «Assessing urban population exposure risk to extreme heat: Patterns, trends, and implications for climate resilience in China (2000–2020)», *Sustain. Cities Soc.*, vol. 103, 2024, doi: 10.1016/j.scs.2024.105260.

- [75] N. Bansal, M. Mukherjee, e A. Gairola, «Causes and Impact of Urban Flooding in Dehradun», *Int. J. Curr. Res.*, 2015.
- [76] D. Cherfaoui e N. Djelal, «Assessing the flexibility of public squares the case of Grande Poste square in Algiers», *Cities*, vol. 93, 2019, doi: 10.1016/j.cities.2019.04.017.
- [77] P. Mouroux e B. Le Brun, «Presentation of RISK-UE Project», *Bull. Earthq. Eng.*, vol. 4, n. 4, pagg. 323–339, set. 2006, doi: 10.1007/s10518-006-9020-3.
- [78] R. De Lotto, C. Pietra, e E. M. Venco, «Risk Analysis: A Focus on Urban Exposure Estimation», in *Computational Science and Its Applications – ICCSA 2019*, Springer, Cham, 2019, pagg. 407–423.
- [79] L. Yang, P. Hoffmann, J. Scheffran, S. Ruhe, J. Fischereit, e I. Gasser, «An Agent-Based Modeling Framework for Simulating Human Exposure to Environmental Stresses in Urban Areas», *Urban Sci.*, vol. 2, n. 2, pag. 36, apr. 2018, doi: 10.3390/urbansci2020036.
- [80] J. Li, J. Li, Y. Yuan, e G. Li, «Spatiotemporal distribution characteristics and mechanism analysis of urban population density: A case of Xi’an, Shaanxi, China», *Cities*, vol. 86, n. May 2018, pagg. 62–70, mar. 2019, doi: 10.1016/j.cities.2018.12.008.
- [81] N. Langenheim, M. White, N. Tapper, S. J. Livesley, e D. Ramirez-Lovering, «Right tree, right place, right time: A visual-functional design approach to select and place trees for optimal shade benefit to commuting pedestrians», *Sustain. Cities Soc.*, vol. 52, pag. 101816, gen. 2020, doi: 10.1016/j.scs.2019.101816.
- [82] M. S. Engel, B. Paas, C. Schneider, C. Pfaffenbach, e J. Fels, «Perceptual studies on air quality and sound through urban walks», *Cities*, vol. 83, 2018, doi: 10.1016/j.cities.2018.06.020.
- [83] A. A. Paukaeva, T. Setoguchi, V. I. Luchkova, N. Watanabe, e H. Sato, «Impacts of the temporary urban design on the people’s behavior - The case study on the winter city Khabarovsk, Russia», *Cities*, vol. 117, 2021, doi: 10.1016/j.cities.2021.103303.
- [84] R. Ponce-Lopez e J. Ferreira, «Identifying and characterizing popular non-work destinations by clustering cellphone and point-of-interest data», *Cities*, vol. 113, 2021, doi: 10.1016/j.cities.2021.103158.
- [85] WHO, «Ambient Air pollution: a global assesment of exposure and burden of desease», 2016.
- [86] J. Luo, K. Boriboonsomsin, e M. Barth, «Reducing pedestrians’ inhalation of traffic-related air pollution through route choices: Case study in California suburb», *J. Transp. Heal.*, vol. 10, pagg. 111–123, set. 2018, doi: 10.1016/j.jth.2018.06.008.
- [87] K. Mouratidis e A. Yiannakou, «COVID-19 and urban planning: Built environment, health, and well-being in Greek cities before and during the pandemic», *Cities*, 2021, doi: 10.1016/j.cities.2021.103491.
- [88] J. Song *et al.*, «Resilience-vulnerability balance to urban flooding: A case study in a densely populated coastal city in China», *Cities*, vol. 95, pag. 102381, dic. 2019, doi: 10.1016/j.cities.2019.06.012.
- [89] F. Giuliani, A. De Falco, e V. Cutini, «The role of urban configuration during disasters. A scenario-based methodology for the post-earthquake emergency management of Italian historic centres», *Saf. Sci.*, vol. 127, n. February, pag. 104700, lug. 2020, doi: 10.1016/j.ssci.2020.104700.
- [90] G. Woo, «Understanding the Principles of Terrorism Risk Modeling from Charlie Hebdo Attack in Paris», *Def. Against Terror. Rev.*, vol. 7, n. 1, pagg. 1–11, 2015.

- [91] M. Pietilä, M. Neuvonen, K. Borodulin, K. Korpela, T. Sievänen, e L. Tyrväinen, «Relationships between exposure to urban green spaces, physical activity and self-rated health», *J. Outdoor Recreat. Tour.*, vol. 10, 2015, doi: 10.1016/j.jort.2015.06.006.
- [92] D. Afriyanie, M. M. Julian, A. Riqqi, R. Akbar, D. S. A. Suroso, e I. Kustiwan, «Re-framing urban green spaces planning for flood protection through socio-ecological resilience in Bandung City, Indonesia», *Cities*, vol. 101, pag. 102710, giu. 2020, doi: 10.1016/j.cities.2020.102710.
- [93] G. Bernardini e T. M. Ferreira, «Combining Structural and Non-structural Risk-reduction Measures to Improve Evacuation Safety in Historical Built Environments», *Int. J. Archit. Herit.*, vol. 16, n. 6, pagg. 820–838, 2022, doi: 10.1080/15583058.2021.2001117.
- [94] X. Romão, E. Paupério, e O. Tikhonova, «The DALIH Database for Recording Disaster Damage and Loss Data in Cultural Heritage BT - Structural Analysis of Historical Constructions», 2024, pagg. 1080–1092.
- [95] A. Faiella *et al.*, «Enabling Knowledge through Structured Disaster Damage & Loss Data Management System», *Sustainability*, vol. 14, n. 10. 2022, doi: 10.3390/su14106187.
- [96] J.-M. Lozano e I. Tien, «Data collection tools for post-disaster damage assessment of building and lifeline infrastructure systems», *Int. J. Disaster Risk Reduct.*, vol. 94, pag. 103819, 2023, doi: <https://doi.org/10.1016/j.ijdr.2023.103819>.
- [97] A. Wirtz, W. Kron, P. Löw, e M. Steuer, «The need for data: natural disasters and the challenges of database management», *Nat. Hazards*, vol. 70, n. 1, pagg. 135–157, 2014, doi: 10.1007/s11069-012-0312-4.
- [98] G. Bernardini, R. Lovreglio, e E. Quagliarini, «Proposing behavior-oriented strategies for earthquake emergency evacuation: A behavioral data analysis from New Zealand, Italy and Japan», *Saf. Sci.*, vol. 116, pagg. 295–309, 2019, doi: 10.1016/J.SSCI.2019.03.023.
- [99] L. Milanesi, M. Pilotti, e B. Bacchi, «Using web-based observations to identify thresholds of a person’s stability in a flow», *Water Resour. Res.*, n. 52, pagg. 7793–7805, 2016, doi: 10.1002/2016WR019182.
- [100] T. M. Ferreira, N. Mendes, e R. Silva, «Multiscale Seismic Vulnerability Assessment and Retrofit of Existing Masonry Buildings», *Buildings*, vol. 9, n. 4. 2019, doi: 10.3390/buildings9040091.
- [101] A. Sharifi, «Resilient urban forms: A review of literature on streets and street networks», *Build. Environ.*, vol. 147, n. July 2018, pagg. 171–187, 2019, doi: 10.1016/j.buildenv.2018.09.040.
- [102] A. Shabani, M. Kioumars, e M. Zucconi, «State of the art of simplified analytical methods for seismic vulnerability assessment of unreinforced masonry buildings», *Eng. Struct.*, vol. 239, pag. 112280, 2021, doi: <https://doi.org/10.1016/j.engstruct.2021.112280>.
- [103] N. Shiwakoti, M. Sarvi, e G. Rose, «Modelling pedestrian behaviour under emergency conditions – State-of-the-art and future directions», pagg. 457–473, 2008.
- [104] G. Bernardini, T. M. Ferreira, P. Baquedano Julià, R. Ramírez Eudave, e E. Quagliarini, «Assessing the spatiotemporal impact of users’ exposure and vulnerability to flood risk in urban built environments», *Sustain. Cities Soc.*, vol. 100, 2024, doi: 10.1016/j.scs.2023.105043.
- [105] V. I. Novelli, D. D’Ayala, N. Makhloufi, D. Benouar, e A. Zekagh, «A procedure for the identification of the seismic vulnerability at territorial scale. Application to the Casbah of Algiers», *Bull. Earthq. Eng.*, vol. 13, n. 1, pagg. 177–202, 2015, doi: 10.1007/s10518-014-9666-1.

- [106] N. Chooramun, P. J. Lawrence, e E. R. Galea, «Hybrid Spatial Modelling, from Modelling People in the Vicinity to Urban Scale Simulation of Pedestrians BT - Information Systems Design and Intelligent Applications», 2019, pagg. 439–448.
- [107] M. Chraïbi, A. Tordeux, A. Schadschneider, e A. Seyfried, «Modelling of Pedestrian and Evacuation Dynamics BT - Encyclopedia of Complexity and Systems Science», R. A. Meyers, A c. di Berlin, Heidelberg: Springer Berlin Heidelberg, 2018, pagg. 1–22.
- [108] A. Borrmann, A. Kneidl, G. Köster, S. Ruzika, e M. Thiemann, «Bidirectional coupling of macroscopic and microscopic pedestrian evacuation models», *Saf. Sci.*, vol. 50, n. 8, pagg. 1695–1703, 2012, doi: <https://doi.org/10.1016/j.ssci.2011.12.021>.
- [109] G. Lämmel, A. Seyfried, e B. Steffen, *Large-scale and microscopic: a fast simulation approach for urban areas*. 2014.
- [110] M. Shi, E. W. M. Lee, Y. Ma, W. Xie, e R. Cao, «The density-speed correlated mesoscopic model for the study of pedestrian flow», *Saf. Sci.*, vol. 133, pag. 105019, gen. 2021, doi: [10.1016/j.ssci.2020.105019](https://doi.org/10.1016/j.ssci.2020.105019).
- [111] J. A. Zambrano, J. A. Huertas, E. Segura-Duran, e A. L. Medaglia, «Time Estimation and Hotspot Detection in the Evacuation of a Complex of Buildings: A Mesoscopic Approach and Case Study», *IEEE Trans. Eng. Manag.*, vol. 67, n. 3, pagg. 641–658, ago. 2020, doi: [10.1109/TEM.2019.2960354](https://doi.org/10.1109/TEM.2019.2960354).
- [112] M. Shi, E. W. M. Lee, e Y. Ma, «A novel grid-based mesoscopic model for evacuation dynamics», *Phys. A Stat. Mech. its Appl.*, vol. 497, pagg. 198–210, mag. 2018, doi: [10.1016/j.physa.2017.12.139](https://doi.org/10.1016/j.physa.2017.12.139).
- [113] Y. Choi, H. Yoon, e D. Kim, «Where do people spend their leisure time on dusty days? Application of spatiotemporal behavioral responses to particulate matter pollution», *Ann. Reg. Sci.*, vol. 63, n. 2, pagg. 317–339, ott. 2019, doi: [10.1007/s00168-019-00926-x](https://doi.org/10.1007/s00168-019-00926-x).
- [114] B. Yıldız e G. Çağdaş, «Fuzzy logic in agent-based modeling of user movement in urban space: Definition and application to a case study of a square», *Build. Environ.*, vol. 169, pag. 106597, feb. 2020, doi: [10.1016/j.buildenv.2019.106597](https://doi.org/10.1016/j.buildenv.2019.106597).
- [115] G. Bernardini, M. D’orazio, e E. Quagliarini, *Towards a “behavioural design” approach for seismic risk reduction strategies of buildings and their environment*, vol. 86. 2016.
- [116] N. Kapucu, «Disaster and emergency management systems in urban areas», *Cities*, vol. 29, pagg. S41–S49, mar. 2012, doi: [10.1016/j.cities.2011.11.009](https://doi.org/10.1016/j.cities.2011.11.009).
- [117] A. Buzási, T. Pálvölgyi, e M. S. Csete, «Assessment of climate change performance of urban development projects – Case of Budapest, Hungary», *Cities*, vol. 114, 2021, doi: [10.1016/j.cities.2021.103215](https://doi.org/10.1016/j.cities.2021.103215).
- [118] M. M. Santos, J. C. G. Lanzinha, e A. V. Ferreira, «Review on urbanism and climate change», *Cities*, vol. 114. 2021, doi: [10.1016/j.cities.2021.103176](https://doi.org/10.1016/j.cities.2021.103176).
- [119] K. Bischiniotis, H. De Moel, M. Van Den Homberg, A. Couasnon, e J. Aerts, «A framework for comparing permanent and forecast-based flood risk- reduction strategies», *Sci. Total Environ.*, vol. 720, 2020, doi: [10.1016/j.scitotenv.2020.137572](https://doi.org/10.1016/j.scitotenv.2020.137572).
- [120] S. Yamashita, R. Watanabe, e Y. Shimatani, «Smart adaptation activities and measures against urban flood disasters», *Sustain. Cities Soc.*, vol. 27, pagg. 175–184, nov. 2016, doi: [10.1016/j.scs.2016.06.027](https://doi.org/10.1016/j.scs.2016.06.027).
- [121] E. J. Plate, «Flood risk and flood management», *J. Hydrol.*, 2002, doi: [10.1016/S0022-1694\(02\)00135-X](https://doi.org/10.1016/S0022-1694(02)00135-X).

- [122] C. Arrighi, M. Pregolato, R. J. Dawson, e F. Castelli, «Preparedness against mobility disruption by floods», *Sci. Total Environ.*, 2019, doi: 10.1016/j.scitotenv.2018.11.191.
- [123] B. Kolen e P. H. A. J. M. van Gelder, «Risk-Based Decision-Making for Evacuation in Case of Imminent Threat of Flooding», *Water*, vol. 10, n. 10, pag. 1429, ott. 2018, doi: 10.3390/w10101429.
- [124] D. Lumbroso e M. Davison, «Use of an agent-based model and Monte Carlo analysis to estimate the effectiveness of emergency management interventions to reduce loss of life during extreme floods», *J. Flood Risk Manag.*, vol. 11, pagg. S419–S433, gen. 2018, doi: 10.1111/jfr3.12230.
- [125] H. Hamacher e S. Tjandra, «Mathematical Modeling of Evacuation Problems: A State of The Art», *Pedestr. Evacuation Dyn.*, vol. 2002, gen. 2002.
- [126] Y. Yuan e D. Wang, «Path selection model and algorithm for emergency logistics management», *Comput. Ind. Eng.*, vol. 56, n. 3, pagg. 1081–1094, apr. 2009, doi: 10.1016/j.cie.2008.09.033.
- [127] G. Galindo e R. Batta, «Review of recent developments in OR/MS research in disaster operations management», *Eur. J. Oper. Res.*, vol. 230, n. 2, pagg. 201–211, 2013, doi: 10.1016/j.ejor.2013.01.039.
- [128] V. Bayram, «Optimization models for large scale network evacuation planning and management: A literature review», *Surv. Oper. Res. Manag. Sci.*, vol. 21, n. 2, pagg. 63–84, 2016, doi: <https://doi.org/10.1016/j.sorms.2016.11.001>.
- [129] Y. Ma, W. Xu, L. Qin, e X. Zhao, «Site Selection Models in Natural Disaster Shelters: A Review», *Sustainability*, vol. 11, n. 2, 2019, doi: 10.3390/su11020399.
- [130] Y. Li, B. Hu, D. Zhang, J. Gong, Y. Song, e J. Sun, «Flood evacuation simulations using cellular automata and multiagent systems -a human-environment relationship perspective», *Int. J. Geogr. Inf. Sci.*, vol. 33, n. 11, pagg. 2241–2258, nov. 2019, doi: 10.1080/13658816.2019.1622015.
- [131] M. Shirvani e G. Kesserwani, «Flood–pedestrian simulator for modelling human response dynamics during flood-induced evacuation: Hillsborough stadium case study», *Nat. Hazards Earth Syst. Sci.*, vol. 21, pagg. 3175–3198, ott. 2021, doi: 10.5194/nhess-21-3175-2021.
- [132] G. Bernardini, F. Finizio, M. Postacchini, e E. Quagliarini, «Assessing the flood risk to evacuees in outdoor built environments and relative risk reduction strategies», *Int. J. Disaster Risk Reduct.*, vol. 64, pag. 102493, ott. 2021, doi: 10.1016/j.ijdr.2021.102493.
- [133] K. Matsuo, L. Natainia, e F. Yamada, «Flood and Evacuation Simulations for Urban Flooding», *5th Int. Conf. Flood Manag.*, pagg. 391–398, 2011.
- [134] G. Bernardini *et al.*, «A preliminary combined simulation tool for the risk assessment of pedestrians’ flood-induced evacuation», *Environ. Model. Softw.*, vol. 96, pagg. 14–29, 2017, doi: 10.1016/j.envsoft.2017.06.007.
- [135] M. Shirvani, G. Kesserwani, e P. Richmond, «Agent-based modelling of pedestrian responses during flood emergency: mobility behavioural rules and implications for flood risk analysis», *J. Hydroinformatics*, vol. 22, n. 5, pagg. 1078–1092, set. 2020, doi: 10.2166/hydro.2020.031.
- [136] J. Kim, J. Park, K. Kim, e M. Kim, «RnR-SMART: Resilient smart city evacuation plan based on road network reconfiguration in outbreak response», *Sustain. Cities Soc.*, vol. 75, pag. 103386, dic. 2021, doi: 10.1016/j.scs.2021.103386.
- [137] C. Burstedde, K. Klauck, A. Schadschneider, e J. Zittartz, «Simulation of pedestrian dynamics using a two-dimensional cellular automaton», vol. 295, pagg. 507–525, 2001.

- [138] V. Blue e J. L. Adler, *Cellular automata microsimulation for modeling bi-directional pedestrian walkways*, vol. 35. 2000.
- [139] C. Gloor, P. Stucki, e K. Nagel, «Hybrid Techniques for Pedestrian Simulations BT - Cellular Automata», 2004, pagg. 581–590.
- [140] M. D’Orazio, E. Quagliarini, G. Bernardini, e L. Spalazzi, «EPES - Earthquake pedestrians’ evacuation simulator: A tool for predicting earthquake pedestrians’ evacuation in urban outdoor scenarios», *Int. J. Disaster Risk Reduct.*, vol. 10, n. PA, pagg. 153–177, 2014, doi: 10.1016/j.ijdrr.2014.08.002.
- [141] K. Cheliotis, «An agent-based model of public space use», *Comput. Environ. Urban Syst.*, vol. 81, n. December 2019, pag. 101476, mag. 2020, doi: 10.1016/j.compenvurbsys.2020.101476.
- [142] M. E. Yuksel, «Agent-based evacuation modeling with multiple exits using NeuroEvolution of Augmenting Topologies», *Adv. Eng. Informatics*, vol. 35, n. November 2017, pagg. 30–55, 2018, doi: 10.1016/j.aei.2017.11.003.
- [143] T. I. Lakoba, D. J. Kaup, e N. M. Finkelstein, «Modifications of the Helbing-Molnár-Farkas-Vicsek Social Force Model for Pedestrian Evolution», *Simulation*, vol. 81, n. 5, pagg. 339–352, mag. 2005, doi: 10.1177/0037549705052772.
- [144] D. Helbing e P. Molnar, «Social Force Model for Pedestrian Dynamics», n. May, 1998, doi: 10.1103/PhysRevE.51.4282.
- [145] D. Helbing e P. Molnár, «Social force model for pedestrian dynamics», *Phys. Rev. E*, 1995, doi: 10.1103/PhysRevE.51.4282.
- [146] A. Johansson, D. Helbing, e P. K. Shukla, «Specification of the Social Force Pedestrian Model by Evolutionary Adjustment», n. May 2014, 2007, doi: 10.1142/S0219525907001355.
- [147] F. Pirlone, I. Spadaro, e S. Candia, «More Resilient Cities to Face Higher Risks. The Case of Genoa», *Sustainability*, vol. 12, n. 12. 2020, doi: 10.3390/su12124825.
- [148] H. Entorf e A. Jensen, «Willingness-to-pay for hazard safety – A case study on the valuation of flood risk reduction in Germany», *Saf. Sci.*, vol. 128, pag. 104657, 2020, doi: 10.1016/J.SSCI.2020.104657.
- [149] S. F. Balica, I. Popescu, L. Beevers, e N. G. Wright, «Parametric and physically based modelling techniques for flood risk and vulnerability assessment: A comparison», *Environ. Model. Softw.*, vol. 41, pagg. 84–92, 2013, doi: 10.1016/j.envsoft.2012.11.002.
- [150] J. Natanian, O. Aleksandrowicz, e T. Auer, «A parametric approach to optimizing urban form, energy balance and environmental quality: The case of Mediterranean districts», *Appl. Energy*, vol. 254, pag. 113637, nov. 2019, doi: 10.1016/j.apenergy.2019.113637.
- [151] X. Li, S. Erpicum, E. Mignot, P. Archambeau, M. Piroton, e B. Dewals, «Laboratory modelling of urban flooding», *Sci. Data*, vol. 9, n. 1, pag. 159, apr. 2022, doi: 10.1038/s41597-022-01282-w.
- [152] T. Osman, «A framework for cities and environmental resilience assessment of local governments», *Cities*, vol. 118, 2021, doi: 10.1016/j.cities.2021.103372.
- [153] A. Yari *et al.*, «Behavioral, health- related and demographic risk factors of death in floods: A case-control study», *PLoS One*, vol. 16, n. 12, pag. e0262005, dic. 2021, doi: 10.1371/journal.pone.0262005.
- [154] M. Russo *et al.*, «Morphological Systems of Open Spaces in Built Environment Prone to Sudden-Onset Disasters», in *Sustainability in Energy and Buildings 2020 (Part of the Smart*

- Innovation, Systems and Technologies book series - SIST, volume 203 - ISSN: 2190-3018*), J. Littlewood, R. J. Howlett, e L. C. Jain, A c. di Springer, Singapore, 2021, pagg. 321–331.
- [155] E. Ronchi, E. D. Kuligowski, P. A. Reneke, R. D. Peacock, e D. Nilsson, «The Process of Verification and Validation of Building Fire Evacuation Models», *NIST Tech. Note*, vol. 1822, 2013.
- [156] J. Xin e C. Huang, «Fire risk analysis of residential buildings based on scenario clusters and its application in fire risk management», *Fire Saf. J.*, vol. 62, pagg. 72–78, 2013, doi: <https://doi.org/10.1016/j.firesaf.2013.09.022>.
- [157] E. Quagliarini, G. Bernardini, G. Romano, e M. D’Orazio, «Users’ vulnerability and exposure in Public Open Spaces (squares): A novel way for accounting them in multi-risk scenarios», *Cities*, vol. 133, pag. 104160, 2023, doi: <https://doi.org/10.1016/j.cities.2022.104160>.
- [158] M. Xofi *et al.*, «On the Multi-hazard Risk Assessment of Urban Areas: Identification and Analysis of Exposure and Physical Vulnerability Indicators», in *Springer Proceedings in Materials*, vol. 16, 2022, pagg. 146–155.
- [159] M. D’Orazio, E. Quagliarini, G. Bernardini, e L. Spalazzi, «EPES – Earthquake pedestrians’ evacuation simulator: A tool for predicting earthquake pedestrians’ evacuation in urban outdoor scenarios», *Int. J. Disaster Risk Reduct.*, vol. 10, pagg. 153–177, 2014, doi: <https://doi.org/10.1016/j.ijdr.2014.08.002>.
- [160] S. Savić *et al.*, «Heat wave risk assessment and mapping in urban areas: case study for a midsized Central European city, Novi Sad (Serbia)», *Nat. Hazards*, vol. 91, n. 3, pagg. 891–911, apr. 2018, doi: [10.1007/s11069-017-3160-4](https://doi.org/10.1007/s11069-017-3160-4).
- [161] J. J. Wang, «Flood risk maps to cultural heritage: Measures and process», *J. Cult. Herit.*, vol. 16, n. 2, pagg. 210–220, 2015, doi: [10.1016/j.culher.2014.03.002](https://doi.org/10.1016/j.culher.2014.03.002).
- [162] M. D’Orazio, S. Longhi, P. Olivetti, e G. Bernardini, «Design and experimental evaluation of an interactive system for pre-movement time reduction in case of fire», *Autom. Constr.*, vol. 52, pagg. 16–28, apr. 2015, doi: [10.1016/j.autcon.2015.02.015](https://doi.org/10.1016/j.autcon.2015.02.015).
- [163] S. R. Shrestha, R. Sliuzas, e M. Kuffer, «Open spaces and risk perception in post-earthquake Kathmandu city», *Appl. Geogr.*, vol. 93, pagg. 81–91, apr. 2018, doi: [10.1016/J.APGEOG.2018.02.016](https://doi.org/10.1016/J.APGEOG.2018.02.016).
- [164] A. B. Aslam, I. A. Rana, S. S. Shah, e G. Mohuddin, «Climate change and glacial lake outburst flood (GLOF) risk perceptions: An empirical study of Ghizer District, Gilgit-Baltistan Pakistan», *Int. J. Disaster Risk Reduct.*, vol. 83, 2022, doi: [10.1016/j.ijdr.2022.103392](https://doi.org/10.1016/j.ijdr.2022.103392).
- [165] S. Boschi, L. Galano, e A. Vignoli, «Mechanical characterisation of Tuscany masonry typologies by in situ tests», *Bull. Earthq. Eng.*, vol. 17, n. 1, pagg. 413–438, 2019, doi: [10.1007/s10518-018-0451-4](https://doi.org/10.1007/s10518-018-0451-4).
- [166] M. Corradi e A. Borri, «A database of the structural behavior of masonry in shear», *Bull. Earthq. Eng.*, vol. 16, n. 9, pagg. 3905–3930, 2018, doi: [10.1007/s10518-018-0328-6](https://doi.org/10.1007/s10518-018-0328-6).
- [167] L. Binda, A. Saisi, e C. Tiraboschi, «Investigation procedures for the diagnosis of historic masonries», *Constr. Build. Mater.*, vol. 14, n. 4, pagg. 199–233, 2000, doi: [10.1016/S0950-0618\(00\)00018-0](https://doi.org/10.1016/S0950-0618(00)00018-0).
- [168] A. Borri, G. Castori, M. Corradi, e E. Speranzini, «Shear behavior of unreinforced and reinforced masonry panels subjected to in situ diagonal compression tests», *Constr. Build. Mater.*, 2011, doi: [10.1016/j.conbuildmat.2011.01.009](https://doi.org/10.1016/j.conbuildmat.2011.01.009).
- [169] A. Borri, M. Corradi, e E. Speranzini, «Caratterizzazione meccanica di murature del XX secolo: alcune sperimentazioni», gen. 2009.

- [170] S. Boschi, C. Bernardini, e A. Vignoli, «The Tuscany Masonry Database Website», *Heritage*, vol. 4, n. 1, pagg. 230–248, 2021, doi: 10.3390/heritage4010014.
- [171] Norme Tecniche per le Costruzioni, *D.M. del Ministero delle Infrastrutture e dei Trasporti del 17/01/2018. Aggiornamento delle “Norme Tecniche per le Costruzioni”*. Rome, Italy, Italy: Gazzetta Ufficiale n.42 del 20 febbraio 2018, 2018, pagg. 1–337.
- [172] Circolare 7/2019, «Circolare del Ministero delle Infrastrutture e dei Trasporti, n.7 del 21 Gennaio 2019: ‘Istruzioni per l’applicazione dell’aggiornamento delle Norme Tecniche per le Costruzioni di cui al D.M. 17 gennaio 2018’». Consiglio Superiore dei Lavori Pubblici. G.U. n.35 del 11.02.2019, Rome, Italy, 2019.
- [173] A. Dall’Asta, G. Leoni, A. Meschini, E. Petrucci, e A. Zona, «Integrated approach for seismic vulnerability analysis of historic massive defensive structures», *J. Cult. Herit.*, vol. 35, pagg. 86–98, 2019, doi: 10.1016/J.CULHER.2018.07.004.
- [174] G. Milani e M. Valente, «Failure analysis of seven masonry churches severely damaged during the 2012 Emilia-Romagna (Italy) earthquake: Non-linear dynamic analyses vs conventional static approaches», *Eng. Fail. Anal.*, vol. 54, pagg. 13–56, 2015, doi: 10.1016/J.ENGFAILANAL.2015.03.016.
- [175] ASTM C1197-20, «Standard Test Method for In Situ Measurement of Masonry Deformability Properties Using the Flatjack Method». pagg. 1–6, 2021, doi: 10.1520/C1197-20E01.
- [176] A. Incerti, A. R. Tilocca, F. Ferretti, e C. Mazzotti, «Influence of Masonry Texture on the Shear Strength of FRCM Reinforced Panels», in *RILEM Bookseries*, vol. 18, 2019.
- [177] ASTM C1531-03, «Standard Test Methods for In Situ Measurement Of Masonry Mortar Joint Shear», vol. 03. pagg. 1–6, 2003.
- [178] P. Mishra, C. Pandey, U. Singh, A. Gupta, C. Sahu, e A. Keshri, «Descriptive statistics and normality tests for statistical data», *Ann. Card. Anaesth.*, vol. 22, n. 1, pag. 67, 2019, doi: 10.4103/aca.ACA_157_18.
- [179] J. P. M. de Sá, *Applied Statistics Using SPSS, STATISTICA, MATLAB and R*. Springer-Verlag Berlin Heidelberg, 2007.
- [180] P. J. Rousseeuw e M. Hubert, «Robust statistics for outlier detection», *Wiley Interdiscip. Rev. Data Min. Knowl. Discov.*, vol. 1, n. 1, pagg. 73–79, gen. 2011, doi: 10.1002/widm.2.
- [181] CEN European Committee for Standardization, «Eurocode 6, EN 1996-1-1: Design of Masonry Structures—Part1-1: General Rules for Reinforced and Unreinforced Masonry Structures». Bruxelles, 2005.
- [182] ASTM E519-15, «Standard Test Method for Diagonal Tension (Shear) in Masonry Assemblages». pag. 5, 2015, doi: 10.1520/E0519_E0519M-15.
- [183] A. Armanasco e D. Foppoli, «A flat jacks method for in situ testing of brick masonry shear characteristics», *Constr. Build. Mater.*, 2020, doi: 10.1016/j.conbuildmat.2020.119840.
- [184] G. Romano, E. Quagliarini, G. Pace, e M. Renzi, «Local masonry typologies still unregulated by the Italian Building Code: how to behave? The case of the stone-and-brick mixed masonry in the Marche Region», in *Colloqui.AT.e 2023 - In Transition: challenges and opportunities for the build heritage*, 2023, pagg. 1183–1195.
- [185] S. Soares-Frazão e Y. Zech, «Dam-break flow through an idealised city», *J. Hydraul. Res.*, vol. 46, n. 5, pagg. 648–658, set. 2008, doi: 10.3826/jhr.2008.3164.

- [186] G. Bernardini, G. Romano, L. Soldini, e E. Quagliarini, «How urban layout and pedestrian evacuation behaviours can influence flood risk assessment in riverine historic built environments», *Sustain. Cities Soc.*, vol. 70, 2021, doi: 10.1016/j.scs.2021.102876.
- [187] M. Velickovic, Y. Zech, e S. Soares-Frazão, «Steady-flow experiments in urban areas and anisotropic porosity model», *J. Hydraul. Res.*, 2017, doi: 10.1080/00221686.2016.1238013.
- [188] E. Mignot, X. Li, e B. Dewals, «Experimental modelling of urban flooding: A review», *J. Hydrol.*, vol. 568, pagg. 334–342, gen. 2019, doi: 10.1016/j.jhydrol.2018.11.001.
- [189] A. Paquier, E. Mignot, e P.-H. Bazin, «From Hydraulic Modelling to Urban Flood Risk», *Procedia Eng.*, vol. 115, pagg. 37–44, 2015, doi: 10.1016/j.proeng.2015.07.352.
- [190] G. Testa, D. Zuccalà, F. Alcrudo, J. Mulet, e S. Soares-Frazão, «Flash flood flow experiment in a simplified urban district», *J. Hydraul. Res.*, 2007, doi: 10.1080/00221686.2007.9521831.
- [191] R. Beretta, G. Ravazzani, C. Maiorano, e M. Mancini, «Simulating the influence of buildings on flood inundation in Urban areas», *Geosci.*, 2018, doi: 10.3390/geosciences8020077.
- [192] V. Te Chow, *Open-Channel Hydraulics*. New York: McGraw-Hill, 1959.
- [193] N. M. De Sousa, W. D. A. Soares, S. R. Da Silva, e E. C. Do Nascimento, «Contribution of public squares to the reduction of urban flooding risk», *Rev. Ambient. e Agua*, 2019, doi: 10.4136/ambi-agua.2374.
- [194] K. Zakariya, N. Z. Harun, e M. Mansor, «Spatial Characteristics of Urban Square and Sociability: A Review of the City Square, Melbourne», *Procedia - Soc. Behav. Sci.*, vol. 153, 2014, doi: 10.1016/j.sbspro.2014.10.099.
- [195] P. Martí, L. Serrano-Estrada, e A. Nolasco-Cirugeda, «Using locative social media and urban cartographies to identify and locate successful urban plazas», *Cities*, vol. 64, pagg. 66–78, 2017, doi: <https://doi.org/10.1016/j.cities.2017.02.007>.
- [196] Q. Dai, X. Zhu, L. Zhuo, D. Han, Z. Liu, e S. Zhang, «A hazard-human coupled model (HazardCM) to assess city dynamic exposure to rainfall-triggered natural hazards», *Environ. Model. Softw.*, vol. 127, n. May 2019, pag. 104684, mag. 2020, doi: 10.1016/j.envsoft.2020.104684.
- [197] K. Haynes *et al.*, «Exploring the circumstances surrounding flood fatalities in Australia—1900–2015 and the implications for policy and practice», *Environ. Sci. Policy*, vol. 76, pagg. 165–176, 2017, doi: 10.1016/J.ENVSCI.2017.07.003.
- [198] J. Nemeškal, M. Ouředníček, e L. Pospíšilová, «Temporality of urban space: daily rhythms of a typical week day in the Prague metropolitan area», *J. Maps*, vol. 16, n. 1, 2020, doi: 10.1080/17445647.2019.1709577.
- [199] F. Lindberg e C. S. B. Grimmond, «Nature of vegetation and building morphology characteristics across a city: Influence on shadow patterns and mean radiant temperatures in London», *Urban Ecosyst.*, vol. 14, n. 4, pagg. 617–634, 2011, doi: 10.1007/s11252-011-0184-5.
- [200] J. C. García-Palomares, M. H. Salas-Olmedo, B. Moya-Gómez, A. Condeço-Melhorado, e J. Gutiérrez, «City dynamics through Twitter: Relationships between land use and spatiotemporal demographics», *Cities*, vol. 72, 2018, doi: 10.1016/j.cities.2017.09.007.
- [201] L. B. L. da Silva, M. H. Alencar, e A. T. de Almeida, «A novel spatiotemporal multi-attribute method for assessing flood risks in urban spaces under climate change and demographic scenarios», *Sustain. Cities Soc.*, vol. 76, n. July 2021, pag. 103501, gen. 2022, doi: 10.1016/j.scs.2021.103501.

- [202] C. Curt, «Multirisk: What trends in recent works? – A bibliometric analysis», *Sci. Total Environ.*, vol. 763, pag. 142951, apr. 2021, doi: 10.1016/j.scitotenv.2020.142951.
- [203] M. Polese, M. Di Ludovico, M. Gaetani d’Aragona, A. Prota, e G. Manfredi, «Regional vulnerability and risk assessment accounting for local building typologies», *Int. J. Disaster Risk Reduct.*, vol. 43, 2020, doi: 10.1016/j.ijdr.2019.101400.
- [204] Ministry of Interior (Italy), «DM 03/08/2015: Fire safety criteria (Approvazione di norme tecniche di prevenzione incendi, ai sensi dell’articolo 15 del decreto legislativo 8 marzo 2006, n. 139.)». 2015.
- [205] Federal Emergency Management Agency, «Risk Management Series. Handbook for Rapid Visual Screening of Buildings to Evaluate Terrorism Risks (FEMA 455)», 2009.
- [206] Y. Hahm, H. Yoon, e Y. Choi, «The effect of built environments on the walking and shopping behaviors of pedestrians; A study with GPS experiment in Sinchon retail district in Seoul, South Korea», *Cities*, vol. 89, 2019, doi: 10.1016/j.cities.2019.01.020.
- [207] M. Bloomberg e A. Burden, «New York City Pedestrian Level of Service Study–Phase 1», New York, NY, USA, 2006.
- [208] E. Bosina e U. Weidmann, «Estimating pedestrian speed using aggregated literature data», *Phys. A Stat. Mech. its Appl.*, vol. 468, pagg. 1–29, feb. 2017, doi: 10.1016/j.physa.2016.09.044.
- [209] P. Jia, Y. Qiu, e A. E. Gaughan, «A fine-scale spatial population distribution on the High-resolution Gridded Population Surface and application in Alachua County, Florida», *Appl. Geogr.*, vol. 50, 2014, doi: 10.1016/j.apgeog.2014.02.009.
- [210] M. Fleischmann, A. Feliciotti, e W. Kerr, «Evolution of Urban Patterns: Urban Morphology as an Open Reproducible Data Science», *Geogr. Anal.*, pag. gean.12302, lug. 2021, doi: 10.1111/gean.12302.
- [211] H. Chang *et al.*, «Assessment of urban flood vulnerability using the social-ecological-technological systems framework in six US cities», *Sustain. Cities Soc.*, vol. 68, 2021, doi: 10.1016/j.scs.2021.102786.
- [212] A. Gandini, L. Garmendia, I. Prieto, I. Álvarez, e J. T. San-José, «A holistic and multi-stakeholder methodology for vulnerability assessment of cities to flooding and extreme precipitation events», *Sustain. Cities Soc.*, 2020, doi: 10.1016/j.scs.2020.102437.
- [213] A. Gandini, L. Quesada, I. Prieto, e L. Garmendia, «Climate change risk assessment: A holistic multi-stakeholder methodology for the sustainable development of cities», *Sustain. Cities Soc.*, vol. 65, 2021, doi: 10.1016/j.scs.2020.102641.
- [214] W. H. M. Wan Mohtar, J. Abdullah, K. N. Abdul Maulud, e N. S. Muhammad, «Urban flash flood index based on historical rainfall events», *Sustain. Cities Soc.*, vol. 56, 2020, doi: 10.1016/j.scs.2020.102088.
- [215] P. Puchol-Salort, J. O’Keeffe, M. van Reeuwijk, e A. Mijic, «An urban planning sustainability framework: Systems approach to blue green urban design», *Sustain. Cities Soc.*, vol. 66, pag. 102677, mar. 2021, doi: 10.1016/j.scs.2020.102677.
- [216] E. L. French, S. J. Birchall, K. Landman, e R. D. Brown, «Designing public open space to support seismic resilience: A systematic review», *Int. J. Disaster Risk Reduct.*, vol. 34, pagg. 1–10, mar. 2019, doi: 10.1016/j.ijdr.2018.11.001.
- [217] Q. Fan, Z. Tian, e W. Wang, «Study on Risk Assessment and Early Warning of Flood-Affected Areas when a Dam Break Occurs in a Mountain River», *Water*, vol. 10, n. 10, pag. 1369, set. 2018, doi: 10.3390/w10101369.

- [218] S. Jamrussri e Y. Toda, «Available Flood Evacuation Time for High-Risk Areas in the Middle Reach of Chao Phraya River Basin», *Water*, vol. 10, n. 12, pag. 1871, dic. 2018, doi: 10.3390/w10121871.
- [219] M. R. Najafi, Y. Zhang, e N. Martyn, «A flood risk assessment framework for interdependent infrastructure systems in coastal environments», *Sustain. Cities Soc.*, vol. 64, 2021, doi: 10.1016/j.scs.2020.102516.
- [220] M. M. M. Piyumi, C. Abenayake, A. Jayasinghe, e E. Wijegunaratna, «Urban Flood Modeling Application: Assess the Effectiveness of Building Regulation in Coping with Urban Flooding Under Precipitation Uncertainty», *Sustain. Cities Soc.*, vol. 75, 2021, doi: 10.1016/j.scs.2021.103294.
- [221] L. Zhuo e D. Han, «Agent-based modelling and flood risk management: A compendious literature review», *J. Hydrol.*, vol. 591, pag. 125600, dic. 2020, doi: 10.1016/j.jhydrol.2020.125600.
- [222] P.-H. Bazin, E. Mignot, e A. Paquier, «Computing flooding of crossroads with obstacles using a 2D numerical model», *J. Hydraul. Res.*, vol. 55, n. 1, pagg. 72–84, gen. 2017, doi: 10.1080/00221686.2016.1217947.
- [223] G. Bernardini, S. Camilli, E. Quagliarini, e M. D’Orazio, «Flooding risk in existing urban environment: from human behavioral patterns to a microscopic simulation model», *Energy Procedia*, vol. 134, pagg. 131–140, ott. 2017, doi: 10.1016/j.egypro.2017.09.549.
- [224] D. Domingo, G. Palka, e A. M. Hersperger, «Effect of zoning plans on urban land-use change: A multi-scenario simulation for supporting sustainable urban growth», *Sustain. Cities Soc.*, vol. 69, 2021, doi: 10.1016/j.scs.2021.102833.
- [225] S. Dong, T. Yu, H. Farahmand, e A. Mostafavi, «Probabilistic modeling of cascading failure risk in interdependent channel and road networks in urban flooding», *Sustain. Cities Soc.*, vol. 62, 2020, doi: 10.1016/j.scs.2020.102398.
- [226] Y. Han e P. Mozumder, «Risk-based flood adaptation assessment for large-scale buildings in coastal cities using cloud computing», *Sustain. Cities Soc.*, vol. 76, 2022, doi: 10.1016/j.scs.2021.103415.
- [227] R. J. Cox, T. D. Shand, M. J. Blacka, e M. J. Shand, T.D.Blacka, *Australian Rainfall & Runoff revision project 10: Appropriate safety criteria for people*, n. April. 2010.
- [228] H. Takagi *et al.*, «Storm surge and evacuation in urban areas during the peak of a storm», *Coast. Eng.*, vol. 108, pagg. 1–9, feb. 2016, doi: 10.1016/j.coastaleng.2015.11.002.
- [229] S. T. Ashley e W. S. Ashley, «Flood fatalities in the United States», *J. Appl. Meteorol. Climatol.*, 2008, doi: 10.1175/2007JAMC1611.1.
- [230] N. N. Samany, M. Sheybani, e S. Zlatanova, «Detection of safe areas in flood as emergency evacuation stations using modified particle swarm optimization with local search», *Appl. Soft Comput.*, vol. 111, pag. 107681, nov. 2021, doi: 10.1016/j.asoc.2021.107681.
- [231] C. Dias, N. A. Rahman, e A. Zaiter, «Evacuation under flooded conditions: Experimental investigation of the influence of water depth on walking behaviors», *Int. J. Disaster Risk Reduct.*, vol. 58, n. November 2020, pag. 102192, 2021, doi: 10.1016/j.ijdr.2021.102192.
- [232] X. Jia, G. Morel, H. Martell-Flore, F. Hissel, e J.-L. Batoz, «Fuzzy logic based decision support for mass evacuations of cities prone to coastal or river floods», *Environ. Model. Softw.*, vol. 85, pagg. 1–10, nov. 2016, doi: 10.1016/j.envsoft.2016.07.018.
- [233] J. M. Bodoque *et al.*, «Improvement of resilience of urban areas by integrating social perception in flash-flood risk management», *J. Hydrol.*, feb. 2016, doi: 10.1016/j.jhydrol.2016.02.005.

- [234] L. Shi, Q. Xie, X. Cheng, L. Chen, Y. Zhou, e R. Zhang, «Developing a database for emergency evacuation model», *Build. Environ.*, vol. 44, n. 8, pagg. 1724–1729, ago. 2009, doi: 10.1016/j.buildenv.2008.11.008.
- [235] E. Ronchi, «Developing and validating evacuation models for fire safety engineering», *Fire Saf. J.*, pag. 103020, mag. 2020, doi: 10.1016/j.firesaf.2020.103020.
- [236] E. Quagliarini, G. Romano, G. Bernardini, e M. D’Orazio, «Leaving or Sheltering? a Simulation-Based Comparison of Flood Evacuation Strategies in Urban Built Environments», in *Sustainability in Energy and Buildings 2021. Smart Innovation, Systems and Technologies*, vol 263, J. R. Littlewood, R. J. Howlett, e L. C. Jain, A c. di Springer Singapore, 2022, pagg. 113–123.
- [237] J. Zhou *et al.*, «Research on earthquake emergency response modes of individuals based on social surveillance video», *Int. J. Disaster Risk Reduct.*, vol. 28, n. November 2017, pagg. 350–362, giu. 2018, doi: 10.1016/j.ijdr.2018.03.015.
- [238] M. Haghani e M. Sarvi, «Crowd behaviour and motion: Empirical methods», *Transp. Res. Part B Methodol.*, vol. 107, pagg. 253–294, gen. 2018, doi: 10.1016/J.TRB.2017.06.017.
- [239] L. Milanesi, M. Pilotti, e R. Ranzi, «A conceptual model of people’s vulnerability to floods», *Water Resour. Res.*, vol. 51, n. 1, pagg. 5375–5377, gen. 2015, doi: 10.1002/2014WR016172.
- [240] J. Xia, Q. Chen, R. A. Falconer, S. Deng, e P. Guo, «Stability criterion for people in floods for various slopes», *Proc. Inst. Civ. Eng. - Water Manag.*, vol. 169, n. 4, pagg. 180–189, 2016, doi: 10.1680/wama.14.00110.
- [241] J. Xia, R. A. Falconer, Y. Wang, e X. Xiao, «New criterion for the stability of a human body in floodwaters», *J. Hydraul. Res.*, n. July, 2014, doi: 10.1080/00221686.2013.875073.
- [242] H. U. Bae, K. M. Yun, J. Y. Yoon, e N. H. Lim, «Human stability with respect to overtopping flow on the breakwater», *Int. J. Appl. Eng. Res.*, 2016.
- [243] H.-K. Lee, W.-H. Hong, e Y.-H. Lee, «Experimental study on the influence of water depth on the evacuation speed of elderly people in flood conditions», *Int. J. Disaster Risk Reduct.*, vol. 39, pag. 101198, ott. 2019, doi: 10.1016/j.ijdr.2019.101198.
- [244] Y. Wang, M. Kyriakidis, e V. N. Dang, «Incorporating human factors in emergency evacuation – An overview of behavioral factors and models», *Int. J. Disaster Risk Reduct.*, vol. 60, pag. 102254, 2021, doi: 10.1016/J.IJDRR.2021.102254.
- [245] H. Nakanishi, J. Black, e Y. Suenaga, «Investigating the flood evacuation behaviour of older people: A case study of a rural town in Japan», *Res. Transp. Bus. Manag.*, vol. 30, pag. 100376, 2019, doi: 10.1016/J.RTBM.2019.100376.
- [246] M. Diakakis, «Types of behavior of flood victims around floodwaters. Correlation with situational and demographic factors», *Sustain.*, vol. 12, n. 11, 2020, doi: 10.3390/su12114409.
- [247] O. Petrucci *et al.*, «Flood fatalities in Europe, 1980-2018: Variability, features, and lessons to learn», *Water (Switzerland)*, vol. 11, n. 8, 2019, doi: 10.3390/w11081682.
- [248] Y. Feng, C. Brenner, e M. Sester, «Flood severity mapping from Volunteered Geographic Information by interpreting water level from images containing people: A case study of Hurricane Harvey», *ISPRS J. Photogramm. Remote Sens.*, vol. 169, pagg. 301–319, 2020, doi: 10.1016/J.ISPRSJPRS.2020.09.011.
- [249] J. Le Coz *et al.*, «Crowdsourced data for flood hydrology: Feedback from recent citizen science projects in Argentina, France and New Zealand», *J. Hydrol.*, vol. 541, pagg. 766–777, 2016, doi: 10.1016/J.JHYDROL.2016.07.036.

- [250] T. H. Assumpção, I. Popescu, A. Jonoski, e D. P. Solomatine, «Citizen observations contributing to flood modelling: opportunities and challenges», *Hydrol. Earth Syst. Sci.*, vol. 22, n. 2, pagg. 1473–1489, 2018, doi: 10.5194/hess-22-1473-2018.
- [251] V. Kutija *et al.*, *Model Validation Using Crowd-Sourced Data From A Large Pluvial Flood* Kutija Vedrana, Bertsch Robert, Glenis Vassilis, Alderson David, Walsh Claire, Robinson John, Kilsby C. 2014.
- [252] B. Alizadeh Kharazi e A. H. Behzadan, «Flood depth mapping in street photos with image processing and deep neural networks», *Comput. Environ. Urban Syst.*, vol. 88, pag. 101628, lug. 2021, doi: 10.1016/j.compenvurbsys.2021.101628.
- [253] P. Chaudhary, S. D’Aronco, M. de Vitry, J. P. Leitão, e J. D. Wegner, «FLOOD-WATER LEVEL ESTIMATION FROM SOCIAL MEDIA IMAGES», *ISPRS Ann. Photogramm. Remote Sens. Spat. Inf. Sci.*, vol. IV-2/W5, pagg. 5–12, 2019, doi: 10.5194/isprs-annals-IV-2-W5-5-2019.
- [254] MassMotion Guide, «MassMotion Guide», 2020.
- [255] D. Helbing, I. Farkas, e T. Vicsek, «Simulating dynamical features of escape panic», *Nature*, vol. 407, n. 6803, pagg. 487–490, set. 2000, doi: 10.1038/35035023.
- [256] E. Quagliarini, G. Romano, e G. Bernardini, «Investigating pedestrian behavioral patterns under different floodwater conditions: A video analysis on real flood evacuations», *Saf. Sci.*, vol. 161, pag. 106083, mag. 2023, doi: 10.1016/j.ssci.2023.106083.
- [257] J. J. Fruin, *Pedestrian planning and design*. New York: Metropolitan Association of Urban Designers and Environmental Planners, 1971.
- [258] A. Schadschneider, W. Klingsch, H. Klüpfel, T. Kretz, C. Rogsch, e A. Seyfried, «Evacuation Dynamics: Empirical Results, Modeling and Applications», *Encyclopedia of Complexity and Systems Science*. Springer New York, pagg. 3142-3176 LA-English, 2009, doi: 10.1007/978-0-387-30440-3_187.
- [259] T. Robin, G. Antonini, M. Bierlaire, e J. Cruz, «Specification, estimation and validation of a pedestrian walking behavior model», *Transp. Res. Part B Methodol.*, 2009, doi: 10.1016/j.trb.2008.06.010.
- [260] M. Kobes, I. Helsloot, B. de Vries, e J. G. Post, «Building safety and human behaviour in fire: A literature review», *Fire Safety Journal*. 2010, doi: 10.1016/j.firesaf.2009.08.005.
- [261] J. Lin, R. Zhu, N. Li, e B. Becerik-Gerber, «How occupants respond to building emergencies: A systematic review of behavioral characteristics and behavioral theories», *Saf. Sci.*, vol. 122, pag. 104540, feb. 2020, doi: 10.1016/j.ssci.2019.104540.
- [262] R. Melo *et al.*, «Defining evacuation travel times and safety areas in a debris flow hazard scenario», *Sci. Total Environ.*, 2020, doi: 10.1016/j.scitotenv.2019.136452.
- [263] S. Opper, P. Cinque, e B. Davies, «Timeline modelling of flood evacuation operations», vol. 3, pagg. 175–187, 2010, doi: 10.1016/j.proeng.2010.07.017.
- [264] British Standards Institution, *The application of fire safety engineering principles to fire safety design of buildings-Part 6: Human factors: Life safety strategies — Occupant evacuation, behaviour and condition (Sub-system 6)*, n. PD 7974-6:2004. 2004.
- [265] T. L. Saaty, «The analytic hierarchy process: planning», *Prior. Setting. Resour. Alloc. MacGraw-Hill, New York Int. B. Co.*, 1980.
- [266] S. Ibri, «An ILP for Joint Districting and Evacuation», in *Lecture Notes in Networks and Systems*, 2022, vol. 359 LNNS, n. November, pagg. 540–549, doi: 10.1007/978-3-030-89880-9_40.

- [267] M. Ahmadi, A. Seifi, e B. Tootooni, «A humanitarian logistics model for disaster relief operation considering network failure and standard relief time : A case study on San Francisco district», *Transp. Res. Part E*, vol. 75, pagg. 145–163, 2015, doi: 10.1016/j.tre.2015.01.008.
- [268] A. Xie, X. Wang, e S. Lu, «Risk Minimization Routing Against Geographically Correlated Failures», *IEEE Access*, vol. 7, pagg. 62920–62929, 2019, doi: 10.1109/ACCESS.2019.2916834.
- [269] G. Bernardini, S. Santarelli, E. Quagliarini, e M. D’Orazio, «Dynamic guidance tool for a safer earthquake pedestrian evacuation in urban systems», *Comput. Environ. Urban Syst.*, vol. 65, pagg. 150–161, 2017, doi: 10.1016/j.compenvurbsys.2017.07.001.
- [270] A. Mu e S. Yu, «Calculation of optimal path in post-earthquake emergency period», *World Earthq. Eng.*, vol. 34, n. 1, pagg. 113–120, 2018.
- [271] P. Guo, J. Xia, M. Zhou, R. A. . Falconer, Q. Chen, e X. Zhang, «Selection of optimal escape routes in a flood-prone area based on 2D hydrodynamic modelling», *J. Hydroinformatics*, vol. 20, n. 6, pagg. 1310–1322, 2018, doi: 10.2166/hydro.2018.161.
- [272] M. Péroche, F. Leone, e R. Gutton, «An accessibility graph-based model to optimize tsunami evacuation sites and routes in Martinique, France», *Adv. Geosci.*, vol. 38, pagg. 1–8, 2014, doi: 10.5194/adgeo-38-1-2014.
- [273] Y. Zhu *et al.*, «Optimal Evacuation Route Planning of Urban Personnel at Different Risk Levels of Flood Disasters Based on the Improved 3D Dijkstra ’ s Algorithm», *Sustain.*, vol. 14, n. 16, pag. 10250, 2022, doi: <https://doi.org/10.3390/su141610250>.
- [274] European Commission, «European Overview Assessment of Member States ’ reports on Preliminary Flood Risk Assessment and Identification of Areas of Potentially Significant Flood Risk». 2015, doi: <https://doi.org/10.2779/576456>.
- [275] VV.AA., «Studi e proposte per la definizione del rischio idraulico e dell’erosione nei bacini idrografici delle aree montane - Parte A: rischio idraulico delle aree montane (in Italian - Studies for defining hydraulic risk and erosion in mountain areas)». Autorità di Bacino della Regione Marche, 2005.
- [276] M. Giandotti, «Previsione delle piene e delle magre dei corsi d’acqua (in Italian - Forecast of floods and low levels of watercourses)», *Ist. Poligr. dello Stato*, vol. 8, pagg. 107–117, 1934.
- [277] T. Haq, G. Halik, e E. Hidayah, «Flood routing model using integration of Delft3D and GIS (case study: Tanggul watershed, Jember)», in *AIP Conference Proceedings*, 2020, vol. 2278, n. October, pag. 020052, doi: 10.1063/5.0014607.
- [278] K. Hassaballah, Y. Mohamed, A. Omer, e S. Uhlenbrook, «Modelling the Inundation and Morphology of the Seasonally Flooded Mayas Wetlands in the Dinder National Park-Sudan», *Environ. Process.*, vol. 7, n. 3, pagg. 723–747, set. 2020, doi: 10.1007/s40710-020-00444-5.
- [279] M. A. Al Baky, M. Islam, e S. Paul, «Flood Hazard, Vulnerability and Risk Assessment for Different Land Use Classes Using a Flow Model», *Earth Syst. Environ.*, vol. 4, n. 1, pagg. 225–244, mar. 2020, doi: 10.1007/s41748-019-00141-w.
- [280] S. D. Sandbach *et al.*, «Hydrodynamic modelling of tidal-fluvial flows in a large river estuary», *Estuar. Coast. Shelf Sci.*, vol. 212, n. June, pagg. 176–188, nov. 2018, doi: 10.1016/j.ecss.2018.06.023.
- [281] A. Borri, M. Corradi, e A. De Maria, «The Failure of Masonry Walls by Disaggregation and the Masonry Quality Index», *Heritage*, vol. 3, n. 4. pagg. 1162–1198, 2020, doi: 10.3390/heritage3040065.

- [282] F. Porco, G. Porco, G. Uva, e M. Sangirardi, «Experimental characterization of “non-engineered” masonry systems in a highly seismic prone area», *Constr. Build. Mater.*, vol. 48, 2013, doi: 10.1016/j.conbuildmat.2013.07.028.
- [283] M. C. J. Delgado e I. C. Guerrero, «Earth building in Spain», *Constr. Build. Mater.*, vol. 20, n. 9, pagg. 679–690, nov. 2006, doi: 10.1016/j.conbuildmat.2005.02.006.
- [284] MOPT, «Bases para el diseno y construcción con tapial. Madrid: Centro de Publicaciones Secretaria General Técnica Ministerio de Obras Publicas y Transportes». 1992.
- [285] E. Quagliarini, S. Lenci, e M. Iorio, «Mechanical properties of adobe walls in a Roman Republican domus at Susa», *J. Cult. Herit.*, vol. 11, n. 2, 2010, doi: 10.1016/j.culher.2009.01.006.
- [286] E. Quagliarini e S. Lenci, «The influence of natural stabilizers and natural fibres on the mechanical properties of ancient Roman adobe bricks», *J. Cult. Herit.*, vol. 11, n. 3, 2010, doi: 10.1016/j.culher.2009.11.012.
- [287] Ministero per i Beni e le Attività Culturali Regione Marche, *Architetture di Terra nelle Marche*. Edizioni Tecnostampa, Recanati, IT, 2005.
- [288] P. Walker, *Australia Standards, Australian Earth Building Handbook - HB 195*. Sydney, Australia, 2002.
- [289] D. Thompson, C. Augarde, e J. P. Osorio, «A review of current construction guidelines to inform the design of rammed earth houses in seismically active zones», *J. Build. Eng.*, vol. 54, n. February, pag. 104666, 2022, doi: 10.1016/j.job.2022.104666.
- [290] Standards Association Zimbabwe, «SAZS 724:2001: Standard Code of Practice for Rammed Earth Structures. Harare: Standards Association of Zimbabwe.» 2001.
- [291] Edict of Government, *NZS 4297 (1998): Engineering design of earth buildings*, vol. 4297. New Zealand, 1998, pag. 63.
- [292] «Construction Industries Division of the Regulation and Licensing Department the New Mexico Earthen Building Materials Code, Title 14, (Chapter 7), Part 4.» 2016.
- [293] G. Marcari, M. Basili, e F. Vestroni, «Experimental investigation of tuff masonry panels reinforced with surface bonded basalt textile-reinforced mortar», *Compos. Part B Eng.*, 2017, doi: 10.1016/j.compositesb.2016.09.094.
- [294] G. Marcari, G. Fabbrocino, e P. Lourenco, *Mechanical properties of tuff and calcarenite stone masonry panels under compression*. 2010.
- [295] N. Augenti e F. Parisi, *Mechanical characterization of tuff masonry*. 2009.
- [296] M. Guadagnuolo, M. Aurilio, A. Basile, e G. Faella, «Modulus of Elasticity and Compressive Strength of Tuff Masonry: Results of a Wide Set of Flat-Jack Tests», doi: 10.3390/buildings10050084.
- [297] Z. M. Memluk, «Designing Urban Squares», in *Advances in Landscape Architecture*, InTech, 2013.
- [298] ISTAT, «Popolazione residente al 1° gennaio 2018», 2018. http://dati.istat.it/Index.aspx?DataSetCode=DCIS_POPRES1 (consultato mag. 30, 2019).
- [299] K. Abass *et al.*, «Rising incidence and risks of floods in urban Ghana: Is climate change to blame?», *Cities*, vol. 121, pag. 103495, 2022, doi: 10.1016/J.CITIES.2021.103495.
- [300] J. Xia, R. A. Falconer, B. Lin, e G. Tan, «Numerical assessment of flood hazard risk to people and vehicles in flash floods», *Environ. Model. Softw.*, vol. 26, n. 8, pagg. 987–998, ago. 2011, doi: 10.1016/j.envsoft.2011.02.017.

- [301] T. Ishigaki, R. Kawanaka, Y. Onishi, H. Shimada, K. Toda, e Y. Baba, «Assessment of safety on evacuating route during underground flooding», in *Advances in Water Resources and Hydraulic Engineering - Proceedings of 16th IAHR-APD Congress and 3rd Symposium of IAHR-ISHS*, 2009, pagg. 141–146, doi: 10.1007/978-3-540-89465-0_27.
- [302] M. Pearson e K. Hamilton, «Investigating driver willingness to drive through flooded waterways», *Accid. Anal. Prev.*, vol. 72, pagg. 382–390, 2014, doi: 10.1016/J.AAP.2014.07.018.
- [303] K. Papagiannaki, M. Diakakis, V. Kotroni, K. Lagouvardos, e G. Papagiannakis, «The role of water depth perception in shaping car drivers' intention to enter floodwaters: Experimental evidence», *Sustain.*, vol. 13, n. 8, 2021, doi: 10.3390/SU13084451.
- [304] C. Arrighi, J. C. Alcèrreca-Huerta, H. Oumeraci, e F. Castelli, «Drag and lift contribution to the incipient motion of partly submerged flooded vehicles», *J. Fluids Struct.*, 2015, doi: 10.1016/j.jfluidstructs.2015.06.010.
- [305] K. Hamilton, A. E. Peden, M. Pearson, e M. S. Hagger, «Stop there's water on the road! Identifying key beliefs guiding people's willingness to drive through flooded waterways», *Saf. Sci.*, vol. 89, pagg. 308–314, nov. 2016, doi: 10.1016/j.ssci.2016.07.004.
- [306] H. Chanson, R. Brown, e D. McIntosh, «Human body stability in floodwaters: The 2011 flood in Brisbane CBD», in *ISHS 2014 - Hydraulic Structures and Society - Engineering Challenges and Extremes: Proceedings of the 5th IAHR International Symposium on Hydraulic Structures*, gen. 2014, n. June, pagg. 1–9, doi: 10.14264/uql.2014.48.
- [307] K. Hamilton, D. Demant, A. E. Peden, e M. S. Hagger, «A systematic review of human behaviour in and around floodwater», *Int. J. Disaster Risk Reduct.*, vol. 47, pag. 101561, 2020, doi: 10.1016/J.IJDRR.2020.101561.
- [308] M. Tanaka e M. Shimomura, «Making Evacuation Routine Behavior: Impact of Experiencing Severe Flood Damage on Recognition and Advance Evacuation Behavior», *J. Disaster Res.*, vol. 16, n. 2, pagg. 250–262, feb. 2021, doi: 10.20965/jdr.2021.p0250.
- [309] S. Alonso Vicario *et al.*, «Unravelling the influence of human behaviour on reducing casualties during flood evacuation», *Hydrol. Sci. J.*, vol. 65, n. 14, pagg. 2359–2375, ott. 2020, doi: 10.1080/02626667.2020.1810254.
- [310] T. Haer, W. J. W. Botzen, e J. C. J. H. Aerts, «The effectiveness of flood risk communication strategies and the influence of social networks—Insights from an agent-based model», *Environ. Sci. Policy*, vol. 60, pagg. 44–52, giu. 2016, doi: 10.1016/j.envsci.2016.03.006.
- [311] J. Cools, D. Innocenti, S. O'Brien, e S. O'Brien, *Lessons from flood early warning systems*, vol. 58. Elsevier Ltd, 2016, pagg. 117–122.
- [312] K. Haynes *et al.*, «'Shelter-in-place' vs. evacuation in flash floods», *Environ. Hazards*, vol. 8, n. 4, pagg. 291–303, gen. 2009, doi: 10.3763/ehaz.2009.0022.
- [313] G. Musolino, R. Ahmadian, e J. Xia, «Enhancing pedestrian evacuation routes during flood events», *Nat. Hazards*, 2022, doi: 10.1007/s11069-022-05251-9.
- [314] A. Gissing, K. Haynes, L. Coates, e C. Keys, «Motorist behaviour during the 2015 Shoalhaven floods», vol. 31, pagg. 25–30, apr. 2016.
- [315] J. Sörensen *et al.*, «Re-Thinking Urban Flood Management—Time for a regime Shift», *Water (Switzerland)*, pagg. 1–15, 2016, doi: 10.3390/w8080332.
- [316] T. Fujimi e K. Fujimura, «Testing public interventions for flash flood evacuation through environmental and social cues: The merit of virtual reality experiments», *Int. J. Disaster Risk Reduct.*, vol. 50, pag. 101690, 2020, doi: 10.1016/J.IJDRR.2020.101690.

- [317] X. Zhao, R. Lovreglio, e D. Nilsson, «Modelling and interpreting pre-evacuation decision-making using machine learning», *Autom. Constr.*, vol. 113, pag. 103140, mag. 2020, doi: 10.1016/j.autcon.2020.103140.
- [318] A. Banerjee, A. K. Maurya, e G. Lämmel, «A Review of Pedestrian Flow Characteristics and Level of Service over Different Pedestrian Facilities», *Collect. Dyn.*, vol. 3, n. 0 SE-, pagg. 1–52, lug. 2018, doi: 10.17815/CD.2018.17.
- [319] F. Hu, S. Yang, e W. Xu, «A non-dominated sorting genetic algorithm for the location and districting planning of earthquake shelters», *Int. J. Geogr. Inf. Sci.*, vol. 28, pagg. 1482–1501, mar. 2014, doi: 10.1080/13658816.2014.894638.
- [320] M. Gama, B. Santos, e M. Scaparra, «A multi-period shelter location-allocation model with evacuation orders for flood disasters», *EURO J. Comput. Optim.*, vol. 4, n. 3, pagg. 299–323, 2016, doi: <https://doi.org/10.1007/s13675-015-0058-3>.
- [321] M. Mohammadi, Z. K. Dashti, e A. Mirzazadeh, «MCLP and SQM models for the emergency vehicle districting and location problem», *Decis. Sci. Lett.*, vol. 3, n. 4, pagg. 479–490, 2014, doi: 10.5267/j.dsl.2014.7.001.
- [322] S. Kazazi Darani e M. Bashiri, «A multi-district asset protection problem with time windows for disaster management», *Int. J. Eng. Trans. B Appl.*, vol. 31, n. 11, pagg. 1929–1934, 2018, doi: 10.5829/ije.2018.31.11b.17.
- [323] E. Quagliarini, G. Bernardini, G. Romano, e M. D’Orazio, «Simplified flood evacuation simulation in outdoor built environments. Preliminary comparison between setup-based generic software and custom simulator», *Sustain. Cities Soc.*, vol. 81, pag. 103848, 2022, doi: 10.1016/J.SCS.2022.103848.
- [324] E. Quagliarini e G. Maracchini, «Experimental and FEM Investigation of Cob Walls under Compression», *Adv. Civ. Eng.*, vol. 2018, pagg. 21–29, 2018, doi: 10.1155/2018/7027432.
- [325] M. Bertagnin, *Architetture di Terra in Italia: tipologie, tecnologie eculture costruttive*. 1999.
- [326] E. Sori e A. Forlani, *Case di Terra e Paglia delle Marche*. Ascoli Piceno: Centro Beni Culturali Regione Marche,., 2003.
- [327] P. Croce *et al.*, «Shear modulus of masonry walls: A critical review», in *Procedia Structural Integrity*, 2018, vol. 11, doi: 10.1016/j.prostr.2018.11.044.
- [328] V. Alecci, G. Stipo, A. La Brusco, M. De Stefano, e L. Rovero, «Estimating elastic modulus of tuff and brick masonry: A comparison between on-site and laboratory tests», *Constr. Build. Mater.*, 2019, doi: 10.1016/j.conbuildmat.2019.01.224.
- [329] A. Prota, G. Marcari, G. Fabbrocino, G. Manfredi, e C. Aldea, «Experimental In-Plane Behavior of Tuff Masonry Strengthened with Cementitious Matrix–Grid Composites», *J. Compos. Constr.*, vol. 10, n. 3, 2006, doi: 10.1061/(asce)1090-0268(2006)10:3(223).
- [330] G. Faella, G. Manfredi, e R. Realfonzo, «Experimental evaluation of mechanical properties of old tuffmasonry panels subjected to axial loadings», in *Proceedings of the 9th International Brick/Block Masonry Conference*, 1991, pagg. 172–179.
- [331] B. Calderoni, E. A. Cordasco, L. Guerriero, G. Manfredi, e P. Lenza, «Mechanical behaviour of postmedieval tuff masonry in the Naples area», *Mason. Int.*, vol. 21, pagg. 85–96, gen. 2009.
- [332] E. Grande e A. Romano, «Experimental investigation and numerical analysis of tuff-brick listed masonry panels», *Mater. Struct.*, vol. 46, n. 1, pagg. 63–75, 2013, doi: 10.1617/s11527-012-9884-4.

- [333] L. Miccoli, U. Müller, e P. Fontana, «Mechanical behaviour of earthen materials: A comparison between earth block masonry, rammed earth and cob», *Constr. Build. Mater.*, vol. 61, 2014, doi: 10.1016/j.conbuildmat.2014.03.009.
- [334] G. Lan, Y. Wang, G. Zeng, e J. Zhang, «Compressive strength of earth block masonry: Estimation based on neural networks and adaptive network-based fuzzy inference system», *Compos. Struct.*, vol. 235, pag. 111731, 2020, doi: <https://doi.org/10.1016/j.compstruct.2019.111731>.
- [335] M. Mahdad, A. Benidir, e A. Brara, «Experimental assessment of mechanical behavior of a compressed stabilized earth blocks (CSEB) and walls», *J. Mater. Eng. Struct.*, vol. 8, n. May, pagg. 95–110, 2021.
- [336] C. Röhlen, U.;Ziegert, *Lehmbau-Praxis: Planung und Ausführung*, 3rd ed. Berlin, Germany, 2020.
- [337] E. Vicente e D. Torrealva, «Mechanical properties of historical adobe in Perú», *9th Int. Conf. Struct. Anal. Hist. Constr.*, pagg. 1–11, 2014, [In linea]. Available at: https://f-origin.hypotheses.org/wp-content/blogs.dir/1981/files/2018/05/TERRA-2016_Th-4_Art-216_Vicente.pdf.
- [338] G. Lan, G. Weng, e K. Zhang, «Assessment of optimal specimen to measure the compressive strength of earthen-based masonry», *Measurement*, vol. 208, n. May 2022, pag. 112484, feb. 2023, doi: 10.1016/j.measurement.2023.112484.
- [339] H. N. Abhilash *et al.*, «Mechanical Behaviour of Earth Building Materials BT - Testing and Characterisation of Earth-based Building Materials and Elements: State-of-the-Art Report of the RILEM TC 274-TCE», A. Fabbri, J.-C. Morel, J.-E. Aubert, Q.-B. Bui, D. Gallipoli, e B. V. V. Reddy, A c. di Cham: Springer International Publishing, 2022, pagg. 127–180.
- [340] F. Wu, G. Li, H.-N. Li, e J.-Q. Jia, «Strength and stress–strain characteristics of traditional adobe block and masonry», *Mater. Struct.*, vol. 46, n. 9, pagg. 1449–1457, 2013, doi: 10.1617/s11527-012-9987-y.
- [341] S. Dora, V. Humberto, C. Aníbal, e C. José, «Mechanical Properties and Behavior of Traditional Adobe Wall Panels of the Aveiro District», *J. Mater. Civ. Eng.*, vol. 27, n. 9, pag. 4014253, set. 2015, doi: 10.1061/(ASCE)MT.1943-5533.0001194.
- [342] R. Illampas, R. Silva, D. Charmpis, P. Lourenco, e I. Ioannou, *Experimental Investigation of the Structural Response of Adobe Buildings to Lateral Loading Before and After the Implementation of Compatible Grout Repairs*. 2018.
- [343] E. Quagliarini, A. Stazi, E. Pasqualini, e E. Fratolocchi, «Cob construction in Italy: Some lessons from the past», *Sustainability*, vol. 2, n. 10, 2010, doi: 10.3390/su2103291.
- [344] Ziegert C. *Lehmwellerbau*, «Konstruktion, Schäden und Sanierung, Berichte aus dem Konstruktiven Ingenieurbau.», Technical University of Berlin, 2003.
- [345] M. Gomaa, J. Vaculik, V. Soebarto, e M. Griffith, «Feasibility of 3DP cob walls under compression loads in low-rise construction», *Constr. Build. Mater.*, vol. 301, n. June, pag. 124079, 2021, doi: 10.1016/j.conbuildmat.2021.124079.
- [346] R. H. Saxton, «Performance of cob as a building material», *Struct. Eng. London*, vol. 73, n. 7, pagg. 111–115, 1995, [In linea]. Available at: <https://www.scopus.com/inward/record.uri?eid=2-s2.0-0029635311&partnerID=40&md5=d53f8c36c6d96b0209bc0b10b34ae41b>.
- [347] O. O. Akinkurole, C. Jiang, A. T. Oyediran, O. I. D.- Salawu, e A. K. Elensinnla, «Engineering Properties of Cob as a Building Material», *J. Appl. Sci.*, vol. 6, n. 8, pagg. 1882–1885, apr. 2006, doi: 10.3923/jas.2006.1882.1885.

- [348] Q. M. Pullen e T. V Scholz, «Index and Engineering Properties of Oregon Cob», *J. Green Build.*, vol. 6, n. 2, pagg. 88–106, 2011, doi: 10.3992/jgb.6.2.88.
- [349] T. Vineslas, E. Hamard, A. Razakamanantsoa, e F. Bendahmane, «Further development of a laboratory procedure to assess the mechanical performance of cob», *Environ. Geotech.*, vol. 7, n. 3, pagg. 200–207, 2020, doi: 10.1680/jenge.17.00056.
- [350] A. Jiménez Rios e D. O’Dwyer, «Experimental validation for the application of the flat jack test in cob walls», *Constr. Build. Mater.*, vol. 254, pag. 119148, 2020, doi: <https://doi.org/10.1016/j.conbuildmat.2020.119148>.
- [351] C. M. Jaquin, P.A.; Augarde, C.E.; Gerrard, «Analysis of Historic Rammed Earth construction». New Delhi, India.
- [352] A. Romanazzi, D. V. Oliveira, e R. A. Silva, «Experimental Investigation on the Bond Behavior of a Compatible TRM-based Solution for Rammed Earth Heritage», *Int. J. Archit. Herit.*, vol. 13, n. 7, 2019, doi: 10.1080/15583058.2019.1619881.
- [353] Q. B. Bui, J. C. Morel, S. Hans, e N. Meunier, «Compression behaviour of non-industrial materials in civil engineering by three scale experiments: The case of rammed earth», *Mater. Struct. Constr.*, vol. 42, n. 8, 2009, doi: 10.1617/s11527-008-9446-y.
- [354] T. T. Bui, Q. B. Bui, A. Limam, e S. Maximilien, «Failure of rammed earth walls: From observations to quantifications», *Constr. Build. Mater.*, vol. 51, 2014, doi: 10.1016/j.conbuildmat.2013.10.053.
- [355] M. Hall e Y. Djerbib, «Rammed earth sample production: Context, recommendations and consistency», *Constr. Build. Mater.*, vol. 18, n. 4, 2004, doi: 10.1016/j.conbuildmat.2003.11.001.
- [356] M. F. Sabbà, M. Tesoro, C. Falcicchio, e D. Foti, «Rammed earth with straw fibers and earth mortar: Mix design and mechanical characteristics determination», *Fibers*, vol. 9, n. 5, 2021, doi: 10.3390/fib9050030.
- [357] F. Champiré, A. Fabbri, J.-C. Morel, H. Wong, e F. McGregor, «Impact of relative humidity on the mechanical behavior of compacted earth as a building material», *Constr. Build. Mater.*, vol. 110, pagg. 70–78, 2016, doi: <https://doi.org/10.1016/j.conbuildmat.2016.01.027>.
- [358] D. Ciancio, P. Jaquin, e P. Walker, «Advances on the assessment of soil suitability for rammed earth», *Constr. Build. Mater.*, vol. 42, pagg. 40–47, 2013, doi: <https://doi.org/10.1016/j.conbuildmat.2012.12.049>.
- [359] V. Maniatis e P. Walker, «Structural Capacity of Rammed Earth in Compression», *J. Mater. Civ. Eng.*, vol. 20, n. 3, 2008, doi: 10.1061/(asce)0899-1561(2008)20:3(230).
- [360] F. Ávila, E. Puertas, e R. Gallego, «Characterization of the mechanical and physical properties of unstabilized rammed earth: A review», *Constr. Build. Mater.*, vol. 270, 2021, doi: 10.1016/j.conbuildmat.2020.121435.
- [361] F. Ávila, E. Puertas, e R. Gallego, «Characterization of the mechanical and physical properties of unstabilized rammed earth: A review», *Constr. Build. Mater.*, vol. 270, pag. 121435, 2021, doi: <https://doi.org/10.1016/j.conbuildmat.2020.121435>.
- [362] Q. Liu e L. Tong, «Engineering properties of unstabilized rammed earth with different clay contents», *J. Wuhan Univ. Technol. Sci. Ed.*, vol. 32, n. 4, pagg. 914–920, 2017, doi: 10.1007/s11595-017-1690-y.
- [363] T. D. Dulal e S. K. Darunkumar, «Characteristic Properties of Cement-Stabilized Rammed Earth Blocks», *J. Mater. Civ. Eng.*, vol. 27, n. 7, pag. 4014214, lug. 2015, doi: 10.1061/(ASCE)MT.1943-5533.0001170.

- [364] R. El Nabouch, «Mechanical behavior of rammed earth walls under Pushover tests», Université Grenoble Alpes, 2017.
- [365] R. Silva, D. Oliveira, L. Schueremans, P. Lourenco, e T. Miranda, *Modelling of the Structural Behaviour of Rammed Earth Components*. 2014.
- [366] T.-T. Bui, Q.-B. Bui, A. Limam, e J.-C. Morel, «Modeling rammed earth wall using discrete element method», *Contin. Mech. Thermodyn.*, vol. 28, n. 1, pagg. 523–538, 2016, doi: 10.1007/s00161-015-0460-3.
- [367] A. Arrigoni, R. Pelosato, G. Dotelli, C. T. S. Beckett, e D. Ciancio, «Weathering’s beneficial effect on waste-stabilised rammed earth: a chemical and microstructural investigation», *Constr. Build. Mater.*, vol. 140, pagg. 157–166, 2017, doi: <https://doi.org/10.1016/j.conbuildmat.2017.02.009>.
- [368] M. Pakand e V. Toufigh, «A multi-criteria study on rammed earth for low carbon buildings using a novel ANP-GA approach», *Energy Build.*, vol. 150, pagg. 466–476, 2017, doi: <https://doi.org/10.1016/j.enbuild.2017.06.004>.
- [369] M. Kosarimovahhed e V. Toufigh, «Sustainable usage of waste materials as stabilizer in rammed earth structures», *J. Clean. Prod.*, vol. 277, pag. 123279, 2020, doi: <https://doi.org/10.1016/j.jclepro.2020.123279>.
- [370] D. M. Lilley e J. Robinson, «ULTIMATE STRENGTH OF RAMMED EARTH WALLS WITH OPENINGS.», *Proc. Inst. Civ. Eng. - Struct. Build.*, vol. 110, n. 3, pagg. 278–287, 1995, doi: 10.1680/istbu.1995.27872.
- [371] V. Toufigh e E. Kianfar, «The effects of stabilizers on the thermal and the mechanical properties of rammed earth at various humidities and their environmental impacts», *Constr. Build. Mater.*, vol. 200, pagg. 616–629, 2019, doi: <https://doi.org/10.1016/j.conbuildmat.2018.12.050>.
- [372] C. A. Freimund, G. M. Garfin, L. M. Norman, L. A. Fisher, e J. L. Buizer, «Flood resilience in paired US–Mexico border cities: a study of binational risk perceptions», *Nat. Hazards*, 2022, doi: 10.1007/s11069-022-05225-x.
- [373] A. Sadeghi-Pouya, J. Nouri, N. Mansouri, e A. Kia-Lashaki, «Developing an index model for flood risk assessment in the western coastal region of Mazandaran, Iran», *J. Hydrol. Hydromechanics*, 2017, doi: 10.1515/johh-2017-0007.
- [374] S. Santoro, V. Totaro, R. Lovreglio, D. Camarda, V. Iacobellis, e U. Fratino, «Risk perception and knowledge of protective measures for flood risk planning. The case study of Brindisi (Puglia region)», *Saf. Sci.*, vol. 153, pag. 105791, 2022, doi: 10.1016/J.SSCI.2022.105791.
- [375] F. Mahdavian, M. Wiens, S. Platt, e F. Schultmann, «Risk behaviour and people’s attitude towards public authorities – A survey of 2007 UK and 2013 German floods», *Int. J. Disaster Risk Reduct.*, vol. 49, pag. 101685, ott. 2020, doi: 10.1016/j.ijdr.2020.101685.
- [376] S. Rufat e W. J. W. Botzen, «Drivers and dimensions of flood risk perceptions: Revealing an implicit selection bias and lessons for communication policies», *Glob. Environ. Chang.*, vol. 73, 2022, doi: 10.1016/j.gloenvcha.2022.102465.
- [377] G. Gomes, V. Marchezini, e M. Sato, «(In)visibilities About the Vulnerabilities of People with Visual Impairments to Disasters and Climate Change: A Case Study in Cuiabá, Brazil», *Int. J. Disaster Risk Sci.*, 2022, doi: 10.1007/s13753-022-00394-6.
- [378] H. S. Na e R. Grace, «Influence of social networks and opportunities for social support on evacuation destination decision-making», *Saf. Sci.*, vol. 147, pag. 105564, 2022, doi: 10.1016/J.SSCI.2021.105564.

-
- [379] H. Chanson e R. Brown, «Stability of Individuals during Urban Inundations: What Should We Learn from Field Observations?», 2018, doi: 10.3390/geosciences8090341.
- [380] T. Ishigaki, Y. Onishi, Y. Asai, K. Toda, e H. Shimada, *Evacuation criteria during urban flooding in underground space*. 2008.
- [381] M. Yee, «Human stability in floodways», *Undergrad. Honours Thesis, Sch. Civ. Environ. Eng. Univ. New South Wales, Sydney, Aust.*, 2003.
- [382] O. Petrucci *et al.*, «MEFF: The database of MEDiterranean Flood Fatalities (1980 to 2015)», 2018, doi: 10.1111/jfr3.12461.
- [383] J. Adrian *et al.*, «A Glossary for Research on Human Crowd Dynamics», *Collect. Dyn.*, vol. 4, pagg. 1–13, 2019, doi: 10.17815/cd.2019.19.
- [384] S. Soares-Frazão, J. Lhomme, V. Guinot, e Y. Zech, «Two-dimensional shallow-water model with porosity for urban flood modelling», *J. Hydraul. Res.*, 2008, doi: 10.1080/00221686.2008.9521842.

